Effect of Al-5Ti-1B Master Alloy Grain Refiner on Mechanical Properties and Hot Tearing Susceptibility of Cast Al-7Si-3Cu Alloy

Ph.D. THESIS

by

Sachin Kumar Rathi
(ID: 2013RMT9039)

DEPARTMENT OF METALLURGICAL AND MATERIALS ENGINEERING

MALAVIYA NATIONAL INSTITUTE OF TECHNOLOGY JAIPUR,

JAIPUR-302017, RAJASTHAN (INDIA)

JANUARY 2018

Effect of Al-5Ti-1B Master Alloy Grain Refiner on Mechanical Properties and Hot Tearing Susceptibility of Cast Al-7Si-3Cu Alloy

A THESIS

Submitted in partial fulfillment of the requirements for the award of degree

of

DOCTOR OF PHILOSOPHY

in

METALLURGICAL AND MATERIALS ENGINEERING

by

Sachin Kumar Rathi
(ID: 2013RMT9039)

DEPARTMENT OF METALLURGICAL AND MATERIALS ENGINEERING

MALAVIYA NATIONAL INSTITUTE OF TECHNOLOGY JAIPUR,

JAIPUR-302017, RAJASTHAN (INDIA)

JANUARY 2018

This thesis is dedicated to

***My Parents**: Sh. Ravindra Singh & Smt. Sharvesh Devi*

***My Wife**: Sonia*

For their unconditional love, support and especially never ending patience

DEPARTMENT OF METALLURGICAL AND MATERIALS ENGINEERING

MALAVIYA NATIONAL INSTITUTE OF TECHNOLOGY JAIPUR, RAJASTHAN (INDIA)

CERTIFICATE

This is to certify that the thesis entitled **"Effect of Al-5Ti-1B Master Alloy Grain Refiner on Mechanical Properties and Hot Tearing Susceptibility of Cast Al-7Si-3Cu Alloy"** being submitted by me to the Malaviya National Institute of Technology Jaipur for the award of the degree of **Doctor of Philosophy** is a bonafide record of original research work carried out by me. The content of the thesis has been checked using software "Turnitin" for Plagiarism.

I have incorporated all the suggestions/queries/changes raised by the Examiner in the Thesis Evaluation Reports.

(Sachin Kumar Rathi)

This is to certify that above statement made by the candidate is true to our knowledge.

Prof. Dr. Ashok Sharma
(Supervisor)

Ph.D. viva-voce examination of Mr. Sachin Kumar Rathi, Research Scholar, was held on 02-01-2018 in Department of Metallurgical & Materials Engineering, MNIT Jaipur. The candidate defended the viva-voce successfully to the satisfaction of Oral Defense Committee. The Committee recommends for the award of Ph.D. Degree.

Signature of Supervisors **Signature of External Examiner**

DEPARTMENT OF METALLURGICAL AND MATERIALS ENGINEERING

MALAVIYA NATIONAL INSTITUTE OF TECHNOLOGY JAIPUR, RAJASTHAN (INDIA)

CERTIFICATE

This is to certify that the thesis entitled **"Effect of Al-5Ti-1B Master Alloy Grain Refiner on Mechanical Properties and Hot Tearing Susceptibility of Cast Al-7Si-3Cu Alloy"** is being submitted by **Mr. Sachin Kumar Rathi (ID: 2013RMT9039)** to the Malaviya National Institute of Technology Jaipur for the award of the degree of **Doctor of Philosophy** is a bonafide record of original research work carried out by him under our supervision and guidance. This thesis work, in our opinion, has reached the requisite standard fulfilling the requirement of **Doctor of Philosophy**.

The results contained in this thesis have not been submitted, in part or full, to any other university or institute for the award of any degree or diploma.

Prof. Dr. Ashok Sharma
(Supervisor)
Dept. of Met. & Mat. Engg.
Malaviya National Institute
of Technology Jaipur
Rajasthan (India)

Assoc. Prof. Dr. Marisa Di Sabatino
(External Supervisor)
Norwegian University of Science and
Technology Norway

Date:

DECLARATION

I, Sachin Kumar Rathi, declare that this thesis titled, "Effect of Al-5Ti-1B Master Alloy Grain Refiner on Mechanical Properties and Hot Tearing Susceptibility of cast Al-7Si-3Cu Alloy" and the work presented in it, are my own. I confirm that:

- This work was done wholly or mainly while in candidature for a research degree at this university.
- Where any part of this thesis has previously been submitted for a degree or any other qualification at this university or any other institution, this has been clearly stated.
- Where I have consulted the published work of others, this is always clearly attributed.
- Where I have quoted from the work of others, the source is always given. With the exception of such quotations, this thesis is entirely my own work.
- I have acknowledged all main sources of help.
- Where the thesis is based on work done by myself, jointly with others, I have made clear exactly what was done by others and what I have contributed myself.

Date: Sachin Kumar Rathi (2013RMT9039)

ACKNOWLEDGEMENT

First I would like to express my earnest gratitude and humble regards to my supervisors **Prof. Dr. Ashok Sharma** and **Prof. Dr. Marisa Di Sabatino** who provided me precious opportunity to pursue research under their guidance. Their guidance put me on a new platform of wonderful and challenging materials world. Their unique guiding quality, interest, working enthusiasm and analytical approach towards the experimental results impressed me so much. It is great honour for me to work with them. I would like to express my sincere thanks to **Prof. Dr. A.K. Bhargava (HOD), Prof. Dr. Upender Pandel and Dr. V.K. Sharma** for being in my DREC committee and to **Dr. R.K. Duchaniya** (convener, DPGC) for their encouragement, analytical insights and recommendations. I would like to thank **Mr. Lalchand Kumawat (Sr. Technician)**, **Mr. Chidarapu Rishikesh Babu (Technician)** and **Mr. Lala Ram** of department of Metallurgical and Materials Engineering, MNIT Jaipur for their help during PhD work.

I further extend my thanks to all the staff members of **Materials Research Center (MNIT Jaipur)** for providing characterization facilities. I express my deep appreciation to my collogues **Mr. Himanshu Sharma, Dr. Avnish Kumar, Mr. Robin Gupta, Mr. Anurag Hamilton, Ms. Vatsala Chaturvedi, Mr. Rahul Sen, Mr. Samir Pradhan, Mr. Arun Kumar, Mr. Akshay Kumar, Dr. Arnav Anuj Kasar, Mr. Shushant kumar, Mr. Dheeraj Mehta, Mr. Nitesh Kumar** and the post graduate students of the department of Metallurgical and Materials Engineering, MNIT Jaipur for their moral support and help. I would like to extend my sincere thanks to all the faculty and staff members of MNIT, Jaipur for their support during my Ph.D.

I would like to thank my parents and my family members for their unconditional love and support. Without them, this thesis would not be possible.

(Sachin Kumar Rathi)

ABSTRACT

In the present investigation, the effect of Al–5Ti–1B grain refiner on the microstructure, mechanical properties and hot tearing tendency of Al-7Si-3Cu alloy have been studied. Al-7Si-3Cu alloy is a relatively new Al-Si-Cu alloy with good strength and excellent wear resistance at both room and elevated temperature. However, despite their advantages, when these alloys are cast via the permanent mould casting (PMC) process, they show a high susceptibility to hot tearing. Grain refinement has shown promises as a mean to increase mechanical properties and to reducing hot tear in aluminium alloys via achieving finer grains. The refinement of Al-7Si-3Cu alloy is carried out by the addition of varying amount of titanium 0.035 wt.% to 0.050 wt.% of Ti.

The present work is focused on improving the grain refining efficiency of Al-5Ti-1B master alloy via ball milling, annealing and hot rolling. By these processes more number of heterogeneous nucleating sites are ($TiAl_3$ particles) formed of smaller size. After ball milling and hot rolling $TiAl_3$ particles reduce in size from 80 µm to 9 and 15 µm, respectively. The improvement in grain refining performance of Al-5Ti-1B master alloy is due to the fracture of larger $TiAl_3$ particles into fine particles during rolling. The improved grain refining efficiency of the Al-5Ti-1B master alloy on annealing is ascribed to the increased volume fraction of $TiAl_3$ and the possible formation of $(Ti,Al)B_2$ phase. The mechanical properties are enhanced by 40% MPa and 31% HB respectively by addition 0.035 wt.% Ti hot rolled master alloy.

For hot tear test, a permanent mould having test bar of size 260 mm long and 20 mm in height with constraint at the end has been used. The effect of mould temperature and grain refinement on hot tearing tendency of Al-7Si-3Cu alloy has also been investigated. The results indicate that mould temperature and grain refiner show significant influence on reducing the hot tearing tendency of the alloy. Effect of mould temperature on hot tear formation has been studied at room temperature, 90 ºC, 160 ºC, 230 ºC and 300 ºC. Higher mould temperature upto 300 ºC helps in reducing hot tear susceptibility of the alloy by refilling the material in later stage of solidification. The results showed that the hot tearing tendency of the Al-7Si-3Cu alloy was removed with the addition of cast master alloy at 0.050 wt.% Ti. When master alloy was further treated using ball milled, annealed and hot rolled the mechanical properties were improved

significantly and hot tear was reduced. The addition level of wt.% titanium also reduced from 0.05 wt.% to 0.045 wt.%, 0.040 wt.% and 0.035 wt.% Ti respectively.

During later stage of the solidification higher volume fraction of solid forms and as a subsequence, hot tears directly nucleate in the interdendritic liquid from pre-existing micropores. The hot tearing surface morphology shows the formation of spikes either by the necking of solid bridges established across the grain boundaries prior to pulling, or by the sudden break-up of the liquid film during pulling. Further, thermal analysis suggested that grain refinement delayed the onset of dendrite coherency in Al-7Si-3Cu alloy and therefore increased the duration of bulk liquid metal feeding for the grain refined casting conditions. As a consequence, the influence of such factors resulted in a more uniform distribution of strain, and subsequent higher resistance to hot tearing for the refined Al-7Si-3Cu alloy. The addition of hot rolled master alloy in Al-7Si-3Cu alloy showed more fine and equiaxed grain structure in comparison to as cast, ball milled and annealed master alloy at lower addition level. Characterization study has been carried out by OM, DSC, XRD, SEM and TEM analysis.

CONTENTS

List of Tables

List of Figures

List of Appendix

List of Abbreviations

PMC	Permanent mould casting
GR	Grain refiner
SDAS	Secondary dendritic arm spacing
ASTM	American society for testing and materials
OM	Optical micrographs
XRD	X-ray diffraction
SEM	Scanning electron microscope
TEM	Transmission electron microscope
EDS	Energy Dispersive X-Ray Spectroscopy
DSC	Differential scanning calorimetric
UTS	Ultimate tensile strength
QI	Quality index
GRF	Growth restriction factor
FCC	Face centered cubic
µm	Micrometer
wt.%	Weight percentage
ºC	Degree Celsius
Al	Aluminium
Ti	Titanium
B	Boron
h	Hour
mm	Millimeter
CSC	Cracking susceptibility coefficient
HCS	Hot cracking sensitivity

1 Chapter one

Introduction

1.1 Background

Aluminium alloy castings are used in the automotive industry for several components such as engine blocks and cylinder heads, due to their favorable combination of low weight, recyclability, easy machinability and low cost [1,2]. The most common class of aluminum alloys is of aluminum-silicon-copper (Al-Si-Cu) system [3,4]. These alloys produce lighter and more fuel efficient vehicles. Cost reduction and product optimization have been the driving force for research in the field of alleviating casting defects. It was nearly 1969 when Campbell [5] issued a research paper on the feeding mechanisms in casting. A notable literature view by many researchers [6-8] depicted attention to the scientific and technical knowledge on metal related castability effects in aluminum foundry alloys. Experimental work has been started though not on a wide scale, paying special attention to the feeding mechanisms and their influence on mechanical properties and porosity formation. The dendrite coherency point is a vital characteristic in cast aluminium-silicon alloys [9-13], because it marks the transition from mass feeding to interdendritic feeding in the solidification process [6, 14-17]. Recent investigations across a large range of aluminium alloys have reported that the fraction of solid at which dendrite coherency is reached varies systematically as a function of alloying composition, cooling rate, and grain refinement [9,11,18-23].

Grain refinement plays a vital role in improving metallurgical characteristics and mechanical properties of aluminum alloys [24-32]. Fine equiaxed grains [33] ensure the following benefits: (a) uniform and improved mechanical properties throughout the material,(b) distribution of secondary phases and micro-porosity on a fine scale which in turn improves machinability, (c) better feeding to eliminate shrinkage porosity, (d) better surface finishes on both the basic casting and the machined parts, (e) reduced ingot cracking and improved resistance to hot tearing, (f) better strength, toughness, fatigue life and corrosion resistance [34-41]. The addition of Al–5Ti and Al–5Ti–1B master alloy to the Al-Si-Cu alloy melt discharge a large number of intermetallic particles, for example $TiAl_3$, TiB_2 and $(Al,Ti)B_2$ into the melt. These particles act as heterogeneous nucleating sites for the solid grain during solidification [42-45]. The $TiAl_3$ and TiB_2 particles exhibit a

particular orientational relationship with α-Al phase, along which the grain refinement occurs having minimum lattice mismatch. However, the dimension, distribution, and morphology of heterogeneous particles play an imperative role in the process of grain refinement. Furthermore, many researchers [46-51] have investigated the improvement in grain refining response of Al-Si-Cu alloys, with variation in contact time. It has been observed that grain refinement increases with increase in contact time, but only up to a certain extent, beyond which, with increase in contact time the grain refining efficiency remains unaffected. This has primarily been attributed to the agglomeration and settlement of $TiAl_3$ and TiB_2 particles with greater contact time. Nevertheless, a conventional method of achieving higher grain refinement of Al-7Si-3Cu is through the proportion of Al-5Ti-1B master alloy.

By now, various attempts have been made to improve the grain refinement response on the Al–Si-Cu alloys. Ghadimi [52] and Murty et al. have [53,54] additionally demonstrated that ball milling, annealing and hot rolling enhances the grain refining efficiency of Al-5Ti and Al-5Ti-1B master alloy by aggregate the $TiAl_3$ phase. One effective route is to increase the addition level of Al–5Ti–B master alloy, which is undesirable in practice [55]. In the present investigation, possibility is explored to refine the $TiAl_3$ particles in Al-5Ti-1B grain refiner by ball milling, annealing and hot rolling technique and to achieve equiaxed grain structure in Al-7Si-3Cu alloy at lower addition level of grain refiner. Ball milling and rolling consequences in the fracture of $TiAl_3$ particles [56]. During rolling, a high concentration of stress is accommodated on the particle matrix interface, which leads the fracture of $TiAl_3$ nucleating particles. Since the particles are brittle in nature so, stress concentration results in their fracture. Rolling provides larger number of heterogeneous nucleating sites in the melt [57,58]. Murty et al. [53] investigated that as the hot rolled reduction level of master alloy is increased the grain refining efficiency of the master alloy is increased in Al alloy resulting in finer grains and enhance mechanical properties [59-61]. When Al-7Si-3Cu alloy is cast through permanent mould casting (PMC) process, it has higher susceptibility to hot tearing. This defect limits the use of Al-Si-Cu alloy as their outstanding mechanical properties are offset by its hot tearing tendency [62-69]. The hot tearing is a casting defect and induced during the solidification in aluminium alloys by pulling the columnar dendrites in the transverse direction. Eskin et al. [63] predicted that hot tearing tendency of the alloy depends on various casting parameters such as pouring temperature, mould temperature and chemistry of the alloy. Furthermore, grain refinement,

geometry of mould, and superheat of the melt also affect the hot tearing tendency of the alloy [70-72]. Recent investigation [65,63] proposed that hot tearing is a strain controlled phenomenon and occurs when it reaches a critical value in hot spot zone. In the first stage of solidification, liquid film is relatively thick enough and continuous throughout, while in the latter stage, the film is thinner and thinner and the deformation is localized on a few hot zones, giving rise to high strains [73,74]. Furthermore, Campbell [5] quantified Pellini's [75] theory and stated that strain in the hot spot is directly influenced by the coefficient of thermal expansion, the length of mushy zone, length of the casting, and length of a hot spot. Hot tear is formed in a critical region of the mushy zone where the liquid film of interdendriritic is more or less continuous and permeability is less [76-80].

The size of the mushy zone and the solidification behavior of molten metal in the mushy zone also affect hot tearing. Bala et al. [81] investigated that solidification of casting depends upon various parameters such as mould wall temperature, metal mould interface, material of the mould and mould wall thickness. Various studies [82-84] also emphasized the role of tensile stresses in the mushy Zone, which imposed due to the insufficient feeding of melt in interdendritic region. Hot tearing probability of many binary alloys has been investigated such as Mg-Zn [85], Mg-Y [86], Mg-Gd [7] and Mg-Ca [77]. In addition, the hot tearing tendency of ternary alloy Mg-Zn-Y [87], [87], Al-Mg-Cu [79], Mg-2Ca-xZn [84], Al-Mg-Sr [88] and Al-Mg-Ca [15] alloys have also been investigated. Wang et al. [79] reported that hot tearing in Al-Zn-Mg-Cu alloy is completely eliminated by grain refinement. As per Saveiko theory [16] presence of thin and continuous interdendritic film in the later solidification has low tendency toward hot tearing. Eskin et al. [63] suggested that impurities can considerably affect the ductility and the freezing range of alloys. It has been thoroughly investigated that fine equiaxed structure prompts to various paybacks such as high yield strength, improved machinability, improved feeding to eliminate the shrinkage porosities, diminished hot tearing tendency, and lessened mould filling time in Al-7Si-3Cu alloy [37,52,84,89,90].

Recent studies by Eskin et al. [63] reported that grain refinement reduces the onset time of thermal contraction and pushed it at an advanced stage of solidification giving fewer thermal strain in the mushy zone. This grain refinement decreases hot tear propensity in Al-Si-Cu alloys. These potent nucleating particles act as substrate for heterogeneous nucleation, and eventually refines the α-Al phase [29,45,49,91,92]. Finer grain morphology, subsequent from grain refinement, enables improvement in feeding of liquid

melt during solidification and also improves solidification strain homogeneity. Titanium silicide has lower chemical stability with molten metal. Therefore, Ti:B inoculation produce poisoning effect with higher Ti level. The morphology, size, size distribution or $TiAl_3$ particles in the Al-5Ti-1B grain refiner also play a vital role in deciding the grain refining performance of the grain refiner [53,54,93]. The ball milling, annealing and hot rolling of grain refiner are done, to eliminate the hot tearing tendency at lesser addition level of Ti:B via improved grain refining efficiency. This also eliminates the possibility of poisoning. The improvement in grain refining efficiency is a key variable to limit hot tearing in Al-7Si-3Cu alloy, for example, this defect can be eliminated at lower addition level of Ti:B. After outlining the recent studies, this research concentrates on advance in grain refining efficiency of Al-5Ti-1B master alloy. The entire body of effort is far too vast to experimental comprehensively; the study is focus on eliminated hot tearing tendency of Al-7Si-3Cu alloy at lower addition level of grain refiner. Starting here of view a point by point investigation of the microstructure, grain refining proficiency, XRD and SEM of the annealed Al-5Ti-1B master alloy and Al-7Si-3Cu alloy are carried out in the present investigation.

1.2 Objectives of Present Study

The primary aim of the study was to improve the mechanical properties and hot tearing resistance of Al-7Si-3Cu alloy with addition of Al-5Ti-1B grain refiner master alloy. The objectives of the present research work are subcategorized in following heads.

- Study of different processing conditions on the shape, size and particles distribution of $TiAl_3$ particles of Al-5Ti-1B master alloy.
- Assessment of grain refinement in Al-7Si-3Cu alloy with addition of as cast, ball milled, annealed and hot rolled master alloy.
- Investigation of above effects with different characterization techniques such as microstructure, XRD, DSC, SEM and TEM with EDX.
- Study about mechanical properties of Al-7Si-3Cu alloy with addition of as received and treated master alloy. Comparison between the as cast, with ball milled, annealed and hot rolled master alloy.
- The effect of mould temperature and grain refinement on hot tearing susceptibility in Al-7Si-3Cu alloy.

- Examination of hot tearing by addition of as received and treated master alloy with different content of Al-5Ti-1B master alloy. The addition of optimum grain refiner in Al-7Si-3Cu alloy to observe the effect of grain refiner on the hot tearing tendency of the alloy.

1.3 Outline of Thesis

The contents of the thesis have been organized into seven chapters.

Chapter 1 deals with the overall idea about the thesis. The applications of Al-Si-Cu alloys in various industries and their importance are given in this chapter. The major problem faced by Al-7Si-3Cu alloy i.e. inadequate mechanical properties and susceptibility to hot tearing are also discussed. Effective ways to enhance the mechanical properties of the alloy are also given.

Chapter 2 presents a concise review of the literature available on alloy solidification, mechanical properties, thermo-mechanical treatment of grain refiner, the theories of hot tearing, and the factors affecting hot tearing, including alloy composition, grain size and processing parameters. The various techniques used to characterize mechanical properties and hot tearing susceptibility are also critically reviewed. The mechanism of grain refinement and the hot tearing tendency by inoculants have also been discussed.

Chapter 3 includes the detailed experimental procedure employed for alloy preparation and characterization. Al-7Si-3Cu alloy was prepared using commercial purity Al (99.7%), Al-13Si and Al-33Cu master alloy. As received Al-5Ti-1B master alloy was given the following treatments, (i) Ball-milled into a fine powder (10 µm). This was achieved by cutting the starting master alloy by lathe machine and then ball-milled for 10h, 30hand 50h, respectively, (ii) Annealing was performed at 500 ºC, 600 ºC, 700 ºC and 800 ºC in a muffle furnace with an accuracy of ± 5 ºC. This was done to improve the volume of $TiAl_3$ particles, and (iii) Hot rolling was done at 250 ºC and 350 ºC with achieving reduction level 25%, 50% and 75%, respectively. Table 1 shows the type of master alloy with different treatments.

To identify the phases, present in the Al-7Si-3Cu and Al-5Ti-1B alloy, XRD studies were carried out using an X'Pert Powder PAN alytical diffractometer with CuKα radiation. The microstructures were characterized using an optical microscope (OM, Leica DMLA), scanning electron microscope (SEM, NOVA NANO 450) and transmission electron microscope (TEM, G^2 20(FEI)) with EDS micro-analysis facility was used for

microstructural examinations. Solidification behavior was studied by Differential Scanning Calorimeter (DSC 404 F3). The tensile test was performed for experimental samples in as-cast state and grain refined on a tensile tester. Values of ultimate tensile strength are determined by the average value of three test samples. Hardness measurement was performed by a Brinell hardness tester. The Brinell hardness value at each state was obtained by the average of at least five measurements. For hot tear test, melt was poured in a steel test bar of size 260 mm long and 20 mm in height, at varying amount of master alloy with various processing conditions. Table 1.1 shows the types of master alloy which are carried out to investigate the effect of various treatments on mechanical properties and hot tear tendency.

Table 1.1 Types of master alloy

Si. No.	Alloy type	Treatment
1	Type A	As cast
2	Type B	Ball milling
3	Type C	Annealing
4	Type D	Hot rolling

Chapter 4 covers the results and discussions about microstructure, macrostructure, porosity and mechanical properties of the cast and grain refined Al-7Si-3Cu alloy. Various amount of Al-5Ti-1B master alloy was added to the Al-7Si-3Cu alloy under different treatment such as ball milling, annealing and hot rolling. $TiAl_3$ particles have better grain refining efficiency in comparison to TiB_2 particles and present in microscopic form, whether TiB_2 particles are is submicroscopic form. Therefore, to notice the effect of ball milling, annealing and hot rolling on morphology of heterogeneous nucleating particles, $TiAl_3$ particles were mainly focused. However, the presence of TiB_2 particles on $TiAl_3$ surface increase the grain refining efficiency of the master alloy. It is observed that the hot rolling showed maximum grain refiner efficiency at lower addition level of Ti as a comparison to type A, B and C master alloys. An X-ray diffraction pattern of the as received Al-5Ti-1B master alloy was studied, which showed that the alloy consisted of $TiAl_3$ phase with a tetragonal crystal structure (JCPDF No. 01-072-5006), TiB_2 phase with a hexagonal crystal structure (HCP) (JCPDF No. 01-085-2084) and α (Al) phase with a face-centered cubic (FCC) crystal structure (JCPDF No. 00-004-0787). The XRD patterns after ball milling, annealing and hot rolling showed that the relative peak intensity of $TiAl_3$ particles

is increased in comparison to as cast master alloy. The higher peak intensity confirms that the grain refining performance of Al-5Ti-1B master alloy increased from as cast to ball milled to annealed and finally by hot rolled. The improvement of $TiAl_3$ peak intensity during ball milling and hot rolling is due to the fracture of these brittle intermetallic particles, resulting in more number of heterogeneous nucleating sites. The increase in the $TiAl_3$ peak intensity with annealing temperature suggests an increase in the volume fraction of the phase. The increase in the $TiAl_3$ peak intensity is a confirmation of higher volume fraction of the $TiAl_3$ phase. The increase in the $TiAl_3$ peak after annealing suggests that the alloy does not grasp equilibrium during its synthesis.

Optical microstructures of as cast and grain refined Al-7Si-3Cu alloy showed that the addition of master alloy under various processing conditions refined the α-Al phase. A change is observed in the microstructure from columnar grain structure to a mixture of fine columnar and equiaxed grain structure within 10 min of holding time. This is given as follows;

As the addition level of wt.% Ti of as cast master alloy is increased in the Al-7Si-3Cu alloy, the refinement of α-phase improved. The optimum grain refinement of α-Al phase is obtained with the addition of type A master alloy with 0.050 wt.% Ti. However, the higher addition level (0.055 wt.% Ti) could not show the further refinement of α-phase rather negative effect of Ti addition was observed. The optimum grain refinement of Al-7Si-3Cu alloy is achieved with the addition of type B master alloy at 0.045 wt.% Ti for 30h with average particles size 20 µm. However, Al-7Si-3Cu alloy inoculated with type B master alloy at 0.045 wt.% Ti for 50h does not show the further refinement in the microstructure. Which was due to the smaller particles of 10 µm in size after 50h. Smaller particles of 10 µm size of $TiAl_3$ may dissolve quickly into the melt.

The improved grain refining efficiency of master alloy after annealing could be attributed to the increase in volume fraction of $TiAl_3$ particles. At higher annealing temperatures of 700 ºC, the grain refining performance of master alloy increased to that at 500 ºC and 600 ºC. However, annealing at 800 ºC shows poor performance of master alloy to other temperature due to the segregation the $TiAl_3$ and TiB_2 particles at upper and lower region, respectively. The best response of grain refinement on Al-7Si-3Cu alloy is achieved with the addition of hot rolled master alloy at 75% reduction level at 0.035 wt.% Ti. At, 75% reduction level there are more number of $TiAl_3$ particles of size 15 µm in comparison to 10 µm after ball milling. The $TiAl_3$ particles of size 15 µm is more stable into the melt in respect to size of 10 µm.

It is observed that porosity can be minimized with the addition of Al-5Ti-1B master alloy. The finer grains permit to drift the liquid melt into the mushy zone which is needed to heal the pores in the later stage of solidification. This reduces hot tearing tendency of the Al-7Si-3Cu alloy besides improvement in mechanical properties. The as cast Al-7Si-3Cu alloy displays the porosity formation (2.6%). With addition of type A master alloy at 0.05 wt.% Ti it decreased upto (2.3%). The Al-7Si-3Cu alloy inoculated with type D master alloy shows the minimum porosity (0.6%) at same addition level with 50% and 75% reduction level.

The coarser primary α-dendritic structure exhibited low tensile values in the unrefined alloy. The tensile properties of Al-7Si-3Cu alloy inoculated with type A master alloy increases with increase in wt.% Ti upto 0.050 wt.% Ti, which was due to the change in the morphology of primary α-phase from coarser dendritic structure to fine equiaxed structure. The hardness properties of the alloy increases with increase in wt.% Ti upto 0.050wt.% Ti, and increased further with the addition 0.055 wt.% Ti. This was due to the presence of higher number of heterogeneous nucleating particles and large intermetallic phase. The Al-7Si-3Cu alloy inoculated with type D master alloy exhibited optimum results of tensile and hardness values in comparison to the type A, B, and C master alloy. The tensile and hardness properties of refined Al-7Si-3Cu alloy with the addition of type D master alloy at 0.035 wt.% Ti, roughly increased by 40 and 34% respectively. This shows that the optimum value of Al–5Ti–1B master alloy gives us the maximum tensile values (292 MPa) and hardness (89 HB) at 0.035 wt.% Ti.

Chapter 5 deals with the effect of mould temperature and grain refinement on hot tearing tendency in Al-7Si-3Cu alloy. Al-5Ti-1B master alloy is added in Al-7Si-3Cu alloy as received type A and with treated master alloy of type B, type C and type D at varying wt.% Ti for each case. The study of various process parameters to minimize hot tear tendency of Al-7Si-3Cu alloy is given as follows.

It is observed that the mould temperature has a major effect on hot tearing tendency of Al-7Si-3Cu alloy. It is seen that the fracture is generated in test bar at room temperature, 90 °C, 160°C and 230 °C mould temperature. It is observed that as the mould temperature increased up to 300 °C, the hot tearing got eliminated. At higher mould temperature principal strain was lower and hence, a reduced tendency to form hot tears resulted. The results suggest that the grain refinement reduces hot tearing severity of Al-7Si-3Cu alloy by restricting the growth of α-phase. When, type A master alloy with 0.050 wt.% Ti was

added to the melt, the hot tearing got eliminated. This has happened due to the sufficient nucleation sites available for grain refinement.

The Al-7Si-3Cu alloy inoculated with type B alloy at 0.045 wt.% Ti for 10h shows crack near the down sprue in the test bar. However, at the same addition level of type B alloy for 30h and 50h, hot tear got eliminated. Ball milling for 30h and 50h has caused higher fragmentation of existing $TiAl_3$ particles resulting in more number of finer $TiAl_3$ particles. The Al-7Si-3Cu alloy inoculated with type C master alloy with 0.040 wt.% Ti, at 400ºC, 500 ºC and 600 ºC temperature shows hairline fracture in the test bar. By addition of type C master alloy at 700 ºC, crack got eliminated at the same addition level. However, the same addition of type C master alloy at 800 ºC has caused appearance of crack again in the test bar. Hot rolled master alloy has extraordinary abilities to refine the dendritic structure as compared to other type A, B, and C master alloys due to the fracture of $TiAl_3$ particles. In this case the $TiAl_3$ particles after rolling fragmented to 15 µm particles size. The particles of size 15 µm showed best response towards grain refinement. The Al-7Si-3Cu alloy inoculated with type D master alloy with 0.035 wt.% Ti of 25% reduction level is added to the melt, a minor crack is observed in the test bar. Same addition level of type D master alloy with 50% and 75% reduction level were sufficient to remove the crack from the test bar.

The cracks noticed in the test bar were examined under SEM to understand the cause of fracture. Evidence of density difference from liquid to solid is seen at the fracture surfaces, which proves the tensile loading present during tearing. It is obvious that hot tearing occurs due to porosity formation. Solid skeleton formation begins to transfer tensile forces at the early stage, which suggests that a continuous dendritic network formed in the mushy zone begins to separate under the applied tensile force. It is indicated that hot tearing is initiating and propagating under the applied tensile force.

Chapter 6 summarizes the important outcome of the present investigations and suggestions for future work.

Appendix (I – VI) introduce the wt.% grain refiner calculation, the mean particle size of nucleating particles, phase transformation reaction and a list of publications.

1.4 Advantages of Addition of Grain Refiner

Addition of grain refiner exhibited several advantages

(i) Refinement of dendritic structure into the equiaxed structure.

(ii) Improved feeding and reduced ingot cracking.

(iii) Better homogeneity with reduced porosity.

(iv) Improved mechanical properties.

(v) High productivity and reduced costs.

1.5 Industrial Applications of Al-Si-Cu alloy

There are various companies which are working to produce Al-Si-Cu alloy components and lead to the application in automotive industry, especially for automotive engines, crankcases, intake manifolds, cylinder blocks, cylinder heads, pistons, cast oil pans and valve lifters [48].

2 Chapter Two

Literature Review

This chapter contains the fundamental aspects of solidification, grain refinement, mechanical properties and hot tearing tendency of the alloy. This chapter covered the relevant literature about the effect of different process parameters on mechanical properties and hot tearing tendency. Review of grain size and mechanical properties by various investigators was also carried out.

2.1 Principle of Solidification

When liquid metal cools then transformation from liquid to solid takes place. During solidification nucleation of new grains takes place which may further grow, so solidification comprises two different processes; nucleation and growth [19]. Nucleation is of two types; homogeneous and heterogeneous. Homogeneous nucleation occurs in pure metals, while heterogeneous nucleation takes place in alloys due to foreign particles [12, 94-98]. During the solidification of a casting, most alloys freeze over a temperature range and solidification occurs gradually with decreasing temperature. As the temperature decreases, the developing solid fraction leads to a continuously changing mush microstructure and increasing difficulties of feeding liquid [99]. Further, the freezing liquid continuously contracts to form solid and generating a pressure difference between the inside and outside of the casting. This internal pressure might decrease enough to become negative, as a hydrostatic tension, and is undesirable in casting, as it is the driving force for the initiation and development of defects including porosity and hot tearing [14].

2.1.1 Homogeneous nucleation

When pure metal cools in a liquid state, then it transforms in a solid state at fixed temperature. Thermodynamically for pure metals, there is only one temperature where solid and liquid can coexist [100] Critical radius and free energy for homogeneous nucleation can be given as

$$r^*_{homogeneous} = \frac{-2\,\gamma_{sl}}{\Delta G_v} \tag{2.1}$$

$$\Delta G_c = \frac{16}{3}\frac{\pi\gamma_{sl}^3}{(\Delta G_v)^2} \tag{2.2}$$

Where, γ_{SL} is the surface energy (J/m^2) of solid–liquid interface. For an undercooling ΔT, per unit volume, Gibb's free energy ΔGv can be given as

$$\Delta G_v = \Delta T \Delta S = \frac{\Delta H_f \Delta T}{T_m} \quad (2.3)$$

ΔT = undercooling (K) below liquidus temperature, ΔS = change in entropy (J/K/m3) for liquid to solid phase transformation, ΔHf = enthalpy of solidification and Tm = temperature for melting. If embryo of solid is bigger than the critical radius (r*), then the embryo survives and develop into a nucleus [101]. Figure 2.1 shows the change in Gibb's free energy for homogeneous nucleation.

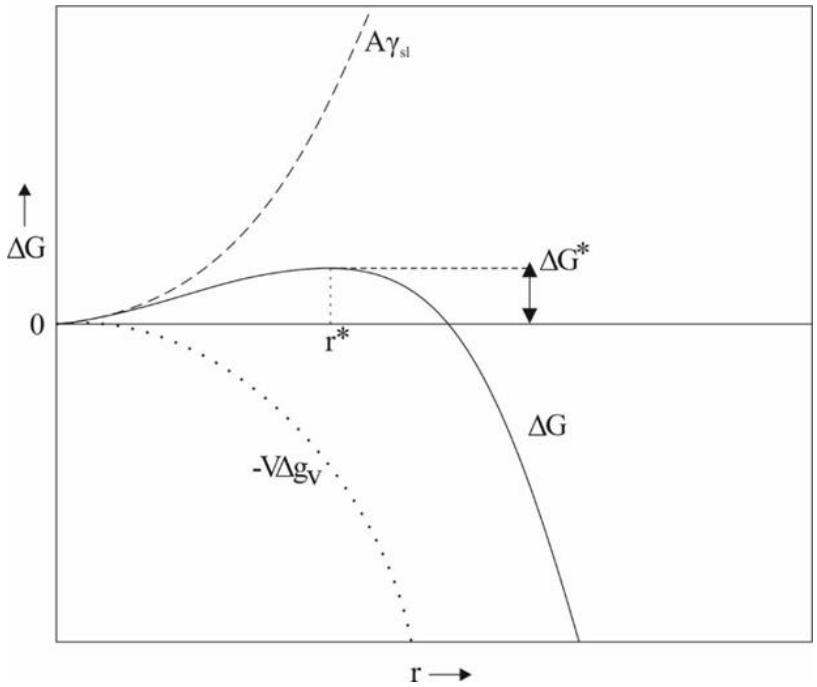

Fig.2.1 Change in Gibb's free energy for homogeneous nucleation [102]

2.1.2 Heterogeneous nucleation

Heterogeneous nucleation occurs due to foreign particles which reduced critical free energy so that stable nuclei may form at lower energy or the nucleation may take place at certain points (Fig.2.2). Heterogeneous nucleation required less energy as compared to the homogeneous nucleation. Hence, heterogeneous nucleation occurred more rapidly than homogeneous nucleation**.** In heterogeneous nucleation the foreign particles worked as nucleus if wet by the liquid, it should make low contact angle and liquid should have some structural affinity with solid [103]. If foreign particle is wetted by both solid and liquid, then force equilibrium can be given as

$$\gamma_{ms} = \gamma_{ml} - \gamma_{sl} Cos\theta \quad (2.4)$$

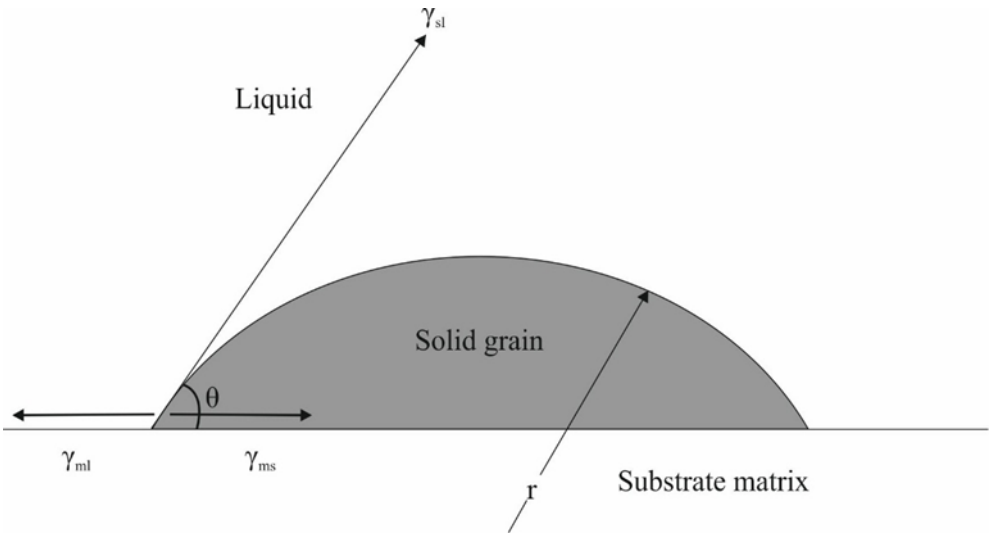

Fig.2.2 Heterogeneous nucleation of spherical cap on a flat mould wall [102]

Now from Eq. (2.4)

$$\cos\theta = \frac{\gamma_{ml}-\gamma_{ms}}{\gamma_{sl}} \tag{2.5}$$

Gibb's free energy for heterogeneous nucleation can be given regarding wetting angle θ and cap radius r as;

$$\Delta G_{hetro} = \left(-\frac{4}{3}\pi r^3 \Delta G_v + 4\pi r^2 \gamma_{sl}\right) G(\theta) \tag{2.6}$$

$$\Delta G_{hetro} = \Delta G_{homo} G(\theta) \tag{2.7}$$

$$G(\theta) = \left(\frac{2-3\cos\theta+\cos^3\theta}{4}\right) \tag{2.8}$$

Now by differentiating Eq. (2.6) it can be shown that

$$r_c = -\frac{2\gamma_{sl}}{\Delta G_v} \tag{2.9}$$

$$\Delta G_c = \left(\frac{16}{3}\frac{\pi\gamma_{sl}^3}{(\Delta G_v)^2}\right) G(\theta) \tag{2.10}$$

So from above equations, it is cleared that critical energy or free energy barrier for heterogeneous nucleation (ΔG_c) is less when compared to the energy barrier of homogeneous nucleation (ΔG_c) by factor G(θ) and is shown in Fig. 2.3.

It can be shown that critical radius r^x is given as,

$$r^x_{het} = -2\gamma_{sl} / \Delta G \tag{2.11}$$

and

$$\Delta f^x_{het} = \Delta f^x_{homo} (2 - 3\,COS\,\theta + COS^3\,\theta)/4 \tag{2.12}$$

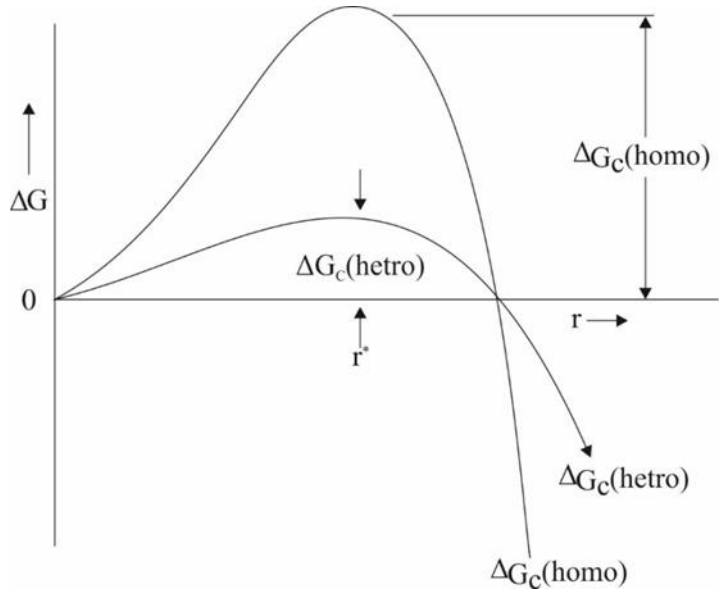

Fig.2.3 Free energy curve for homogeneous and heterogeneous nucleation [102]

As the contact angle changes from 0^o to 180^o, some important conclusions can be made from the following cases:

- At $\theta = 0^o$, $\Delta f^x_{het} = 0$
- At $\theta = 90^o$, $\Delta f^x_{het} = \frac{1}{2}\Delta f^x_{homo}$
- At $\theta = 180^o$, $\Delta f^x_{het} = \Delta f^x_{homo}$

Hence as the contact angle θ decreases, the value of r^x_{het} decreases, which indicates that the volume of the heterogeneous nucleus becomes smaller and hence requires fewer atoms for its formation. So it can be concluded that rate of homogenous nucleation is much faster than the rate of heterogeneous nucleation.

2.1.3 Solidification and growth of alloy

The solidification of pure metal is not so common. Even commercially available pure metal exhibited such amount of impurities which change the characteristics of pure metal to alloy [9]. Therefore, solidification in alloy studied with equilibrium and non-equilibrium solidification. Constitutional super-cooling takes place due to segregation of alloying element ahead of the solid-liquid front as shown in Fig. 2.4.

Constitutional supercooling occurs in alloy while thermal super-cooling operates in both pure metal and alloy. At the time of growth, rejection of solute formed a constitutional super-cooled zone at the solid-liquid interface. The constitutional super-cooling can be given as

$$G_L \geq -m_L C_0 (1-k)/k D_L \qquad (2.13)$$

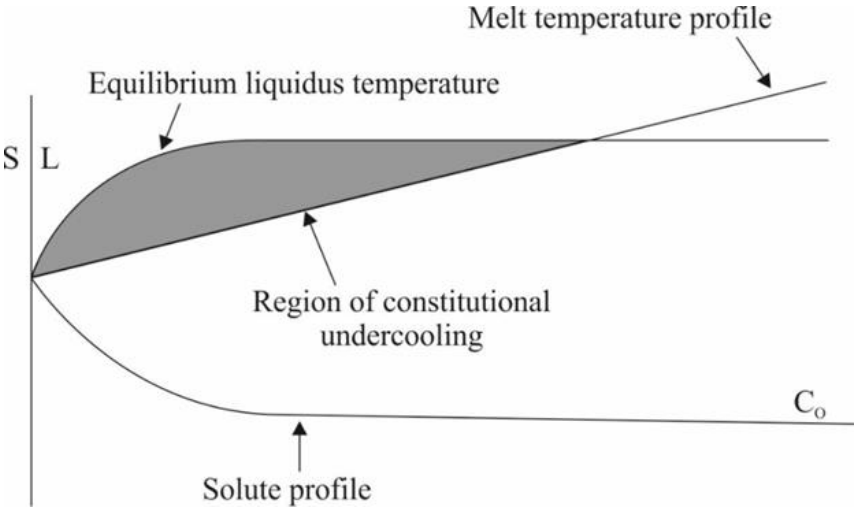

Fig.2.4 Constitutional undercooling on solidification [103]

Where, G_L = temperature gradient (K/m) in liquid ahead of solid–liquid interface. R = growth rate (K/ wt.%) of phase diagram, C_0 = bulk alloy composition (wt.%) in liquid, k = partition coefficient and D_L = diffusion coefficient (m^2/s) of solute in liquid [10].

Growth is the increase in size of the solid nucleus after it has been nucleated (Fig. 2.5). It usually occurs by the thermally activated jump of atoms from the liquid to the solid phase.

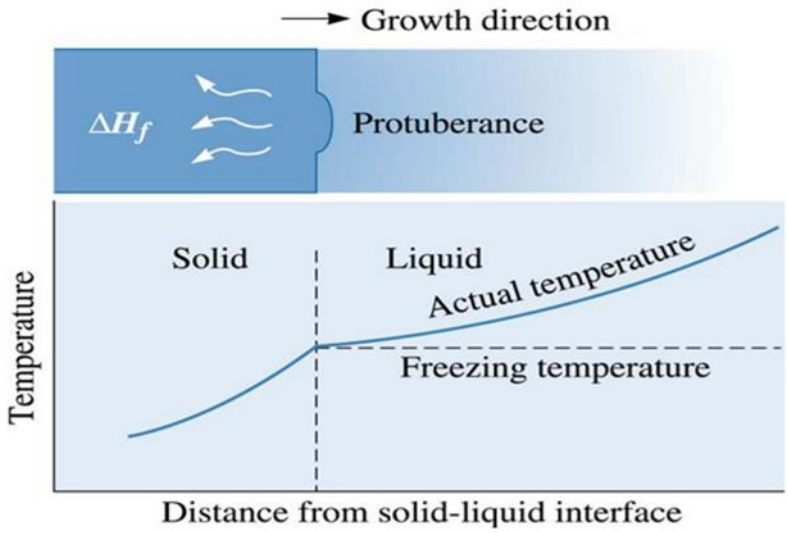

Fig.2.5 Growth of the solid on solidification [104]

When the temperature of liquid is below the freezing temperature, a protuberance on the solid-liquid interface will grow. Campbell [11] identified five feeding mechanisms (i.e. liquid feeding, mass feeding, interdendritic feeding, burst feeding and solid feeding) that take place during alloy solidification. Fig. 2.6 displays a schematic of the five feeding mechanisms during solidification. The mechanisms are described hereunder in the order in which they generally take place.

(i) Liquid feeding is the first feeding mechanism to take place during casting. At the beginning of solidification, the liquid drifts freely before any solid formation or through large channels between solid regions [12].

(ii) As solidification progresses and the alloy temperature cools, nucleation of solid particles take place. Such nuclei, are responsible for the growth of grains in alloys. Each nucleant develops into a grain and therefore the number of nuclei is key in determining the ultimate grain size of the casting. If the more nuclei present in the melt then these produce the finer grain size [13]. Once nuclei exist in the melt, shrinkage (i.e. pressure differential) prompted flow occurs by what is termed as 'mass feeding' [14]. At this stage, crystals are suspended in the flowing melt. Both liquid and mass feeding are effective at feeding the solidification shrinkage since there is no barrier to the liquid movement. Further, the casting's solid structure has very little coherence and therefore no stress accumulation in the casting at this stage. Thus, the casting is not prone to porosity or hot tearing during this stage of solidification.

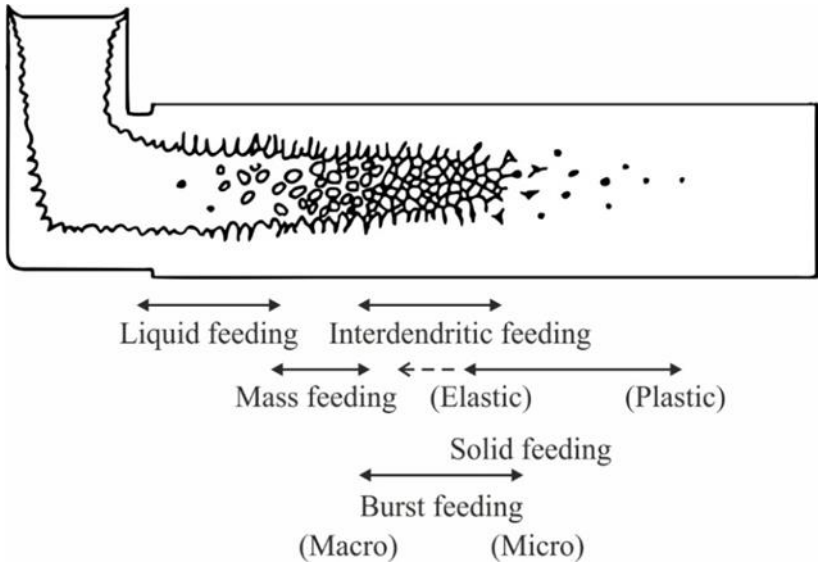

Fig.2.6 Schematic diagram of the five feeding mechanisms during casting [105]

(iii) As solidification progresses, growing dendrite arms begin to impinge on one another and eventually form a solid network. The solid fraction at which this occurs is called the dendrite coherency point and typically ranges between 0.25 and 0.60 [106, 107]. At this stage of solidification, stresses arise in the network as the dendrite arms begin to mechanically interact with one another. Further, the solidifying mass loses the characteristics of a viscous liquid and becomes a semi-solid paste. As a result, the mobility of liquid metal is reduced and the remaining liquid is limited to regions through the dendrite network. Thus, the dendrite coherency point marks the onset of interdendritic feeding,

although some mass feeding can still continue due to small-scale movement of dendrites [108,109].

(iv) With increasing solid fraction the dendrite network becomes more closely packed leading to smaller interdendritic feeding channels. In turn, this makes it increasingly difficult for the remaining liquid to flow and accommodate solidification shrinkage. If a shrinking region in a casting is not fed by interdendritic flow, a hydrostatic tension develops in the liquid and this imposes an increasing stress on the solid network. The increasing stress at this region may exceed the strength of the solid network and cause the network to collapse or "burst". This feeding mechanism is hence termed burst feeding. During burst feeding, the broken or "burst" portions of dendrite arms are suspended in the melt, similar to that which occurs during mass feeding. Burst feeding occurs at select regions within a casting (i.e. where stresses are high enough to collapse the solid network) and takes place simultaneously with interdendritic feeding.

The regions along the casting may also exist whereby either the imposed stress on the solid network is not sufficient to yield the barrier to interdendritic flow, or the strength of the barrier is substantial such that it may not yield. In this case, the stress will continuously increase and any release of stress will correspond to the creation and growth of a pore [110]. Thus, burst feeding is a desirable mechanism that enhances the permeability of the solidifying network and limits the formation of defects. During the final stage of solidification, the dendrite network develops into a rigid solid skeleton and regions of liquid become isolated.

(v) At this stage, the feeding mechanism that takes place was identified as solid feeding. Pools of liquid remain in pockets between dendrite arms due to the high enrichment of solute at these regions [111]. As solidification progresses, it results an increasing number of dendrite arms and dendrites coalesce resulting in more liquid regions becoming isolated [112]. Hence, the permeability of the solid network becomes too low for liquid to flow through and further thermal contraction will cause pores to grow and hot tears to form.

2.2 Casting characteristics of Al-Si and Al-Cu System

Aluminium has numerous remarkable intrinsic properties. Al is a light metal, with a low melting point. It has virtuous thermal and electrical conductivity. It has high electro positivity, even though its oxidation forms an impermeable layer of alumina that keeps protect from further corrosion. Aluminium alloy surface properties can be improve by

various surface treatments. In form of pure substance, aluminium is an extremely malleable and ductile metal. The addition of elements can significantly improve its strength but certainly alter the other properties of the metal. Therefore, a huge array of aluminium alloys has been developed. Use of aluminium castings in automobiles has increased from non-structural demanding, as it is the case of cylinder heads and engine blocks. To structural parts, such as suspension struts due to the beneficial effects that arise by combining light weight and mechanical properties [113-116]. The alloys of the series 2xxx, 6xxx, 7xxx are precipitation hardening alloys which exhibit high strength. The 2xxx and 7xxx alloys have the best mechanical properties which are used in applications where high specific properties are required (aeronautics, aerospace, transport, military applications). The presence of copper in these alloys increases their sensitivity to corrosion. The 6xxx has lower mechanical properties but have excellent forming abilities and good resistance to corrosion. These alloys are used for profiled products. They can also be used as electrical conductors. The other series are hardened by mechanical treatment. The 1xxx alloys have capability to be cold formed. They are widely used for common goods (packaging, cookware, heat exchangers, and thin foils). High purity alloys (99.99 %) are used in electronics and optics. The 3xxx series have the same applications as the 1xxx series but with increased mechanical properties. The 5xxx series have relatively good mechanical properties, a good welding ability and a good resistance to corrosion. The Al-Si alloys (4xxx) are seldom used as wrought alloys, but are intensively used as cast alloys. Now a day, aluminium castings are more demanding in the automotive industry for assemble of several components such as cylinder heads and engine blocks. This credit goes to their favourable combination of low weight, recyclability, easy machinability, and low cost [117].

2.2.1 Al-Si alloys

Developments and optimization of aluminium alloys casting techniques have promoted to advance material properties which enable aluminium castings to assure the new market necessities and have permitted to provide substitute. Silicon is the well-known alloying element of cast Al alloy. In hypoeutectic alloy, the silicon percentage usually varies from 5 to 12 wt.%. Silicon is principally responsible for “superior castability”, i.e., the capability to completely fill dies and to freeze alloy without hot tearing formation. Silicon plays a significant role to improve the wear resistance of the alloy due to its hard phase property. By addition Si with other alloying elements, improve the mechanical properties and make alloy heat treatable.

An alloy which persists more than 7 wt.% of Si forms three-dimensional eutectic Si networks containing interconnected Si platelets inserted in the ductile-Al matrix upon solidification [118]. Silicon content in Al-Si cast alloys effects tensile properties at both room and elevated temperature; while its character becomes more emphasized in the deficiency of alloy elements (e.g. Cu, Mg and Fe) [119]. Two main alloying elements which have been extensively added to Al-Si cast alloys are Mg and Cu, which upturn the strength of the alloy. These alloys are mostly used for a wide series of applications, such as engine cooling fans, structural aerospace components, air compressor pistons, fuel pumps, machine fragments, etc. [120-121]. The strengthening phases like θ($CuAl_2$), β(Mg_2Si) and/or S($CuAl_2Mg$) tend to become unstable above 200 ºC, coarsen rapidly, and at last melt, primary to the production of an alloy which has a damaging microstructure for high temperature applications. Cooper addition was found to improve the tensile strength and creep resistance of Al-Si alloys at higher temperatures (up to ~200 ºC) [122].

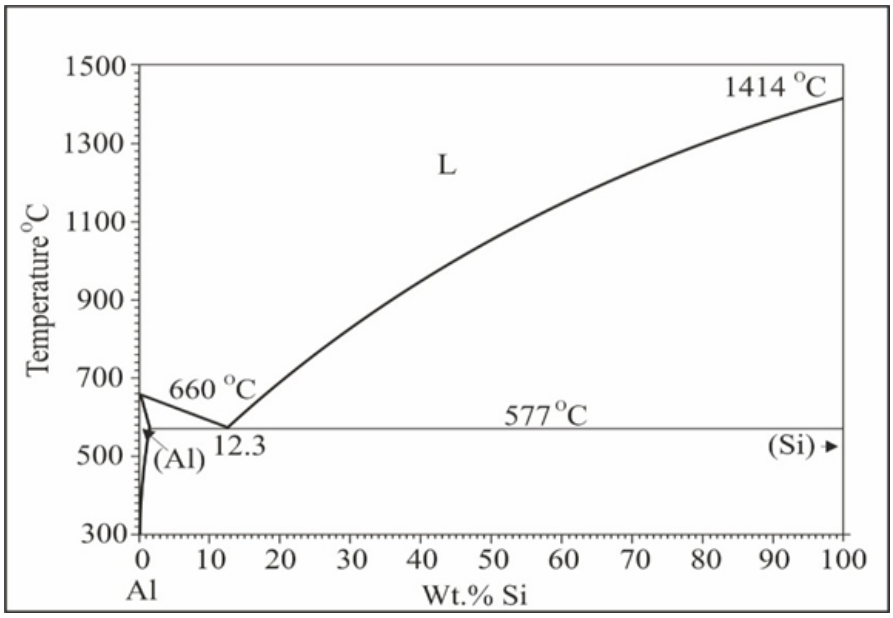

Fig.2.7 Schematic phase diagram of Al-Si [121]

Fig. 2.7 presents a phase diagram of the Al-Si system with a eutectic point. The eutectic point is at 12.3 wt.% Si and the eutectic temperature is 577 °C. Aluminium melts a determined of 1.6 wt.% of Si while the solubility of Al in Si is nearly zero [123].

The microstructure of the Al-Si cast alloys mainly consists of a major phase (α-Al) and eutectic mixture of Al-Si. By increasing the cooling rate we can achieve finer grains with small SDAS, changes the morphology of eutectic Si to small and rounder ones from large

and elongated plates-like. Plate-like morphology of eutectic Si-particles remained unaffected by increasing cooling rate.

2.2.2 Al-Cu alloys

Al-Cu alloy is a high strength-ductility cast alloy. It is widely used to cast large shape and bearing components. Some forging blank can be replaced by Al-Cu alloy may decrease production cost. Therefore, the Al-Cu alloys have been extensively used in various applications like aerospace, automobile, and airplane [124,125]. It is observed that the alloy with 4 wt.% Cu [126,127] exists as a single phase ***α***-solid solution near 550 ºC, and at room temperature as a mixture of ***α*** (with less than 0.5 wt.% Cu) and an inter-metallic compound, $CuAl_2$ (***θ***) with 52 wt.% Cu (Fig. 2.8). **α**-rejects excess Cu as precipitate particles of θ on slow cooling. These coarser particles moderate the strengthening of the alloy.

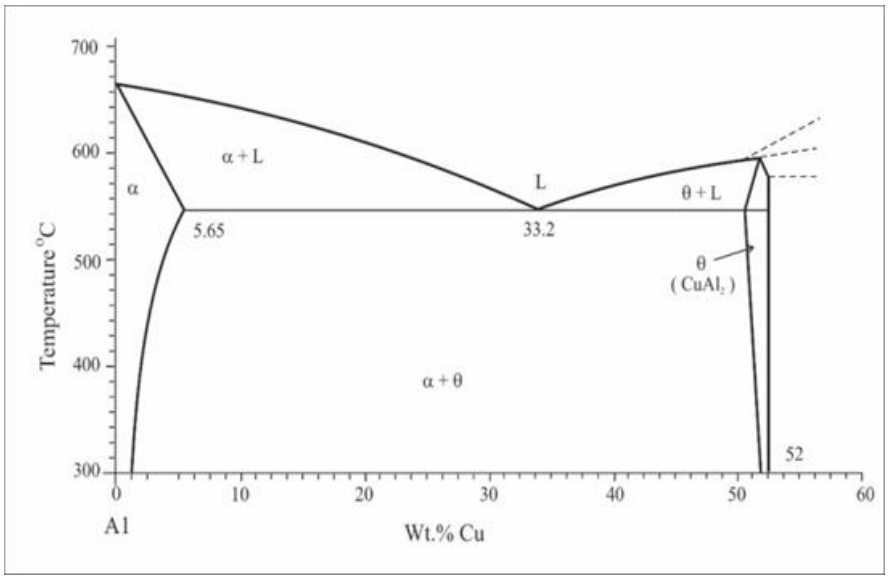

Fig.2.8 Schematic phase diagram of Al-Cu [128]

A supersaturated solution of the alloy can be obtained at room temperature by rapid cooling, at higher temperatures up to 200 ºC, the diffusion of Cu atoms occurs and the precipitate particles are formed. For this particular alloy, Al-4wt.% Cu, five successive structures occurred: (a) supersaturated solid solution ***α***, (b) GP1 zones, (c) GP2 zones (***θ"*** phase), (d) ***θ'*** phase and (e) ***θ*** phase, $CuAl_2$. ***θ'*** and ***θ*** phases produced at higher temperature and GP1 and GP2 zones are occur at lower temperatures.

The extremely small size of particles and their uniform distribution precipitates in the initial stages and the most difficult to analyze. *Guinier-Preston* zones (GP) have a definite composition and structure that is differ as that of the final stable precipitate [129-131].

Evidently these particles nucleate easier than the final precipitate. Eventually they disappear as later more stable phases appear. ***θ"*** and ***θ'*** are meta-stable transition precipitates with distinct crystal structure of their own, while ***θ*** is the equilibrium stable precipitate of $CuAl_2$.

2.2.3 Al-Si-Cu alloys

No ternary compound is formed in Al-Si-Cu system. Here, Aluminium base saturated solid solution remains in equilibrium only with $CuAl_2$ and Si. The ternary eutectic (Al) + ($CuAl_2$) +Si is formed at temperature between 520-525 °C and contains 5 - 6.5 wt.% Si and 26 – 31 wt.% Cu (Fig. 2.9). Table 2.1 shows the solubility of Cu and Si in solid aluminium at various temperature.

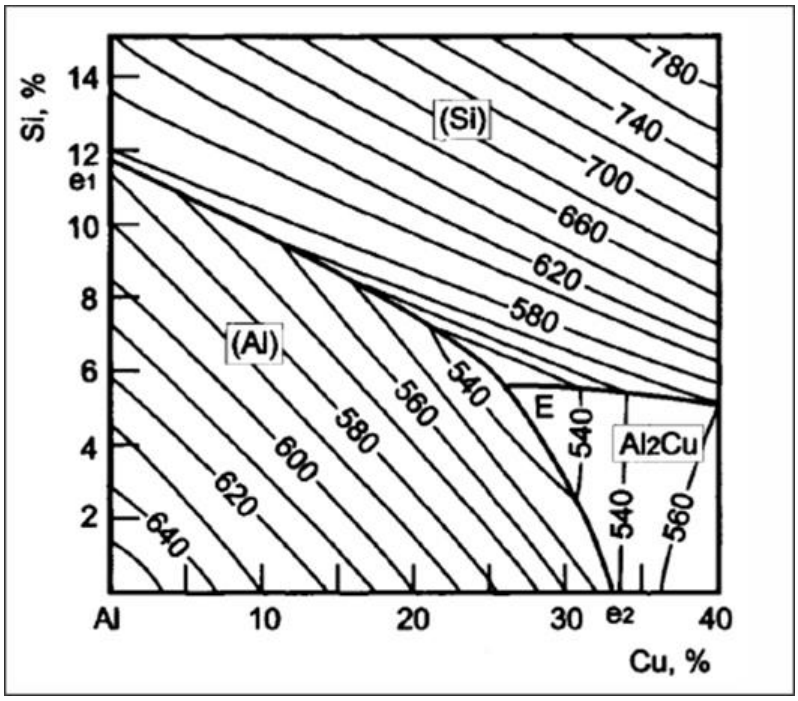

Fig.2.9 Al-Si-Cu phase diagram [132]

Table 2.1 Solubility of Cu and Si in solid Aluminium [100]

T (°C)	500	460	400	300
Cu (%)	4.1	3.6	1.5	0.4
Si (%)	0.85	0.6	0.25	0.1

The solubility of copper and silicon in $CuAl_2$ is negligibly small. The maximum solubility of copper and silicon in solid aluminium is 4.5 wt.% Cu and 1.1 wt.% Si respectively at room temperature. As the temperature decreases, the solubility of Si and Cu also decreases.

2.3 Grain Refinement of Aluminium Alloys

In grain refinement, the grain size of α-Al phase reduced which improve the feed ability, reduce porosity, hot tearing and leads to better mechanical properties of Al-Si alloy than the alloy with coarser grains size. The grain refinement is carried out with the addition of grain refiner in melt which provides more number of heterogeneous nucleating sites and formed the grain of smaller size [133]**.** In the industry, various types of grain refiner available for aluminium alloys, based on Al-Ti, Al-Ti-B, Al-Ti-C master alloys, and Ti or Ti-B containing salt tablets. Al-Ti-B master alloys are available in several forms, most commonly as piglet, waffle plate, nugget and cut rod. Al-Ti alloys are commonly supplied as Al-10 wt.% Ti, Al-Ti-B alloys as Al-5Ti-1B (though in both cases alternative compositions are available [134 -136].

2.3.1 Types of grain refiners

The Al-Ti-B master alloys containing unstable $TiAl_3$ and stable TiB_2 particles have been dominant in Al industry for 30 years or so and formed in a wide range of chemical compositions. However, Al-Ti-B master alloys face some problems like agglomeration of the borides particles, defects during subsequent forming operations and poisoning by certain elements like Zr, V and Cr. The Al-Ti-B master alloy exhibited superior grain refining efficiency in comparison to Al-Ti-C for aluminum alloys with slight Si and Fe content, it is observed that the refining performance of Al-Ti-C was delicate to the content of Si and Fe impurities [137,138]. The selection of grain refiner depends on principal alloying element as follows-

(i) 1xxx series aluminium alloy

For this series of alloy, Al-5Ti-1B and Al-5Ti-1C is used as grain refiner and vanadium is also added in the melt for appropriate result. Addition of vanadium limits the adverse effect of grain refiner [5, 139,140].

(ii) 2xxx series aluminium alloy

The main refiners used for this series are Al-3Ti-1B and Al-5Ti-1B for Al-Cu alloys [141].

(iii) **3xxx series aluminium alloy**

Al-5Ti-1B and Al-3Ti-1B are used as main grain refiner in this series [142]. Al-Ti-C are not suitable for this series, the presence of Mg reduces the effect of Al-Ti-C grain refiner.

(iv) 4xxx series aluminium alloy

In this series Al-5Ti, Al-5Ti-1B, Al-5Ti-1C and Al-4B are used as main grain refiner. Sr is also used as modifier for better grain refining effect [143,144].

(v) 5xxx series aluminium alloy

Due to presence of Mg, Al-Ti-B master alloys are not used for this series. Al-Ti-C grain refiners are used as main grain refiners for this purpose and grain refining efficiency is improved in the presence of Scandium (Sc) [145, 146].

(vi) 6xxx series aluminium alloy

This series is unused series and no grain refiner is developed till now for this series [147].

(vii) 7xxx series aluminium alloy

Al-Ti-C and Al-Ti-B both are used as grain refiner for Al-Zn alloy [148].

(viii) 8xxx series aluminium alloy

The main refiners used are Al-3Ti-1B and Al-5Ti-1B for Al-Sn alloys [149].

(ix) 9xxx series aluminium alloy

The refiners used for this series are dependent on the application of the alloy. Generally modifiers are used in this series [150].

2.3.2 Grain refiner additional level

The adding amount of grain refiners depend on various parameters such as the composition of the alloy, casting practice, product requirements and the types of the grain refiner. Titanium based grain refiner alloys have their limitations and can be added only

when to achieve at least 0.15wt.%Ti in the alloy, otherwise $TiAl_3$ particle formation on solidification will absent and no grain refinement will took place. For Al-Ti-B master alloys the most common system of addition is Al-5Ti-1B which is typically added, matter to the silicon percentage. The certain addition level required in a casting may be vary than this, depending on various parameter such as geometry of the casting, cooling circumstances and degree of refinement required. For example, rapidly cooled castings (thin section gravity) require lower additions level of grain refiners to obtain small grains. Slowly cooled castings (sand or heavy section gravity die) may need more. In some cases, a very fine equiaxed grain structure is required to fully optimize the casting and mechanical properties whereas in others conditions, it is only necessary to limit the formation of larger grains. For these such reasons addition levels can only choose as a guide, and castings produced from parallel alloys using similar dies may require significantly different levels [151,152].

2.3.3 Grain refinement mechanism

Many investigators [153-155] observed the grain refinement effect and purposed that it can be understood in two steps- (a) nucleant paradigm and (b) solute paradigm. Nucleant particle provides the heterogeneous nucleating sites at which primary phase nucleate at low undercooling, whereas solute gives the constitutional undercooling which restrict the grain growth and help in nucleation. So far the available theories can be grouped into two paradigms;

(a) Nucleant paradigm

(b) Solute paradigm

The former provides more nucleating sites while later restrict the growth of these nucleated particles i.e. the complementary role of nucleant and solute particles in refining the grain size.

(a) Nucleant paradigm

Many investigators purposed various theories to explain the mechanism of grain refinement such as phase diagram theory, hyper nucleation theory, peritectic theory and duplex theory. Among them, duplex nucleation theory is more popular and widely accepted. This theory was suggested by Mohanty et al. [104, 106] and further by Tao et al. [145]. Birol et al. [146] added TiB_2 particles in the melt at varying percentages of titanium. According to this theory when Ti was not present in the melt in sufficient amount then TiB_2 occurred at the grainboundary and grain refinement was not observed. However, when Ti

was in hyper-peritecticconcentration, then TiB_2waspresent at the center of Al grains with a surrounding layer of $TiAl_3$ on TiB_2 particles and α-Al layer formed on $TiAl_3$. In case of hypo-eutectic concentrations of Ti, a layer of $TiAl_3$ between TiB_2 and α-Al was also observed. There was no solid evidence for this theory and this theory has much criticism. Schumacher et al. [147] investigated that the presence of $TiAl_3$ at the interface of boride and aluminide due to adsorption effect. However, the reason for the stability of $TiAl_3$ layer was not cleared. So the stability of $TiAl_3$ layer can be explained based on the impurity of Tantalum, which shifts the peritectic concentration due to peritectic reaction with Al and provides stability to $TiAl_3$ [148- 154].

(b) Solute paradigm

The solute paradigm theory was recommended by Arnberg et al. [161] and explained the effect of grain refinement by nucleants and segregating solutes both. According to the solute paradigm, nucleation is quite important, but the influence of the reject solute on the growth of dendrites and the constitutionally undercooled zone in front of the liquid-solid interface are very important. On understanding this theory, it was realized that the nucleation process could not be explained without the influence of segregants, so paradigm was needed to shift. Many researchers [162 - 165] disputed on the mechanism that borides are not good nucleants. In his investigation, borides was found in the center part of the grains at hypo-peritectic additions of Al-3Ti-1B master alloys even no grain refinement was observed. He also calculated a low dis-registry of 4.3 pct. between the α-Al and the TiB_2particles for (111)Al//(001)TiB_2, [110]Al //[110]TiB_2 [166,167]. Low dis-registry suggests that TiB_2 should be a good nucleant, although not as good as $TiAl_3$. So, although TiB_2 does not appear to grain refine without additional titanium being present, it appears that, when solute titanium is present, effective grain refinement can occur. Furthermore, it is proposed that titanium and silicon (solute elements) produce the undercooling needed for TiB_2 to be a good nucleant, while, without the solute element, TiB_2 do not nucleate aluminum. AlB_2 particles were also grain refine aluminum alloy to some extent at concentrations above the Al-B eutectic, *i.e.*, 0.022 pct. B, [18, 169-172] and Robles [130] found a dis-registry of 3.5 pct. between the α-Al and the AlB_2 particles for $(111)_{Al}$//(001)TiB_2, [110]Al//[110]TiB_2 orientation relationship between the AlB_2 particles. Since both TiB_2 and AlB_2 are isomorphous and have similar lattice parameters, this

confirms the nucleating potency of borides. The segregation was calculated by growth restriction factor (GRF) (Fig. 2.10).

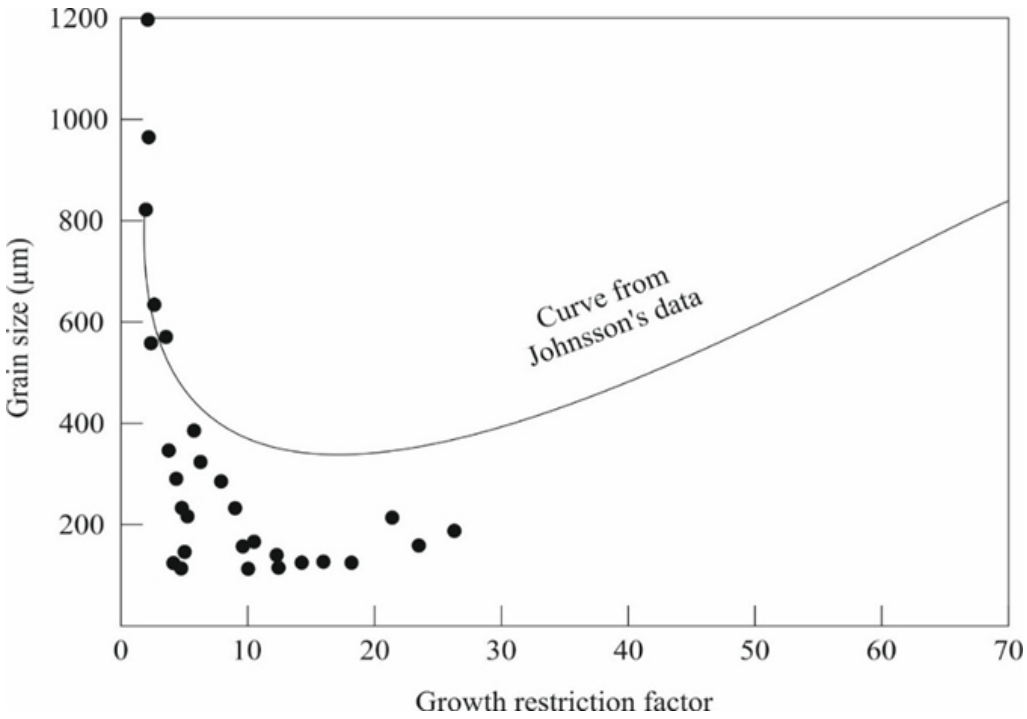

Fig.2.10 Variation of grain size with growth restriction factor [168]

Actuality, solutes control the grain growth due to nucleant effect in grain refinement, but for this no complete and reliable theory was developed. Therefore, it was proposed that the nucleant particles and the segregation of solute elements (e.g. Ti, Si) exhibited a significant role in grain refinement. The GRF determined the segregation ability of solute in the melt and can be given as;

$$GRF = mc_o (k_o-1) \quad (2.14)$$

Where, m = gradient of the liquidus, c_o = solute concentration in the alloy and k_o= partition coefficient of solute at the solid-liquid interface.

2.3.4 Effect of grain refinement on mechanical properties

Recently, many researchers have investigated the effect of master alloy on average grain size and tensile strength of Al alloys. Farahani et al. [127] studied the effect of addition Al-5Ti-1B master alloy on 7042 aluminum alloy. The ideal amounts of added Ti in the alloy was found to be 0.03 wt.%. They noticed considerable enhancement in tensile properties by addition of master alloy. Fig. 2.11a to Fig. 2.11c show the consequence of several amounts added Ti, by using Al–5Ti–1B master alloy, on the microstructure and grain size of the alloy samples. It is found that the heterogeneous nucleation in the occasion of Al–5Ti–1B master alloys is a two-step process. When Al–5Ti–1B grain refiner is added to the alloys, two types of intermetallic elements ($TiAl_3$ and TiB_2) are formed and distributed in the melt and perform active locations during solidification. Fig. 2.11a reveals coarser grains with dendrites structure.

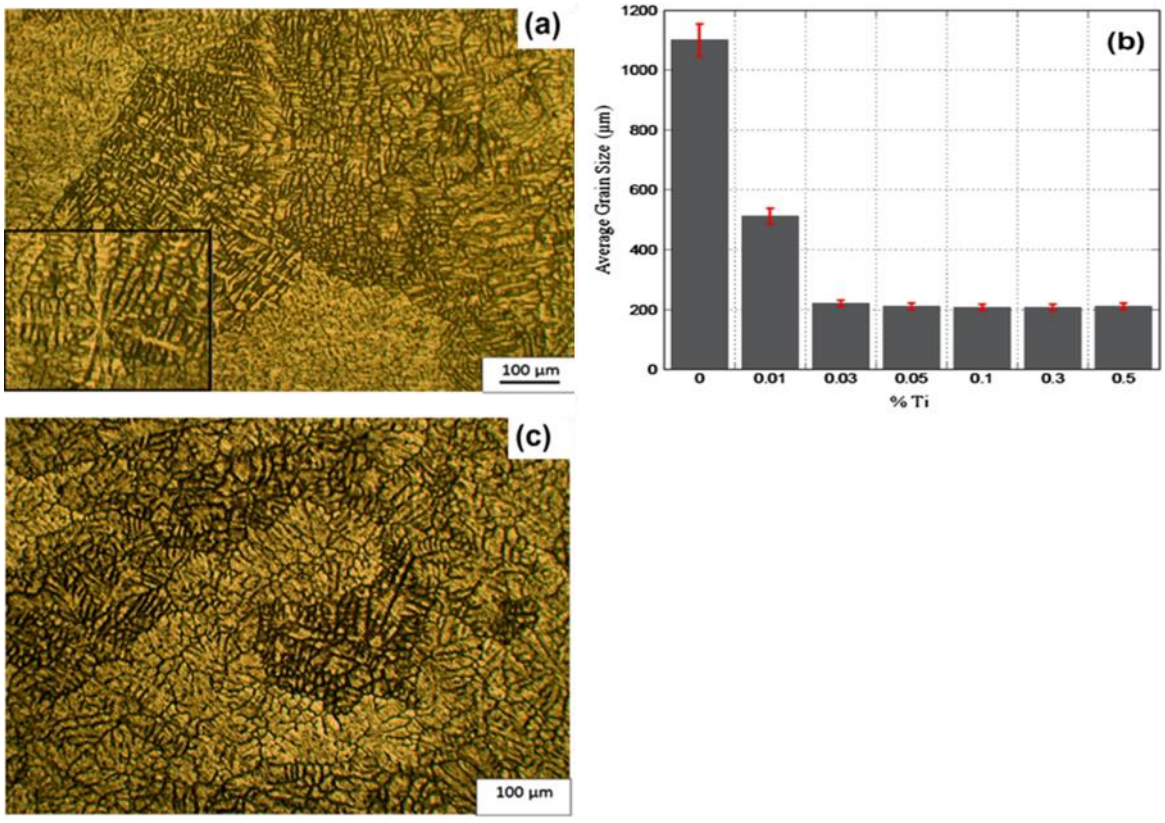

Fig.2.11 The optical micrographs of: (a) Un-refined alloy, (b) Grain size variations with Ti contents and (c) Ti-refined alloy [127].

Effects of master alloys on mechanical properties of the alloy are summarized in Table 2.2. The addition of master alloy in the alloy in optimum amount significantly improves the tensile strength and elongation to fracture. The finer grains are resulting in improvement in both properties (Fig. 2.11b), primary to a finer distribution of second phases.

Table 2.2 Hardness, UTS and El.% results of the un-refined and refined alloy [127]

Alloys	Hardness	UTS (MPa)	EI. %	QI (MPa)
Un-refined	84 ± 0.91	310 ± 13.2	14.8 ± 2.7	759
Ti-refined	110 ± 0.70	335 ± 5.6	14.5 ± 1.0	799

Furthermore, E. Torre et al. [124] studied the effect of grain refiner effect on the microstructure and mechanical properties of the A356 automotive wheels. The obtained results from mechanical testing provide evidence that additions of 0.13 and 0.27 wt.% of Al-5Ti-1B have an improvement on the mechanical performance of the automotive wheels. This can be compared with the use of a grain refiner's higher concentrations, leading to a significant reduction in the cost-benefit ratio for the manufacturing of A356 automotive wheels. Z. Chen et al. [135] investigated the grain refining responses of Al–Zn, Al–Cu, Al–Mg and Al–Si binary systems to inoculation of Al–B master alloy. They observed a significant grain refinement and improvement in tensile properties due to the addition of Al–3B master alloy for Al-7Si-Mg alloy. G. Liu, et al. [2] investigated comparatively the effects of individual or combined additions of grain refiners and modifiers on the mechanical properties, microstructures, grain refining and modification, and intermetallic compounds of Al-7.5Si-4Cu alloy. The results show that the addition of 0.8 wt.% Al−5Ti−1B master alloy obtain superior tensile strength, brinell hardness and finer equiaxed α-(Al) dendrites. AB Pattnaik et al. [92] also reported that addition of the Al–5Ti–1B grain refiner in Al5052 aluminium alloy has significant effect on the microstructure, mechanical properties and acoustic emission characteristics.

2.3.5 Mechanical working of Al−Ti−B master alloy

K. Venkateswarlu et al. [53,54] studied the grain refining performance of pure aluminium with addition as cast, rolled and heat-treated Al-5Ti-1B master alloys. The results indicate that the annealed and hot rolled master alloy have improved grain refining efficiency as compare to as cast master alloy. The enhancement in grain refining efficiency was due to the fracture and increase volume fraction of $TiAl_3$ particles through rolling and annealing, respectively. The SEM analysis clearly show (Fig. 2.12) the evidence of fracture of these nucleating particles.

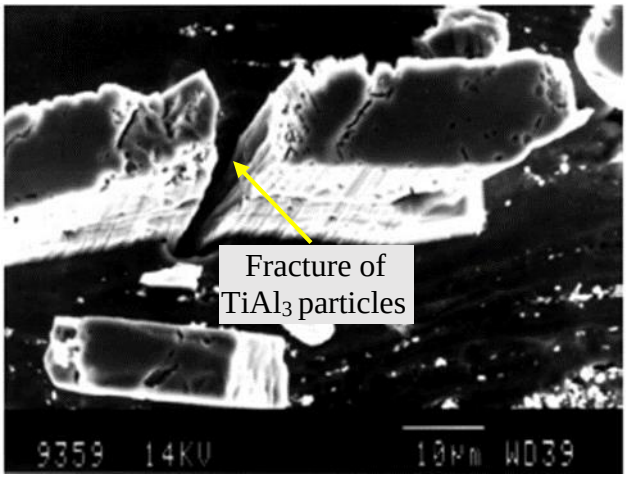

Fig.2.12 SEM micrographs of Al-5Ti-1B master alloy rolled at a reduction level of 40%, displaying the fracture of $TiAl_3$ particles [53].

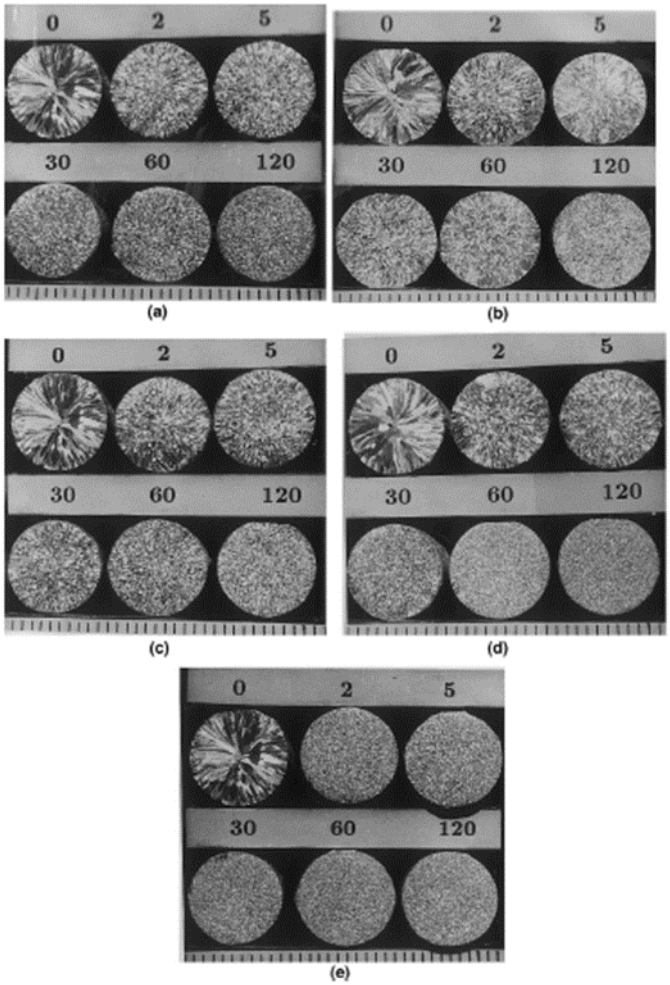

Fig.2.13 Macrostructures of Al grain refined by Al–5Ti–1B master alloys (a) as cast; (b) 20; (c) 40; (d) 60; (e) 80% reduction [53].

The results also suggested that at lower rolling temperature the fracture is more in $TiAl_3$ particles. His results showed that grain refining efficiency can be enhancing by ball milling techniques. Fig. 2.13 (a-e) show the macrostructure analysis of pure Al with addition of as cast and hot rolled grain refiner at different holding time 0, 2, 5,30, 60 and 120 minutes, respectively. From the macrostructure analysis (Fig. 2.13a), it is observed that Al exhibited coarser structure but some refinement occurs with holding time. Equiaxed structure is obtained with addition of hot rolled master alloy at 80% reduction level. H. Ghadimi et al. [52] established that annealing increases the grain refining performance but he showed that annealing at higher temperature produce adverse effect on grain refining performance of master alloy.

2.4 Hot Tearing

Hot tearing is also known as hot cracking, hot shortness, super solidus cracking, and shrinkage brittleness. This is a common and severe defect that takes place during the last stage of solidification of liquid metals. Schematic diagram of the hot tears formation at the 90º junction of I-bar is shown in Fig. 2.14. To better understand the mechanism of hot tearing various modeling methods have been developed since last 30 years. M. Rappaz [80] has always pioneered idea in the field of solidification. Rappaz et al. [82] investigated the hot tearing mechanism in the mushy zone and his results led Flemings to be more and more interested in semi solid processing of metallic alloy (e.g. production of car components by thixocasting). For many years, the main criterion applied to characterize the hot cracking sensitivity (HCS) of an alloy was based on the solidification interval [28, 85,86]: the HCS increases with the width of the mushy zone. Feurer [157] tried to derive a criterion based on the pressure drop of the interdendritic liquid but only driven by solidification shrinkage. Clyne and Davies [158] and much earlier Pellini [159] derived a HCS criterion based on a critical time spent by the mushy zone in the last stage of the solidification.

Shimin Li [17] pursued the following methodology and strategies as given as

(a) Developed a reliable experimental methodology/apparatus to quantitatively characterize hot tearing tendency of aluminum alloys.

(b) Investigated the effects of process variables on hot tearing such as effect of mould and pouring temperature on A356 and 206 alloy.

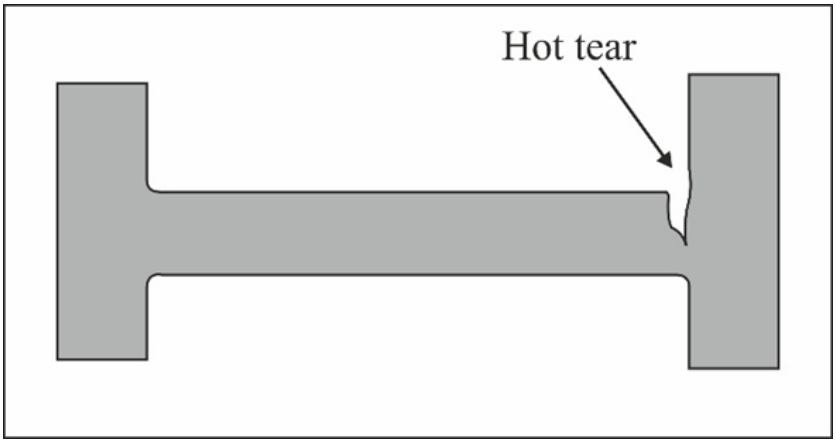

Fig.2.14 Hot tears formation at the 90º junction of I-bar.

(c) Simulation of Hot Tearing

- Computer simulation on filling and solidification processes;
- Simulation on strain and hot tearing.

Constrained rod mould with load cell/LVDT was developed and used to characterize and quantify the contraction behavior of cast aluminum alloys during solidification (Fig. 2.15). The mould temperature is controlled precisely with using heater plates. Different castings dimensions can be obtained by replacing the inserts. The test piece has two arms. One test arm is constrained at one end with threads to keep the bar from contraction; this causes tension to be developed and hence cracking is induced during solidification. The other arm is for temperature and load/displacement measurement with one end connected to a load

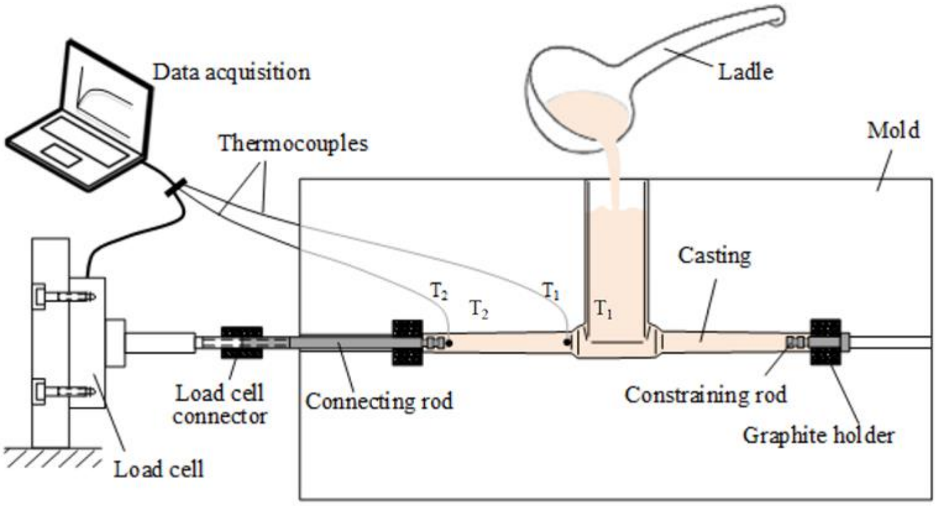

Fig.2.15 Diagram of Experiment Set-up [17].

cell or Linear Variable Differential Transformer (LVDT). The casting rod was designed with a slight taper to reduce friction between the mold and casting. The results show that mould temperature has a significant effect on hot tearing tendency. Elevated mould temperature (low cooling rate) reduced hot tearing tendency in alloy significantly by promoting uniform casting contraction and therefore alleviating stress concentration

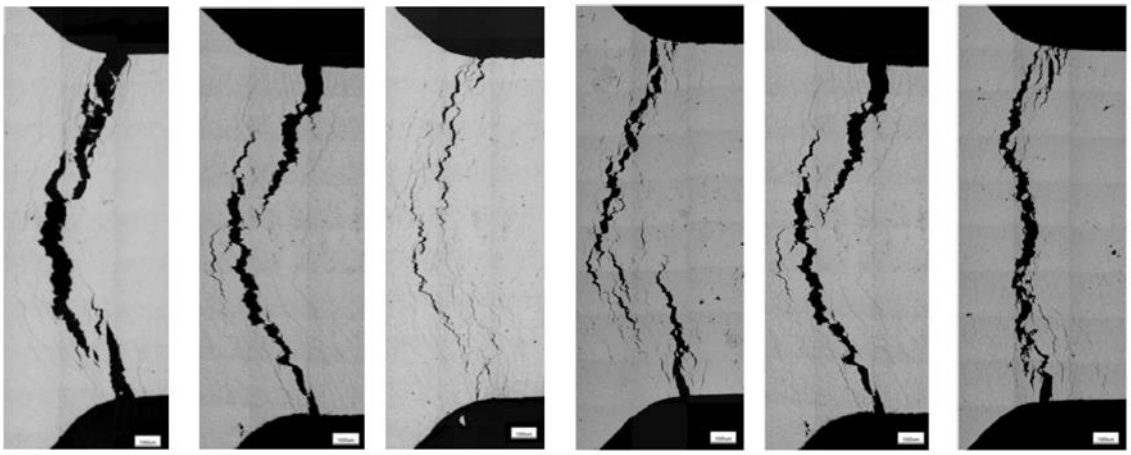

Fig.2.16 Effect of process parameters on hot tearing in 206 alloy (a) mould temperature 200, 300 and 370 ˚C; and (b) pouring temperaturer 700, 750 and 800 ˚C [91].

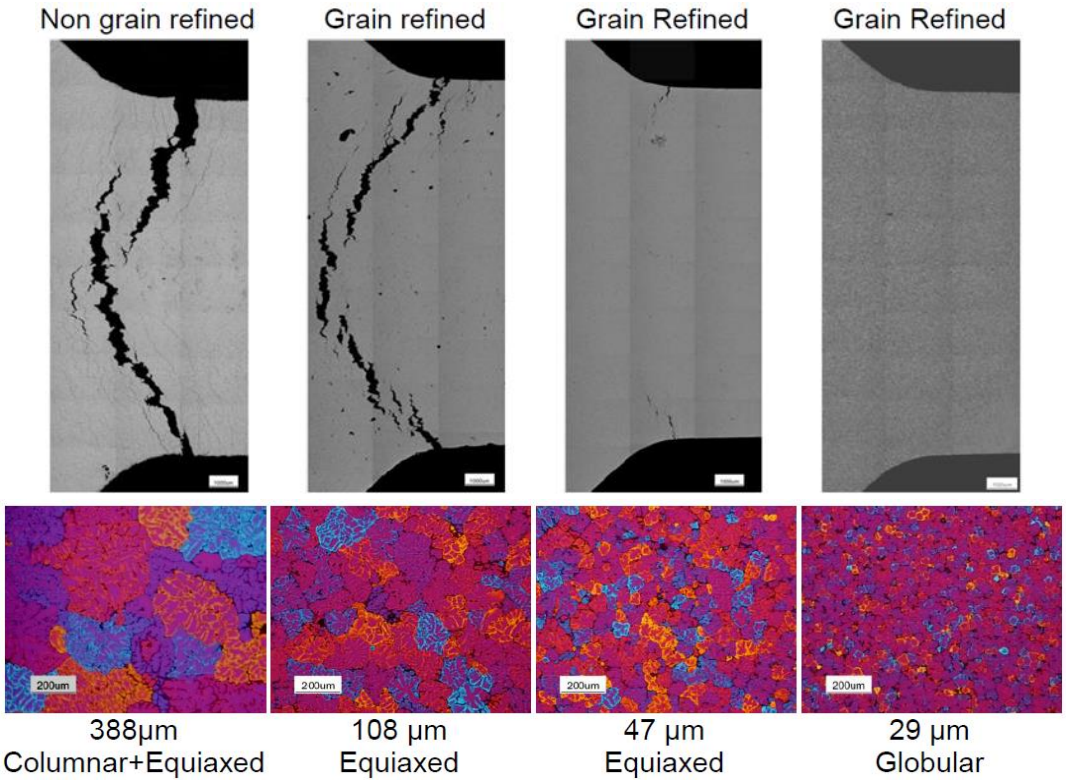

Fig.2.17 Effect of Grain Refinement in B206 alloy [91].

(Figure 2.16 (a). Hot tearing was not significantly affected by varying pouring temperature in 206 in this test within the temperature range between 700-800 ˚C (Fig. 2.16 (b). Grain size and grain morphology are important to reduce hot tearing susceptibility in alloy 206. It was found that a fine globular structure is necessary to prevent the formation of hot tearing during solidification of alloy 206 (Fig. 2.17).

Hot tearing generally occurs as macroscopic and microscopic crack in the casting due to strains developed in a solidified region. When liquid-to-solid phase change occurs, this change advances the strains because of the volumetric shrinkage. The macrostructure analysis of hot tearing is demonstrated in Fig. 2.18 [160]. During solidification, the critical temperature is the temperature at which hot tearing occurs and many metallurgical and mechanical factors are also determined. If the critical temperature lies between the solidification interval Tc, and the solidus temperature, Ts than chances of developing hot tearing tendency are increased. Metallurgical factors include freezing range, eutectic percentage, and second phases that establish the strength and ductility of the alloy at semisolid stage. Casting geometry, mould material, and casting parameters are the variables which results in contraction stresses and hot spots.

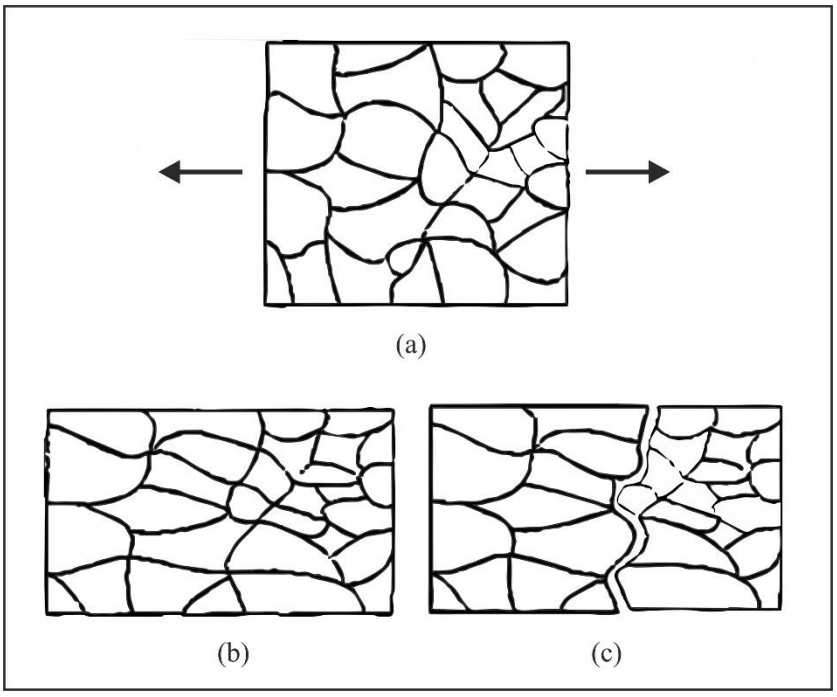

Fig.2.18 Representation of macro-structure of hot tearing, (a) developed stress, (b) flow of metal (no tears), and (c) flaw of metal (with tears) [160].

Various test methods have been adopted in aluminium alloys to measure the hot tearing susceptibility. Casting methods demonstrate better results in comparison to other test methods [3,11,24, 93-96]. However, casting methods are not widely accepted due to their certain limitations such as variation in grain refinement sensitivity and to changes in alloy composition. Many investigators used computable methods to evaluate hot cracking propensity in binary alloys. Mechanical and physical methods [97,98] successfully used by many researchers to measure and evaluate hot tearing vulnerability.

For different casting conditions different mathematical models have been developed to predict hot tearing. Many theories have been purposed by researchers to describe the mechanism of hot tearing, but disagreements still be present [94, 99-103]. In this point of view further investigation is necessary to understand the mechanism of hot tearing, and the parameters are responsible for hot tearing. This section includes a sequential review of hot tearing mechanism and experimental procedures.

There are various theories have been purposed of hot tearing in the recent years which is categorized as (a) Shrinkage-brittleness theory, (b) Stress and strain theories and (c) Generalized theories.

2.4.1 Shrinkage-brittleness theory

The shrinkage-brittleness theory [100–105] results from numerous studies of hot tearing susceptibility of aluminum alloys. A theory accounting for the hot tearing observed in specify aluminum alloy systems (Al-Si) was first advanced by Vero [167]. During the liquid-solid stage, the primary crystals growing at the expense of the decreasing volume of liquid come into contact (coherency temperature) and form a coherent network.

The theory postulated that hot tearing was occurred due to contraction strains of the primary dendrites during subsequent cooling between the liquidus and solidus. Figure 2.19 summarizes Vero's results according to the Al-Si phase diagram. However, Vero [167] stipulated that the healing process was prevented by the narrowness of the interdendritic channels when the remaining liquid was less than the critical proportion. In addition, he assumed that the formation of a crack could occur only during contraction of the dendrites and that no tearing was possible when the amount of liquid freezing at eutectic temperature was greater than the critical value. The experimental results indicated in Al-Si alloys that hot tearing increased from zero at low silicon content to a maximum at approximately 1.6 wt.% silicon and then decreased abruptly to zero at 1.88 wt.% silicon. Alloys with higher silicon content were not prone to hot tearing. The critical amount of liquid (necessary to

heal cracks) was calculated between 12 and 13 percent for the Al-Si binary system using the effective solid solubility at the eutectic temperature of approximately 0.4 percent.

However, it was indicated [51,52,157] that the sudden decrease in hot tearing cannot be explain by Vero's theory as it stands. In fact, based on a simple binary system, the modified theory, which included, in a modified form, the concept of freezing range [107,108] and the volume proportion of eutectic (eutectic index [109]), specify that the severity of tearing

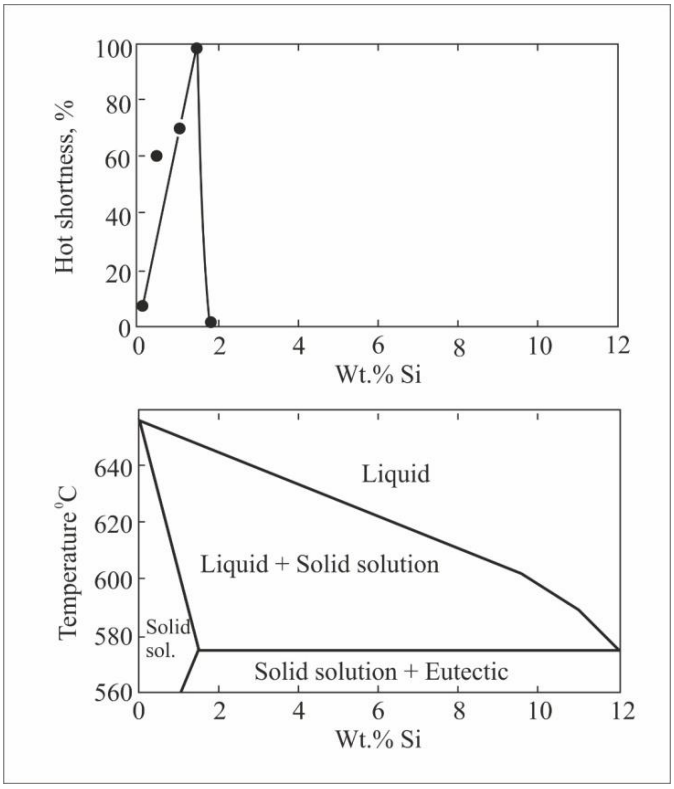

Fig.2.19 Relationship between hot tearing and alloy constitution for the Al-Si binary system [107].

will depend on the amount of contraction while the hottest zone of the casting passes through the critical hot tearing range. It appeared that tearing was possible even though the residual liquid solidifies at constant temperature. Consequently, the hot tearing of castings was accounted for theoretically by a single factor, the extent of the hot tearing temperature range. The tears are unlikely to be formed when the alloy has passed below the solidus line. Hot tearing is only likely to occur in the "brittle range" or the so-called “in effective interval of solidification” which is the range of temperature between the coherency temperature and the solidus (Fig. 2.20).

Hot tearing in last stage of solidification is prevented during the "brittle range" by "accommodation”[108]. The latter designates the degree to which an alloy is able to withstand shrinkage strains by movement of the grains within the semi-solid mass. It has

been stated [109] that the hot tearing propensity is proportional to the degree of the "brittle range". Other factors affecting the occurrence of hot tearing were given by Lees [171,172]. These factors included the effect of mould variables (moulding materials, cores in hindering contraction), constitution of the alloy (especially the proportion of eutectic), grain size, and gas content.

The basic relationship between these factors is related to the extent of mechanical restraint, the promotion of grain boundary film, coherent temperature modification, and their impact on the mobility of the grains and the liquid feeding behaviour. Vero [167] proposed an early theory called the "Brittleness Theory" in 1936. This theory suggests that hot tearing was formed due to the contraction of the primary dendrites. In the semi-solid stage, the primary

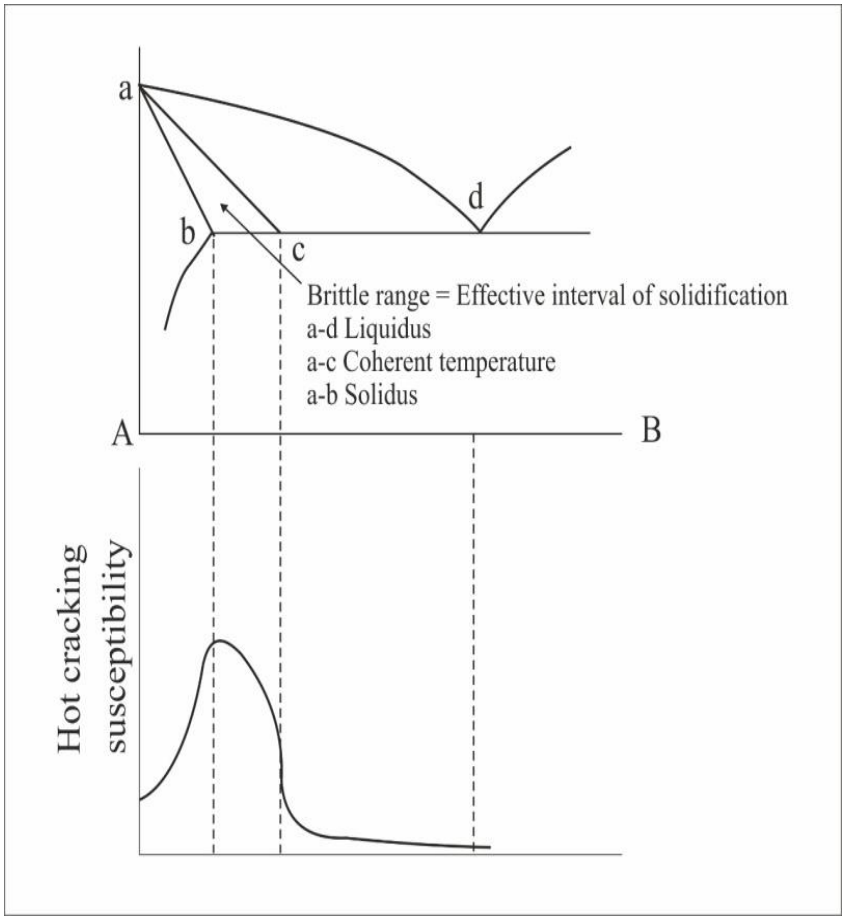

Fig.2.20 Hot tearing susceptibility of eutectiferous alloy (Shrinkage-Brittleness theory) [111].

dendrites grow and formed a coherent network. This contraction would build up stresses in the mushy zone. If these build stresses are very high or the lasting eutectic melt is not sufficient to heal the opening, cracks will continue. Later on, Pumphrey [173] gave some useful ideas to improve the excellence of brittleness theory. Hot tearing propensity depends

on the various factors such as duration level of brittle range, shrinkage stresses during solidification or some other external factors also contribute. Simply, if any factor stimuluses the time of the brittle range it affects hot tearing tendency. To good resistance to hot tearing the alloys should consists a narrow brittle temperature range. This has been shown in the study of as cast and grain refined Al-Si, Al-Si-Cu and Al-Mg-Si alloys [48-50]. If the strength of the material not able to resist the tensile stresses which is developed in the mushy zone hot tearing may occur. If there is sufficient remaining liquid is present in the last stage of solidification, the most tears may have healed. A theoretical and practical curve is derived between the brutality of hot tearing and the brittle-shrinkage range is shown in Fig. 2.21 [111].

It is seen that hot tearing sensitivity become stable after reaching to the maximum brittle range [112]. Furthermore, M. Vedani et al. [129] corrected the earlier theory. He introduced a liquid film perception in their novel theory. It was proposed that a thin liquid film is formed above the solidus temperature between the solidified dendrites. This liquid film region consists more stresses and propagate hot tearing in the casting. But this theory could not give complete details about the aspect that hot tearing developed at temperatures lower the solidus [180-182].

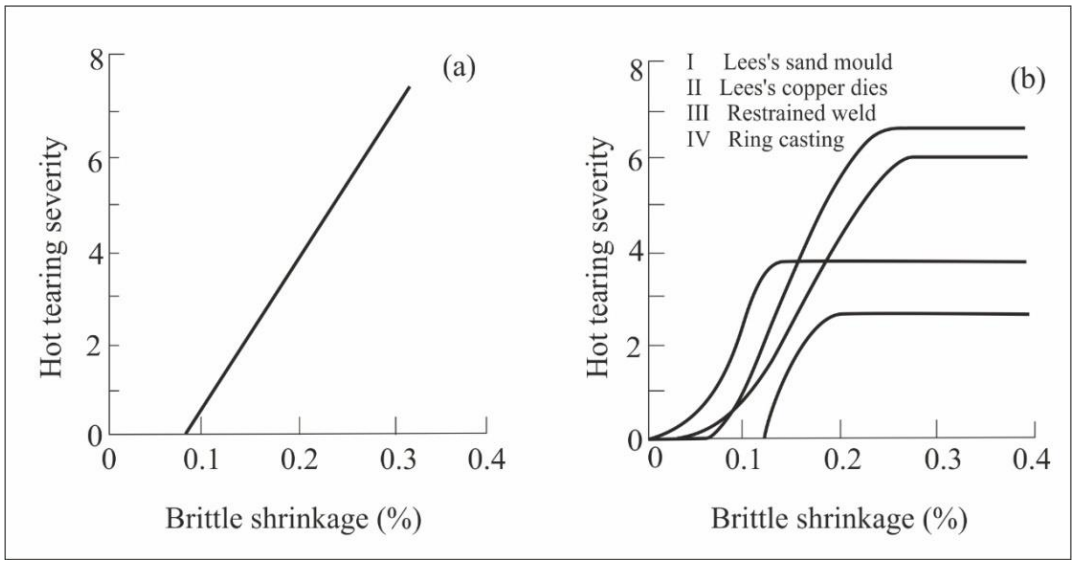

Fig.2.21 Brittle-shrinkage range and hot tearing sensitivity relationship: (a) in theoretical state, (b) in practical test state [111].

2.4.2 Stress and strain theories

Hot tearing generates in the casting due to the formation of stress built up in the metal. This stress builds up due to the volume shrinkage, p⁄related to phase change (usually

β = 6%), but the stress can be multiple by thermal contraction and/or by the constraints of the mould. The earliest study of the process of development of hot tears was assumed by F. Korber in 1928 [183]. On the basis of the experimental results, it was understood that hot tears were generated after the complete solidification of the metal [184-186]. In restrained casting, the induced stresses might be exceeding the tensile strength of the solid and hot tearing propagate.

Pellini proposed [159], *Strain Theory* with the assumption that the hot tearing occurs above the solidus temperature and most scientists accepted this theory by today. Pellini [159] "Strain Theory" was developed on the basis of liquid films concept and believe that liquid films formed above the solidus temperature at grain boundaries. Tearing is known as a strain controlled phenomenon, which generally occurs when the accumulate strain reaches to a critical value. The strain distributions resulting of the hot zone at numerous periods of solidification is presented in Fig. 2.22 [118].

The new theory to explain the mechanisms of hot tearing is undoubtly that attributed to Pellini [159] and his co-workers [160]. They published a new idea about the strain theory based on the film stage concept. This theory suggests that hot tearing is caused by the localized strains, generated by thermal gradients that tend to pull apart solid masses of material separated by essentially continuous films of liquid. This liquid film results from the segregated residual melt. Because of its fundamental nature, the strength and ductility of a mass of solid grains separated by liquid films is of an extremely low order. The strain theory provides a generalized explanation of the mechanism of hot tearing in terms of the strain rate imposed on the liquid film regions. The strain rate and time duration decide the strain in crack region and it shown in Fig. 2.23. It can be predicting that extent the strain rate of the liquid film regions may vary widely due to various factors that propagate hot tearing. These factors include; (a) large regions undergoing contraction, (b) fast cooling of regions undergoing contraction, and (c) small regions undergoing extension.

In slight contrast to the previous theory (Shrinkage-Brittleness), it has been suggested that hot tearing cannot take place during the mushy-stage of solidification since the shrinkage strains are uniformly distributed. In fact, the interdendritic liquid zones are relatively large

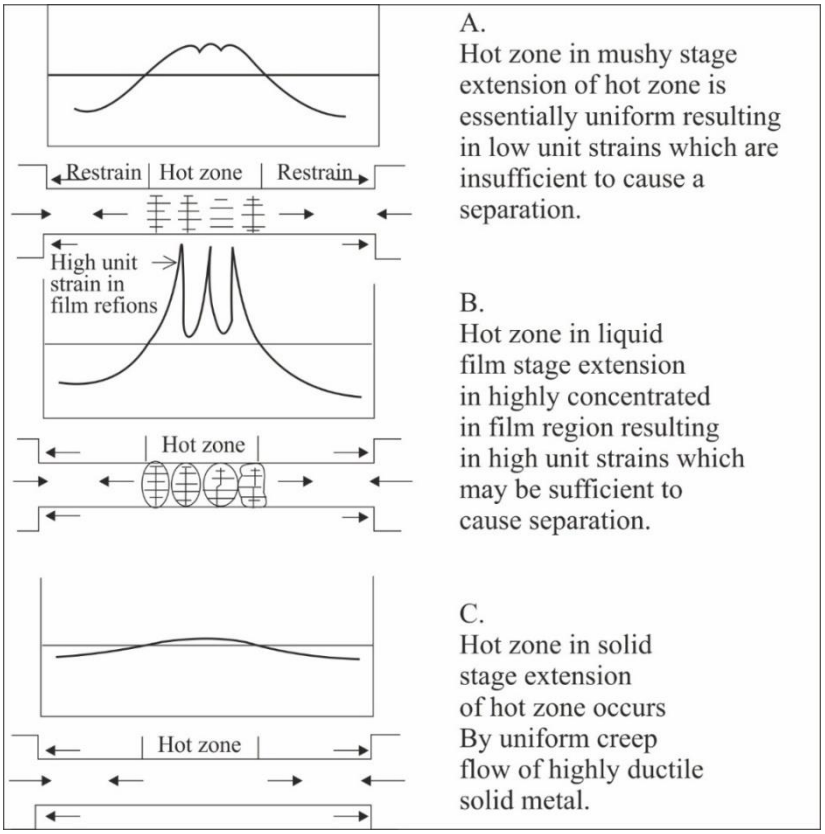

Fig.2.22 Strain distribution character at various stages of solidification [160].

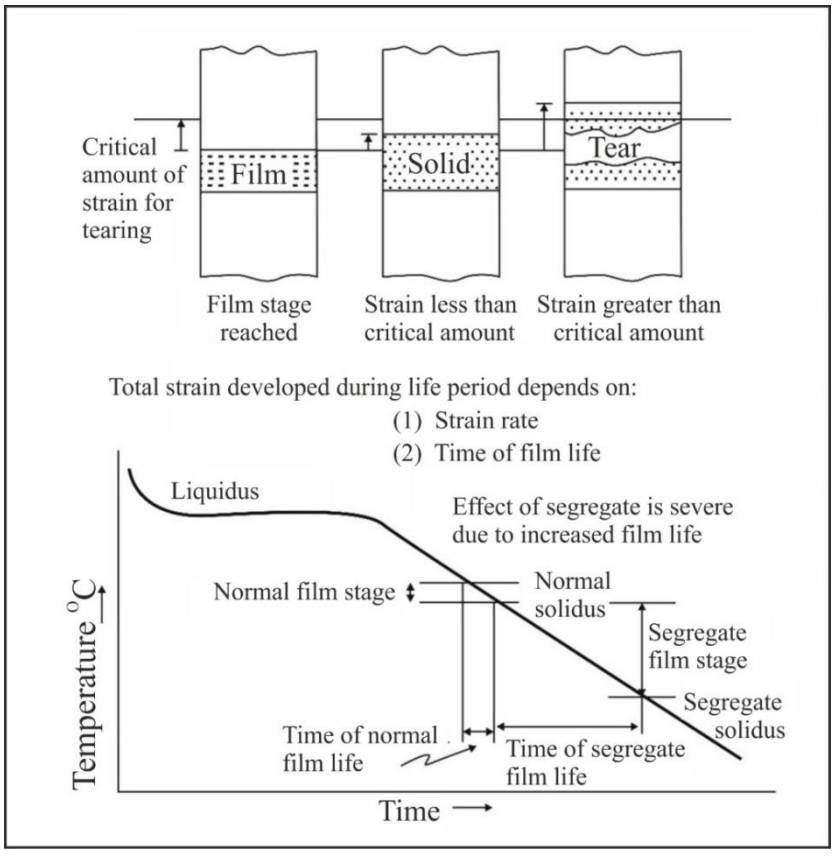

Fig.2.23 Diagram of the result of stain rate and time of film life on hot tearing [160].

and general feeding of the mushy mass could result. Hot tearing occurs only when the film stage is reached and the strain within the hot spot is concentrated into narrow liquid films of low strength. Low melting point segregates which exist, in the molten state, below the equilibrium solidus of the material are the most detrimental in this respect.

2.4.3 Generalized theory

Various attempts to explain hot tearing formation lead to various theories that are supported by experimental evidence. Among them it is one of the generalized theory by A. Bochvar [166] (supported by others [185-189]. It is intended to explain the mechanisms of hot tearing as a combination of the *"*Shrinkage-Brittleness *Theory"* (brittle temperature range), and the *"Strain Theory"* (liquid film stage). The main objective was to modify and extend both theories and explain how the liquid quantity and distribution during solidification affects the hot tearing tendency.

The theory on the liquid film stage is limited to the temperature range around the solidus. On the other hand, the shrinkage-brittleness theory commences at the so-called coherency temperature. The coherency temperature is defined [190,191] as the temperature at which the fraction of solid (f_s) at which the growing equiaxed dendrites begin to interact mechanically and grow to form a coherent network. If contraction region of casting is wide and fast cooling rate, which result in to a more strain rate, it may have more hot tearing propensity. Pellini [163] experienced the result of giant sulphur content on developing hot cracking in steel castings. It was established that more sulphur contents enhance hot cracking tendency of the alloy because due to the presence of an extended liquid film stage, it provides a further opening for strain (Fig. 2.24) [192]. Since the last theory postulated that the solidus temperature is below the hot tearing temperature of an alloy, the temperature period has become a key and is significant for hot tearing [193]. This period has been called "Critical Solidification Range (CSR)" [194]. This temperature range is close to the solidus (Fig. 2.25) [195].

Newly, Oya et al. [186] studied of hot tearing temperature in an Al-7Si alloy with the Acoustic Emission (AE) technique. From his research it is observed that the acoustic emission signals of hot cracking had elevated peak voltage values and were all the time found in the later stage of solidification. In engineering practice, generally used materials for castings are non-metals. Equilibrium conditions comprise higher solidus temperature. Hot tearing in a critical temperature range may not persist high strength and ductility.

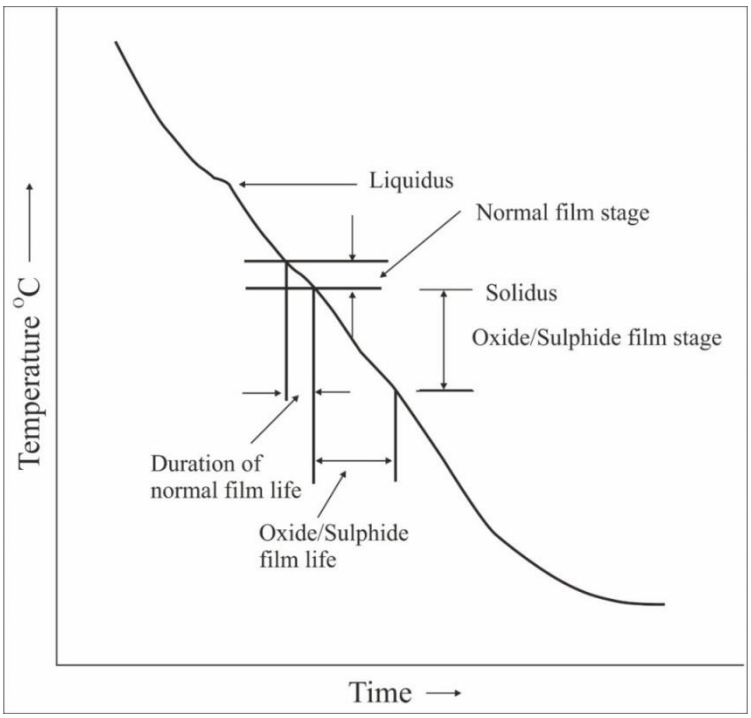

Fig.2.24 The effect of high sulphur wt.% in the alloys on hot tearing [186].

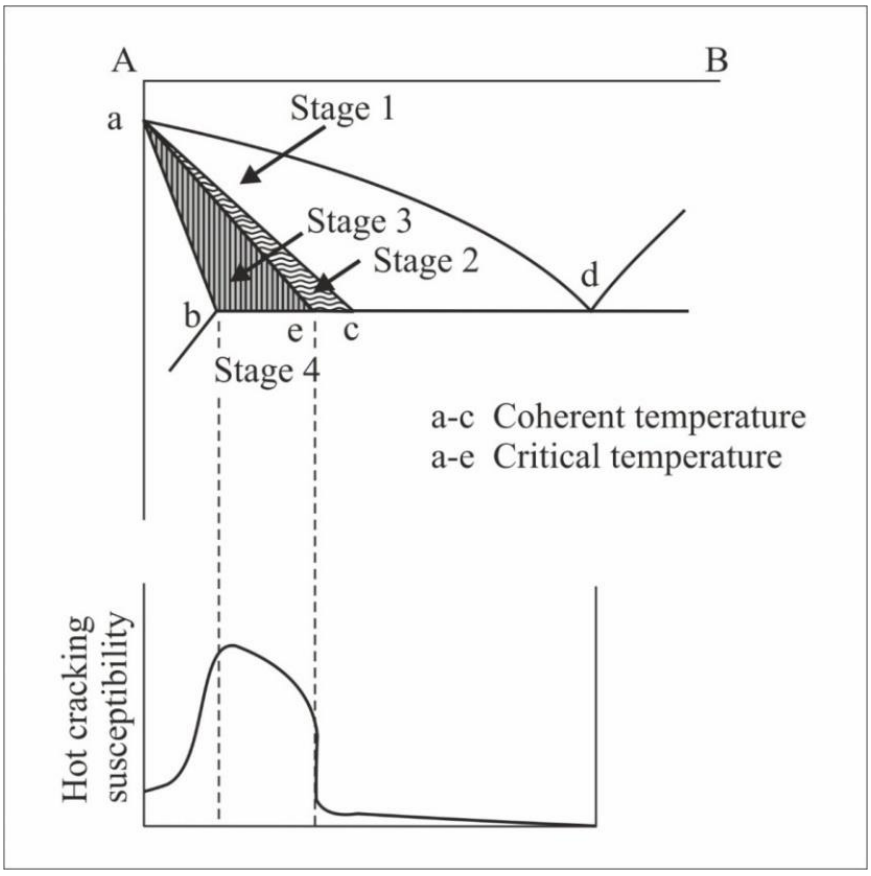

Fig.2.25 Critical temperature period of hot cracking in a binary alloys [187].

Lastly Flinn [187] purposed that solidification process could be categorized on the basis of metal properties. Which are given as

Step 1 - Absolutely liquid. It is not possible that hot tearing take place.

Step 2 - Liquid with a little solid. Cracks can be propagating or can be refill by liquid melt into the openings in the interdendritic state since there is adequate liquid present at this stage.

Step 3 - Liquid films formed in the freezing metal. Solid crystals start to propagate and strains are developed by contraction of dendrites and form an interlocking structure. Since due to contraction strains in the interdendritic region, hot tearing may originate, and since both the liquid and solid is greatly impeded in this stage so hot tearing cannot heal without difficulty.

Step 4- In this stage solid metal reaches to the plastic range. The metal flow takes place at low stress due to high ductility of the alloy and the applied stresses can be relieved by plastic flow.

Step 5- Solid metal reaches in "the elastic range".

Rosenberg et al. [188] thought that the different effects of different alloy additions were due in part to the shape or the resultant film or pockets. When enough alloying elements were added to a pure metal so that eutectic was present in amounts greater than necessary to completely surround the primary grains with a thin film, resistance to hot tearing increased due to improved feeding. However, Pumphrey et al. [160] indicated in their brittleness theory that stress modification and refilling were more important with an increase in the aggregate of eutectic. Eskin et al. [232] presented a comprehensive review on hot tearing susceptibility of aluminum alloys. The review covered many alloy systems, including Al-Cu, Al-Mg binary alloys, Al-Cu-Mg, Al-Cu-Si, Al-Mg-Si and Al-Cu-Li ternary alloys, and AA2XXX (Al-Cu-Mg), AA6XXX (Al-Mg-Si) and AA7XXX (Al-Zn-Mg) series commercial alloys, etc. To “continue” the work in Eskin’s review, many other alloy systems were studied to relate their hot tearing susceptibility or other features to alloy compositions.

Figure 2.26 shows the decrease in the elongation during the transition from the early liquid film stage to the late film stage. It has been shown schematically that the development of the microstructure decreases the overall mobility of the grains. It has been mentioned [200-204] that during the solidification interval of almost every casting material, the tensile strength and elongation-to-fracture were very low compared with the values in the solid

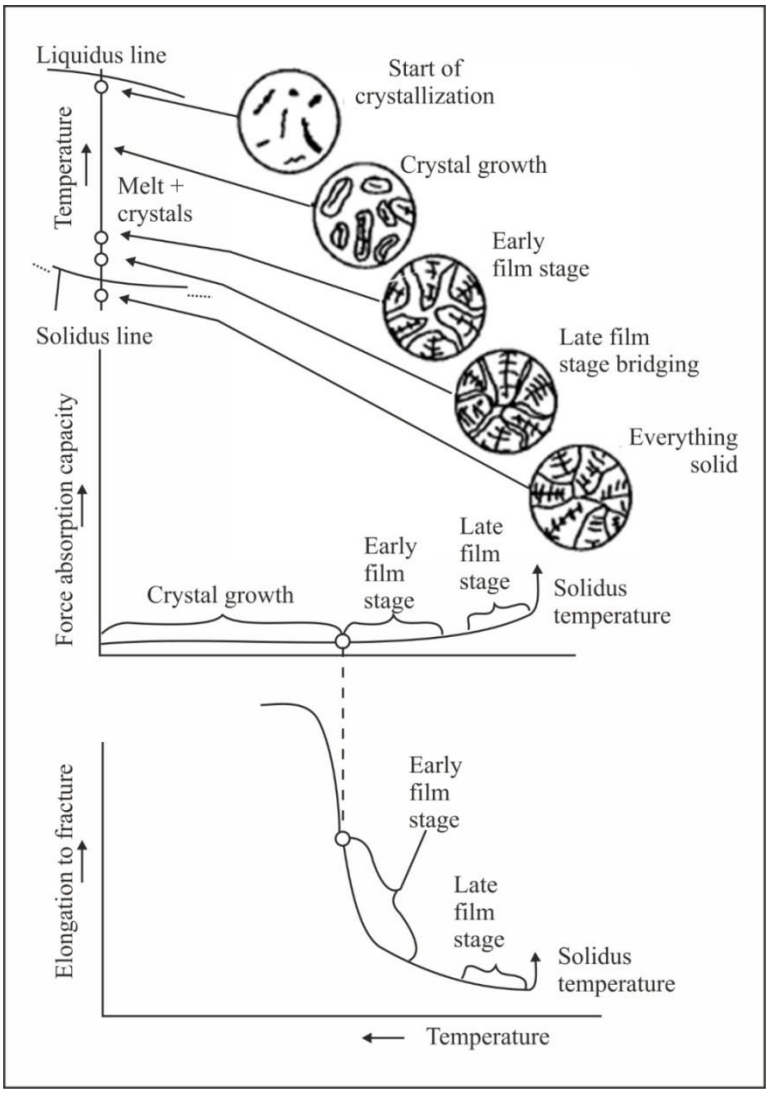

Fig.2.26 Diagram showing the tensile strength and elongation versus the microstructure [200].

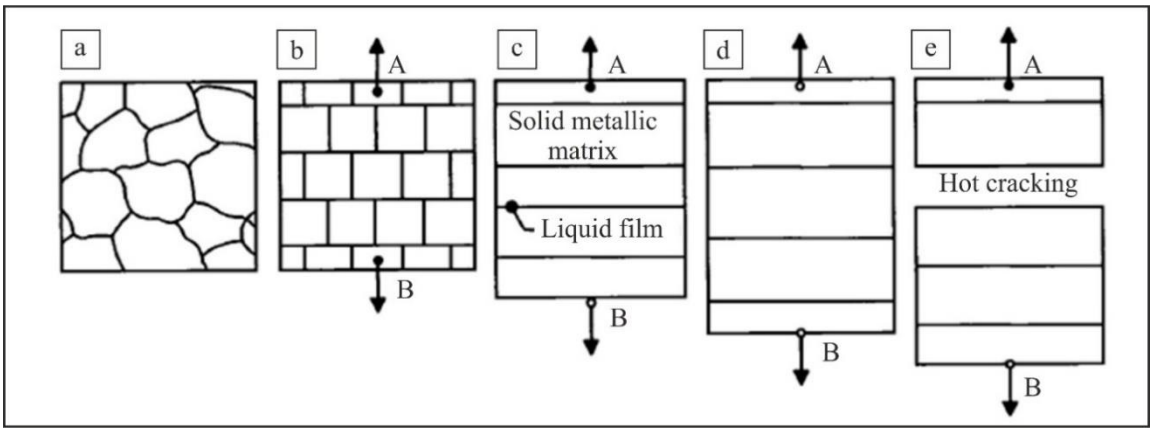

Fig.2.27 Hot tearing mechanism based on liquid film perpendicular to the stress axis [201].

region. The eventual occurrence of hot cracking during the critical temperature range depends mainly on the strain rate, the increase of the liquid film stage as a function of time and the amount of segregated material, and grain size. It has been mentioned [205,206] that only the interdendritic liquid films which are perpendicular to the stress axis will be decisive for the tensile strength. Figure 2.27 shows that hot tearing mechanisms based on this assumption. This theory could be used for both columnar and equiaxed grain structures. The measured elongations are attributed to the plastic deformation of the solid matrix. The tensile strength corresponds only to the stress required to separate two grains (assuming plane surfaces) between which exist a liquid film of thickness "b" with a known surface tension γ_{LG}. The required tensile stress 'σ' can be determined by equation 2.15.

$$\sigma = \frac{2\gamma_{LG}}{b} \qquad (2.15)$$

A similar description was given by Pellini [180] but without mention a specific orientation of the stress axis in relation to the liquid films. It is seen that the present approach will be used in the theoretical model to determine the Al-Si binary alloy fracture stress.

2.5 Factors of Hot Tearing

There are various factors which affect the hot tearing tendency of the Al-Si-Cu alloy. These are discussed in brief here

2.5.1 Effects of alloy chemistry

Alloy composition is a key factor which affects the hot tearing tendency. Al-Cu alloy shows high hot tearing tendency in comparison to Al-Si alloy. While Al-7Si-3Cu alloy persist enhance mechanical properties with hot tearing tendency. These are categorized as.

2.5.1.1 Binary alloys

In the past, most of the studies [207] had been performed with variations in alloy composition. The former studies show that the amount of eutectic is very important feature of the alloy structure. Hot tearing susceptibility is related to the aggregate of eutectic liquid existing during the last stage of solidification. Brittleness Theory [208] explained this phenomenon that stress modification and refilling are very important with rise content of eutectic. The effect of alloy composition on hot tearing has been established.

For many binary alloys, the correlation between hot tearing tendency and alloy composition is known as the lambda curve [209] as presented in Fig. 2.28. Generally, the wide freezing range, the more the alloy is susceptible to hot tearing since the alloy spend much more time in the susceptible stage.

Chamberlain et al. [196] and Sigworth et al.'s [8] work presented that not only the amount of the alloy additions but also their interactions had effect on the hot tearing [210]. It was found that both Mg:Zn ratio and total Mg+Zn content in Al-Mg-Zn alloy system were critical to hot tearing. The propensity to hot tearing decreased with increasing Mg:Zn ratio. There was no hot tearing with Mg:Zn ratio greater than 1.4:1 and with the same Mg:Zn ratio the resistance to hot tearing increased with increasing magnesium content.

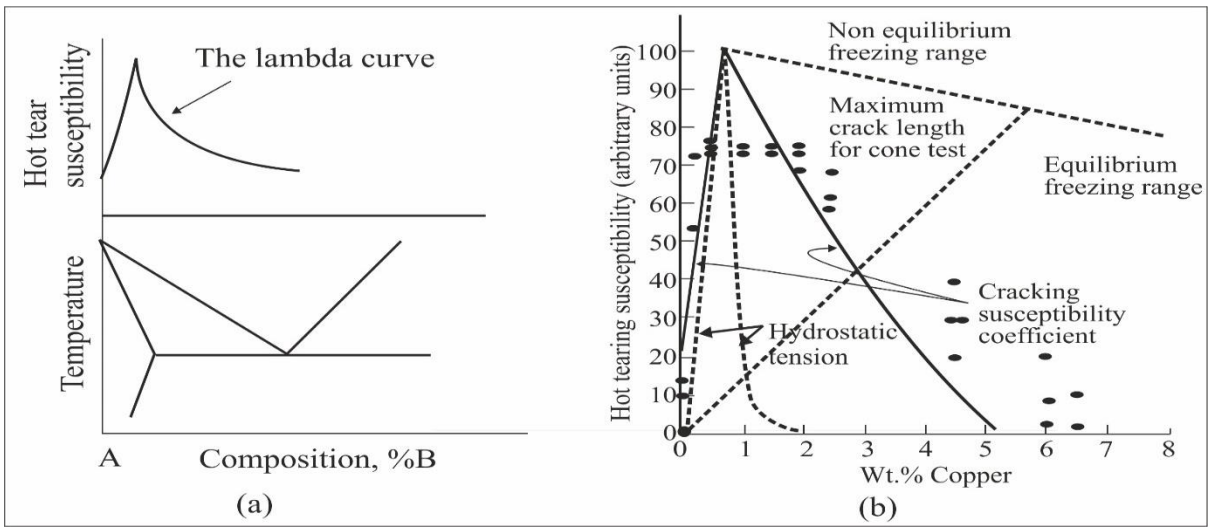

Fig.2.28 Schematic illustration of hot tearing susceptibility (a) binary alloy, presented as a lambda curve [133] **and (b) Hot tearing for Al-Cu alloys, presenting a peak at approximately 0.7 wt.% Cu [210].**

Al-Sn and Al-Cu alloys have revealed that the alloys had minimum lower tendency of cracking when the remaining liquid was insufficient surround the solid [18,104,137,138]. In, Al-Sn alloy, to overlay the interdendritic region only 0.5 wt.% eutectic liquid was required. However, the Al-Cu system, required 12 wt.% eutectic liquid. Furthermore, Pumphrey and Jennings [160] gave a good idea to discover a relationship between the small proportions of eutectic and the typical cooling proportion for an Al-Si alloy.

2.5.1.2 Multi-phase alloys

Recently many work is focused on multi-phase aluminium alloys, earlier it was not carried out. Pumphrey and Jennings [160] investigated the hot tearing vulnerability of Al-Cu-Mg alloys by using Ring Casting and Restrained Weld methods. Before them this technique was used in binary alloys. They keep constant Cu content and increased Mg content and vice versa. The experimental results of the two systems were shown by contour maps as displayed in Fig. 2.29 [111].

Nishimura [139], Pumphrey and Jennings [161] used this system and proved the adjacent connection between the system of the tearing phase diagram and the ternary diagram. To investigate the hot tearing vulnerabilities of ternary Al-Cu-Mg aluminium alloys the Annular Casting method [96] was selected. It was seen that hot tearing tendency of the alloy is influenced by the transformation of the last stage of the solidification.

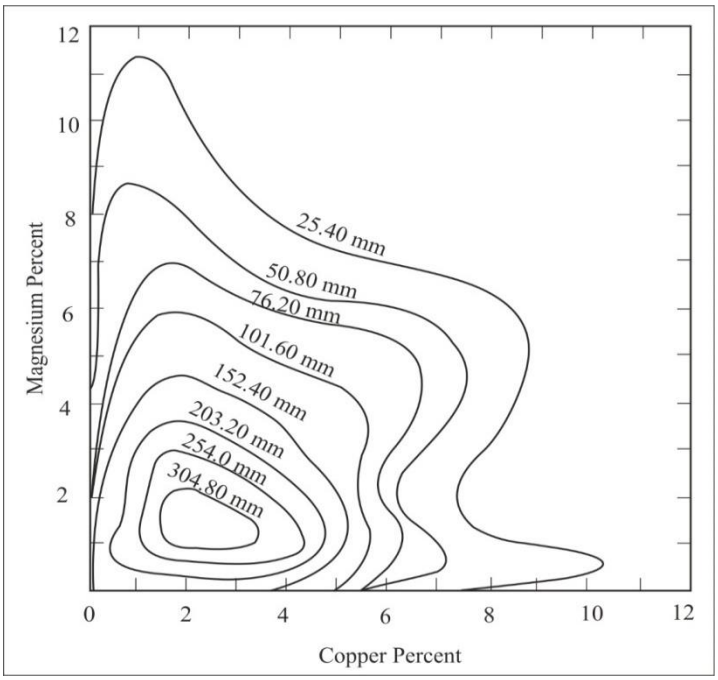

Fig.2.29 Contour of hot cracking vulnerability of an Al-Cu-Mg system measured with RC method [111].

2.5.2 Influence of Various Process Parameters

There are various process parameters which affect the hot tearing susceptibility of the Al alloys. These are discussed here

2.5.2.1 Influence of grain refiner

A fine equiaxed grain structure is always desired in metal castings. The addition of grain refiners decides the size and shape of grains which provide sites for heterogeneous nucleation. Grain size is also affected by the type and the amount of grain refiners added. Fig. 2.30 shows the microstructure of as cast and grain refined of pure aluminium.

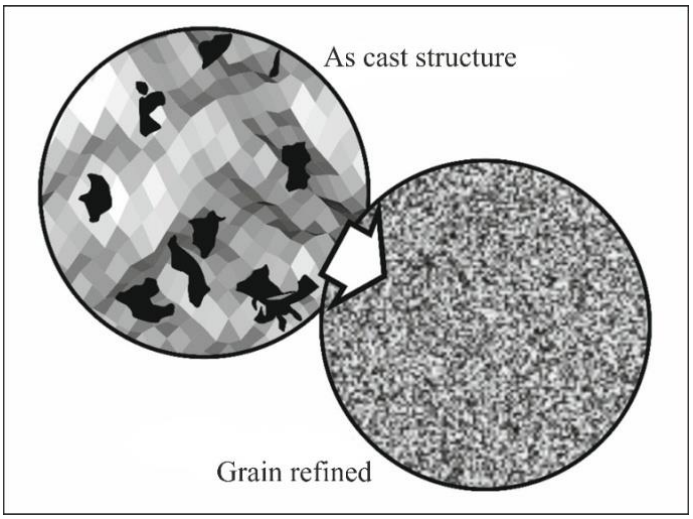

Fig.2.30 Typical macrostructures of pure aluminum castings: (a) as cast structure; (b) grain refined [140].

Matsuda et al. [199] tested the hot tearing tendency of Al alloy, as expected, Cu was produced negative effect. Frequently used grain refiners in aluminium industry are master alloys of Ti, or of Ti and B with Al. Titanium (Ti) and boron (B) are used to refine primary aluminum grains. Titanium separately, added as a titanium aluminum master alloy, forms $TiAl_3$, which serves to nucleate primary aluminum dendrites. More frequent nucleation or initiation of dendrites means a larger number of smaller grains. The results presented a good correlation between cracks and grain size, as a decrease in hot tearing tendency was attended by a reduction in grain size in Al-7Si alloy [59,142]. Grain refining efficiency is better when titanium and boron are used in combination. Master alloys of aluminum with 5% titanium and 1% boron are commonly used additives for this purpose. They form TiB_2 and $TiAl_3$, which together are more effective grain refiners than $TiAl_3$ separately. The most efficient grain refiner for Al-Si alloys has a Ti-B ratio closer to 1:5:1. That is a special case, applicable to 3XX and 4XX alloys and not to the other alloy systems.

Elia et al. [14] displays the effect of Ti-B grain refiner on hot tearing tendency of A319 aluminum alloy. They found that hot tears were present at the 90° junction between the downsprue and the casting bar. The location of hot teared is displayed in the Fig. 2.31,

instead of complete casting. Hot tearing tendency considerably decreased in A319 with additions of Al-5Ti-1B master alloy. A hot tear was primarily existing in the A319 alloy, as displayed in Fig. 2.29a. At 0.02 wt.% and 0.05 wt.% Ti concentrations, hot tear tendency was reduced but was not eliminated, as only minor cracks were notice on the sample surface.

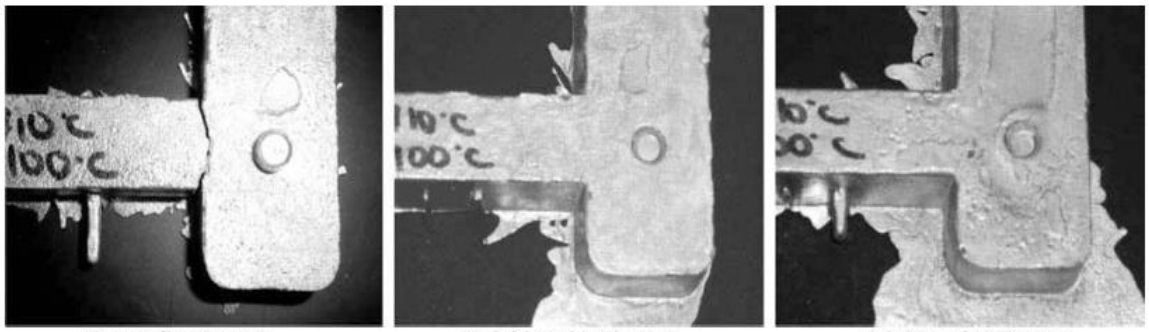

a) unrefined alloy b) 0.02 wt% Ti alloy c) 0.05 wt% Ti alloy

Fig.2.31 Effect of grain refinement on hot tearing in A319 alloy [14].

Their examined outcomes show that fine equiaxed grained structure is less prone to tearing than coarse columnar grained casting. In the presence of equiaxed grains, there is more chance of eutectic being present at this region on boundaries and thermal contraction was shelter by a slight broad mobility of the grains. Amount of eutectic at the grain boundaries permit free movements of the grains to accommodate the strain in the casting.

K. Lee et al. [171,172] studied the freezing range and hot tearing in AZ91E alloy and found that there was not a significant change in the freezing range when Al-5TiB_2 or Al-Al4C_3 refiners were added. While, addition of 2 wt.% ZNO increased the freezing range, which affect the castability of AZ91E (such as increasing hot tearing susceptibility). Li. et al.[17] studied the effect of Yttrium(Y) on the hot-tearing resistance of Al–5 wt.% Cu based alloy. It was found that Y promoted the end-solidification temperature and decreased the quantity of eutectic in grain boundary. Y-rich phase precipitation caused a depression of the begin-solidifying temperature of α-(Al), contracted the crystallization range, increased the hot tearing resistance and decreased the hot-tearing susceptibility significantly. F.D Elia et al. [14] investigated on hot tearing in B206 alloy with addition of titanium (0.02 wt.% and 0.05 wt.%) to examine the role of cooling rate and grain refinement. The additions of titanium to B206 were effective at removing hot tears by transforming the grain structure from coarse dendrites to equiaxed.

2.5.2.2 Influence of mould temperature

Generally, it is considered that the effect of cooling rate of mould temperature play a significant role in hot tearing. Mould temperature directly affects the casting cooling rate and thus the casting microstructure and performance, including hot tearing. On the other hand, controlling cooling rate is generally through controlling mould temperature. In most of the studies on hot tearing, cooling rate was controlled by changing the mould temperature, like in Clyne et al. [158] and Spittle et al.'s tests [201]. Very limited work on this topic was found in the published literatures. Bichler et al. [74] considered the effects of mould temperature on Mg alloy, AZ91D. The tests were performed at pouring temperature was 700ºC and mould temperatures of 140 ºC, 180 ºC, 220 ºC, 260 ºC, 300 ºC, 340 ºC, and 380 ºC, respectively. It was found that mould temperature had significant effect on hot tearing. The severity of hot tearing decreased progressively with increasing mould temperature. Zhen et al. [76] studied the effect of mould temperature in the range of 250 ºC to 500 ºC for Mg-Al alloys. They found that as increase the mould temperature as decrease hot tearing susceptibility and the higher mould temperature led to higher crack onset temperature and longer propagation time. The mechanism they gave was that cracks were initiated at all the mould temperatures, but at higher mould temperature the cracks could be refill by the remaining liquid and healed. H. Huang et al. [77] investigated the effect of pouring and mould temperature on hot tearing susceptibility of AZ91D and Mg−3Nd−0.2Zn−Zr Mg alloys. The results showed that mould temperature shows much more significant influence on the HTS of both alloys than pouring temperature which influence only can be distinguish at low mould temperature (341 K for AZ91D alloy and 423 K for NZ30K alloy). In AZ91D alloy (Fig. 2.32), at a relatively low mould temperature, 341 K (TDSM: 400 K), severe hot cracks occur on all the castings. Even the minimum value of HTS reaches 132 and the average HTS is about 154. Then, the HTS reduces gradually with the increase of mould temperature.

F.D Elia et al. [14] investigated the mechanisms of hot tearing in B206 aluminum alloy and found the same trend as earlier researcher. In this investigation castings were produced at three mould temperatures (250 °C, 325 ° C and 400 °C). Hot tears were present at solid fractions ranging from 0.810 to 0.870. Different studies showed controversies about casting temperature effect but all of the limit work about the effect of mould temperature shown that higher mould temperature reduces hot tearing susceptibility and gave the mechanism of better feeding and initial crack refilling.

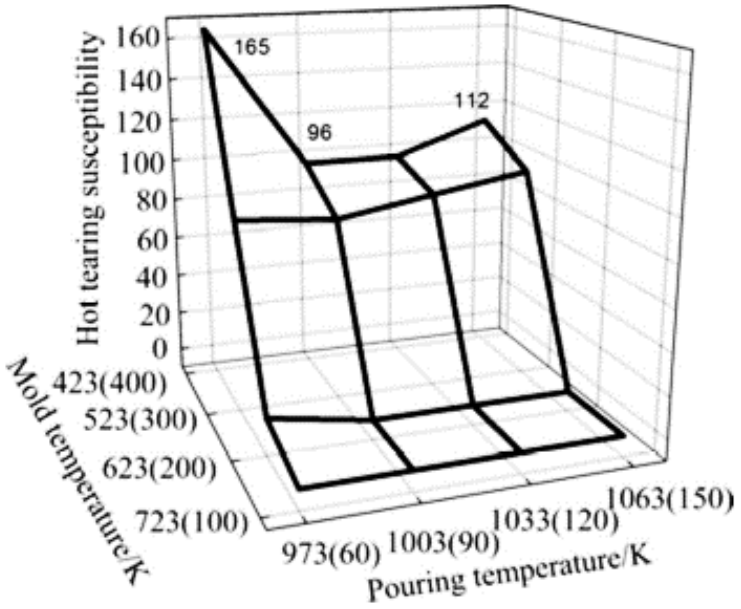

Fig.2.32 Influence of pouring and mould temperatures on hot tearing susceptibility (HTS) of NZ30K alloy (TDSM: $T_{solidus}-T_{mould}$; superheat: $T_{pouring}-T_{liquidus}$; Data in parentheses are TDSM and superheat temperature, respectively) mould [14].

2.5.2.3 Influence of pouring temperature

Pouring temperature has minor effect on hot tearing tendency of the Al-alloy. So, there are limited study was conducted to investigate the effect of pouring temperature on

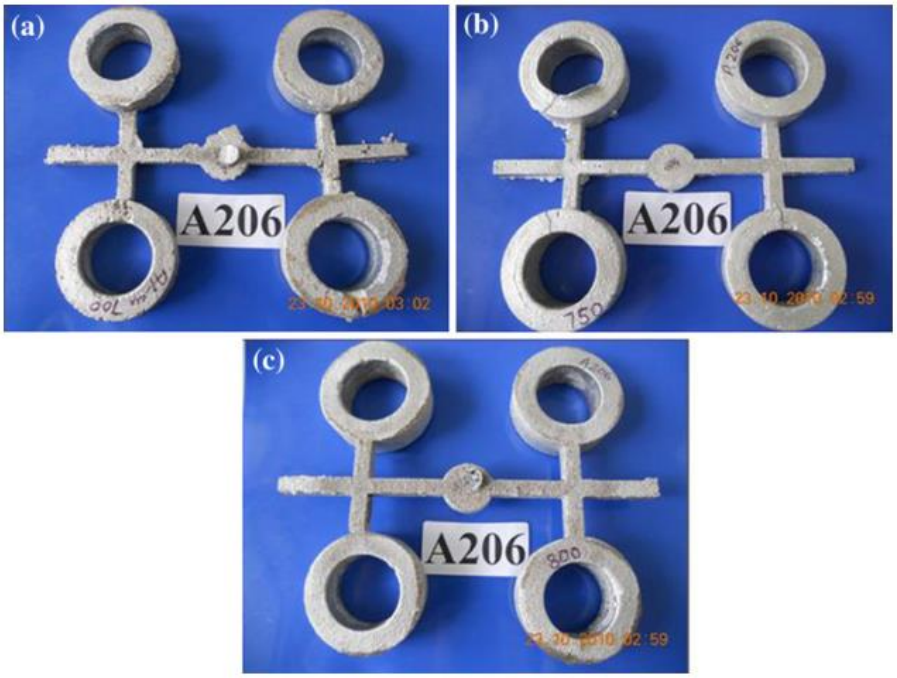

Fig.2.33 Picture showing cast surface of A206 cast alloy (a) Casting poured at 700 ºC, avg. crack length 13.75 mm; (b) Casting poured at 750 ºC, avg. crack length 41 mm; (c) Casting poured at 780 ºC, avg. crack length 12.75 mm [14].

hot tearing susceptibility. A. K. Birru et al. [85] showed the hot tearing vulnerability of Al–Cu, Al–Mg, and Al–Zn alloys. The hot tearing tests of the listed alloys were conducted at three different pouring temperatures using sand mould casting. The results revealed a good correlation between pouring temperatures, crack susceptibility, and grain size, as declining of crack susceptibility were observed at minimum and maximum pouring temperatures for A206. The influence of pouring temperature on HTS is less significant than mould temperature, and it is very clear in Fig. 2.33. Such influence is only obvious at lower mould temperatures (TDSM: 300−400 K), while very limited at higher mould temperatures (TDSM: 100−200 K).

2.5.2.4 Influence of metal segregation

Metal segregation improves the hot tearing resistance by extending the life of the film stage (impurities). For example, hot tearing in steels is commonly allied with micro-segregation of such as P and S elements [148]. When the S or P addition go beyond the solid solubility value, the hot tearing vulnerability of plain carbon steel improves significantly [89]. However, strength and ductility of the semi-solid casting decrease gradually by small additions of impurities, which reduce the hot tearing resistance of pure metals [149,150]. Various experimental [151] effort has been done to recognize the mechanism of the formation of inverse segregation. Pousset et al. [207] gave a model to analyze inverse segregation. It was found from their study that inverse segregation developed due to solidification shrinkage in the mushy zone.

2.5.2.5 Influence of gas content

The effect of gas content in hot tearing tendency has been investigated in alloys. These alloys contain 4 wt.% Cu and 6 wt.% Cu [110] respectively. Only the hot tearing tendency of 424 alloy was influenced by the gas content. An investigation [153] illustrated the two-fold effect of gas content in Al alloy. The presence of gas can drive residual liquid into tear holes which improves the hot tearing resistance. During the melting hydrogen gas was entrapped in the melt. During solidification this gas starts to reject out which develop an internal pressure and force liquid eutectic to heal the tears [173]. Since excessive gas porosity is undesirable and produce adverse effect such as poor strength, low ductility, strapped surface finish, etc., [68,154].

2.5.2.6 Influence of metal treatment

It is well known that metals and alloys usually solidify with coarse columnar grain structure under normal casting conditions unless the mode of solidification is carefully controlled. It is possible to develop fine equiaxed grains in the as cast structure either by increasing the number of nucleation sites or by grain multiplication. More refine grain has lower tendencies towards casting defects. So, metal treatment can be done by adding grain refiners in the melt [82,155,156].

2.6 Identification of Research gap

Grain refinement is an effective way to improve the tensile behavior and to minimize hot tearing and porosity of Al-Si alloys. The theories of hot tearing postulate that stress, strain, strain-rate and alloy microstructure are all underlying factors. Further, various factors including alloy composition, grain size and morphology and casting process parameters are seen to influence hot tear formation. However, quantification of stress and strain generated during casting is lacking in many hot tearing investigations. Moreover, since hot tearing is a solidification phenomenon, an understanding of microstructure development during solidification will help to paint a clearer picture of the hot tearing mechanisms. With this consideration, the current research extends the use of microstructure studies for residual strain and stress measurements to the Al-7Si-3Cu aluminum alloy. Specifically, the effect of grain refinement on hot tearing and subsequent residual strain is investigated. The addition of Al-5Ti-1B grain refiner refines the average grain size of α-Al phase. By now, various attempts have been made to improve the grain refinement response in commercial Al-alloys. One effective route is to increase the addition level of Al–5Ti–1B master alloy, which is undesirable in practice. There is one more possibility which is to improve the efficiency of Al-5Ti-1B master alloy through ball milling, annealing, and hot rolling of the master alloy. However, studies on the processing of the ball milling, annealing and hot rolling of Al-5Ti-1B master alloys on the grain refining performance of Al-Si alloys are scarce.

3 Chapter Three

Materials And Methods

This chapter will provide all the details on the alloy that was prepared for this study, which includes the melting and casting procedures, mechanical working of grain refiner, preparation of samples for metallographic examination, the mechanical testing procedures and hot tearing testing method.

3.1 Alloy Preparation

The experimental alloy was prepared by careful melting and dilution of master alloys of compositions such as Al-20%Si and Al-33%Cu, in combination with Al of 99.99% purity in the electric resistance furnace at 720 ^{o}C provided with ±5 ^{o}C accuracy for 30 minutes. Necessary allowances for melting losses were also taken into account in the computation of charges. Melting material was covered with flux to avoid oxidation. This was followed by degassing with hexachloroethane tablet (C_2Cl_6) to ensure removal of hydrogen. After proper mixing, the molten alloy was cast in steel mould (height 180 mm, diameter 20 mm). The chemical composition of the base alloy is given in Table 3.1. All the compositions have been expressed in wt. %.

Table 3.1 Chemical Composition of Al-7Si-3Cu Alloy (wt.%)

Cu	Si	Mg	Ni	Mn	Zn	Pb	Cr	Ti	Al
3.0	6.97	0.001	0.026	0.14	0.015	0.008	< .001	0.005	Rem.

3.2 Grain Refiner

Al-5Ti-1B master alloy grain refiner used in this investigation was supplied by M/s Sharu Aikoh Chemicals Limited Meerut (UP). The chemical composition of the master alloy is given in Table 3.2.

Table 3.2 Chemical composition of Al-5Ti-1B master alloy (wt.%)

Al	*Ti*	*B*	*Si*	*Fe*	*V*	*Zn*	*Co*
93.68	*4.99*	*1.0*	*0.05*	*0.15*	*0.09*	*0.01*	*0.02*

3.3 Mechanical Working of Grain Refiners

The grain refining efficiency of the Al-5Ti-1B master alloy was majorly decided by the size, size distribution and morphology of $TiAl_3$ particles. These intermetallic particles act as heterogeneous nucleation sites during solidification of Al-7Si-3Cu alloy resulting in grain refinement. If the size and shape of the $TiAl_3$ particles is changed the response of grain refiner can be changed towards aluminium alloys. The morphology of $TiAl_3$ particles may be changed by using ball milling, heat treatment and hot rolling methods. In this section, Al-5Ti-1B master alloy grain refiner has been given different treatments such as ball milling, heat-treatment and hot rolling.

3.3.1 Ball Milling

As cast Al−5Ti−1B master alloy was cut in small chips with the help of lathe machine then it cleaned by acetone to remove dirt and oil. After cleaning, chips were ball-milled under controlled atmosphere of argon gas into fine powder of size; 55 µm, 30 µm and 10 µm for 10h, 30h and 50h, respectively. The ratio of ball to powder was kept 15:1 and the rotational speed of 400 r/min was used.

3.3.2 Annealing

Heat treatment of as cast Al-5Ti-1B master alloy was carried out at different temperatures; 400 °C, 500 °C, 600 °C, 700 °C and 800 °C for 8 h in a muffle furnace of an accuracy of ±5 ºC, in order to stimulate the intermetallic particles. Heat treatment process increases volume fraction of $TiAl_3$ particles.

3.3.3 Hot rolling

Furthermore, as cast Al-5Ti-1B master alloy was subjected to rolling at 250 °C and 350 °C for three reduction levels of 25%, 50% and 75%, respectively. A 20 x 70 x 150 mm^3 size cast plate was used for rolling purpose. The rolling process includes a 25% reduction level in the beginning at 250 °C temperature. For further higher reduction levels, the samples were again heated in muffle furnace to 250 °C temperature and then rolled. Same process was carried out for sample hot rolled at 350 °C. Thus samples at 25%, 50% and 75% reduction levels were prepared at 250 °C and 350 °C temperature. During rolling coarser brittle $TiAl_3$ particles fragmented into finer particles due to stress concentration at

the particles matrix interface. Thus the total numbers of $TiAl_3$ particles are increased by the fracture of brittle particles at higher stress level.

3.4 Characterization Study of Al-5Ti-1B Master Alloy

The as cast and treated Al-5Ti-1B master alloy under different conditions were characterized by XRD, optical microscopy, SEM and TEM.

3.4.1 X-ray diffraction analysis

XRD studies were carried out on as cast and treated Al-5Ti-1B master alloy to study the nature of second phase particles present in the master alloy. I vs θ for the given alloy is determined by X-ray diffraction (XRD, X'Pert Powder PAN alytical) automated X-ray diffractometer within the angle range of 20-90º with the Cu target with $\lambda_{k\alpha}$ = 1.540Aº. As per requirement of range selected for the master alloys were such that all the major intense peaks of the phases expected in the sample were covered.

3.4.2 Optical microscopy analysis

Samples for microstructural studies were sectioned from as cast and treated master alloys. The sectioned (size 10 × 10 × 10 mm^3) surface so obtained was initially polished on a belt grinder and then on a series of SiC water proof emery papers with increasing grit size. Final stages of polishing were performed on a disc polisher using 75 µm Al_2O_3 powder with water until a scratch free surface is obtained. The polished samples were eatched using Keller's reagent (2.5% HNO_3 + 1.5% HCl + 1% HF + 95 % H_2O by volume) for about 30s in order to develop microstructure. Optical microscopy (OM, Leica DMLA), optical microscope was used for examination of microstructure of the samples.

3.4.3 Scanning Electron Microscopy analysis

The cast and treated Al-5Ti-1B master alloy samples were observed under scanning electron microscopy (SEM, NOVA NANO 450). The procedure adopted for the preparation of SEM samples was exactly the same as that used for optical microscopy. However, metallographic sample was deep etched with Keller's regent. A number of regions were examined in each alloy to have a complete understanding of the microstructural features of the master alloy. The machine is interfaced with Link ISIS software for EDX which was used for bulk analysis of particles.

3.4.4 Transmission Electron Microscope analysis

As cast Al-5Ti-1B master alloy sample was observed under transmission electron microscopy (TEM, G^2 20 (FEI)) with EDX micro-analysis facility. The given alloy was sectioned into thin slice with thickness of the order 250 µm. A low speed diamond saw (BuechlerIsomet Model 11-1180) was used for slicing. From the slices prepared with the desired diameter (3 mm) were punched by using a disc punch. Then disc was mechanically polished to about 100-120 m thickness using grinding media (such as SiC). For polishing, a disc grinder (Model 623) was used as it offers the removal of material with good control. A twin jet electro-polisher (Fishione polisher, Model 110) was used for electro polishing. At last, sample was examined under a table lamp to verify the quality of polishing. For optimal conditions, the surfaces appear shiny. Then sample was removed from the holder using forceps and cleaned in methanol and dried on a filter paper. It can be preliminarily examined in the TEM. The crystal structure of Al-5Ti-1B master alloy has been examined by TEM techniques.

3.5 Grain Refining Procedure

The Al-5Ti-1B master alloy has been tested for its grain refining efficiency in Al-7Si-3Cu alloy. For grain refinement studies the 1.0 Kg charge of Al-7Si-3Cu alloy was melted in a preheated graphite crucible using an electric resistance furnace under a cover flux (45% NaCl+45% KCl+10%NaF) to avoid the oxidation and the melt was held at 720 ± 5 ^{o}C for 30 minutes. Degassing was carried out by using hexachloroethane (C_2Cl_6) tablets. After fluxing and degassing, different wt.% (0.6, 0.7, 0.8, 0.9, 1.0 and 1.1 wt. %) of grain refiner were added separately for each experiment, 10 min before casting. The melt was stirred for 60 second with zirconia coated graphite rod, in order to speed up the dissolution and to separate the titanium borides particles in the melt. Part of the melt was poured at 720 ^{o}C into a circular steel ring (80 mm in diameter and 20 mm height) surrounded by a fire clay brick with its top open. For microstructure and mechanical properties analysis, the melt was poured in a preheated graphite mould (25 mm in diameter and 100 mm height).

Assessment of the grain refining efficiency of as cast and treated Al-5Ti-1B master alloy grain refiner on Al-7Si-3Cu alloy.

The grain refining efficiency of as cast and treated Al-5Ti-1B master alloys have been studied in detailed with the view to understand the nucleation behavior of α-Al on

intermetallic particles such as $TiAl_3$, TiB_2, and ($TiAl_3$+TiB_2). Table 3.3 and 3.4 gives the details of grain refinement studies conducted on Al-7Si-3Cu alloy under various process conditions.

Table 3.3 Details of grain refinement studies on Al-7Si-3Cu by Al-5Ti-1B grain refiner

Metal	Master Alloy	Heterogeneous nucleation particles	Wt.% Addition level	Elemental addition level wt.%	
				Ti	B
Al-7Si-3Cu	Al-5Ti-1B	$TiAl_3$ and TiB_2	0.60	0.030	0.006
			0.70	0.035	0.007
			0.80	0.040	0.008
			0.90	0.045	0.009
			1.0	0.050	0.010
			1.1	0.055	0.011

Table 3.4 Addition of grain refiner in various process conditions

Al-5Ti-1B Master alloy		Treatment	Master alloy wt.%			Wt.% Ti			Wt.% B		
As cast	A_0	-	0.90	1.0	1.1	0.045	0.050	0.055	0.009	0.010	0.011
Ball milled	B	10 H	0.80	0.90	1.0	0.040	0.045	0.050	0.008	0.009	0.010
		30 H	0.80	0.90	1.0	0.040	0.045	0.050	0.008	0.009	0.010
		50 H	0.80	0.90	1.0	0.040	0.045	0.050	0.008	0.009	0.010
Annealed	C	500 ºC	0.70	0.80	0.90	0.035	0.040	0.045	0.007	0.008	0.009
		600 ºC	0.70	0.80	0.90	0.035	0.040	0.045	0.007	0.008	0.009
		700 ºC	0.70	0.80	0.90	0.035	0.040	0.045	0.007	0.008	0.009
		800 ºC	0.70	0.80	0.90	0.035	0.040	0.045	0.007	0.008	0.009
Hot rolled	D	25 %	0.60	0.70	0.80	0.030	0.035	0.040	0.006	0.007	0.008
		50 %	0.60	0.70	0.80	0.030	0.035	0.040	0.006	0.007	0.008
		75 %	0.60	0.70	0.80	0.030	0.035	0.040	0.006	0.007	0.008

3.6 Characterization of Al-7Si-3Cu Alloy

The Al-7Si-3Cu alloy with and without grain refinement has been subjected to macroscopy, microscopy, and grain size analysis. The mechanical properties (tensile strength, yield strength, % elongation and hardness) and were also performed to observe

the effect of grain refinement on these properties. Selected fractured samples of tensile tests were subjected to SEM studies.

3.6.1 Microstructural analysis

Poulton's Reagent and Keller's reagent were used for revealing macro and microstructure and SDAS values. Compositions of these reagents are listed in Table 3.5.

Table 3.5 Chemical composition of reagents used for etching

Etchant	Composition	Specific use
Poulton's Reagent	30% HNO_3, 30% HCI, 35% H_2O and 5% HF by volume	Macroetchant
Keller's Reagent	95% H_2O, 2.5% HNO_3, 1.5% HCl, 1% HF by volume	Good general purpose etchant for Al and alloys. Reveal grain structure and secondary dendrite arm spacing.

The grain-refined samples were characterized by macroscopic examination. For macro-structural study samples were sectioned from ingot from the bottom above 25mm height. They were polished on a series of emery papers from 1/0 to 4/0 grade and finally wheel polished on sylvet cloth with 9, 6, and 1μm diamond paste as an abrasive. With diamond polishing, diamond extender was used as a lubricant as well as to disperse the diamond onto the cloth for uniform abrasion. These samples were carefully cleaned with soap solution and alcohol followed by drying. The samples so obtained were etched for about 30s by the Poulton's reagent for Al-7Si-3Cu alloy for developing the macrostructure. All possible precautions were taken during polishing and etching of samples. All the samples were kept group wise in desiccators. The photo-macrographs were taken directly from the macroetched samples. Macroscopy was performed on all the samples with and without grain refinement.

3.6.2 Grain size measurement

The grain size is measured by using the linear intercept method. The test grid, containing many parallel, straight test lines with spacing greater than the apparent mean grain diameter, was overlaid over the current microscope picture. Then, the average

intercepts length, τ, was determined from the N measured values of l_i in accordance with the following equation:

$$\tau = \frac{\sum_{i=1}^{N} l_i}{N} \quad (3.1)$$

where each l_i value is in length unit (μm) acquired by dividing the apparent distance on the image by the magnification used, M.

3.6.3 Porosity measurement

The porosity for Al-7Si-3Cu alloy in different processing conditions was calculated using Archimedes principle [157] in the following manner

$$P\ (\%) = [1-(D_a/D_m)]\ x100 \quad (3.3)$$

Where;

Da = Experimental density of sample

D_m = Theoretical density of sample

Here D_m= 2.685 gm/cm^3 for Al-7Si-3Cu alloy.

The experimental density of the samples was calculated using the Mettler Toledo, ME-DNY-4 density measurement kit.

3.6.4 X-Ray diffraction analysis

To identify the stoichiometry of existing phase, XRD analysis was carried out for the Al-7Si-3Cu alloy in different conditions using X'pert Pro PANalytica X-Ray diffractometer unit with a CuKα (λ=0.1540598 nm) source. Diffraction measurements were performed in the angle range of 20^o to 90^{o}at step size 0.05^o with scan step time 0.8 sec using Cu-Kα radiation (40kV, 40mA).

3.6.5 Thermal analysis

Pieces of 10 mg in weight were used as a sample, for differential scanning calorimetry (DSC) (Netzsch DSC 404 F3) analysis was properly cleaned. Nitrogen gas was used for controlled atmospheric conditions and the cooling rate was 10 k/min. DSC was used to record the eutectic and liquidus temperature of the alloy under different conditions.

3.6.6 SEM and EDS analysis

The morphology of cast Al-7Si-3Cu alloy was also examined using SEM (Nova Nano 450SEM, FEI, North America) operated at 15-20 kV. Energy dispersive X-ray spectroscopy (EDS) detector (Bruker, Germany) was employed for phase composition and elemental mapping for phase identification.

3.6.7 Transmission electron microscopy analysis

As cast and grain refined Al-7Si-3Cu alloy samples were observed under transmission electron microscopy (TEM, G^2 20 (FEI)) with EDX micro-analysis facility. The procedure adopted for the preparation of TEM samples were exactly the same as that used for earlier study.

3.7 Mechanical properties

3.7.1 Tensile properties

Ultimate tensile strength is the maximum stress that a material can withstand while being stretched or pulled before necking, which is when the specimen's cross-section starts to significantly contract. The Ultimate tensile strength is found by performing a tensile test and recording the stress versus strain; the highest point of the stress-strain curve is the UTS. It is an intensive property, therefore, its value does not depend on the size of the test specimen. However, it is dependent on other factors, such as the preparation of the specimen, the presence or otherwise of surface defects, and the temperature of the test environment and material.

Samples required for tensile tests were machined from as cast and grain refined Al-7Si-3Cu alloy. Each test was repeated three times. Average value of properties was taken for study. Tensile properties (tensile strength, yield strength and ductility in terms of percentage elongation) were measured using Hounsfield computerized tensile testing machine (20KN). 0.2% proof stress is expressed as yield stress.

Tensile tests were carried out on round samples having a 5.05 mm diameter and 25.2 mm length (Fig. 3.1). The samples were tested at constant strain rate of 1.0mm/min. The ultimate tensile strength (UTS) and ductility in terms of percentage elongation was calculated. Tensile test was not conducted for pure Al.

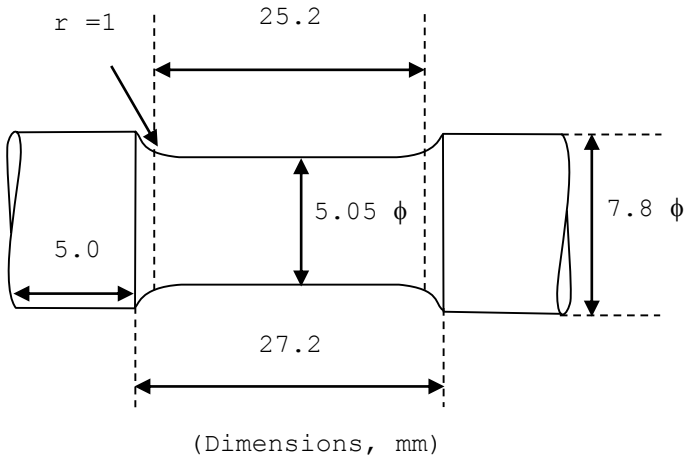

Fig.3.1 Tensile test specimen

3.7.2 Fractography

Fracture surface characterization studies were carried out on the tensile fractured samples in order to provide insight into the various fracture mechanisms operative during tensile loading of samples. Fracture surface characterization studies were primarily accomplished using a scanning electron microscope.

3.7.3 Hardness properties

The hardness of test specimens was calculated using the Brinell hardness testing machine. The polished sample was placed under the microscope for proper selection of the area to obtain the hardness value. The diamond ball indenter of 10 mm was used under the load of 500 kgf for a dwell time of 15s to get the indentation mark (Fig. 3.2). Four readings were taken for each sample and the hardness value was calculated using formula,

$$\mathrm{BHN} = \frac{P}{\frac{\pi D}{2}(D-\sqrt{D^2-d^2})} \qquad (3.4)$$

Where;

D = Diameter of ball indenter

d = diameter of indentation, P =load.

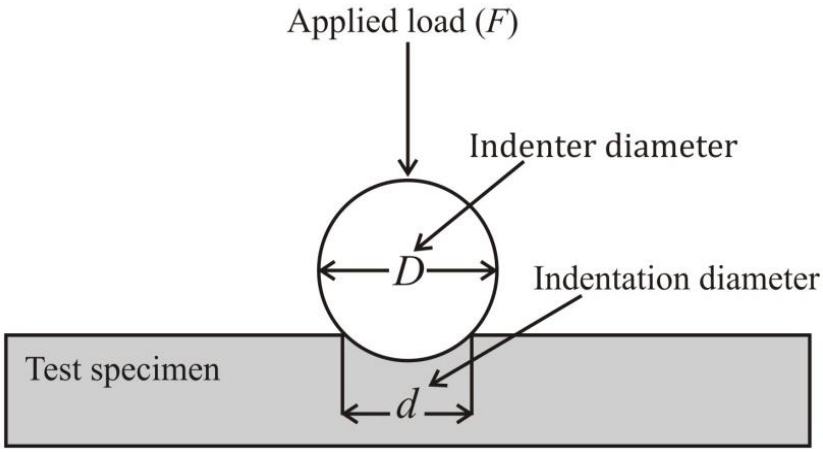

Fig.3.2 Schematic depiction of the Brinell indentation.

3.8 Hot tearing Test

3.8.1 Permanent mould die

Schematic diagram of permanent mould is shown in Fig. 3.3. The sharp corner at the 90º junction of downsprue and casting bar was intentionally given to promote hot tears in the casting. The mould was machined from a block of steel. The thickness of mould was 20 mm. The casting cavity was made up of a 180 mm downsprue and a 260 mm long casting bar with 20 mm end restraint. The mould was also equipped with three vents. The vents confirmed that no entrapped gases remained in the casting cavity during solidification of casting.

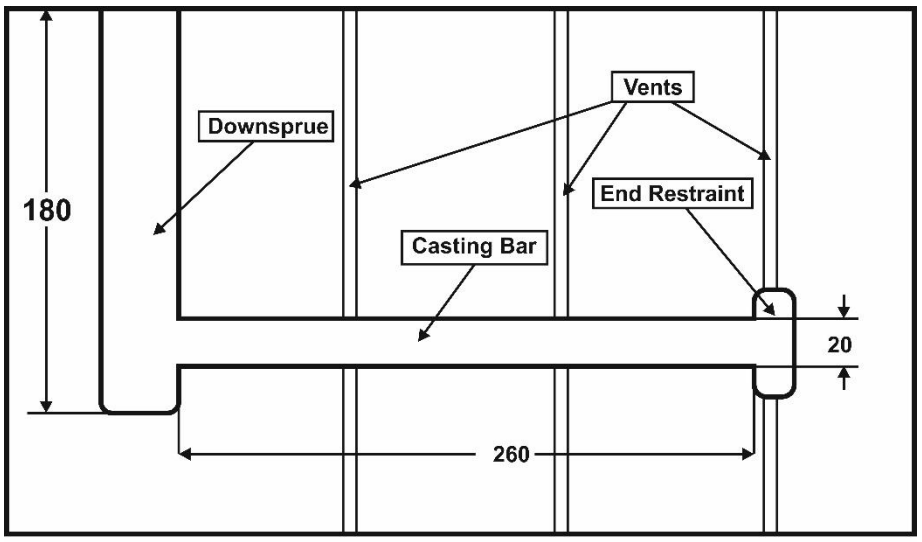

Fig.3.3 Schematic diagram of permanent mould die.

Once molten metal filled the mould cavity, solidification started from the end restraint towards the downsprue. As the casting solidified, it is started to contract. However, contraction of casting is opposed by the end restraint, further, which promoted stresses in the bar. Lastly, these stresses increase continuously and exceeded to the semi-solid strength of the alloy, then hot tear propagated in the casting bar.

Permanent mould is heated with two heating plate to obtained the desired mould temperature. The circuit diagram of heating plate is shown in Fig. 3.4. Two clamps were attached with permanent mould to fix the die, so there is no space for leaking of molten metal. The temperature of molten metal was controlled with k-type thermocouple. Calcium hydroxide coating was applied to the mould, in order to easy with drawl of casting bar from the mould. The permanent mould is then heated to 200 ºC to remove last traces of moisture. The coating was removed after each casting and then re-applied for each casting experiment. The CRC mould cavity is capable of producing cylindrical constrained rod with the size 260 mm long and 20 mm in height, at room temperature. For each pour, the Al-7Si-3Cu alloy was covered under flux and degassed at 740 ºC using hexachloroethane tablets. Finally, the melt was poured in permanent die mould at varying mould temperature, 90 ºC, 160 ºC, 230 ºC and 300 ºC to observe the effect of mould temperature on hot tear.

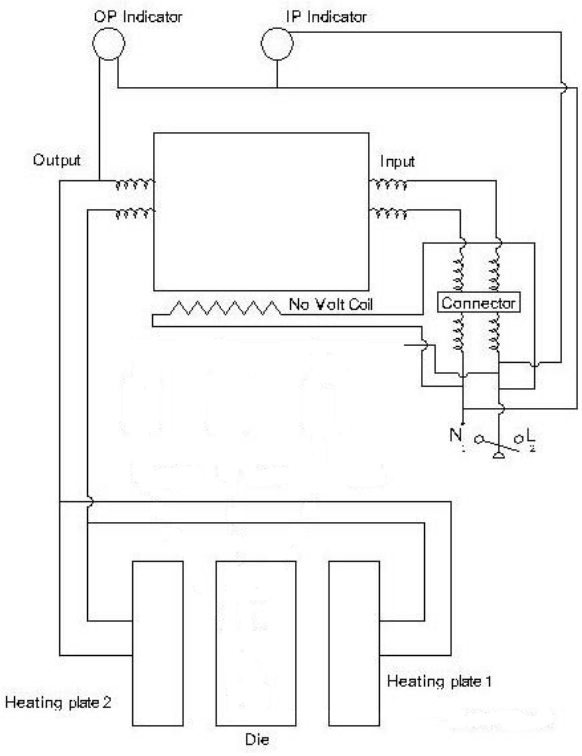

Fig.3.4 Circuit diagram of heating plate.

To observe the effect of as cast and treated grain refiner on hot tearing, the Al-5Ti-1B master alloy in different wt.% were added to the melt at 720 ºC prior to casting. After ten minutes adding of grain refiner, the melt was mechanically stirred for one minute with the help of graphite rod. Finally, the melt was poured in permanent die mould (at mould temperature 200 ºC) at 720 ºC; as shown in Fig. 3.5. During the experiments, mould temperatures were monitored with a K-type thermocouple, which was embedded in or on the surface of the mould. Initially, the horizontal bar filled with molten metal and solidification begins at the end restraint towards downsprue. As the bar solidified, end restraint induced tensile stresses by preventing freely contraction of casting bar. A crack is initiated when tensile stresses are higher than semi solid strength of the alloy. The castings were ejected from the mould after the top of the sprue was completely solidified. Table 3.6 shows summary of procedure adopted for hot tear experiment.

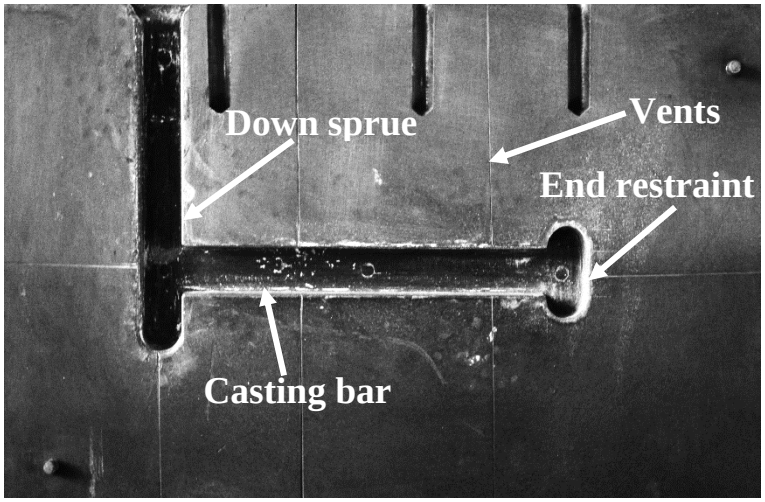

Fig.3.5 Original picture of permanent mould die.

Table 3.6 Experimental procedure for hot tearing test

Order	Procedure
1	Coat the mould with Alumina
2	Preheat mould to 90 ºC, 160 ºC, 200 ºC, 240 ºC and 280 ºC;
3	Maintaining melt temperature at 740°C
4	Preparation of Al-Si-Cu ternary alloy
5	Add cover flux
6	Degas the melt using the hexachloroethane tablet into the melt
7	Add varying wt.% of grain refiners
9	mechanically stir for one minute
10	Pouring melt into preheated mould (230 °C) at 720 °C
11	Recording observations.

3.8.2 Microstructure analysis for hot teared samples

Illustrative samples were extracted from the casting bar at two locations as shown in Fig.3.6, one near the down-sprue and the other near the end restraint. The end restraint is the primarily region where the melt solidified, where down-sprue is the last region. Hot tear in Al-7Si-3Cu alloy occurs near the down-sprue at the last stage of solidification. So these two regions are selected for microstructure, porosity and XRD analysis.

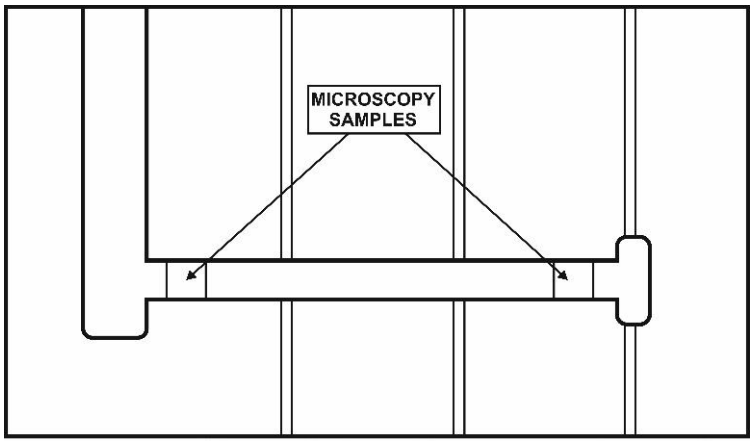

Fig.3.6 Location of sample for microstructure analysis.

The microscopy specimens paper polishing was done on 400, 600, 800 and 1000 grit size silicon carbide paper respectively. After that cloth polishing was done by 600µm, 800µm, 1000µm alumina powder to obtain the crystal clear sample. The Al-Si-Cu alloys were etched to view grain size and general microstructure by Keller's etchant. After etching the microstructure was taken on optical microscope and morphology of the alloy's interdendritic regions were studied.

3.8.3 XRD analysis

The hot teared regions of Al-7Si-3Cu alloy were observed under X-ray diffraction (XRD, X'Pert Powder PAN alytical) automated X-ray diffractometer within the angle range of 10-120º with the Cu target with $\lambda_{k\alpha}$ = 1.540 Aº. As per requirement of range selected for the master alloys were such that all the major intense peaks of the phases expected in the sample were covered. This technique is performed to study the existing phases on hot tear surface.

3.8.4 SEM analysis

The hot teared regions of Al-7Si-3Cu alloy were observed under scanning electron microscopy (SEM, NOVA NANO 450). A number of regions were examined in each alloy to have a complete understanding of the fractured surface. The machine is interfaced with Link ISIS software for EDX which was used for bulk analysis of particles.

3.8.5 TEM analysis

The hot teared regions of Al-7Si-3Cu alloy were observed under transmission electron microscopy (TEM, G^2 20 (FEI)) with EDX micro-analysis facility. The procedure adopted for the preparation of TEM samples were exactly the same as that used for earlier study. This study is carried out to validate the XRD results.

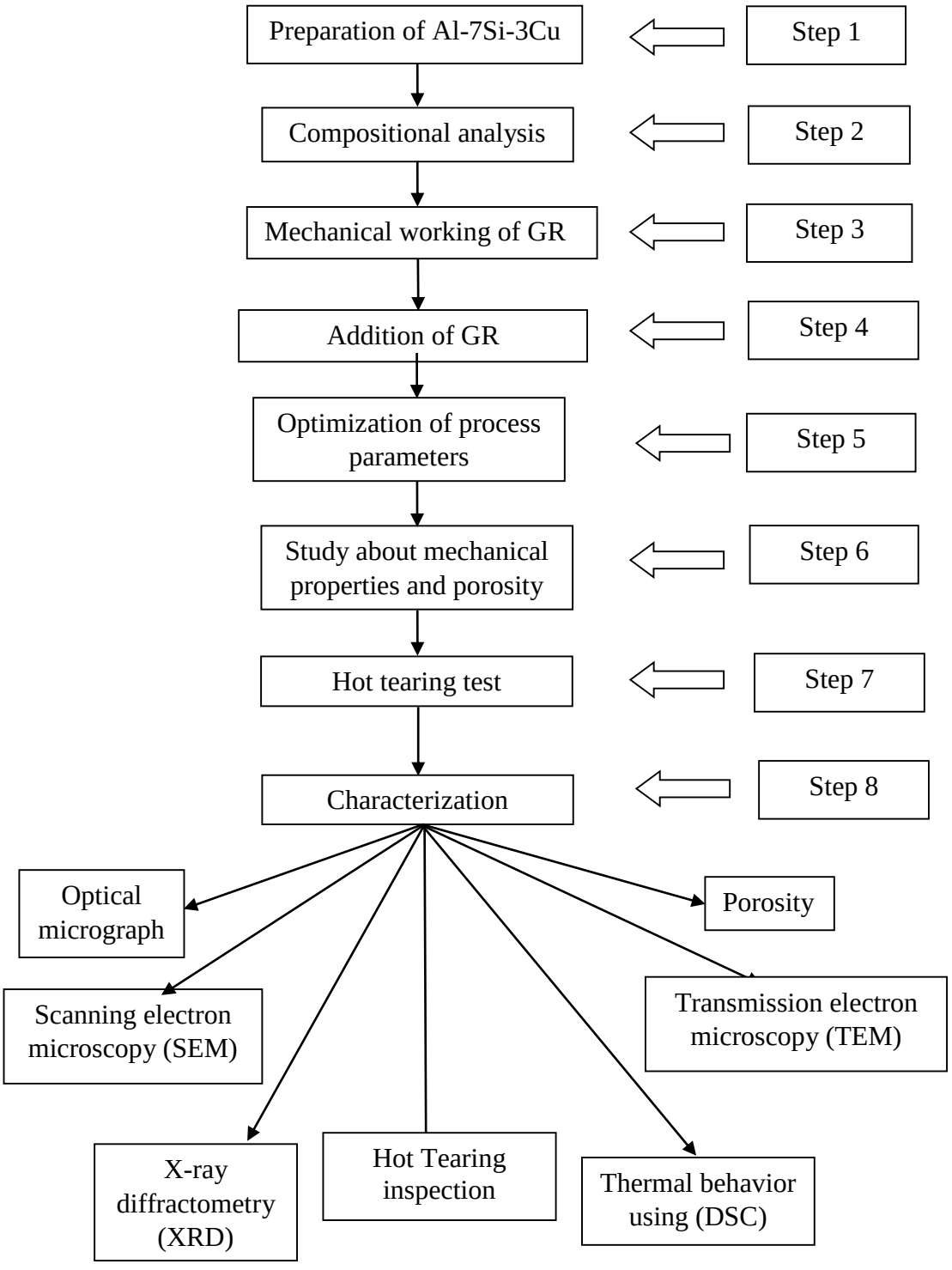

Fig.3.7 Flow chart for materials and methods used in hot tearing test method.

4 Chapter Four

Results and Discussion

Effect of Grain Refiner on Microstructure and Mechanical Properties

This chapter presents a study the effect of grain refiner on microstructure and mechanical properties in Al-7Si-3Cu alloy. Study on the role of ball milling, annealing, and hot rolling of Al-5Ti-1B master alloy on the grain refining performance and mechanical properties have been carried out. The studies have been divided into three parts. Part 1 deals with the effect of various treatments on the master alloy. Part 2 deals with grain refining performance of master alloy in Al-7Si-3Cu alloy. Parts 3 deals a study of mechanical properties with addition of as cast and treated master alloy under different processing conditions such as ball milling, annealing and hot rolling.

4.1 Al-5Ti-1B Master Alloy Grain refiner (GR)

4.1.1 XRD analysis of Al-5Ti-1B master alloy

The XRD patterns for as received Al-5Ti-1B master alloy grain refiner is shown in Fig. 4.1.

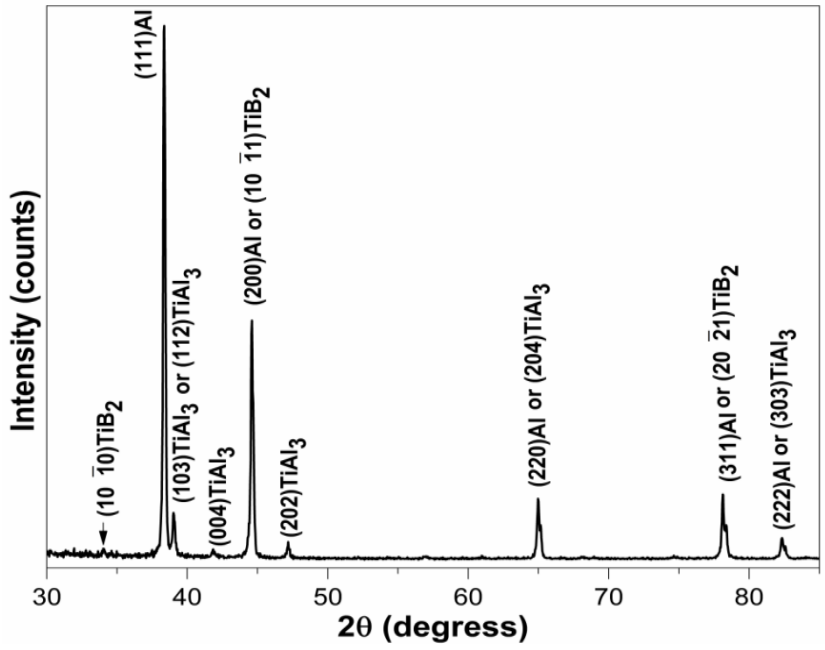

Fig 4.1 XRD analysis of Al-5Ti-1B master alloy

The XRD analysis revealed the presence of $TiAl_3$ phase with a tetragonal crystal structure (JCPDF No. 01-072-5006), TiB_2 phase with a hexagonal crystal structure (HCP) (JCPDF No. 01-085-2084) and α-Al phase with a face-centered cubic (FCC) crystal structure (JCPDF No. 00-004-0787) but no peaks of other phases are directly seen.

4.1.2 Microstructure of Al-5Ti-1B master alloy

Optical microscopy (OM), scanning electron microscopy (SEM) and transmission electron microscopy (TEM) of the Al-5Ti-1B grain refiner was carried out to study the size, shape and distribution of the $TiAl_3$ and TiB_2 particles within the grain refiner. The EDX analysis is carried out to support the XRD results, which shows the presence of $TiAl_3$ and TiB_2 particles. Figure 4.2 shows the microstructure of the as received Al−5Ti−1B master alloy with EDS analysis. Fig.4.2 (a&b) consists blocky and needle like $TiAl_3$ particles of size 5 to 90 μm. Blocky $TiAl_3$ crystals were made in the condition of Ti supersaturated crystallization. The atom starts to form in the crystal due to the sufficient $TiAl_3$ nucleation driving force. If, Ti is in supersaturated state, then it makes fundamental equilibrium of each crystal $TiAl_3$ improves and causes enormous growth in three–dimensions. Arnberg [11] and Liu Xiangfa et al. [34] studied that the temperature of molten aluminum is consequence of morphologies of $TiAl_3$ particles in the melt. Blocky $TiAl_3$ particles are formed at low temperature (< 850 °C), and while needle plate/strip $TiAl_3$ is obtained at high melting temperature (higher than 1000 °C). An EDX analysis showed that the large particles contained Al and Ti. From Table 4.1, it can be seen that at point A in the blocky particles, the molar mass fraction of element Al is 70.34%, the molar mass fraction of element Ti is 23.31%, and the molar mass ratio between element Al and element Ti is 3.07. So these large particles were known as $TiAl_3$ and was expected because the Ti:Al ratio in the Al-5Ti-1B grain refiner is greater than 1:2 [53]. Fig. 4.2(c-e) show the EDX mapping of Al and Ti particles and shows Ti is in the center of aluminium matrix.

Table 4.1 Chemical composition of selected area of Fig. 4.2

Point No.	x(Al)/%	x(Ti)/%	x(B)/%
A	70.34	22.85	6.81

Using SEM, the accurate detection of B in small concentrations is difficult due to the low intensity of B and the limitations of EDS analysis. From earlier studies [76], it is

investigated that the TiB_2 particles are mostly very fine (0.3 µm in size or lesser) they could not be spotted in the present SEM study and hence it is thoughtful to investigate of their structures. For this point of view, TEM studies are carried out on Al-5Ti-1B master alloy sample. Therefore, to study the shape and size of TiB_2 particles TEM study was carried out. TEM analysis is also carried out to validate XRD results, which was found in Fig. 4.1. TiB_2 is a hexagonal crystal structure with lattice parameters, a = 0.3038 nm and c = 0.32392 nm (Arnberg *et al.* 1982). TiB_2 particles are submicroscopic ranging from 0.1-2.0 µm in size present in the matrix.

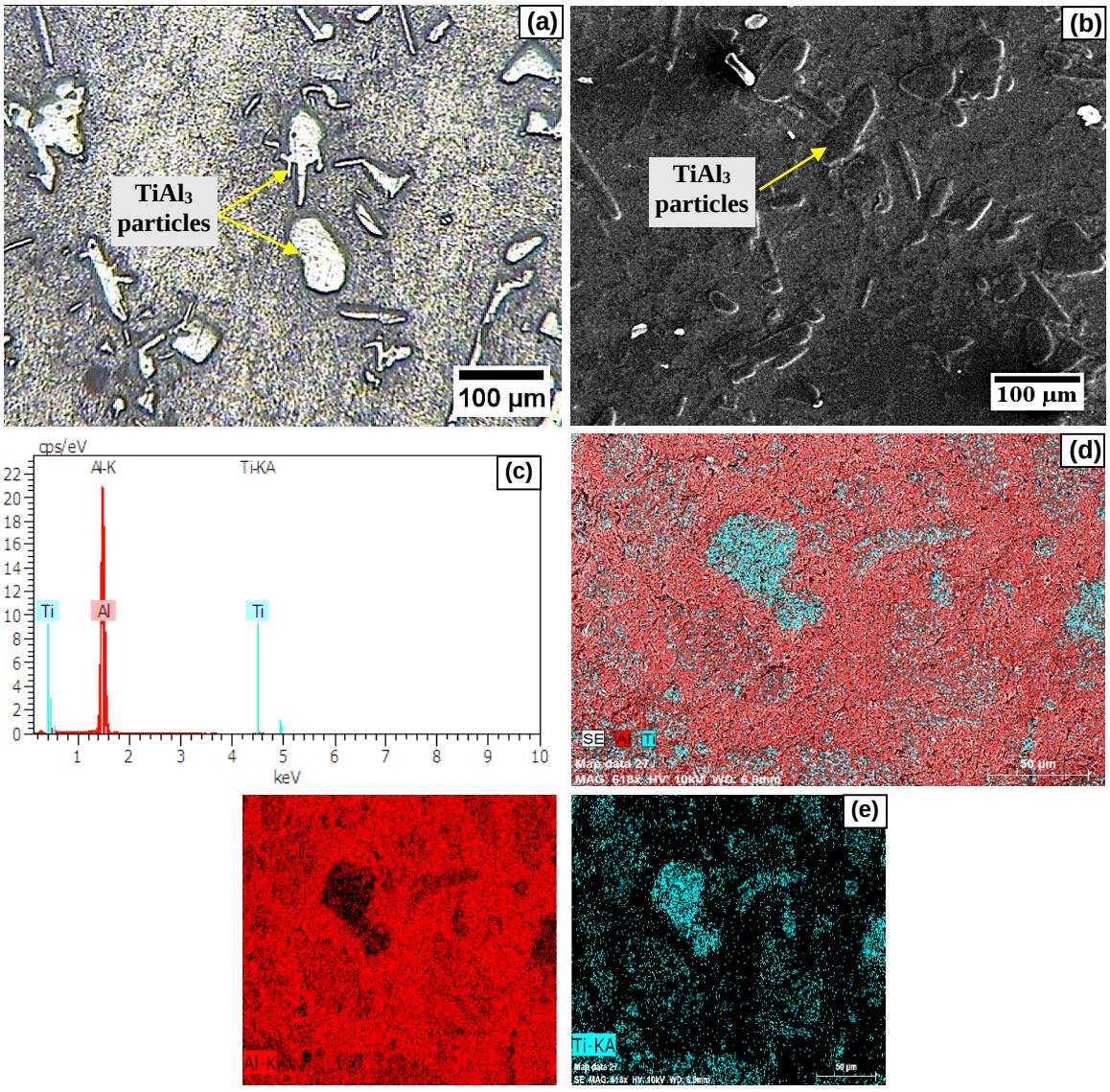

Fig 4.2 Optical microstructure of (a) Al-5Ti-1B master alloy; (b) SEM analysis of Al-5Ti-1B master alloy; (c) corresponding elemental analysis, of point A; (d) and (e) EDX mapping of corresponding area.

Figure 4.3 shows the morphology of TiB_2 particles present in the matrix of Al-5Ti-1B master alloy. It is seen from Fig. 4.3a that TiB_2 particles observed by TEM are of size from 0.2 to 0.8 µm. Fig. 4.3b shows the corresponding SAED pattern of the marked location B. The EDS analysis of the selected area (Fig. 4.3c) also confirmed the presence of boron elements. From Table 4.2, it can be seen that at point B in the small particles, the molar mass fraction of element B is 2.98%, the molar mass fraction of element Ti is 1.46 %, and the molar mass ratio between element B and element Ti is 2.04. The Table 4.2 shows the chemical composition of selected area of Fig.4.3.

Table 4.2 Chemical composition of selected area of Fig. 4.3

Point No.	x(Al)/%	x(Ti)/%	x(B)/%
A	95.44	1.46	2.98

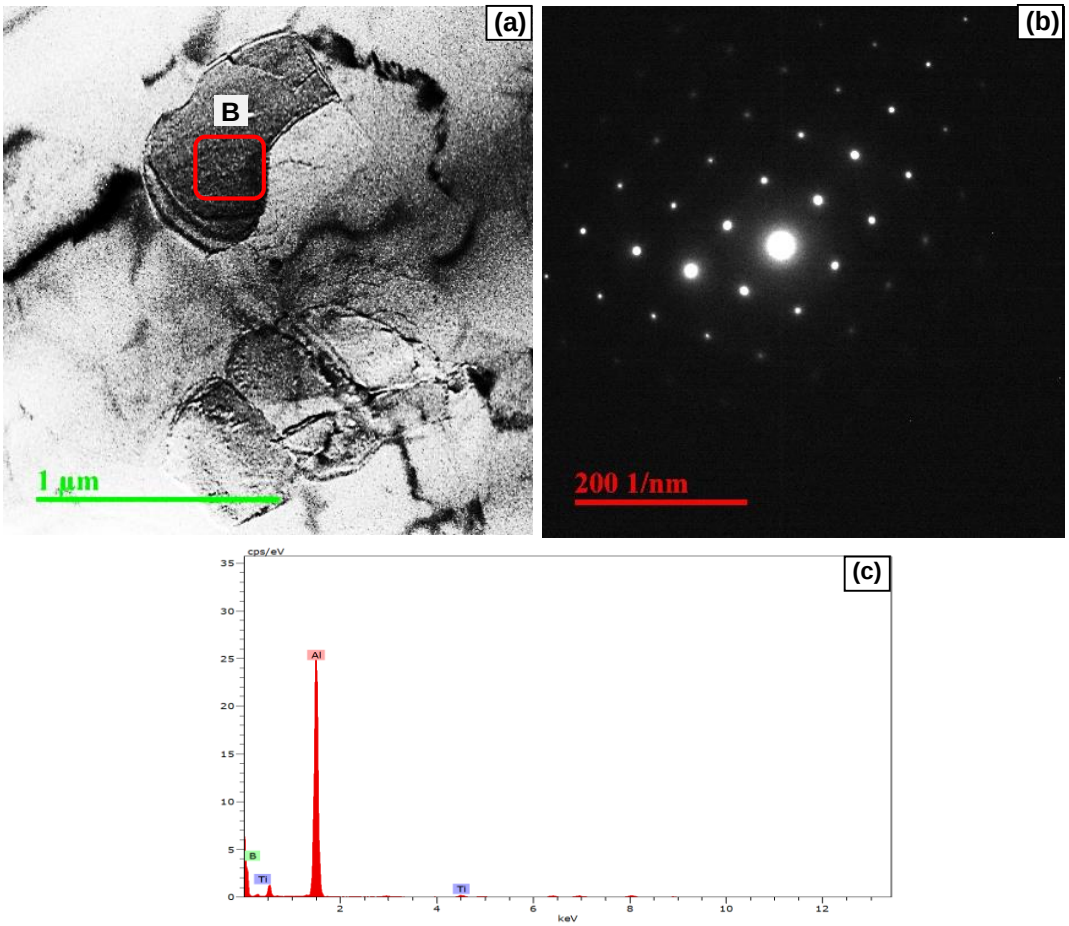

Fig 4.3 TEM analysis of Al-5Ti-1B master alloy (a) Presence of TiB_2 particles; (b) corresponding SAED pattern; (c) corresponding elemental analysis, of point B.

The $TiAl_3$ and TiB_2 particles exhibits a particular orientational relationship with α-Al phase, along which the grain refinement occurs having minimum lattice mismatch. The lattice mismatch for $(110)_{Al}$ // $(110)_{TiAl_3}$ and $(001)_{Al}$ // $(001)_{TiAl_3}$ is substantially greater than for$(111)_{Al}$ // $(111)_{TiAl_3}$. The elastic energy associated with the lattice mismatch will thus be greater for $(110)_{Al}$ // $(110)_{TiAl_3}$ and $(001)_{Al}$ // $(001)_{TiAl_3}$ than for $(110)_{Al}$ // $(111)_{TiAl_3}$. Similarly, the lattice mismatch for $(111)_{Al}$ // $(10\bar{1}1)_{TiB_2}$ is greater than for $(110)_{Al}$ // $(10\bar{1}1)_{TiB_2}$. This, inturn, will restrict any growth on the (110), (001) and (111) surfaces [76]. The optical, XRD and TEM studies of Al-5Ti-1B master alloy show that it contains $TiAl_3$ and TiB_2 particles which act as heterogeneous nucleating sites.

4.2 Ball milling, Annealing and Hot Rolling of Al-5Ti-1B Master Alloy

From the earlier studies it has been observed that ball milling, annealing and hot rolling improve the grain refining efficiency of the Al-Ti, Al-Ti-B and Al-Ti-C types of master alloy.

4.2.1 Ball milling of Al-5Ti-1B master alloy

The as received Al–5Ti–1B master alloy was ball milled at 10h, 30h and 50h to improve its grain refining efficiency. The ball milling was results as the fracture of $TiAl_3$ particles. Higher milling time produces more fracture of the $TiAl_3$ particles. Thus by milling techniques the number of effective nucleating sites for Al-7Si-3Cu alloy is increased.

4.2.1.1 SEM study of ball milled master alloy

Figures 4.4 (a-c) show the morphology of ball milled powder after 10h, 30h and 50h, Al-5Ti-1B grain refiner respectively. From Fig. 4.4b and Fig. 4.4c, it is clearly observed that the $TiAl_3$ particles fragmented after 30h and 50h milling, which leads more number of heterogeneous particles. This improved Al-5Ti-1B master alloy grain refiner efficiency. Table 4.3 shows the mean particle size of nucleating particles of as cast and after ball milling 10h, 30h and 50h respectively.

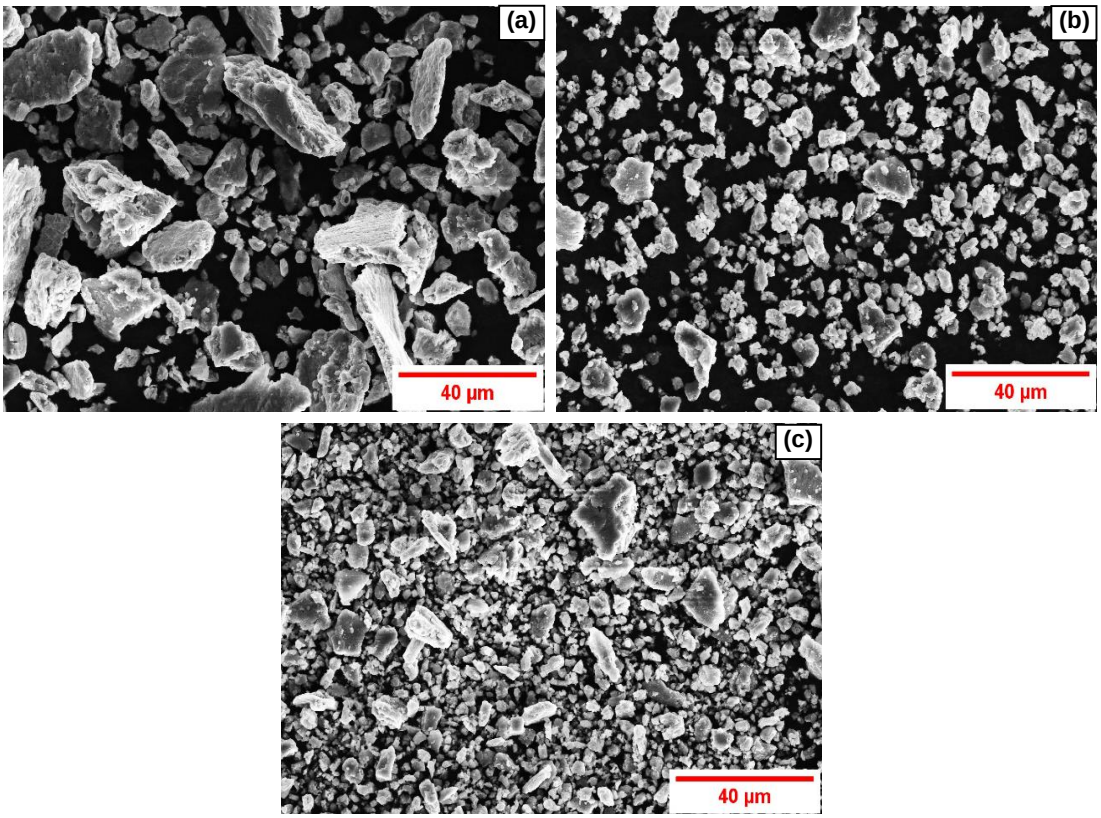

Fig 4.4 SEM analysis of ball milled master alloy (a) 10h; (b) 30h; and (c) 50h.

4.2.1.2 XRD study of ball milled master alloy

Figure 4.5 shows the XRD analysis of as cast, ball milled 10h, 30h and 50h Al-5Ti-1B grain refiner respectively. This analysis confirmed the presence of Al, TiB_2, and $TiAl_3$ phase. $TiAl_3$ phase is a tetragonal crystal structure (JCPDF No. 01-072-5006), TiB_2 phase a hexagonal crystal structure (HCP) (JCPDF No. 01-085-2084) and α-Al phase a face-centered cubic (FCC) crystal structure (JCPDF No. 00-004-0787). This results clearly indicate that as ball milled time is increased the relative intensity of $TiAl_3$ particle is increased. Furthermore, the Fig. 4.6 illustrates the size of $TiAl_3$ particles after ball milling which is measured by particle size analyzer. This figure displays that as ball milling time is increased the average diameter of heterogeneous nucleation particles is decreased from 54.2 µm to 9 µm.

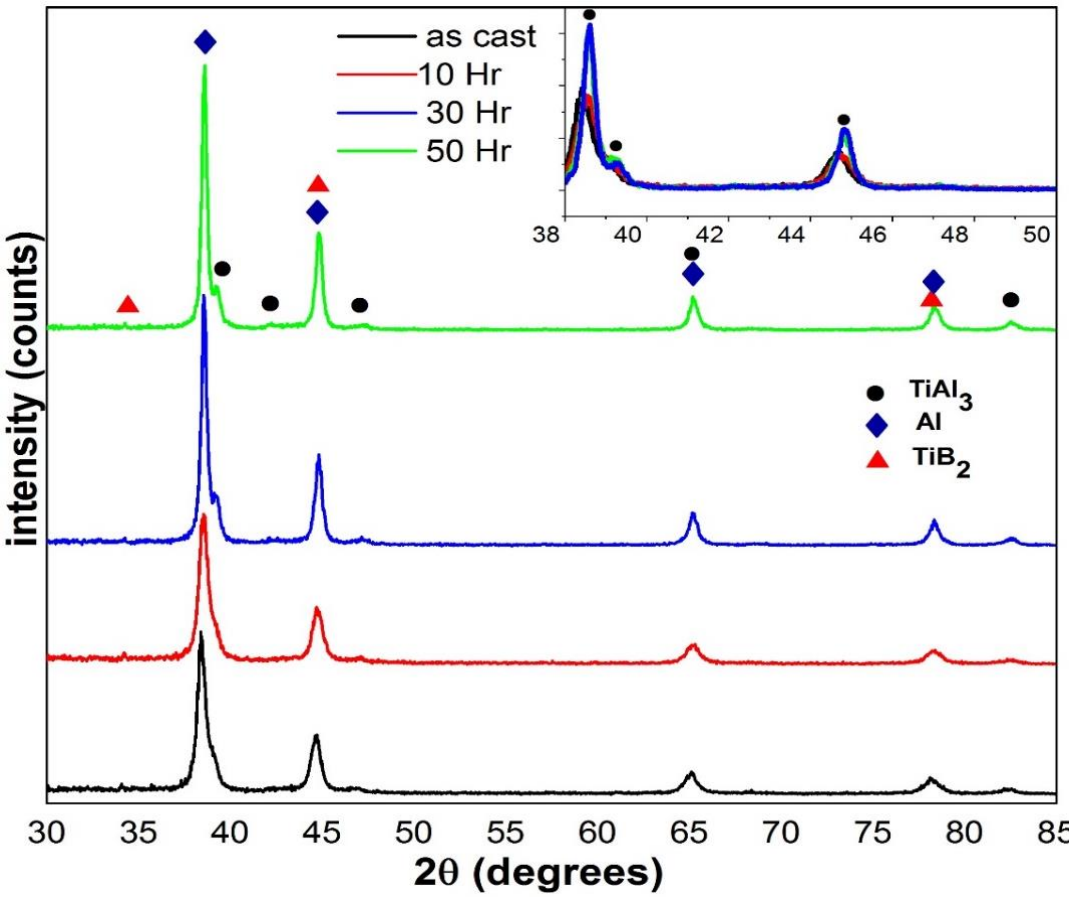

Fig 4.5 XRD analysis of ball milled master alloy (a) as cast; (b) 10h; (c) 30h; and (d) 50h.

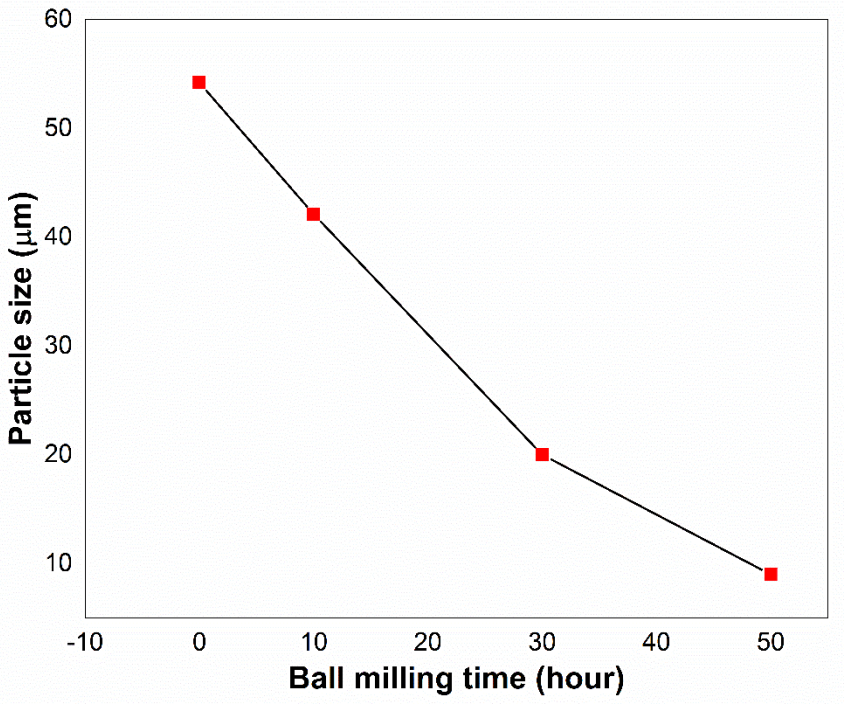

Fig 4.6 $TiAl_3$ particles diameter vs. ball milled time (hour).

4.2.2 Annealing of Al-5Ti-1B master alloy

As cast master alloy was annealed at 400 ºC, 500 ºC, 600 ºC, 700 ºC and 800 ºC for 8 hours to improve its grain refining efficiency. Annealing increases, the volume fraction of $TiAl_3$ particles resulting more heterogeneous nucleating sites present for nucleation.

4.2.2.1 Microstructure study of annealed master alloy

Figure 4.7 (a-d) show the optical microstructure of as cast and annealed Al-5Ti-1B master alloy at 500, 600 and 700 ºC. A noticeable change is observed in the morphology of $TiAl_3$ particles after annealing at 500 ºC for 8h (as shown in Fig. 4.7b). The shape of $TiAl_3$ particles changed from needle type to more globular and plate like structure. Fig. 4.7c and Fig. 4.7d show that there is no significant change in microstructure of Al-5Ti-1B master alloy after annealing at 600 ºC and 700 ºC for 8h, however more nucleating particles are formed at higher annealing temperature (Fig. 4.7d). Table 4.4 displays the mean particle size of nucleating particles of as cast and after annealing at various temperature. From the table, it is clearly observed that there is marginally change in the mean particles size.

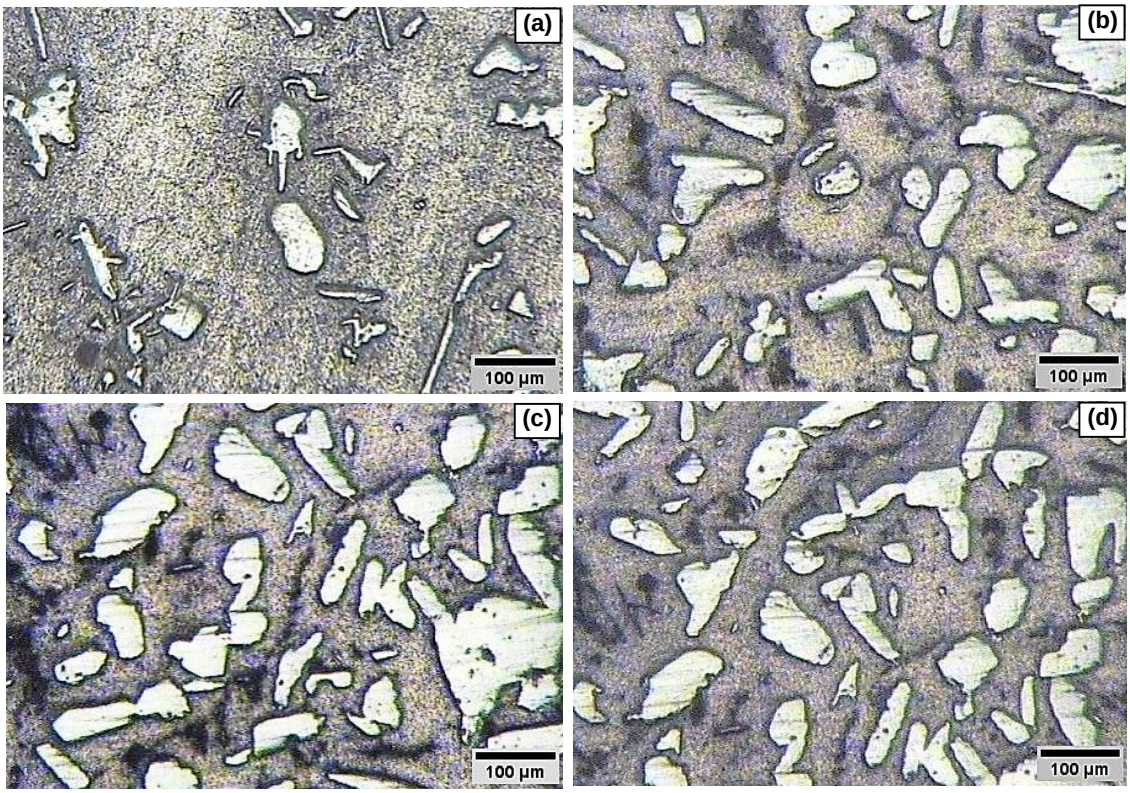

Fig 4.7 Optical microstructure of (a) as cast Al-5Ti-1B master alloy; annealed at temperatures of (b) 500; (c) 600; and (d) 700 ºC for 8 h.

However, standard deviation decreases which suggest that more number of particles are formed of same size at 700 ºC.

4.2.2.2 XRD study of annealed master alloy

The XRD patterns of the as cast Al-5Ti-1B master alloy and after annealing at 400, 500, 600 and 700°C for 8h are shown in Fig. 4.8. From this Fig. 4.8, it is observed that the relative peak intensity of $TiAl_3$ particles increased as the annealing temperature is increased. The variation of relative intensity of $TiAl_3$ peak (in percent) with annealing temperature is shown in Fig. 4.9. Actually, the highest peak relative intensity is the ratio of the intensity of the maximum intensity peak of $TiAl_3$ to that of Al.

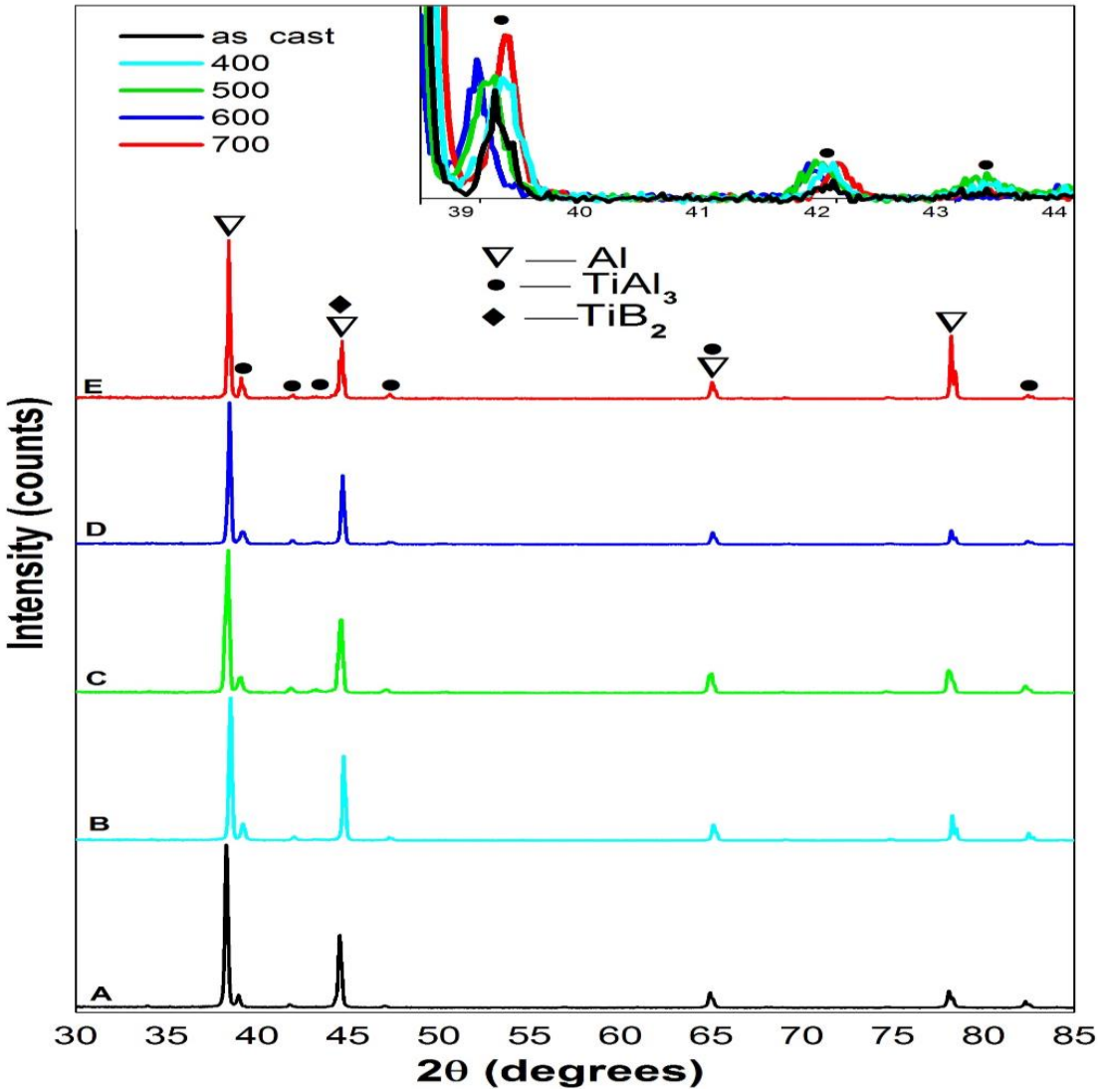

Fig 4.8 XRD analysis of Al-5Ti-1B master alloy (a) as cast grain refiner; annealed at temperatures (b) 400; (c) 500; (d) 600; and (e) 700 ºC for 8.

Higher volume fraction of $TiAl_3$ phase is confirmed by the increase in the $TiAl_3$ peak intensity with annealing temperature. The increase in the $TiAl_3$ fraction after annealing shows that the alloy does not reach equilibrium during its synthesis, wherein liquid Al is allowed to react with K_2TiF_6 and KBF_4. During this reaction, the liquid metal is enriched in Ti from which $TiAl_3$ particles are precipitated. It appears that the precipitation of $TiAl_3$ is not completed during the above reaction and α-Al probably remained in a supersaturated state. Further precipitation of the present $TiAl_3$ particles was due to the sufficient thermal activation energy supplied during annealing. Thus total Ti content in a master alloy is decreased by annealing process and larger fraction of $TiAl_3$ phase is formed at higher annealing temperature. So, the higher fraction of $TiAl_3$ particles at the higher annealing temperature may be ascribed to faster diffusion.

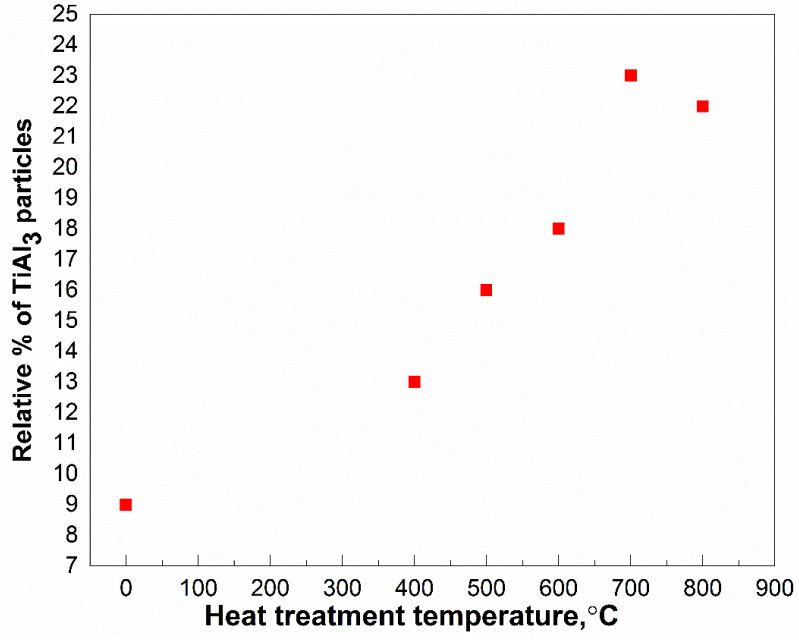

Fig 4.9 Relative percentage of $TiAl_3$ vs. annealing temperature (0 temperature refers to as cast master alloy)

Figures 4.10 (a-f) show the SEM micrographs of Al−5Ti−1B master alloy annealed at 800 °C for 8h. According to Fig. 4.10a and Fig. 4.10b, it can be observed that blocky $TiAl_3$ and TiB_2 particles got segregated to lower region while needle like $TiAl_3$ particles stayed in the upper region of the sample. No blocky particles were observed in the upper region (Fig. 4.10b). Fig. 4.10c shows the microstructure of segregated region where blocky $TiAl_3$ particles are observed with TiB_2 particles. Fig. 4.10d shows the microstructure of segregated region at higher magnification for better understanding of the morphology of nucleating particles in this region. Where, cuboidal rounded TiB_2 particles are observed. The annealing of Al-5Ti-1B was corresponding to the liquid-solid two-phase region and

$TiAl_3$ and TiB_2 particles got segregated at the bottom region due to gravity segregation effect. In the upper part of the sample, acicular particles are flocked; while in the bottom

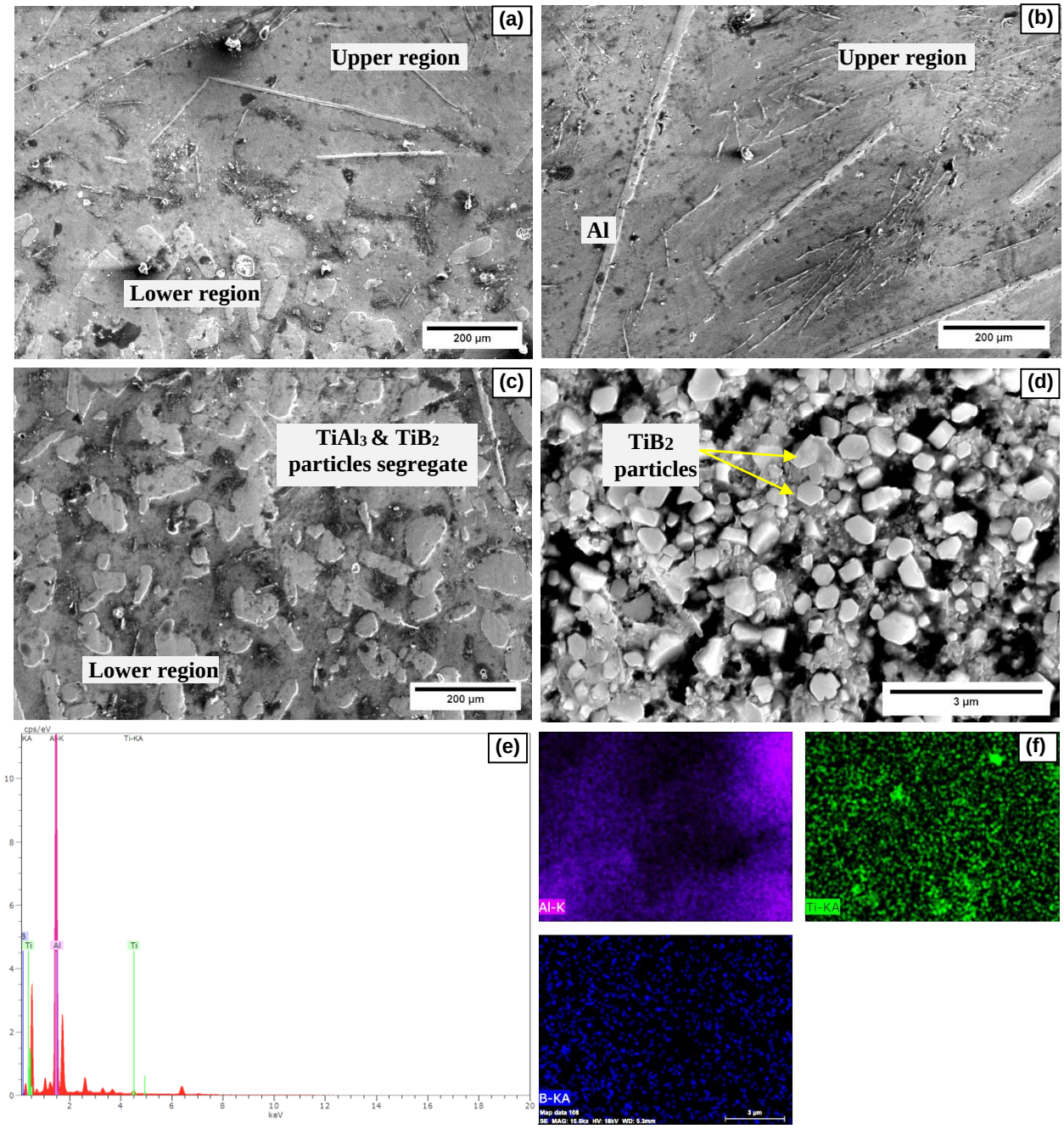

Fig 4.10 SEM analysis of 8 hours annealed sample at 800 ºC, (a) annealed sample; (b) upper region of annealed sample; (c) lower region of annealed sample; (d) SEM micrograph from lower section of annealed alloy showing bimodal particle size distribution at higher magnification; and (e-f) there corresponding elemental analysis and mapping.

region, the aggregation of blocky particles occurs. In accordance with EDS (Energy Dispersive Spectrometer) spectra analysis with mapping of the lower region as shown in

Fig. 4.10 (e-f) confirm the existence of Al, Ti and B particles as dark and white substrates respectively. The elemental analysis demonstrated the results, which consists only Ti, B and Al peak. This confirmed the presence of nucleating TiB_2 particles in this region. Furthermore, elemental mapping of lower region has been carried out which illustrated that titanium is situated along the aluminium matrix and uniformly distributed throughout the matrix. Where, lower region consists TiB_2 and $TiAl_3$ particles [158]. Accordingly, it is understood that TiB_2 and $TiAl_3$ particles isolated into the lower and upper region during the heating operation, respectively. However, XRD analysis of the lower region also confirms the presence of TiB_2 particles which are coarsened and finer in size respectively.

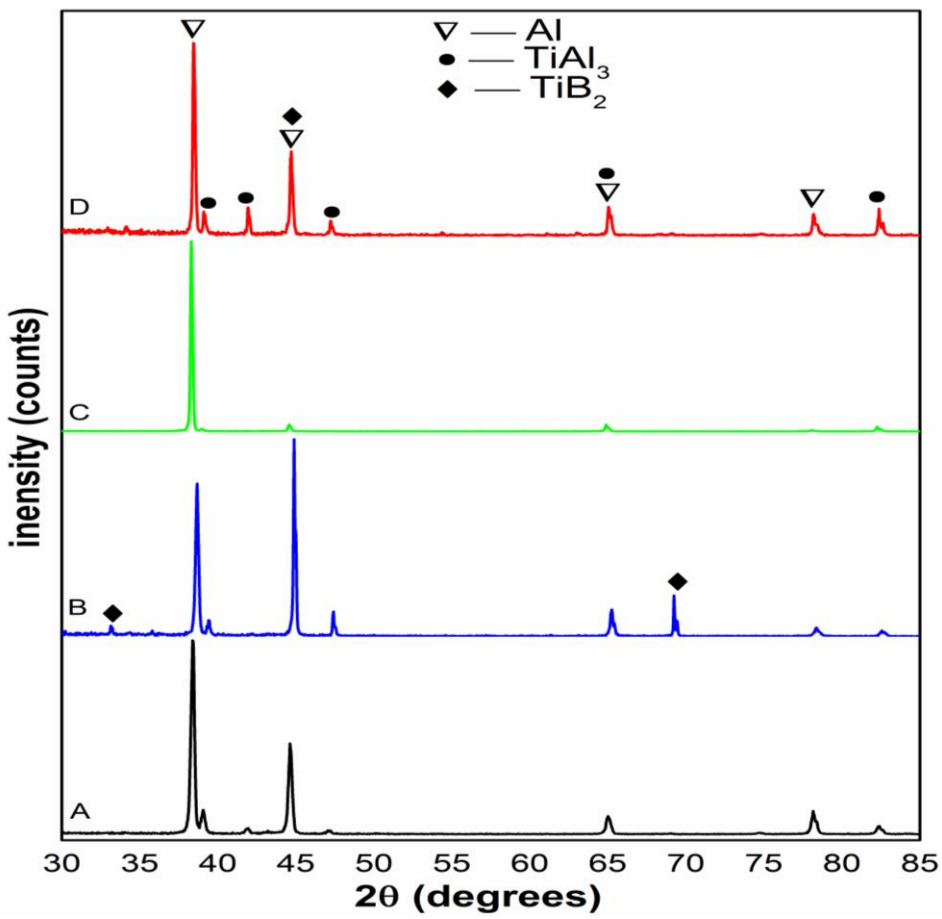

Fig 4.11 XRD analysis of Al-5Ti-1B master alloy (a) as cast Al-5Ti-1B; (b) 8 hours annealed at 800 ºC; (c) upper part of annealed sample; and (d) lower part of annealed sample.

4.2.3 Hot rolling of Al-5Ti-1B master alloy

As received Al–5Ti–1B master alloy was hot rolled at 250 ºC and 350 ºC to enhance its grain refining potency. The three reduction levels were taken; 25%, 50% and 75% to fracture the $TiAl_3$ particles. Higher reduction level produces a lot of fracture of the $TiAl_3$

particles, so increasing the number of effective nucleating sites for Al-7Si-3Cu alloy. The amount of rolling required to attain improved grain refinement decreases with increase in rolling temperature.

4.2.3.1 SEM study of hot rolled master alloy

Figures 4.12 (a-g) display the SEM results of hot rolled samples at 250 ºC and 350 ºC, respectively. SEM images of the samples were acquired with secondary electrons in order to obtain better contrast. Fig. 4.12a, Fig. 4.12c and Fig. 4.12e show the morphology of hot rolled samples at 250ºC. Fig. 4.12b, Fig. 4.12d and Fig. 4.12f show the morphology of hot rolled samples at 350 ºC. It is observed from the SEM micrographs (Fig. 4.12a) of 25% reduction level that mean particle size reduced up to 32.1 µm from 54.2 µm, at 250˚C temperature. However, the mean particles size at 350 ºC is bigger than former (36.8 µm). The mean particles size of $TiAl_3$ are observed 22.2 µm and 15.0 µm, at 50% and 75% reduction level (at, 250 ºC), respectively. However, the mean particle size reached up to 23.9 µm and 17.3 µm, at 50% and 75% reduction level (at, 350 ºC), respectively. It is seen that fracture at 250 ºC is a larger at same reduction level to their respective samples hot rolled at 350 ºC. Subsequently, it is found that as reduction level is increased the mean particles size is decreased at both rolling temperatures, due to fracture of larger $TiAl_3$ particles. Higher stress concentration on particle matrix interface resulting the fracture of $TiAl_3$ particles. From the SEM investigation it is seen clearly that mean particle size of $TiAl_3$ is decreased due to fracture of these brittle intermetallic particles (Fig. 4.12g). The Fig. 4.12g shows the magnified view of Fig. 4.12c, which confirmed the breakdown of $TiAl_3$ particles during hot rolling. Larger particle broke into three or more smaller particles. At lower rolling temperature (250 ºC) the stress concentration is likely to be higher in comparison to 350 ºC and the particles are likely to be more brittle causing wide fracture of these particles as the rolling temperature is decreased. The particle size of hot rolled samples are given in Table in appendix 4, along with those of the as cast alloy. In each case 120 particles have been examined. The results clearly display that as the reduction level is increased the mean particle size is decreased and vice versa (Fig. 4.13).

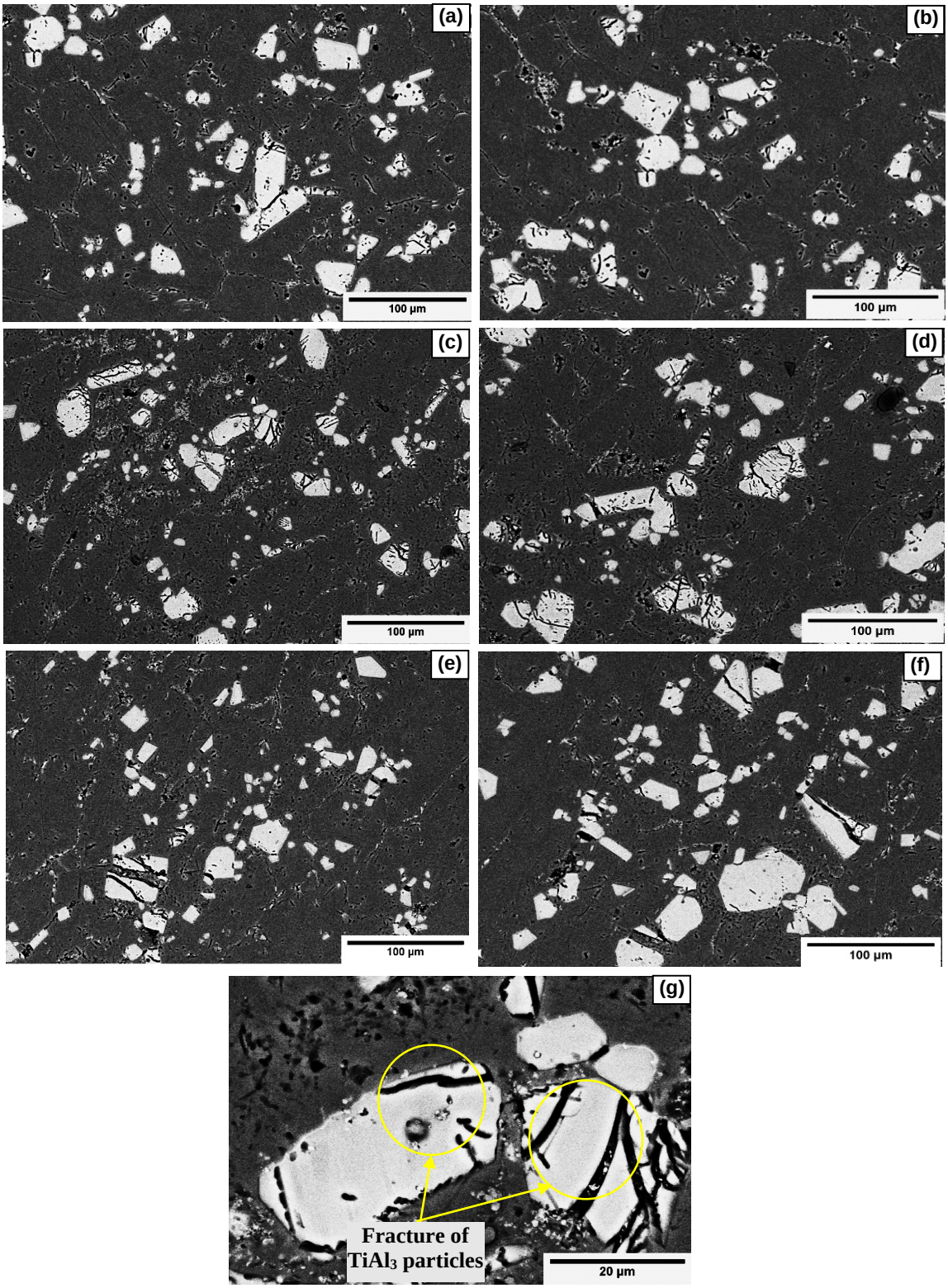

Fig 4.12 SEM micrographs of Al-5Ti-1B master alloy at different rolling reduction levels of (a), (c) and (e) 25, 50 and 75% reduction level at 250 °C, (b), (d)and (f) 25, 50 and 75% reduction level at 350 °C, and (g) fracture of $TiAl_3$ particles in Al–5Ti–1B master alloys at 250 °C, 50% reduction.

The table also provides the results of standard deviation on the mean particle size, which is quite large, instructing that particles differ extensively in their size. The number of particles below 25 µm also greater than before which was at initial reduction level (Table, appendix 4).

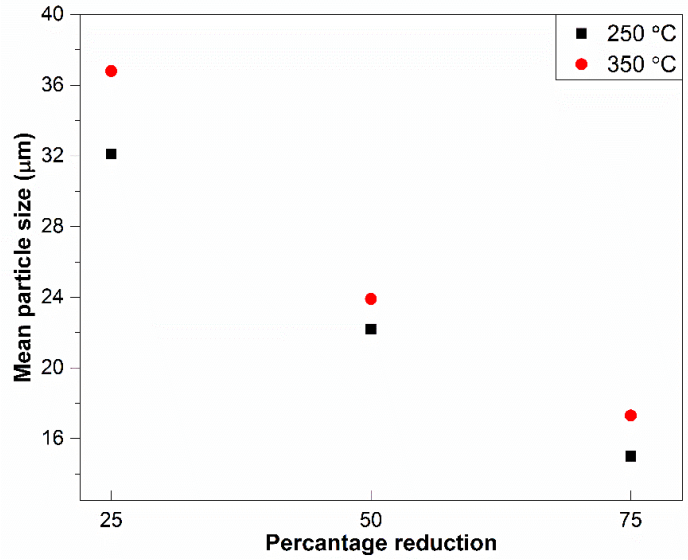

Fig 4.13 Mean particle size vs. percent reduction of Al-5Ti-1B master alloy at 250 and 350 °C temperatures.

4.2.3.2 XRD study of hot rolled master alloy

The XRD patterns of the Al-5Ti-1B master alloy after hot rolling at 250 °C for 25%, 50% and after 75% reduction level is shown in Fig. 4.14.

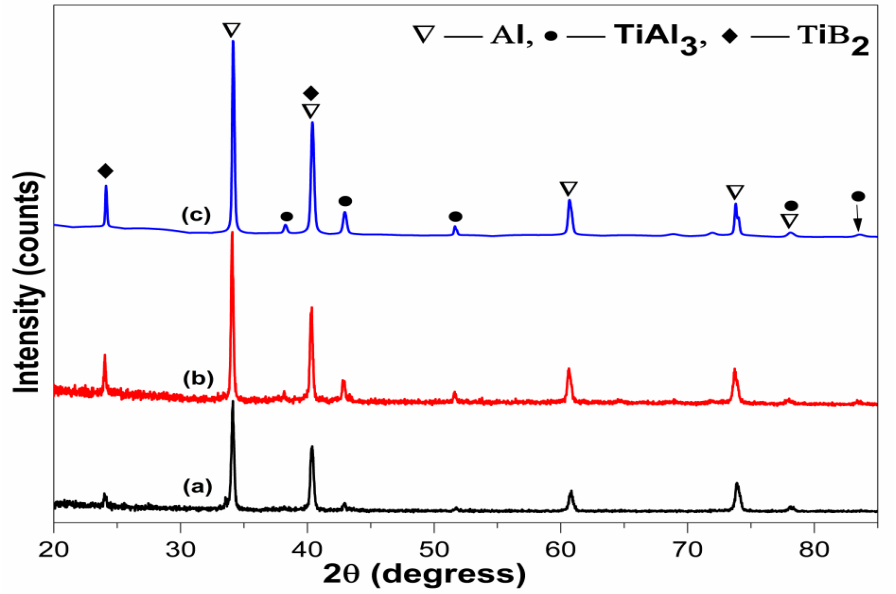

Fig 4.14 XRD analysis of Al-5Ti-1B master alloy at 250 ºC (a) 25; (b) 50; and (c) 75 % reduction.

From the XRD pattern it is observed that the relative peak intensity of $TiAl_3$ particles increases with reduction level. Fig. 4.14a illustrates that Al-5Ti-1B master alloy consists of TiB_2, $TiAl_3$ and Al peak of lower intensity at lower reduction level (at, 25%). While at 50% reduction level the intensity of $TiAl_3$ and TiB_2 peak increased (Fig. 14.4b). Fig. 4.14c confirmed the higher intensity phase of $TiAl_3$ with 75% reduction level and some new $TiAl_3$ phase was also observed.

4.3 Optimization of Grain Refiner in Al-7Si-3Cu Alloy

The grain morphology (microstructure) of the Al-7Si-3Cu alloy samples was analyzed to confirm the effect of grain refinement with addition of Ti. The results are presented in Figures 4.15 to 4.24.

4.3.1 Addition of cast Al-5Ti-1B master alloy

Figure 4.15 (a-d) show the optical microstructure of as cast and grain refined Al-7Si-3Cu alloy. The Fig. 4.15a shows the coarser α-Al dendrites structure. Addition of grain refiner has refined the α-Al dendrites as seen in Fig. 4.15b.

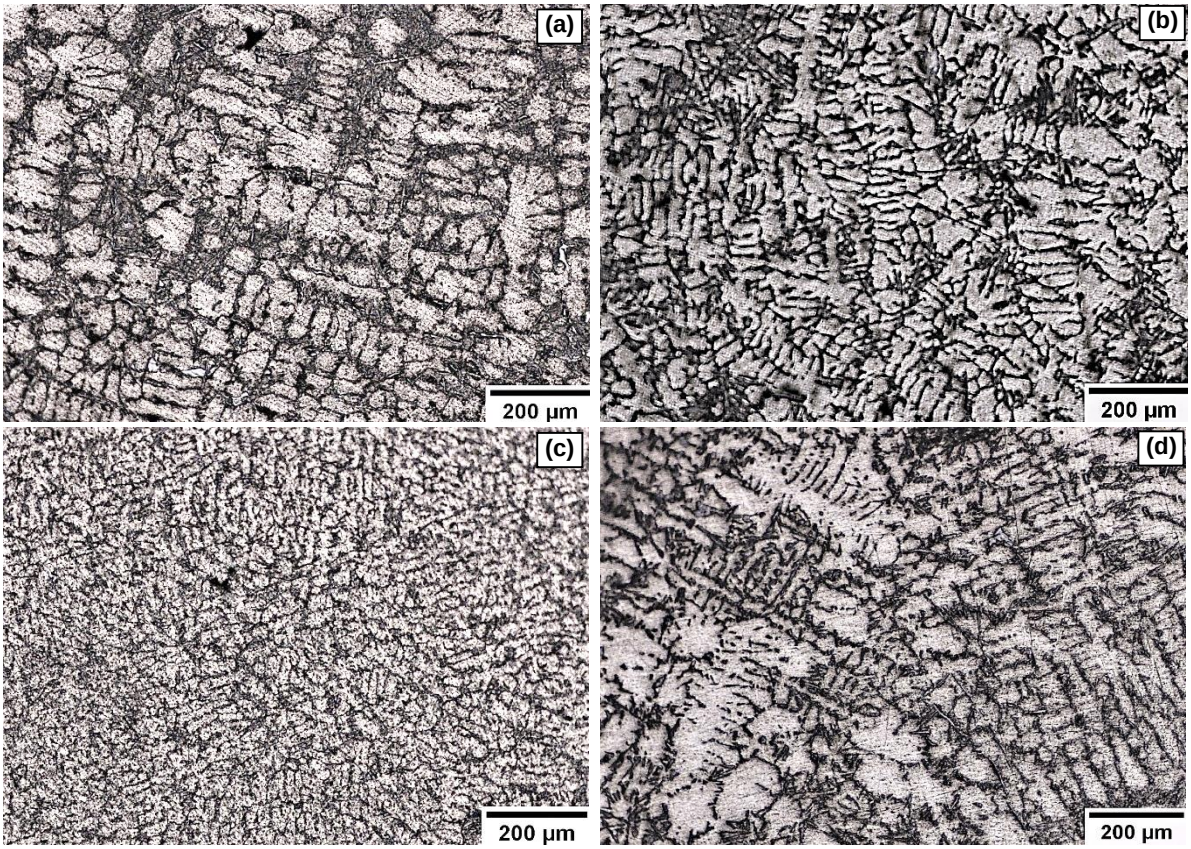

Fig 4.15 Optical microstructure of cast Al-7Si-3Cu alloy inoculated with Al−5Ti−1B master alloy at different wt.% Ti (a) 0; (b) 0.045; (c) 0.050; and (d) 0.055.

However, the grain refinement effect is minor at 0.045 wt.% Ti addition level and is increase further with increase in weight percent (Fig. 4.15c). It is observed that as the wt.% addition of grain refiner increased upto (0.05 wt.% Ti), the size of α-Al phase decreased upto 230 μm. Increasing the Ti addition rate does two things: it improves the grain refining efficiency and reduces the loss of grain refining effect with time i.e. the so called fade effect (Fig. 4.15d). There is hardly any fading effect with very fine grains retained at 10 min after inoculation at this Ti level. Furthermore, at addition level of 0.055 wt.% Ti, the size of α-Al phase is further increased. This is attributed to the formation of Ti_5Si_3 phase with more than 6 wt.% Si in presence of higher Ti level.

4.3.2 Addition of ball milled Al-5Ti-1B master alloy

Figures 4.16-4.18 show the microstructures of cast Al-7Si-3Cu alloy inoculated with ball milled (10h, 30h and 50h) Al−5Ti−1B master alloy with different mass fractions. In comparison with the as-received master alloy, the ball milled master alloy shows the enhanced grain refinement. It is seen that Fig. 4.16a consists coarser structure at 0.040 wt.% Ti, but these are finer in comparison to as cast alloy. When the amount is slightly increased upto 0.045 wt.% Ti, the structure becomes less coarse (Fig. 4.16b). Fig. 4.16c displays the most grain refine structure is obtained at 0.050 wt.% Ti.

The microstructural investigations show that at lower addition level of grain refiner (30h ball milled) fine dendritic structure was obtained for Al-7Si-3Cu alloy (Fig. 4.17a and Fig. 4.17b), in comparison to past alloy. It is seen that from the Fig. 4.17c as mass fraction of Ti is increased up to 0.050 wt.%, the grain structure is changed from dendritic columnar to Equiaxed dendritic grain structures. Further addition level of grain refiner is not required because it shows no further refinement in grain structure. The morphology, size and type of particles are important too.

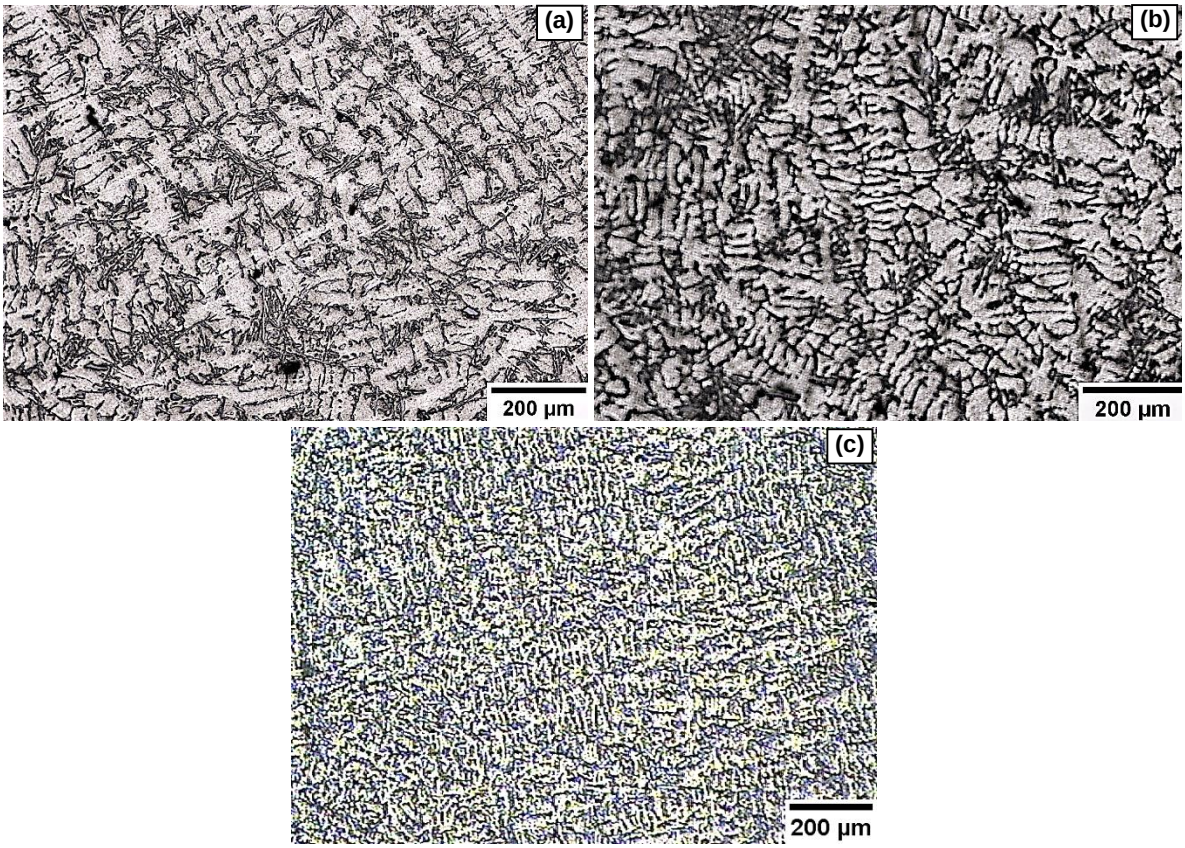

Fig 4.16 Optical microstructure of cast Al-7Si-3Cu alloy inoculated with 10h ball milled Al−5Ti−1B master alloy at different wt.% Ti (a) 0.040; (b) 0.045; and (c) 0.050.

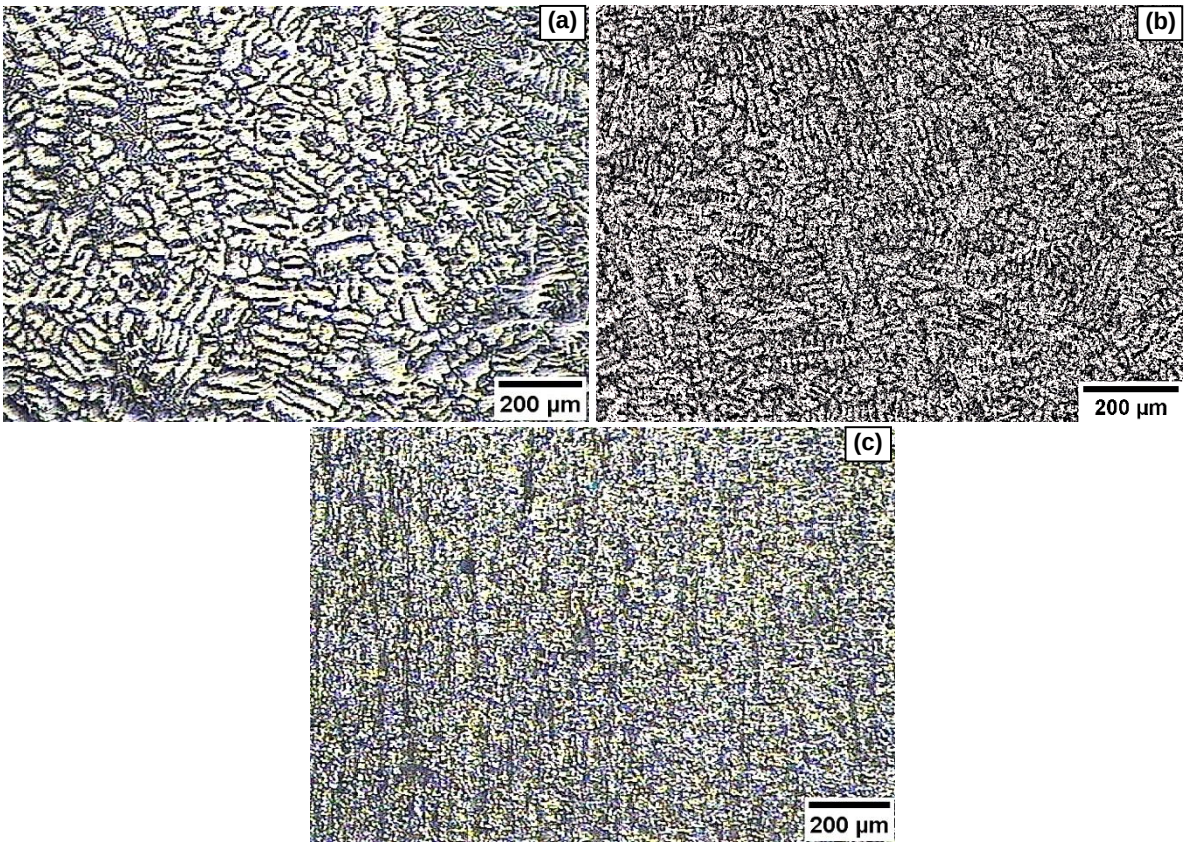

Fig 4.17 Optical microstructure of cast Al-7Si-3Cu alloy inoculated with 30h ball milled Al−5Ti−1B master alloy at different wt.% Ti (a) 0.040; (b) 0.045; and (c) 0.050.

The nucleation potential of $TiAl_3$ particles is better than that of TiB_2 particles, but the presence of TiB_2 particles improves the grain refinement efficiency. It can be contributed to increasing the nucleation sites, preventing the dissolution of boron in the melt and the very high segregating power of Ti. Ti segregates to the nucleant–liquid interface, which leads to constitutional super-cooling, and other nucleant particles get activated for the nucleation.

In continued studies, the effects of different additions of Al–5Ti-1B master alloy on grain size of solidified Al-7Si-3Cu alloy sample were detected (Figures 4.18 a–c). Even at lower addition level of 0.040 wt.%, Ti the alloy shows grain refinement as shown in Fig. 4.18a. With increasing addition level to 0.045 wt.%, and 0.050 wt.%, there is clear evidence of change on the equiaxed grain size (Fig. 18b- Fig.18c). However, as seen in Fig. 4.18b and Fig. 4.18c, Al–5Ti-1B master alloy (50h ball milled) clearly has similar refining efficiency as after addition (30h ball milled) Al–5Ti-1B master alloys when including same content of Al–5Ti-1B master alloy. It could be clearly seen that, when the addition level of Al–5Ti-1B master alloy is 0.045 wt.%, they showed increased grain refining behavior and the average grain size is decreased up to 220 μm.

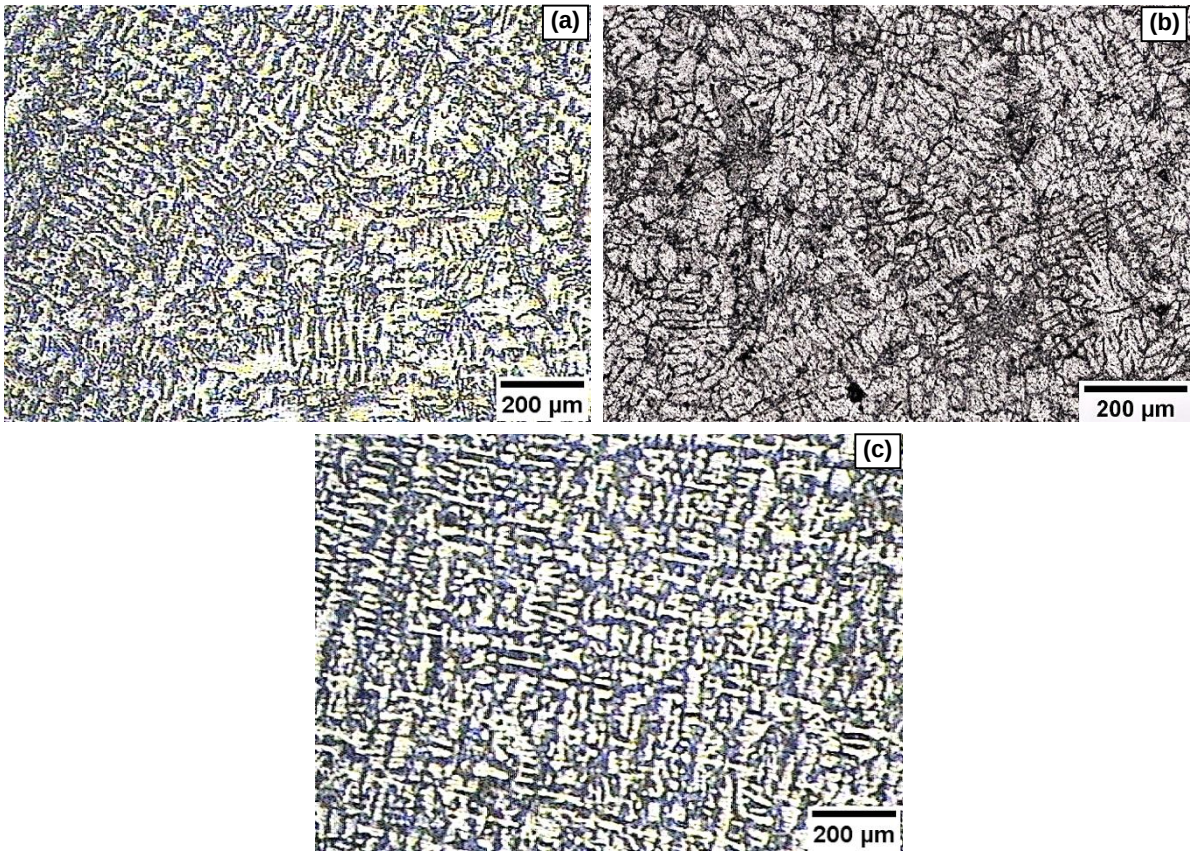

Fig 4.18 Optical microstructure of cast Al-7Si-3Cu alloy inoculated with 50h ball milled Al−5Ti−1B master alloy at different wt.% Ti (a) 0.040; (b) 0.045; and (c) 0.050.

It is seen that after addition of 50h ball milled grain refiner, the finer grains observed only at higher addition level, 0.050 wt.% Ti (Fig. 4.18c). Lower addition level of grain refiner was not able to produce fine grains it may be due to the agglomeration of nucleating particles. After, 50h of ball milling it consists more number of particles with smaller size. These small particles dissolve rapidly into the melt.

4.3.3 Addition of annealed Al-5Ti-1B master alloy

The microstructure of Al-7Si-3Cu alloy, grain refined with Al-5Ti-1B master alloy heat-treated at 500 ºC, 600 ºC and 700 ºC for 8 h showed a change in the macrostructure from columnar grain structure to a mixture of fine columnar and coarse equiaxed grain structure within 10 min of holding. Increased addition level had shown continuous improvement in the grain refinement.

Figures 4.19 (a-c) display the optical microstructure of cast Al-7Si-3Cu alloy and with addition of annealed (at, 500 ºC) Al-5Ti-1B master alloy. It is seen that Fig. 4.19a and Fig.4.19b, exhibit coarser structure in comparison to Fig. 4.19c, it may be due to the inadequate potency of $TiAl_3$ particles at this addition level.

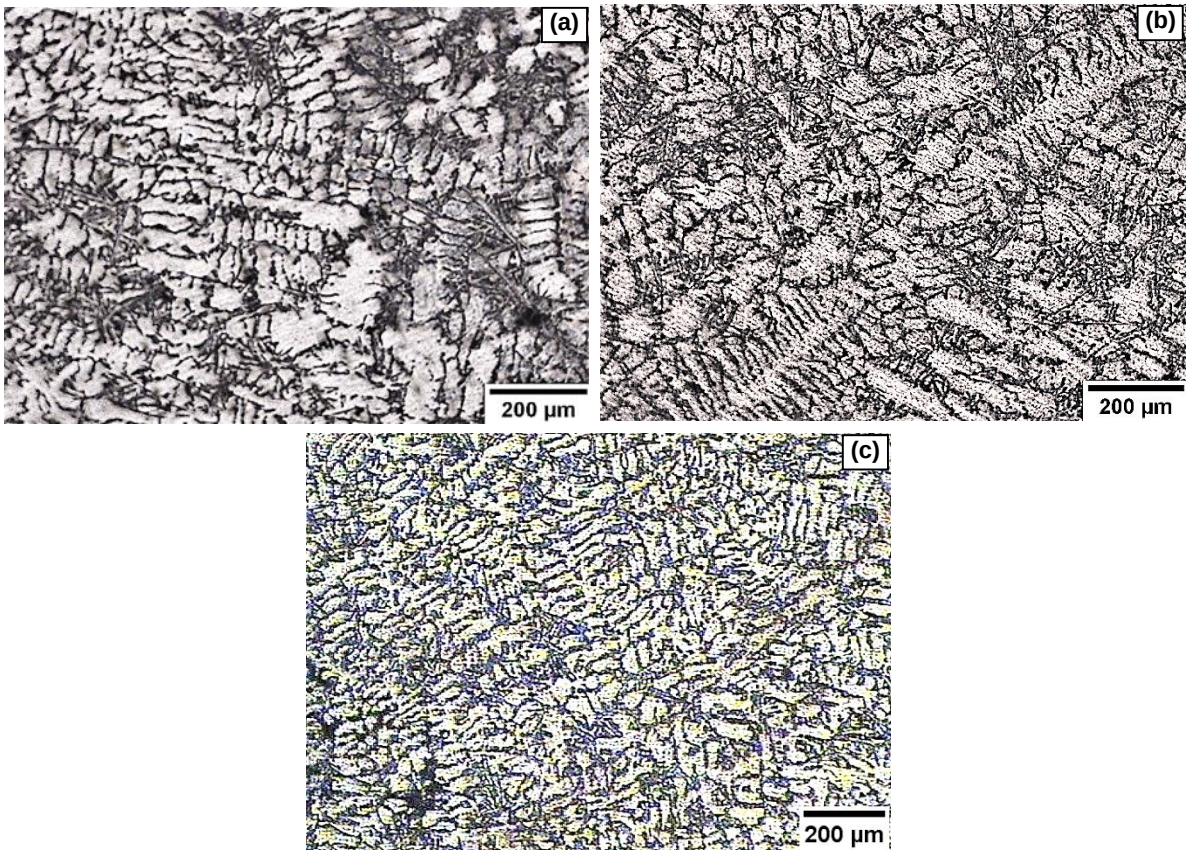

Fig 4.19 Optical microstructure of cast Al-7Si-3Cu alloy inoculated with annealed (500 ºC) Al−5Ti−1B master alloy at different wt.% Ti (a) 0.035; (b) 0.040; and (c) 0.045.

It is observed that annealed grain refiner showed better response towards grain refinement in Al-7Si-3Cu alloy. It is observed that as annealing temperature is increased, the grain refining efficiency is also increased at same addition level. However, this addition level has no significant changes in the microstructures as shown in Fig. 4.20 (a-c) as comparison to Fig. 4.19 (a-c). Beyond which at, the grain refining efficiency of master alloy seemed to be similar to that at 600 ºC, excepting that the grain structure seemed to be finer for the Al-7Si-3Cu grain refined alloy with master alloys heat-treated at higher temperatures.

Fig. 4.21 (a-c) show the optical microstructure of Al-7Si-3Cu alloy with addition annealed grain refiner (at, 700 ºC) at varying amount. Fig. 4.21a shows coarser structure, however, complete conversion of coarse columnar grain structure to fine equiaxed grains occurred within 0.040 wt.% Ti addition level (Fig. 4.21b). The fine equiaxed grains after inoculation is attributed to the blocky morphology and to the increased number of $TiAl_3$ phase, which was approximately 37 µm in size.

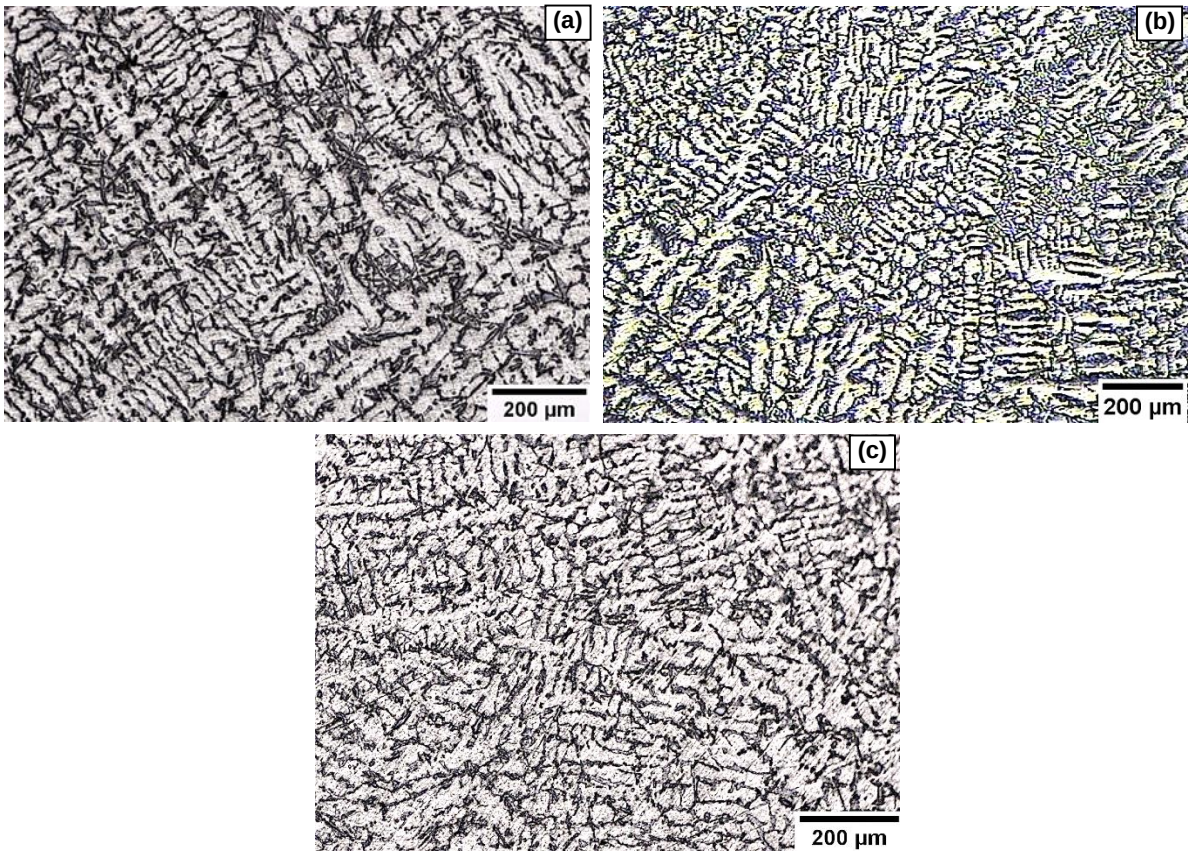

Fig 4.20 Optical microstructure of cast Al-7Si-3Cu alloy inoculated with annealed (600 ºC) Al−5Ti−1B master alloy at different wt.% Ti (a) 0.035; (b) 0.040; and (c) 0.045.

There was a slightly degradation in the grain refinement performance of the master alloy when the mass fraction of Ti increases upto 0.045% (Fig. 4.21c). The grain structure became completely fine equiaxed after 10 min of holding. At higher annealing temperatures of 600 ºC and 700 ºC, the grain refining performance of master alloy looked to be improving to that at 500 ºC, and the grain structure appeared to be finer for the Al-7Si-3Cu alloy grain refined with master alloys annealed at higher temperatures.

4.3.4 Addition of hot rolled Al-5Ti-1B master alloy

The microstructures of the Al–7Si–3Cu cast alloys before and after grain refinement with hot rolled master alloy are shown in Fig. 4.22 to Fig. 4.24. It is observed that, refinement with hot rolled master alloys has profound influence on microstructures of the Al–7Si–3Cu cast alloys. The present experimental results confirmed that the addition of hot rolled master alloy Al–5Ti–1B to Al–7Si–3Cu alloy significantly refines the coarse columnar primary α-Al grains to fine equiaxed α-Al grains (60 μm) due to the presence of $TiAl_3$ and TiB_2particles present in the master alloy which are nucleating agents during the solidification of α-Al grains, while the eutectic silicon particles appear to be unaffected as expected. Since 250 ºC rolling temperature showed large fracture of $TiAl_3$ particles in comparison to 350 ºC, therefore, further study is carried out at this temperature.

Figures 4.22 (a-c) show the optical microstructure of Al-7Si-3Cu alloy grain refined with rolling at 250°C for 25 % reduction levels at varying amount of Ti respectively. It is observed that the hot rolled Al-5Ti-1B master alloy showed better grain refining efficiency as comparison to cast master alloy at lower addition level of grain refiner, which means that the grain refinement efficiency of Al-5Ti-1B master alloy is enhanced after hot rolling. It is interesting to note that the conversion from columnar to equiaxed grain structure occurs, increases with increasing amount of grain refiner.

Figures 4.23 (a-c) show the optical microstructure of Al-7Si-3Cu alloy grain refined with rolling at 250°C for 50 % reduction levels at varying amount of Ti respectively. The Fig. 4.23a displays the fine and coarser α-Al dendrites of size 350 μm. It can be seen that, when mass fraction of Ti is less than 0.035 %, less grain refinement is observed but it is higher than at 25% reduction level. However, the grain size decreases distinctly with the increase mass fraction of Ti upto 0.035wt.% (Fig. 4.23b).

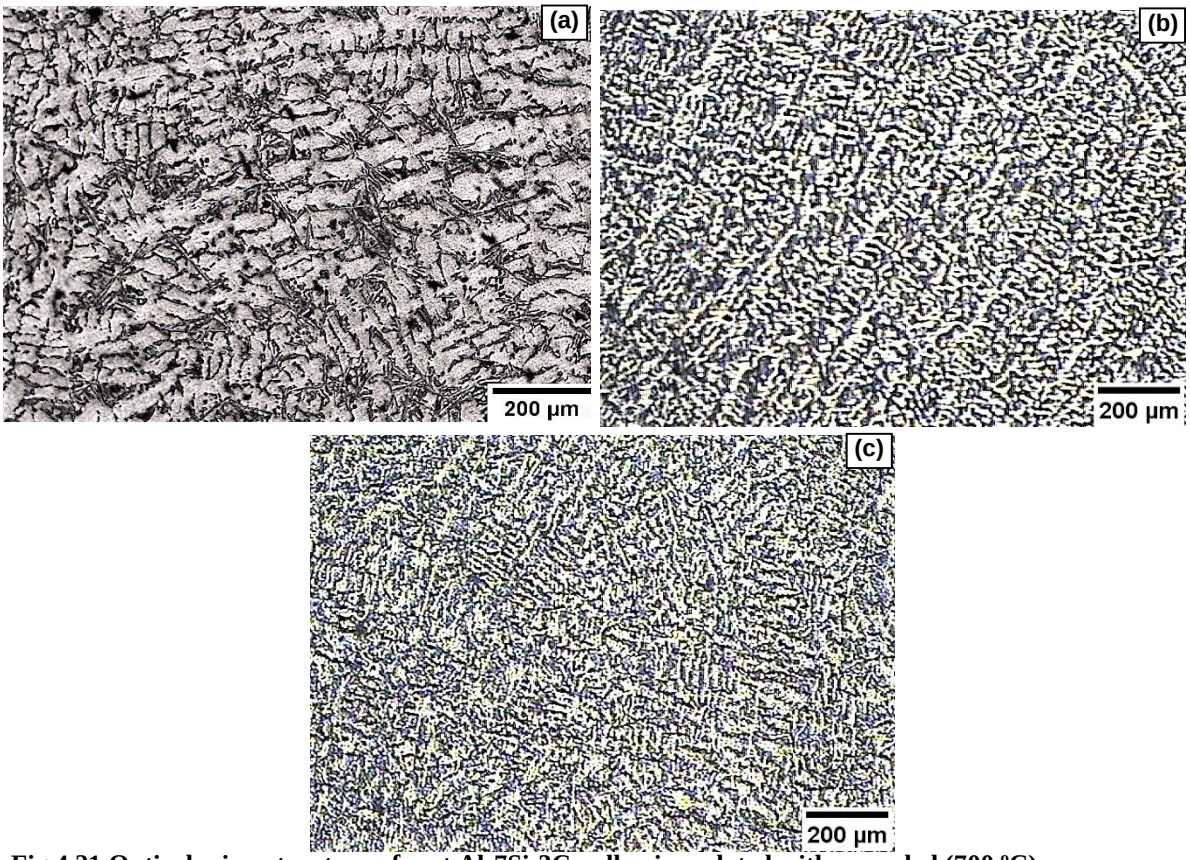

Fig 4.21 Optical microstructure of cast Al-7Si-3Cu alloy inoculated with annealed (700 ºC) Al−5Ti−1B master alloy at different wt.% Ti (a) 0.035; (b) 0.040; and (c) 0.045.

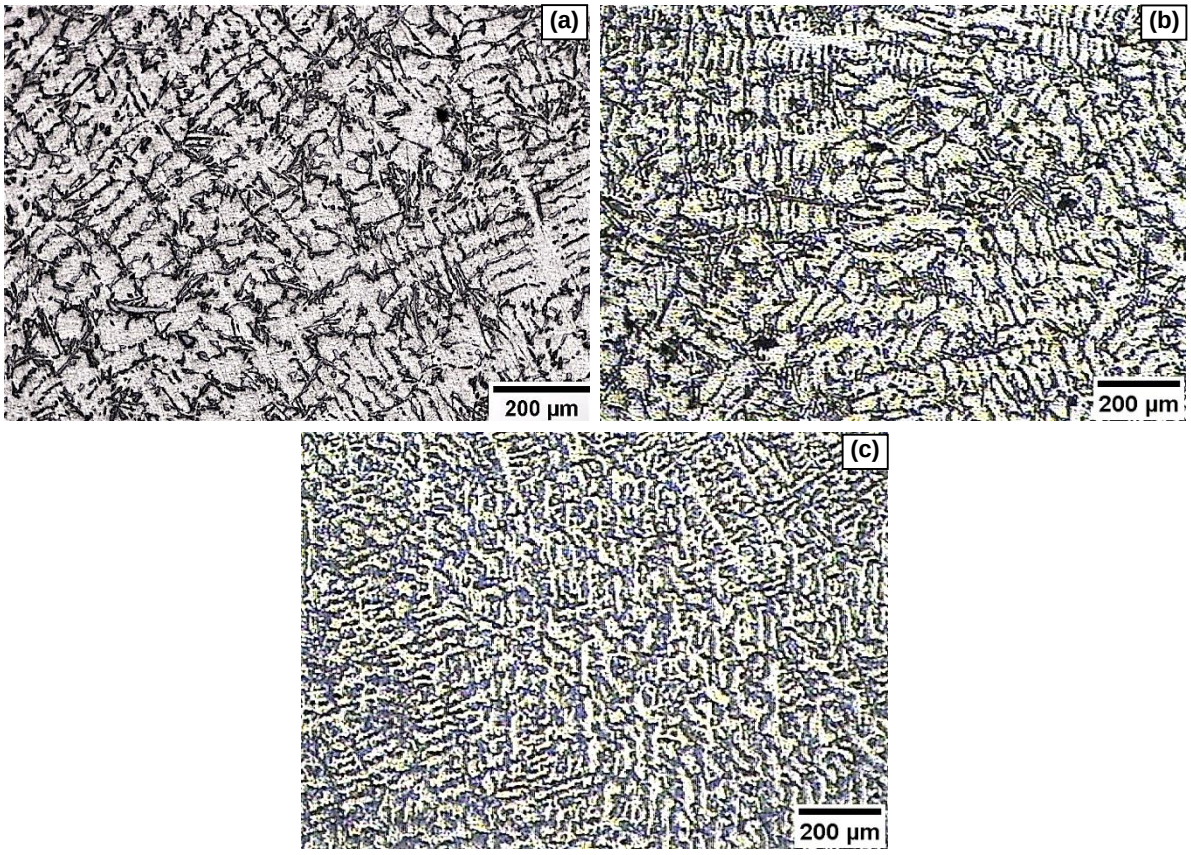

Fig 4.22 Optical microstructure of cast Al-7Si-3Cu alloy inoculated with 25 % hot rolled Al−5Ti−1B master alloy at different wt.% Ti (a) 0.030; (b) 0.035; (c) 0.040.

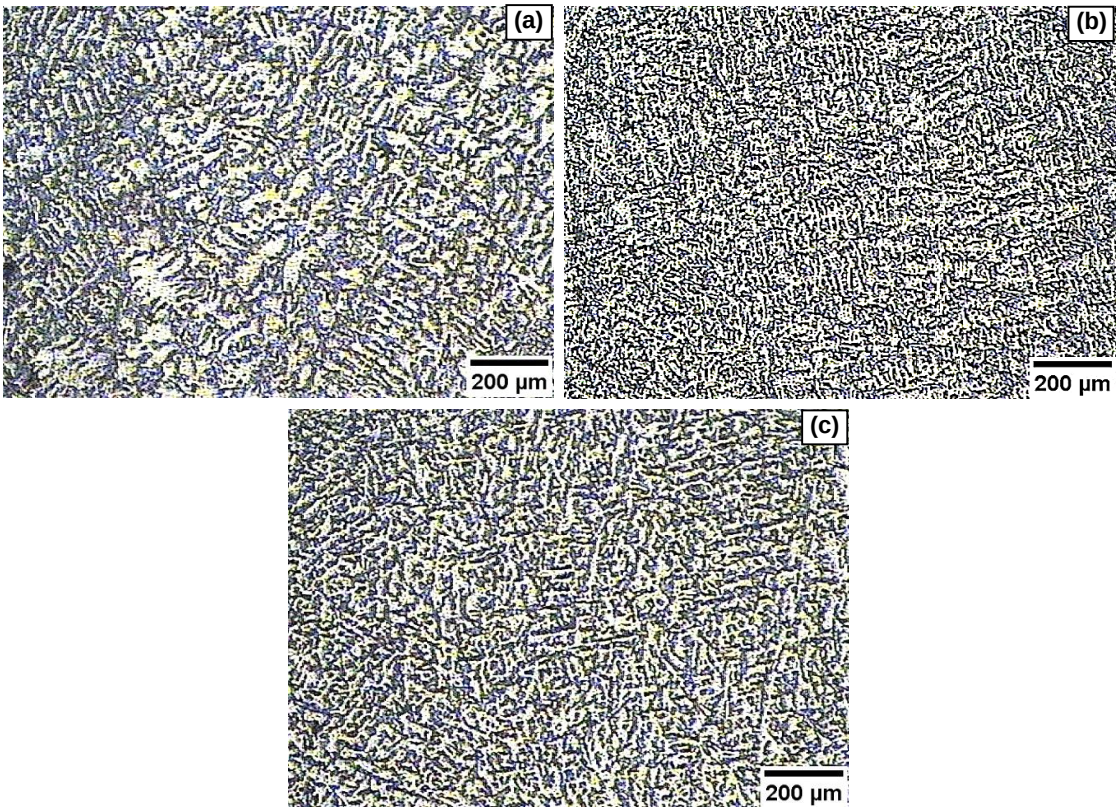

Fig 4.23 Optical microstructure of cast Al-7Si-3Cu alloy inoculated with 50% hot rolled Al−5Ti−1B master alloy at different wt.% Ti (a) 0.030; (b) 0.035; (c) 0.040.

Al-7Si-3Cu alloy. Figure 4.23c demonstrates that when the weight percent of Ti is higher than 0.035, the grain size of Al-7Si-3Cu alloy does not decrease further.

The microstructure of grain refined Al-7Si-3Cu alloy with 75% reduction clearly showed that a complete conversion of dendritic columnar structure to fine equiaxed structure one was achieved within 10 min of holding (Fig. 4.24b). Earlier studies [53] have shown that 10 minutes holding time gives best result with smaller grain size. The hot rolled master alloys with 75 % reduction level had superior grain refining performance compared to the 30 and 50% reduction level of master alloys. The microstructural analysis had clearly displayed (Fig. 4.12) that more number of fine $TiAl_3$ particles formed as reduction level is increased, which improved the number of nucleating sites for α-Al when these rolled GR were used for grain refining Al-7Si-3Cu alloy. The improvement in the grain refining performance of hot rolled master alloys with increase in reduction level could be attributed to the continuous increase in the number of fine $TiAl_3$ particles due to fracture, which increased with the amount of reduction during rolling. Recent investigation [54] also showed that grain refiner efficiency is partially lost when this alloy is hot rolled at higher temperatures. This leads to the fact that $TiAl_3$ particles grow at higher rolling temperatures due to intermediate heating of the alloy between each rolling pass.

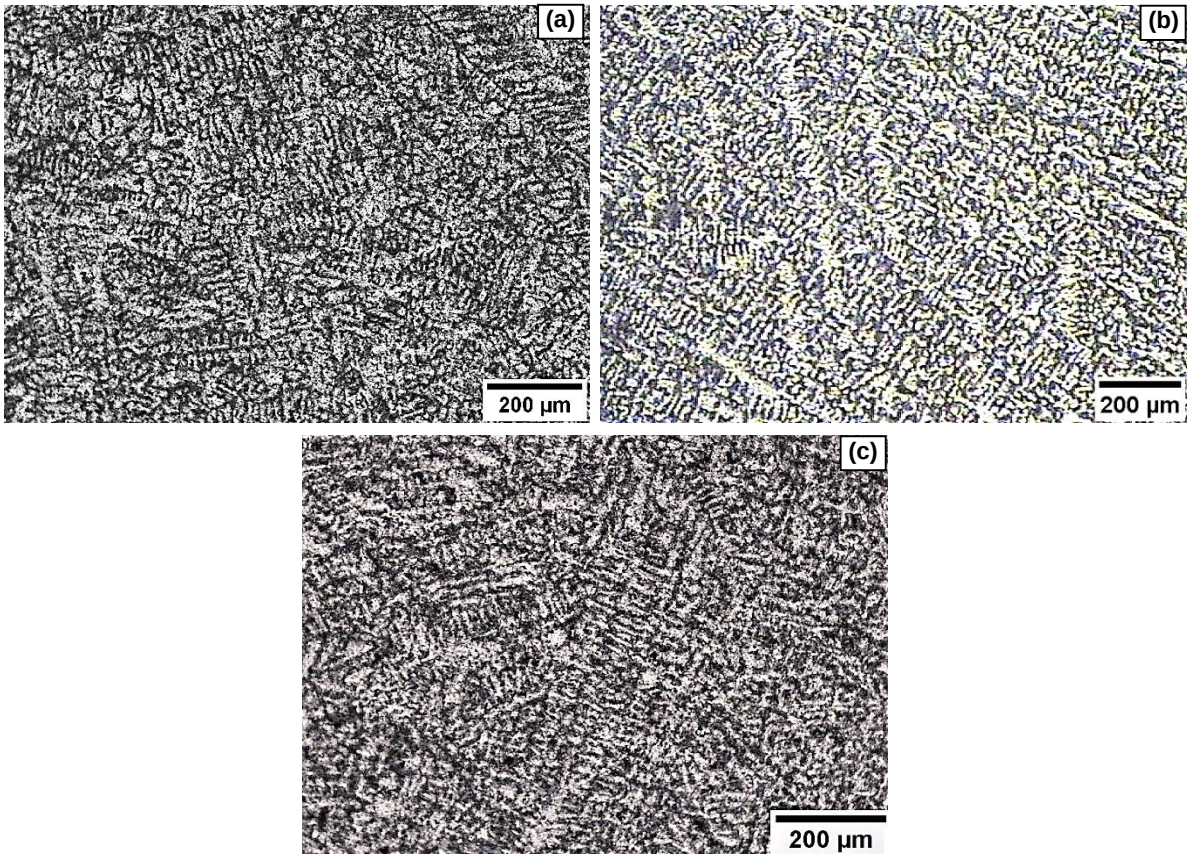

Fig 4.24 Optical microstructure of cast Al-7Si-3Cu alloy inoculated with 75 % hot rolled Al−5Ti−1B master alloy at different wt.% Ti (a) 0.030; (b) 0.035; (c) 0.040.

4.3.5 Macrostructure analysis

The present study aims to explore the potential of $TiAl_3$ and TiB_2 particles in the grain refinement of Al-7Si-3Cu alloys on mechanical properties and hot tearing. In order to study the effect of grain refiner in Al-7Si-3Cu alloy, as cast, ball milled, annealed and hot rolled Al-5Ti-1B master alloys were used to assess their grain refining performance. The photomacrograph of cast Al-7Si-3Cu alloy and grain refined with as cast, ball milled, annealed and hot rolled Al-5Ti-1B master alloy (0.040 wt.% Ti) are shown in Fig. 4.25 (a-e). Fig. 4.25a consists coarser macrostructure in comparison to grain refined Al-7Si-3Cu alloy at any type of master alloy. A change is noticed in the macrostructure from columnar grain structure to a mixture of fine columnar and coarse equiaxed grain structure within 10 min of holding as shown in Fig. 4.25b. Completely equiaxed structures have been obtained by similar addition 30h ball milled grain refiner as presented in Fig. 4.25c.

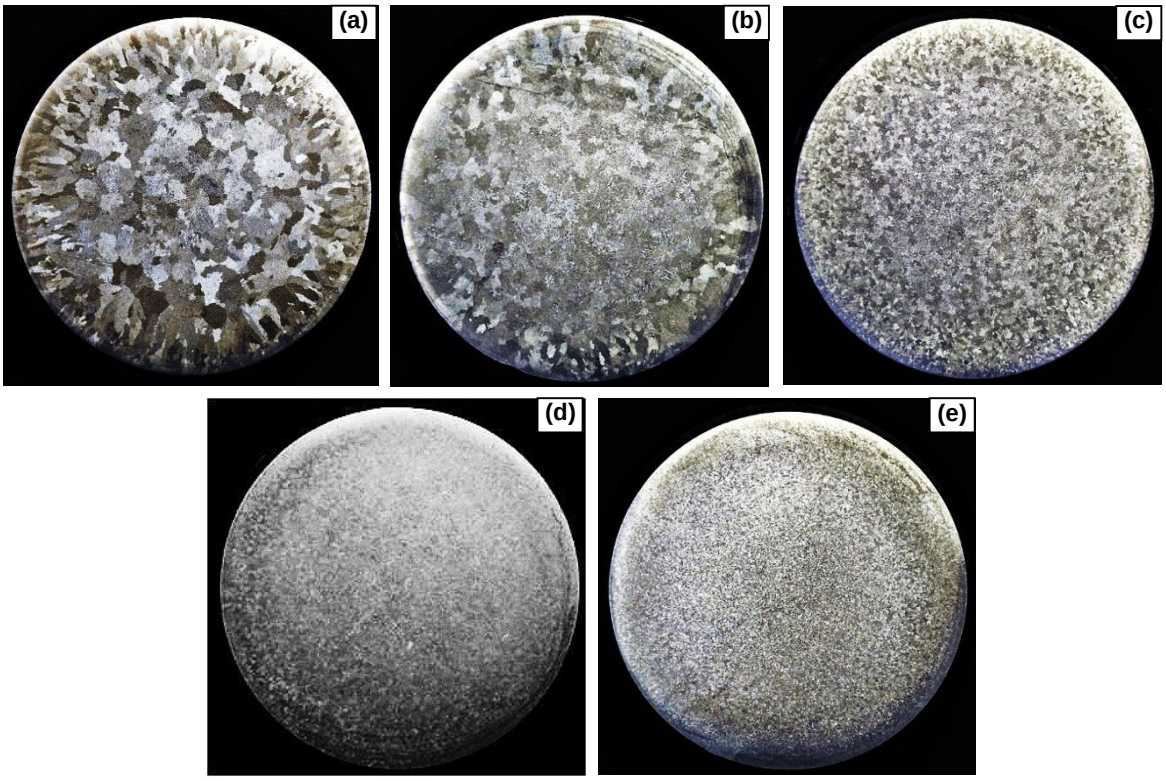

Fig 4.25 Macrostructures of cast Al-7Si-3Cu alloy and inoculated with Al−5Ti−B master alloy with 0.040 wt.% Ti, (a) Starting material as reference; (b) as cast GR; (c) 30h ball milled; (d) 700˚C annealed GR; and (e) 75% HR respectively.

The morphology, size and size distribution of nucleation particles play a vital role in the performance of grain refiner. At higher annealing temperatures 700 ˚C, the grain structure became more fine and equiaxed (Fig. 4.25d). Earlier studies [2,4] established the blocky type of $TiAl_3$ particles make the master alloy a better grain refiner than that containing plate like particles. The increase in the number of fine $TiAl_3$ particles on rolling was probable to increase the number of heterogeneous nucleating sites for α-Al when these hot rolled master alloys were used for grain refining Al-7Si-3Cu alloy. From the Table 4.5, it is seen that the size of $TiAl_3$ particles is reduced upto 15 μm and more number of smaller particles were observed during SEM analysis at 75% reduction level. Hence, this master alloy addition leads to a reduction in the grain size of α-Al in comparison to that achieved with the any type of master alloys (Fig. 4.25e).

4.4 XRD Analysis of Al-7Si-3Cu Alloy with Addition Master Alloy

It is clear from the XRD patterns (Fig. 4.26), as the addition of grain refiner is increased the relative intensity of $TiAl_3$ phase is also increased. Higher intensity of $TiAl_3$ particles improved the mechanical properties and hot tearing resistance by providing more nucleating sites for α-Al phases. The lattice mismatch for $(110)_{Al}//(110)_{TiAl_3}$ and $(001)_{Al}//(001)_{TiAl_3}$ is substantially greater than for $(111)_{Al}//(111)_{TiAl_3}$. The elastic energy associated with the lattice mismatch will thus be greater for $(110)_{Al}//(110)_{TiAl_3}$ and $(001)_{Al}//(001)_{TiAl_3}$ in comparison 0f $(111)_{Al}//(112)_{TiAl_3}$ [36,138,139,142,14]. This, in turn, will restrict any growth on the (110) and (001) surfaces.

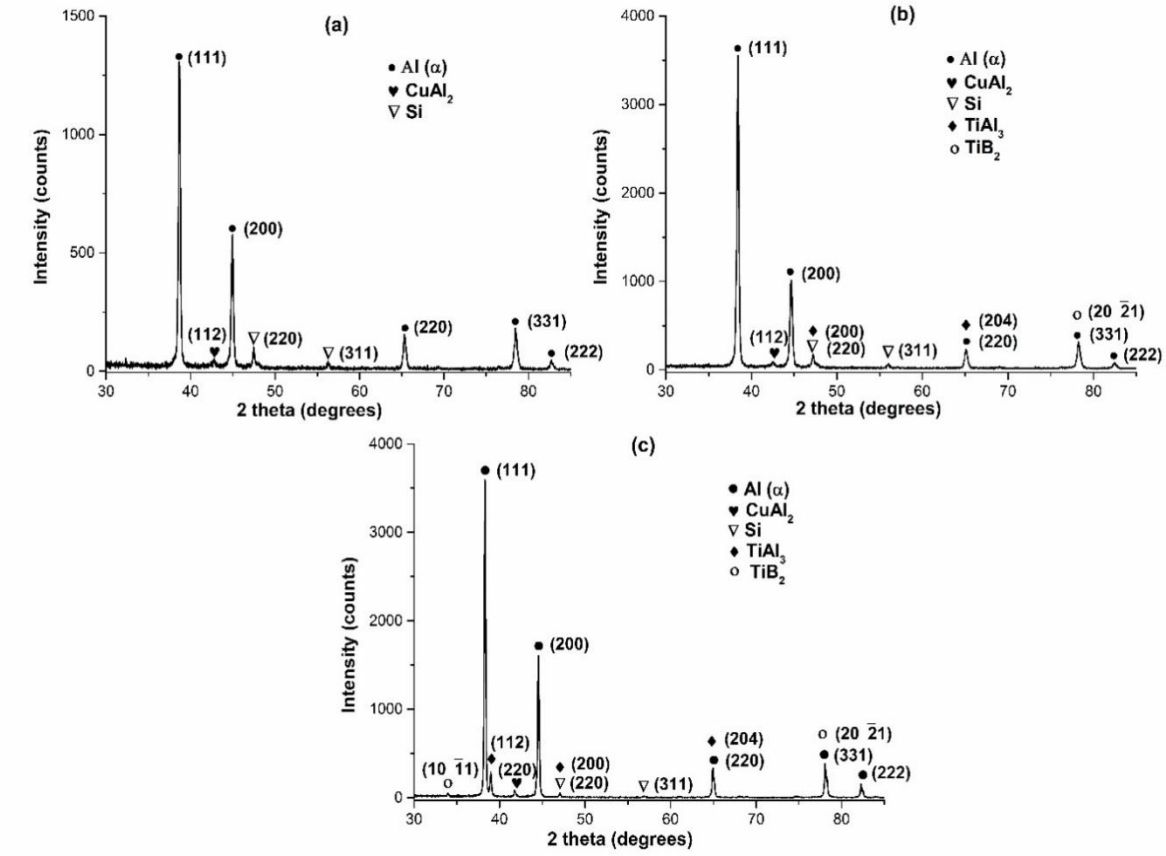

Fig 4.26 XRD analysis of Al-7Si-3Cu alloy (a) without grain refiner, (b) 0.10 wt.% Ti , (c) 0.15 wt.% Ti.

4.5 TEM Analysis of Al-7Si-3Cu Alloy with Addition Master Alloy

The TEM analysis of Al-7Si-3Cu alloy with additions of grain refiner is shown in Fig. 4.27 (a-e). The bright field image shows the presence of TiB_2 particles of size 1 µm – 2 µm, which have hexagonal structure with a = 0.3038 nm and c = 0.32392 nm [159]. The EDS analysis of the selected area (Fig. 4.27b) also confirmed the presence of boron elements. From earlier studies [16] it is known that once $TiAl_3$ and TiB_2 particles are released into the melt, these turns as an excellent heterogeneous nucleation site for Al alloy. However, $TiAl_3$ particles act as best heterogeneous nucleating sites for grain refinement. Our present in situ study demonstrates that the TiB_2 particle also play a vital role in deciding the grain refining efficiency of the master alloy. TiB_2 particles stabilize the $TiAl_3$ phase in a finite temperature range beyond the solidification temperature of the alloy. TiB_2 particles formed a thin layer on the surface of $TiAl_3$ particles. So from this point of view, it can be observed that $TiAl_3$ particles have good orientaional relationship with α-Al in the presence of TiB_2 particles.

Which decrease the dissolving rate of aluminide particles. This in turn, improving the grain refining efficiency of master alloy. The bright and dark field image of Al-7Si-3Cu alloy likewise appeared in Fig. 4.27 (c &d). The relating SAED patterns indicate that $TiAl_3$ particles have tetragonal closed packed structure (002). The SAED pattern associated to $TiAl_3$ confirms the lattice values obtained from the XRD spectrum. Particles with blocky morphology were found in the master alloy; the related SAED pattern is consistent with face centered cubic (fcc) structures and the corresponding lattice parameter a are estimated to be 2.36 A° and affirmed by high magnification observations (as appeared in Fig. 4.27e). There is a certain pre –existing orientation relationship with perfect crystal matching between the Al-matrix and aluminide particles during solidification. The plane $\{111\}_{Al}$is the closed packed plane correspond to $\{112\}_{TiAl_3}$which has the highest structure factor and minimum interplanar spacing or d-value mismatch (1.60 %) [75].The other closed packed or nearly closed packed plane were detected in XRD analysis earlier (Fig. 4.1) which have perfect matching with Al matrix, these are $\{111\}_{Al}$ // $\{004\}_{TiAl_3}$ and $\{200\}_{Al}$ // $\{004\}_{TiAl_3}$ [75,76].

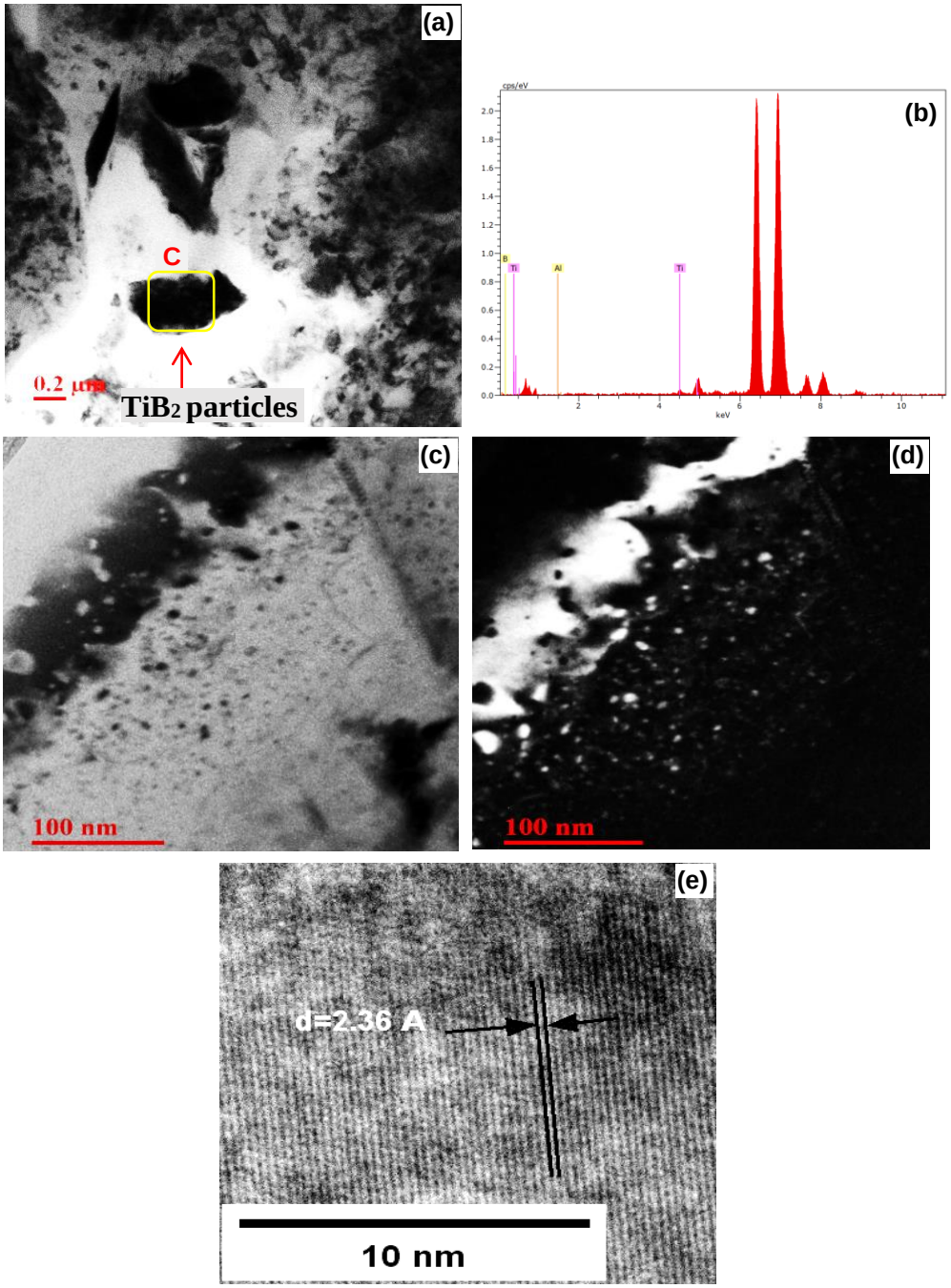

Fig 4.27 TEM bright-field image of Al-7Si-3Cu alloy (a) TiB_2 particles composed of an Al-rich core and Ti-rich shell, found at grain refined Al-7Si-3Cu alloy; (b) EDS spectra obtained from the particle shell; (c) bright field image; (d) dark field image; and (e) distance measurement b/w the two successive planes.

4.6 Effect of higher addition level in Al-7Si-3Cu Alloy

It is observed that titanium silicide (Ti_5Si_3) also formed in the melt at higher addition level of grain refiner at 7.0 wt. % Si as shown in Fig. 4.28 (a-d) [164,165]. This has an adverse effect on reducing hot tear tendency. The EDX analysis confirmed precipitation of Ti_5Si_3, as illustrated in Fig. 4.28. $CuAl_2$ phase was also observed as a hardening precipitates

which increases the hardness properties of the alloy but at the same time it increased the hot tearing tendency of the alloy.

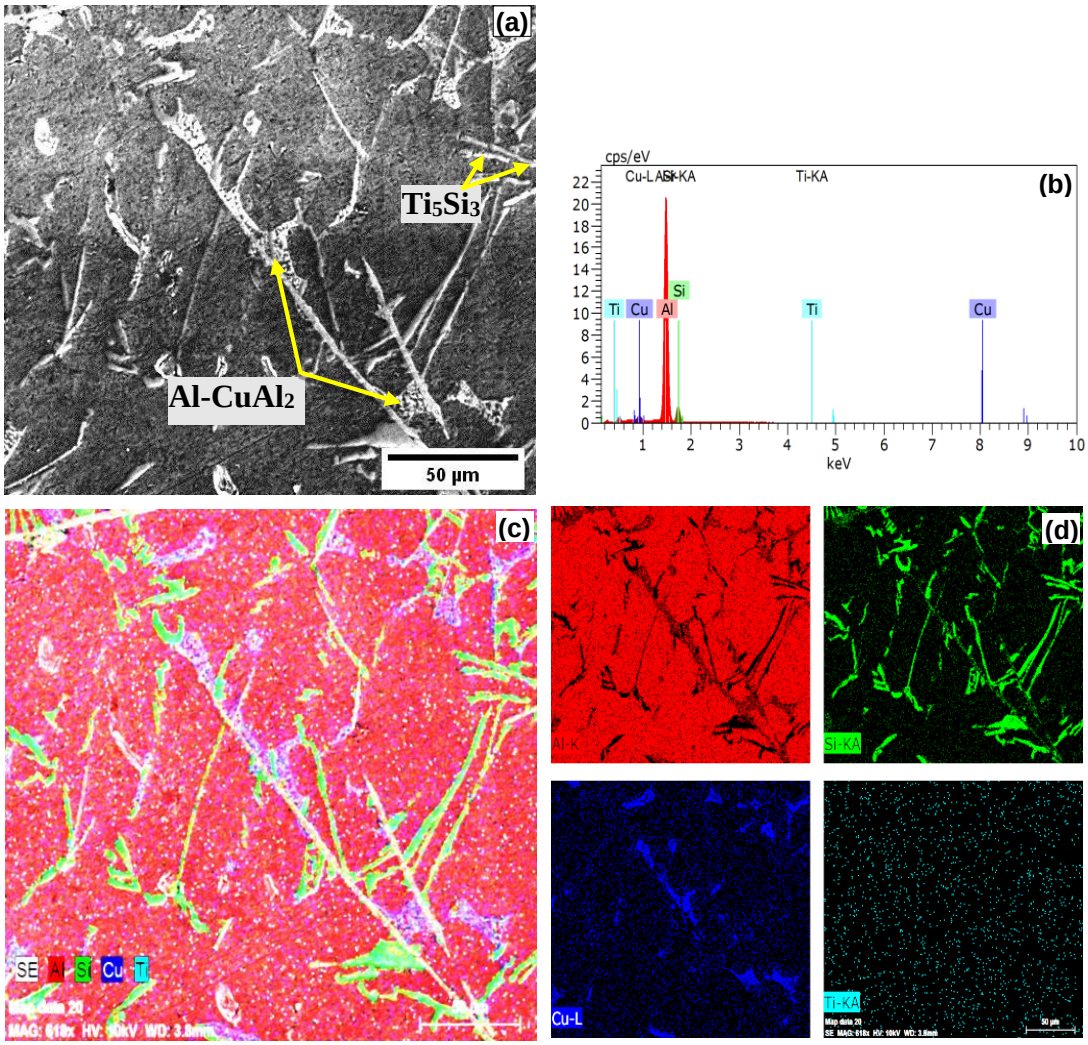

Fig 4.28 FESEM Micrograph of Al-7Si-3Cu alloy (a) with 0.20 wt. % Ti, where the main intermetallic compounds have been indicated; (b) energy dispersive X-ray analysis of the particles, (c); and (d) corresponding EDX composition maps.

4.7 Thermal Analysis of Al-7Si-3Cu alloy with Addition Master Alloy

The cooling curve of cast and grain refined Al-7Si-3Cu alloy is presented in Fig. 4.29. The temperatures for the exothermic reaction thus evaluated in the as cast condition from Fig. 4.29 (Table 4.5, in appendix 5) are Ts= 549 ºC, Tl= 583 ºC and temperatures for Al-7Si-3Cu alloy with 0.10 wt.% Ti from Fig. 4.29 are Ts= 550 ºC, Tl= 589 ºC). While with the addition 0.15 wt.% Ti temperature range is Ts= 551 ºC, Tl= 594 ºC. An intermettalic phase $CuAl_2$ is also present at 508 ºC. From DSC analysis, it is found that the addition of grain refiner increase the liquidus temperature of exothermic reaction. An

increase in the liquidus temperature indicates that lower under cooling is required for nucleation of α-phase, which leads to finer grains [160].

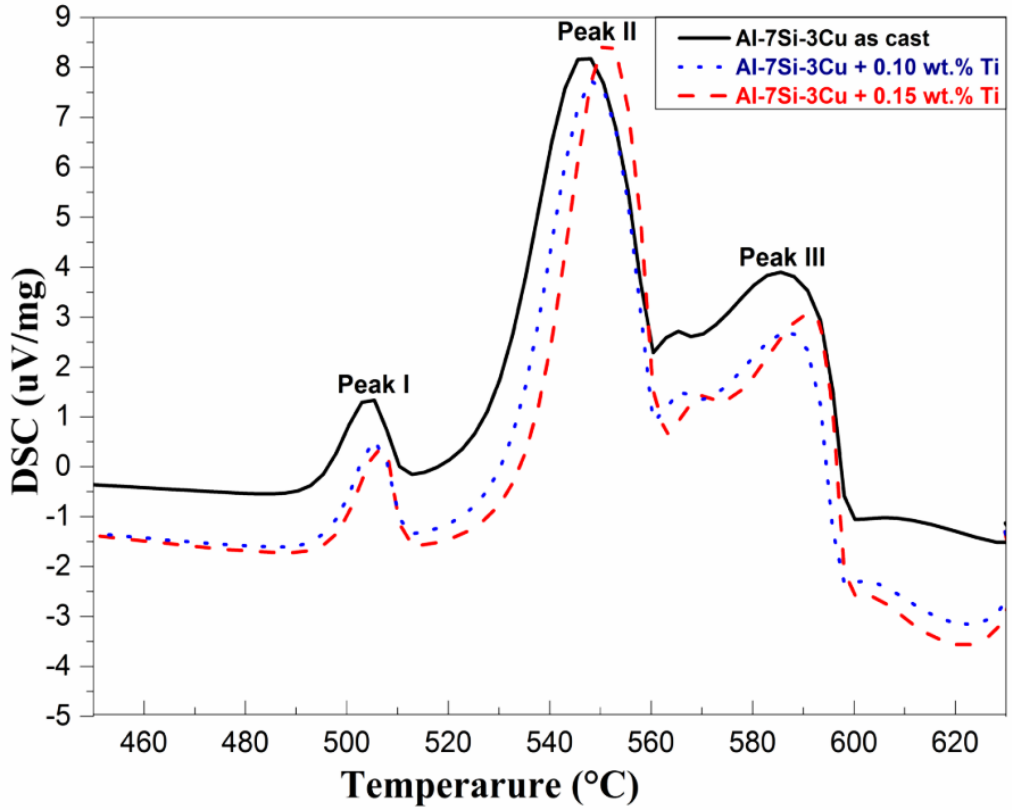

Fig 4.29 DSC analysis of Al-7Si-3Cu alloy (a) without grain refiner; (b) 0.10 wt.% Ti; (c) 0.15 wt.% Ti.

Estrin et al. [164], Cardoso [43] and Xiao [39] have also investigated the nucleation following additions of grain refiner to pure aluminium occurs beyond equilibrium melting temperature. So, growth of α-phase in a grain refined alloy take place rapidly than the un-grain refined alloy due to the presence of $TiAl_3$ particles in the melt [46,160,162–164].

4.8 Effect of Grain Refinement on Grain Size

The grain size examination of cast and grain refined Al-7Si-3Cu alloy is shown in Fig. 4.30. Sr was also added to observe its effect on grain size. When as cast master alloy is added (0.045 wt.%)to Al-7Si-3Cu alloy some refinement was obviously observed and the particle sizes are much exceeding the acceptance level of 580 µm. The grain size of α-Al is attained near the acceptance level within 2 min of holding for each addition level. However, this alloy with addition 0.050 wt.% Ti shows remarkable change in the microstructure and size reduce upto 370 µm, further addition of grain refiner does not show

any significant reduction in grain size. Therefore, further addition level of titanium is undesirable.

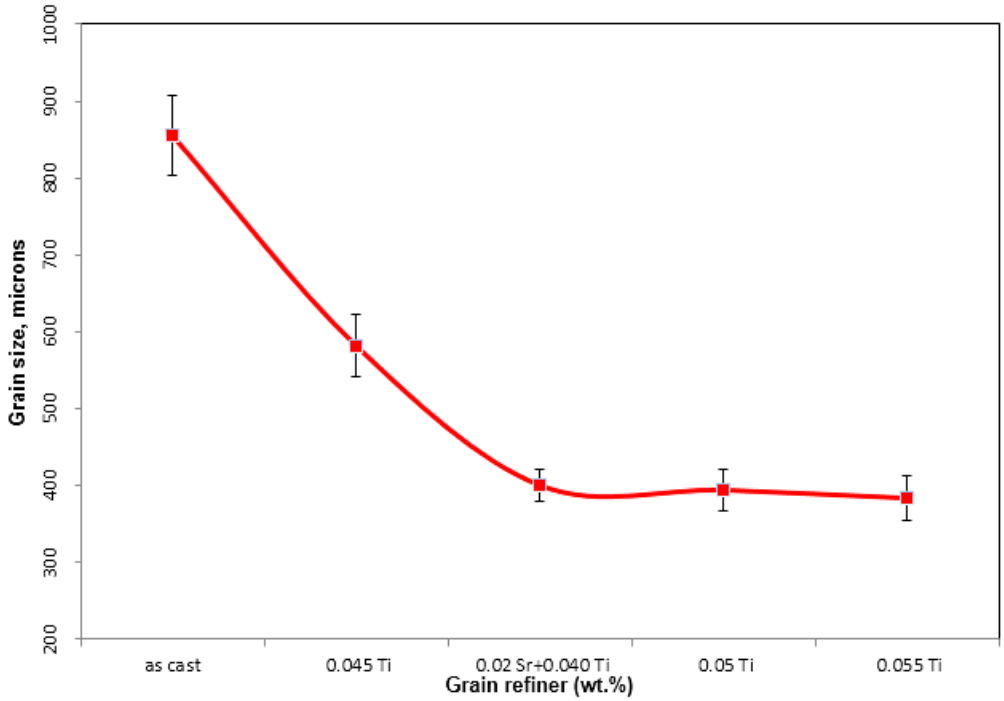

Fig 4.30 Grain size measurements of Al-7Si-3Cu alloy with different levels of grain refiner

4.9 Effect of Grain Refinement on Porosity

Porosity in casting is undesirable and drops the mechanical properties of the alloy. Porosity is specified concerning voids or cavities formed in the casting during solidification [165]. The variations of porosity volume fraction for as cast and grain refined samples in different processing conditions are shown in Fig. 4.31. From the earlier studies [207], it is clearly seen that as the addition level of grain refiner is increased in the casting, the porosity level is decreased respectively. From the Fig. 4.31, the same trend has been observed in Al-7Si-3Cu alloy. The maximum porosity level is observed in as cast Al-7Si-3Cu alloy. The porosity level reaches to minimum value with the addition of type D master alloy.

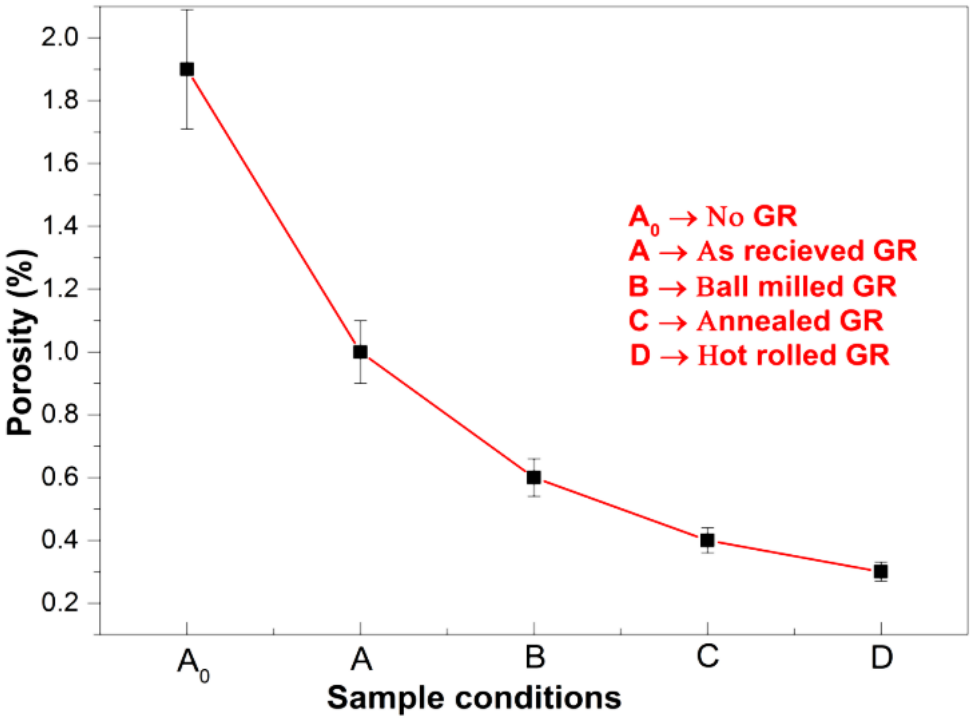

Fig 4.31 Effect of grain refinement on porosity in different processing conditions.

4.10 Mechanical Properties of Al-7Si-3Cu Alloy

The mechanical properties of the Al-7Si-3Cu alloy samples were analyzed to confirm the effect of grain refinement with addition of titanium. The details of the alloys and details of grain refinement are given in Table 3.4. The improvement in the mechanical properties of Al–7Si–3Cu alloys achieved by grain refinement is shown in Table 4.7. The refinement of Al–7Si-3Cu cast alloy has resulted in a 20.5 and 4 % improvement in the UTS and hardness respectively. Further, improvement in the UTS and hardness, to the extent of over 19 and 32 %, could be achieved by adding mechanical worked (Al–5Ti–1B master alloy) in Al-7Si-3Cu cast alloy.

4.10.1 Tensile properties of Al-7Si-3Cu alloy

Tensile properties of Al–7Si–3Cu cast alloys mainly depend on the shape, size and size distribution of the α-Al dendrites, interdendritic networks of eutectic silicon plates and intermetallic $CuAl_2$ phase formed along the interdendritic region. The results of the tensile properties are presented in Figures 4.32 to 4.36. The microstructure of cast Al-7Si-3Cu alloy consists of large elongated primary α-Al grains and the eutectic silicon (plate like) induces poor ductility to the casting (Fig. 4.15a). The addition of Al–5Ti–1B master alloy converts large α-Al dendrites into fine equiaxed α-Al dendrites, eutectic silicon (plate like)

into reasonable particles and fine $CuAl_2$ particles in the interdendritic region resulting in the improved mechanical properties. The improvements which are observed in the present studies are mainly due to structural differences between the cast, grain refined and grain refined with treated master alloy in Al-7Si-3Cu alloy.

As seen earlier from the microstructure observation of Al–7Si–3Cu alloys treated with different type of grain refiner (Al–5Ti–1B) significantly refines the α-Al grains and converts them into fine equiaxed, while the eutectic silicon particles and $CuAl_2$ phase appear to be unaffected, as expected. It is important to note that; the alloy has been cast in a graphite mould surrounded by fireclay brick (slow cooling) after grain refinement. Thus, further improvement in the mechanical properties can be expected for fast cooled castings, as this can lead to further refinement of the microstructures.

The coarser primary α-dendritic structure exhibited low tensile values in the unrefined alloy (Fig. 4.32). The tensile properties of Al-7Si-3Cu alloy inoculated with type A master alloy increases with increase in wt.% Ti upto 0.150 wt.% Ti, which was due to the change in the morphology of primary α-phase from coarser dendritic structure to fine equiaxed structure. Whereas beyond 0.150 wt.% Ti, tensile strength decreases further due to increase in the grain size. The Al-7Si-3Cu alloy inoculated with type B master alloy (Fig. 4.33) exhibited enhanced results of tensile values at lower addition level in comparison to as received grain refiner.

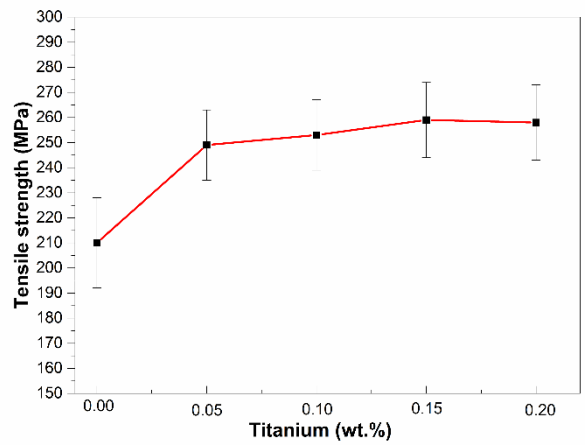

Fig 4.32 Tensile properties of cast Al-7Si-3Cu alloy inoculated with Al−5Ti−1B master alloy at different wt.% Ti (a) 0; (b) 0.05; (c) 0.10; (d) 0.15; and (e) 0.20.

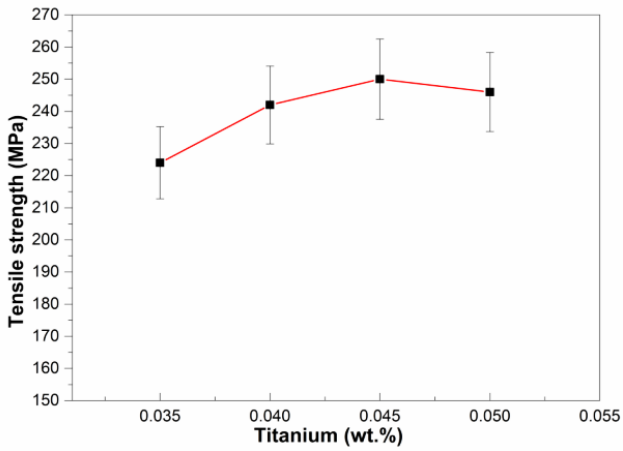

Fig 4.33 Tensile properties of cast Al-7Si-3Cu alloy inoculated with ball milled Al−5Ti−1B master alloy at different wt.% Ti (a) 0.035; (b) 0.040; (c) 0.045; and (d) 0.050.

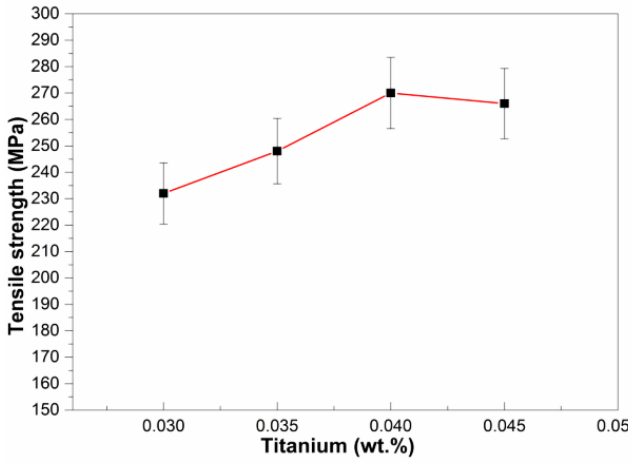

Fig 4.34 Tensile properties of cast Al-7Si-3Cu alloy inoculated with annealed Al−5Ti−1B master alloy at different wt.% Ti (a) 0.030; (b) 0.035; (c) 0.040; and (d) 0.045.

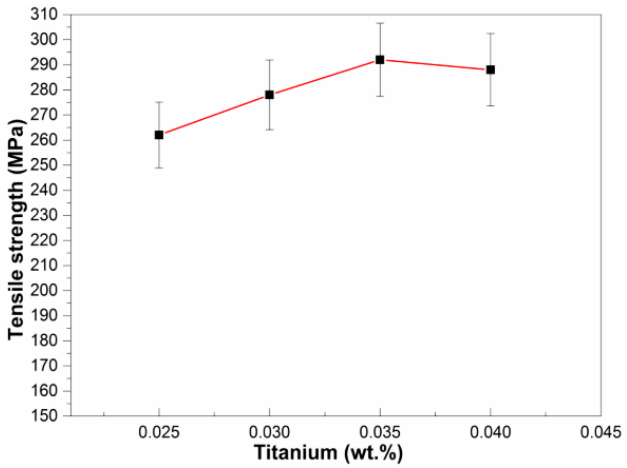

Fig 4.35 Tensile properties of cast Al-7Si-3Cu alloy inoculated with hot rolled Al−5Ti−1B master alloy at different wt.% Ti (a) 0.025; (b) 0.030; (c) 0.035; and (d) 0.040.

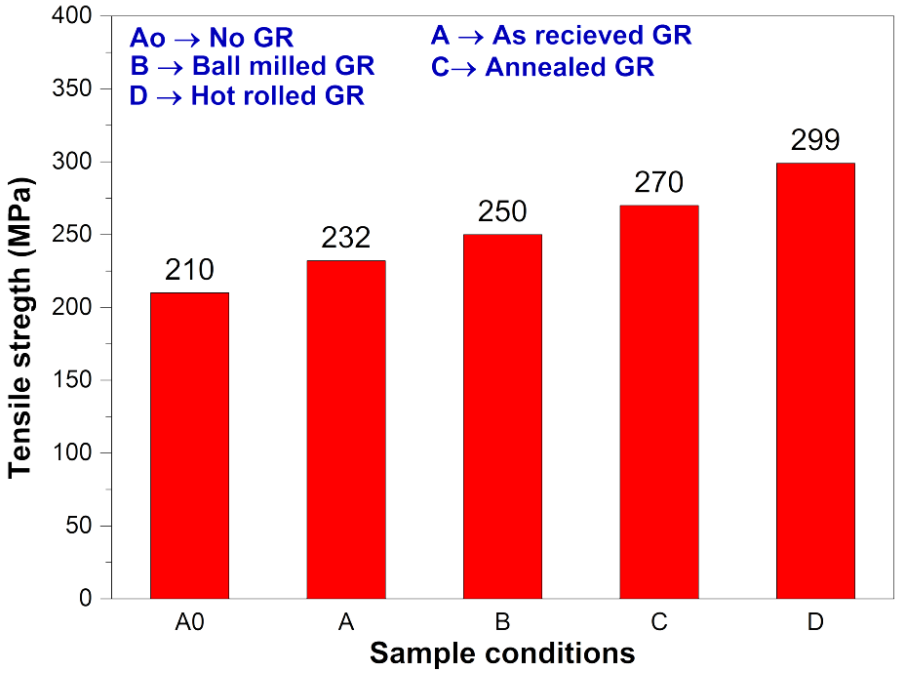

Fig 4.36 Tensile properties of cast Al-7Si-3Cu alloy and inoculated with different types of Al−5Ti−1B master alloy at 0.040 wt.% Ti.

Fig. 4.34 and Fig. 4.35 show that the tensile properties are improved at lower addition level with inoculated type C and type D master alloy, respectively. The tensile properties of refined Al-7Si-3Cu alloy with the addition of type D master alloy (Fig. 4.35) at 0.035 wt.% Ti, roughly increased by 40 %. This shows that the optimum value of Al–5Ti–1B master alloy gives us the maximum tensile values (292 MPa) at 0.035wt.% Ti. The Al-7Si-3Cu alloy inoculated (at, 0.040 wt.% Ti) with type D master alloy (Fig. 4.36) exhibited enhanced results of tensile values in comparison to the all type A, B, and C master alloy.

4.10.2 Hardness properties of Al-7Si-3Cu alloy

The hardness properties of the as-cast and grain refined Al-7Si-3Cu alloy under different conditions are presented in Figures 4.37 to 4.41. The as cast Al-7Si-3Cu alloy has lower hardness value due to the coarser structures. The hardness properties of the alloy increases with increase in wt.% Ti up to 0.050wt.% Ti, and increased further with the addition 0.20 wt.% Ti (Fig. 4.37). This was due to the presence of higher number of heterogeneous nucleating particles and large intermetallic phase. After the comparison of Fig. 4.37, Fig. 4.38, Fig. 4.39 and Fig. 4.40, it has been observed that the Al-7Si-3Cu alloy inoculated with type D master alloy exhibit improved results of hardness values in comparison to the type A, B, and C master alloy. The hardness properties of refined Al-7Si-3Cu alloy with the addition of type D master alloy at 0.035 wt.% Ti, roughly increased by 34%. This shows that the optimum value of Al–5Ti–1B master alloy gives us the maximum hardness (89 HB) at 0.035 wt.% Ti. The Al-7Si-3Cu alloy inoculated (at, 0.040 wt.% Ti) with type D master alloy (Fig. 4.41) showed the enhanced hardness values in comparison to the all type A, B, and C master alloy.

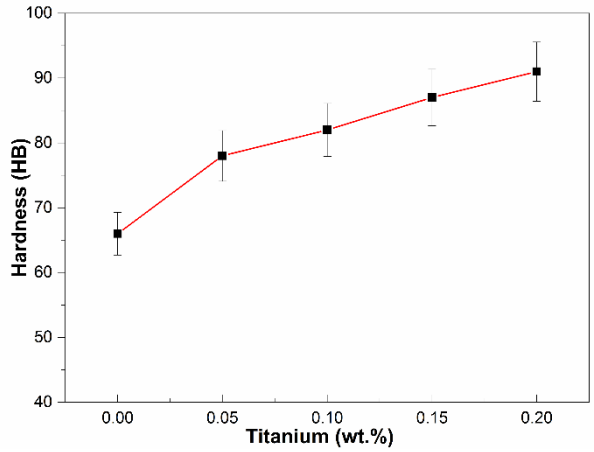

Fig 4.37 Hardness properties of cast Al-7Si-3Cu alloy inoculated with Al−5Ti−1B master alloy at different wt.% Ti (a) 0; (b) 0.05; (c) 0.10; (d) 0.15; and (e) 0.20.

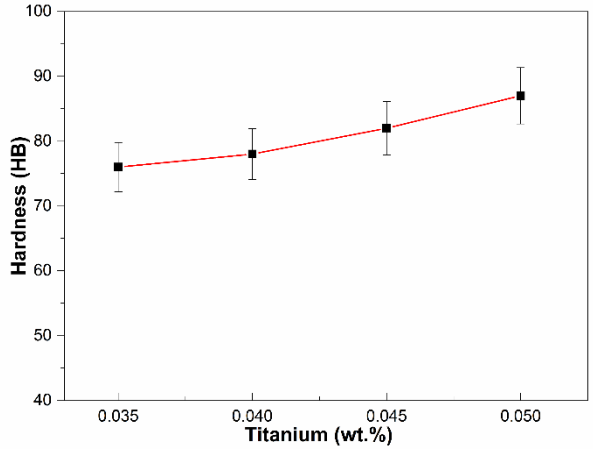

Fig 4.38 Hardness properties of cast Al-7Si-3Cu alloy inoculated with ball milled Al−5Ti−1B master alloy at different wt.% Ti (a) 0.035; (b) 0.040; (c) 0.045; and (d) 0.050.

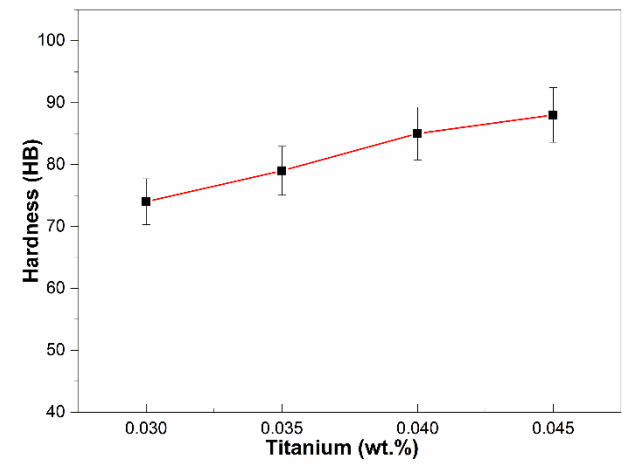

Fig 4.39 Hardness properties of cast Al-7Si-3Cu alloy inoculated with annealed Al−5Ti−1B master alloy at different wt.% Ti (a) 0.030; (b) 0.035; (c) 0.040; and (d) 0.045.

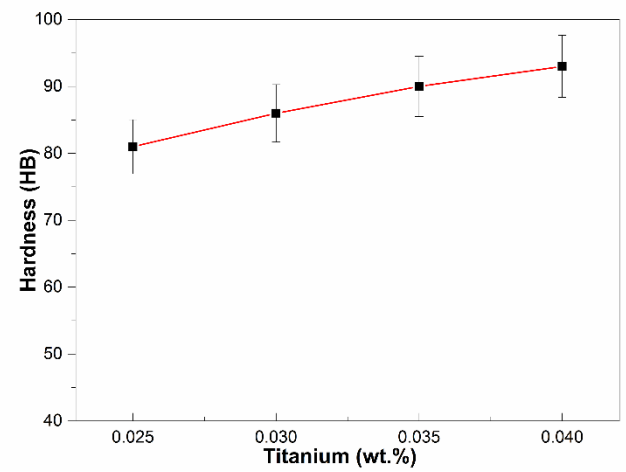

Fig 4.40 Hardness properties of cast Al-7Si-3Cu alloy inoculated with hot rolled Al−5Ti−1B master alloy at different wt.% Ti (a) 0.025; (b) 0.030; (c) 0.035; and (d) 0.040.

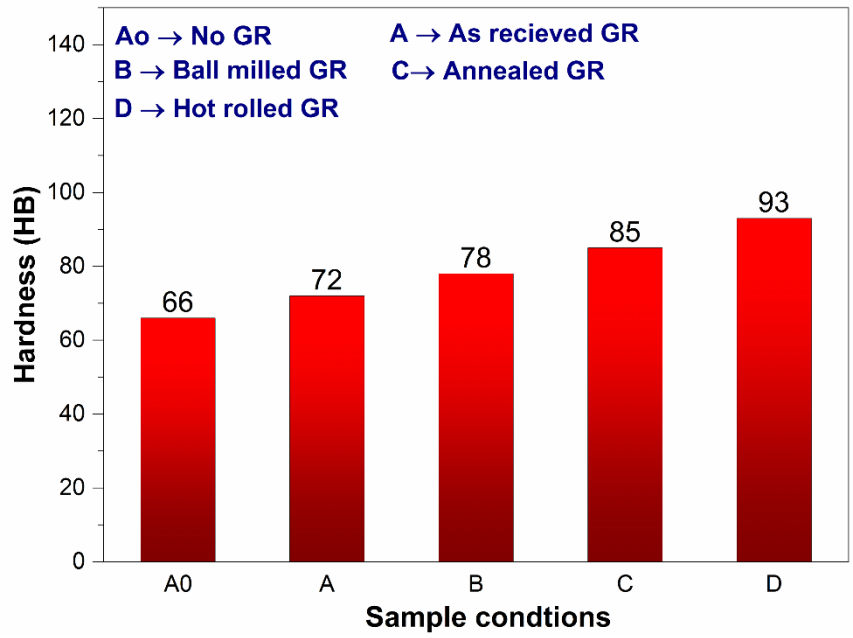

Fig 4.41 Hardness properties of cast Al-7Si-3Cu alloy and inoculated with different types of Al−5Ti−1B master alloy at 0.040 wt.% Ti.

4.10.3 Quality index of Al-7Si-3Cu alloy

The quality index (QI) can be used to observe the effect of grain refinement in different processing conditions [40,57]. The quality index gives the information about the quality of the parts cast with Al-7Si-3Cu alloy. The QI explain the direct relation between

ductility and UTS into a single term. The QI for Al-7Si-3Cu alloy in different processing condition is shown in Fig. 4.42 and can be given by Eq. 51.

$$QI\ (MPa) = UTS\ (MPa) + 150 \log (\%\ E) \quad (51)$$

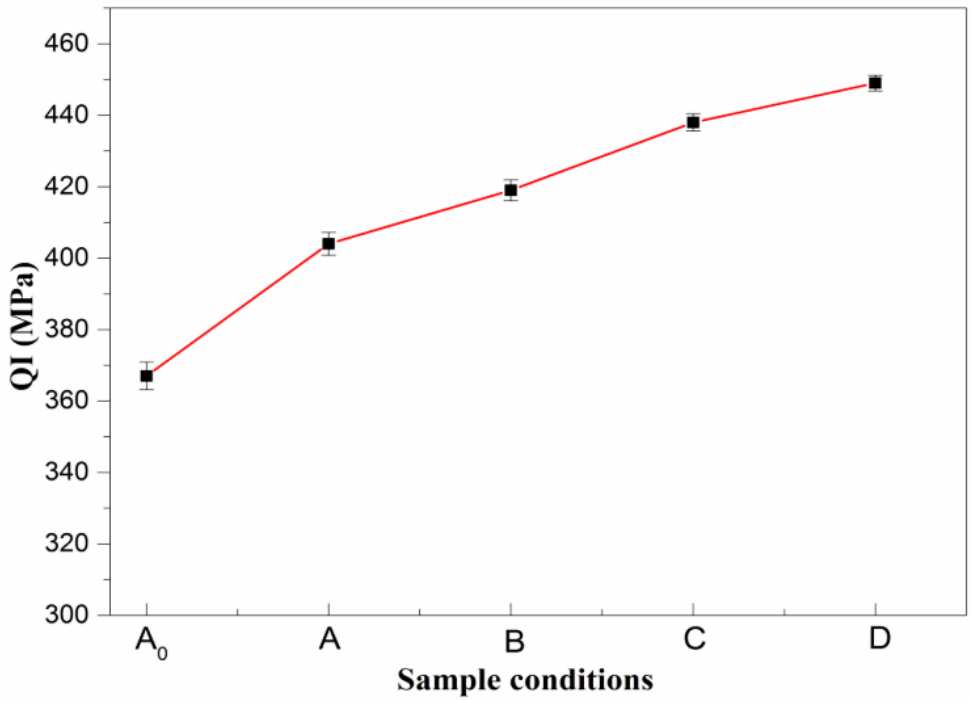

Fig 4.42 Quality index (QI) of Al-7Si-3Cu alloy in different processing conditions.

Moller et al. [224] reported the QI for as cast and grain refined Al-7Si alloy is about 365 and 406 MPa values respectively. In the present investigation, sample D showed 449 MPa with addition of hot rolled master alloy in Al-7Si-3Cu alloy. From above results for QI (Fig. 4.42), it is cleared that addition of treated master alloy significantly improved the tensile properties which are beneficial of Al-7Si-3Cu alloy.

4.10.4 Fractography analysis

SEM technique was employed for fracture surface analysis of Al-7Si-3Cu alloy after the tensile test to observe the mode of fracture. The fracture surfaces of Al-7Si-3Cu alloy with and without addition of grain refiner are shown in Fig. 4.43 (a-c). Fig. 4.43a shows the facture surface of as cast Al-7Si-3Cu alloy. This comprises the cleavage pattern which is the indication of lower ductility and lower mechanical properties. Addition of master alloy (0.025 wt.% Ti) decrease the average grain size of primary α-Al phase and

rounding of eutectic Si, therefore, the analysis of fracture surfaces from Fig. 4.43b reveals a quasi-cleavage pattern with very few dimples, is an suggestion of enhancement in elongation (%) as compared to as cast alloy. While the Fig. 4.43c consist more dimple as compared to other sample at addition level 0.035 wt.% Ti. Presence of dimples at this position showed a further improvement in the ductile behavior of Al-7Si-3Cu alloy.

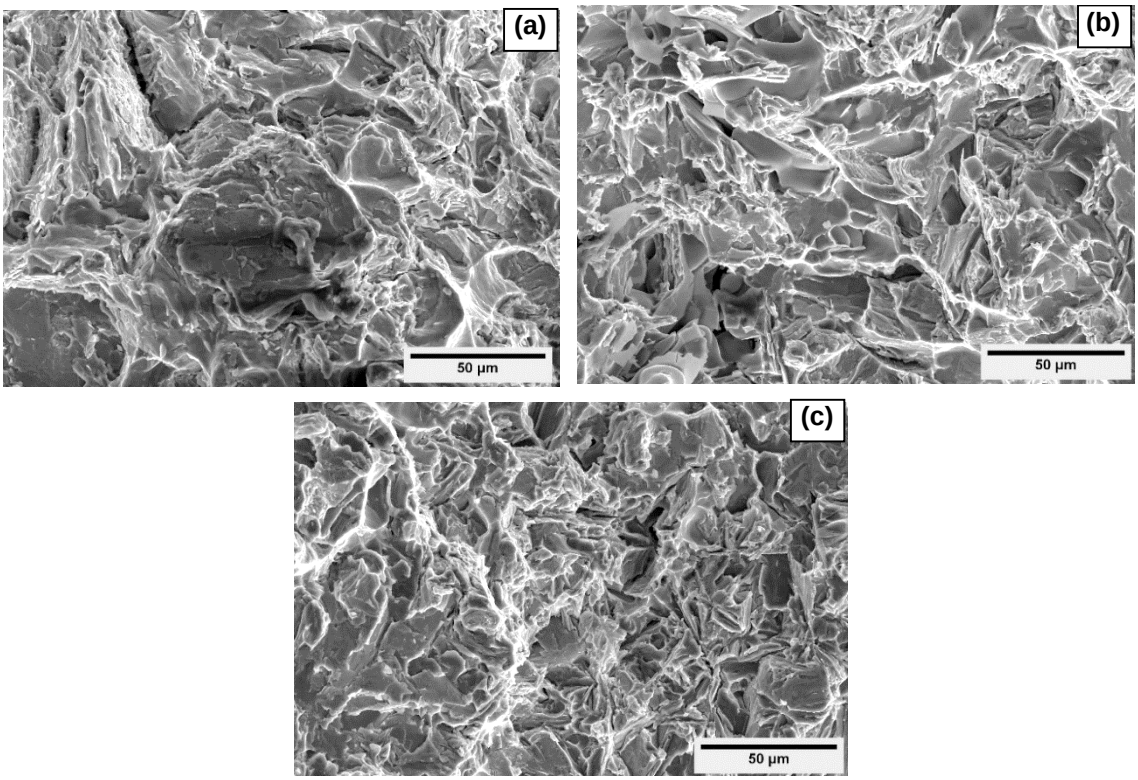

Fig 4.43 Fracture surface of Al-7Si-3Cu alloy; (a) as cast; and inoculated with Type D master alloy (b) 0.025 wt.% Ti; (c) 0.035 wt.% Ti.

5 Chapter Five

Results And Discussion

Hot Tearing Analysis

This chapter presents a study of the effect of grain refiner on hot tearing tendency in Al-7Si-3Cu alloy. This chapter also includes the study of the effect of mould temperature on hot tearing tendency in Al-7Si-3Cu alloy and characterization study of the hot teared surfaces. Al-5Ti-1B master alloy is added in Al-7Si-3Cu alloy as received type A and with treated master alloy of type B, C and D at varying wt.% Ti as shown in Table 3.4 for each case.

5.1 Effect of Process Variables on Hot Tear in Al-7Si-3Cu Alloys

5.1.1 Effect of mould temperature on hot tearing

Figures 5.1 (a-e) show the effect of mould temperatures on hot tearing and the fracture surface of hot teared region at room temperature, 90 °C, 160 °C and 230 °C mould temperature respectively. It is observed that at mould temperature of 90 °C, 160 °C and 230 °C the hot tear persists as shown in Figs. 5.1 (a-d). The crack surface is displayed in the top left corner to better appearance of tear. However, Fig. 5.1e shows that hot tear is eliminated at 300 °C mould temperature. This indicates that the mould temperature has a major effect on hot tearing tendency of Al-7Si-3Cu alloys [21,73,104]. At higher mould temperature principal strain was lower and hence, a reduced tendency to form hot tears resulted. Similar findings were reported by other investigators [142,167]. Mould temperature directly controls casting cooling rate and microstructure by providing an effective thermal gradient which in turn improves bulk feeding of metal at the advanced stage of solidification. Since, at 230 °C mould temperature minute cracks were observed. Therefore, further study is carried out at mould temperature of 230 °C to observe the effect of inoculants.

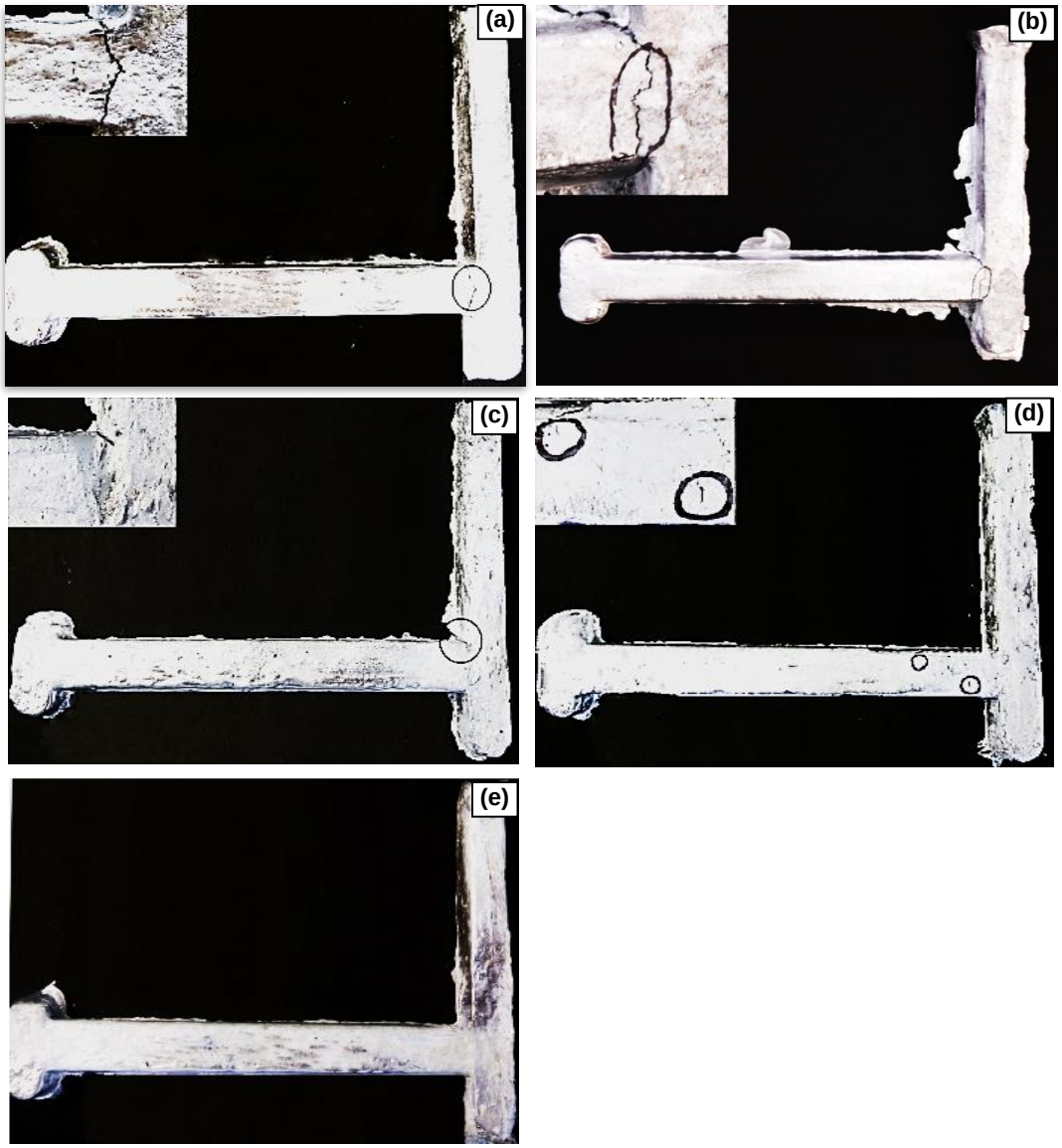

Fig 5.1 Effect of mould temperatures on hot tearing (a) Room temperature (b) 90 ºC temperature (c) 160 ºC temperature (d) 230 ºC temperature (e) 300 ºC temperature.

5.1.2 Effect of GR on hot tearing

Figures 5.2 (a-d) display the results of the castings of as cast and with the addition of 0.040 wt. % Ti, 0.045 wt. % Ti and 0.050 wt. % Ti at 230 ºC mould temperature respectively. The results suggest that the grain refinement reduces hot tearing severity of Al-7Si-3Cu alloy by restricting the growth of α-phase [59, 168-170]. Hot tear crack is present nearby the junction of the down-sprue in casting bar for Al-7Si-3Cu alloy as shown in Fig. 5.2a and Fig. 5.2c. As cast alloy is more prone to hot tearing in comparison to grain refined alloy. The magnified view of hot tear surface is displayed in the top left corner. At 0.05 wt. % addition of titanium level (230 ºC mould temperature) the hot tear was eliminated as shown in Fig. 5.2d. This was also visible on comparing the microstructure of unrefined and refined cast alloy (Figs. 4.15 a-c). The microstructures are coarser dendrites

even at 0.040 and 0.045 wt. % addition level of titanium. This is the reason for the appearance of cracks at 0.040 wt. % and 0.045 wt. % Ti alloy. While at 0.050 wt. % Ti level addition the hot tear was eliminated due to refinement of dendritic structure (Fig. 4.15c). It has been shown that the hot tearing occurs at the mushy zone where the dendrites begin to interlock. For the alloy without grain refinement, the growing tips of the coarse dendrites meet each other at an earlier stage of solidification. This reduces the duration of the mass feeding and therefore increases the hot tearing tendency. However, for the grain refined alloys, the small equiaxed grains form, and the number of paths for the liquid to flow increases, which can increase the refilling capacity and possibly heal the cracks that formed previously.

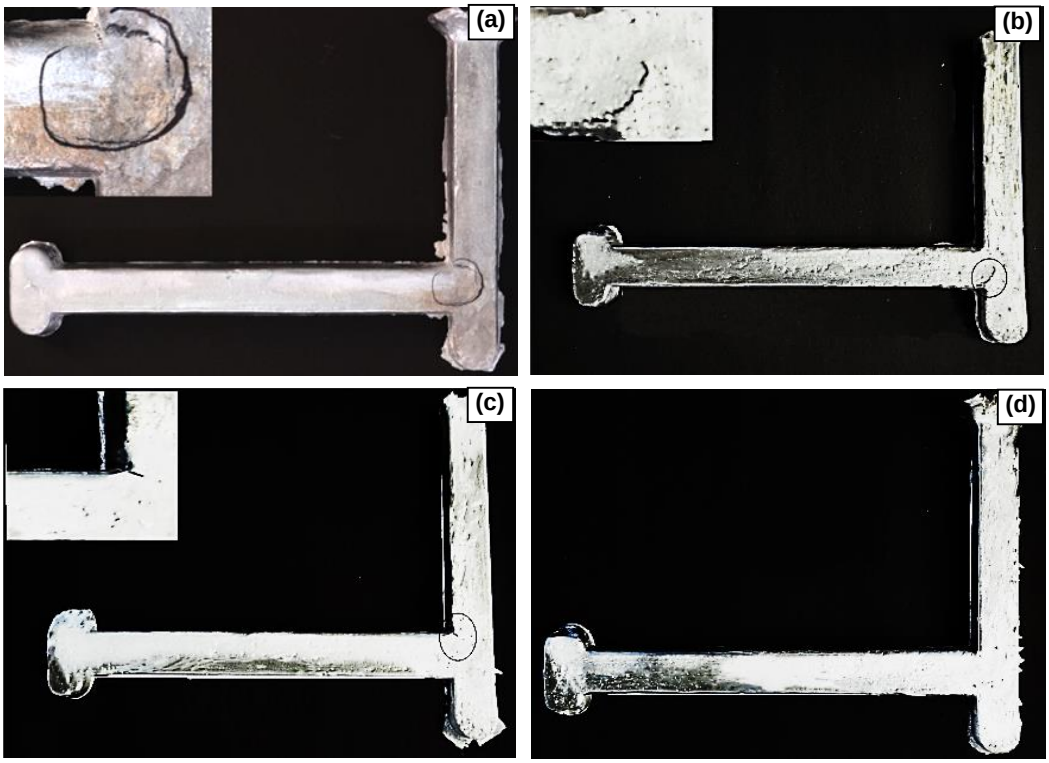

Fig 5.2 Effect of grain refinements on hot tearing in Al-7Si-3Cu alloy (a) as cast; (b) 0.040 wt. % Ti; (c) 0.045 wt.% Ti; (d) 0.050 wt.% Ti; at 230 ºC mould temperature.

5.1.3 Effect of ball milled GR on hot tearing

Figures 5.3 (a-d) show the hot tearing image of Al-7Si-3Cu alloy with addition 0.045 wt.% Ti (type B). Fig. 5.3a and Fig. 5.3b clearly displays that hot tears are present at the 90º junction between the downsprue and casting bar. Grain refinement occurred but this amount was not able to reduce hot tearing and failed to accelerate an effective growth restriction of primary α-Al phase. While the same amount of 30h and 50h ball milled grain refiner is introduced to the melt the crack is completely removed as shown in Fig. 5.3c and

Fig. 5.3d. This has happened due to more heterogeneous nucleation sites present in 30h and 50h ball milled grain refiner in the melt. The grain size is correlated to hot tearing severity of the cast alloy, as an increase in hot tearing severity is due to a larger grain size[171].

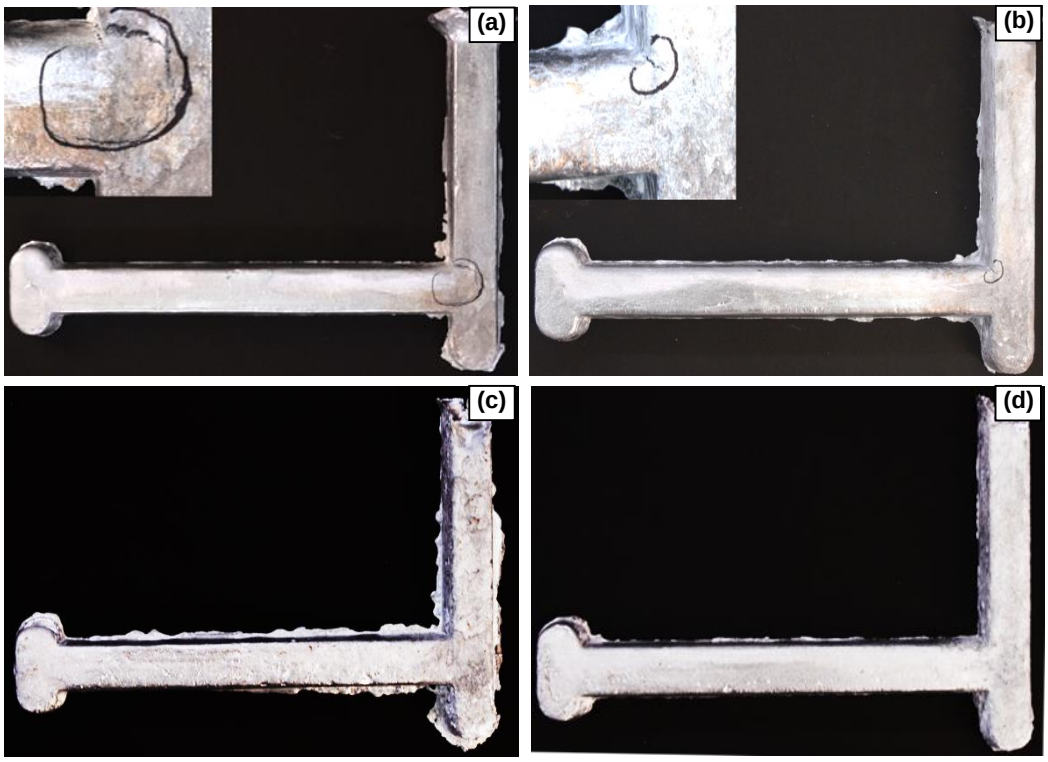

Fig 5.3 Hot tear image of Al-7Si-3Cu alloy of as cast and with addition of ball milled grain refiner (0.045 wt. % Ti) at (a) as cast; (b) 10h; (c) 30h; and (d) 50h.

5.1.4 Effect of annealed GR on hot tearing

The effect of annealed grain refiner on hot tearing is displayed from Figures 5.4 (a-h). Fig. 5.4a shows the hot tear crack of as cast Al-7Si-3Cu alloy with crack length 11 mm. When 400 ºC, 500 ºC and 600 ºC annealed grain refiner (0.040 wt.% Ti) is added to the melt, the crack length is reduced to 7, 5 and 2 mm (Fig. 5.4b to Fig. 5.4d) respectively. The visible cracks on each casting were measured using a measuring scale. The total crack length on each ring was the summation of the all crack lengths. From the Fig. 5.4e, it is observed that the hot tearing crack is completely eliminated by adding 700 ºC annealed grain refiner (0.040 wt.% Ti). It is attributed to the higher volume fraction of $TiAl_3$ particles. However, when 800 ˚C annealed grain refiner (0.040 wt.% Ti) and sectioned upper part of this sample were added to the melt, it showed hot tearing formation with 3 mm and 15 mm crack length (Fig. 5.4f and Fig. 5.4g) respectively. At this temperature, nucleating particles got segregate to the bottom

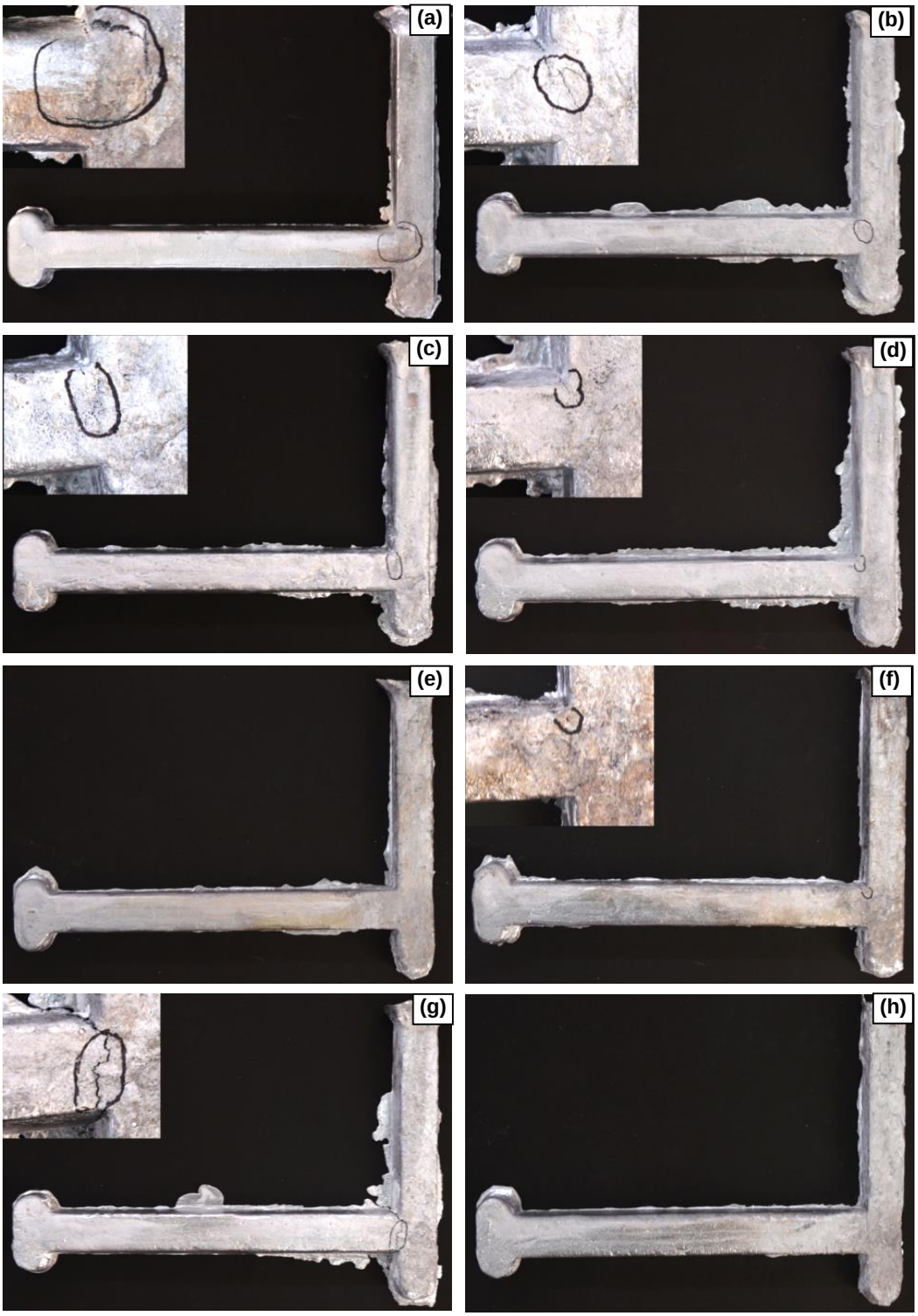

Fig 5.4 Hot tear image of Al-7Si-3Cu alloy of as cast and with addition of annealed grain refiner (0.040 wt.% Ti) for 8 hrs (a) as cast; (b) at 400; (c) 500; (d) 600; (e) 700; and (f) 800 ºC; (g) upper part; and (h) lower part annealed 800˚C.

part of the master alloy (as shown in Fig. 4.10). When bottom part of this sectioned sample was added to the melt in same amount, which consist more nucleating particles, hence crack is eliminated (Fig. 5.4h). A sound casting was produced by addition of bottom part of

annealed sample at 800 ºC. When the added level of Al-5Ti-1B master is too high, the agglomeration phenomenon is apparent. It leads to grain coarsening, grain size non-uniform distribution, and low grain roundness, and then, the hot tearing tendency can be increased. According to the research results, it indicates that the addition of 700˚C annealed GR, 0.040 wt.% (Ti) master alloy is most effective to reduce the grain size and hot tearing of Al-7Si-3Cu alloy.

5.1.5 Effect of hot rolled GR on hot tearing

Figures 5.5 (a-d) show the hot tearing image of Al-7Si-3Cu alloy. Fig. 5.5a illustrates the hot tear image of as cast Al-7Si-3Cu alloy. A large crack is observed near the down sprue. When the 25% hot rolled grain refiner (at, 0.035 wt.% Ti) was added to the melt the crack length was reduced but not completely eliminated (Fig. 5.5b). However, the addition of grain refiner in identical amount at 50 and 75 % reduction level was adequate to eliminate hot tearing (Fig. 5.5c and Fig. 5.5d).

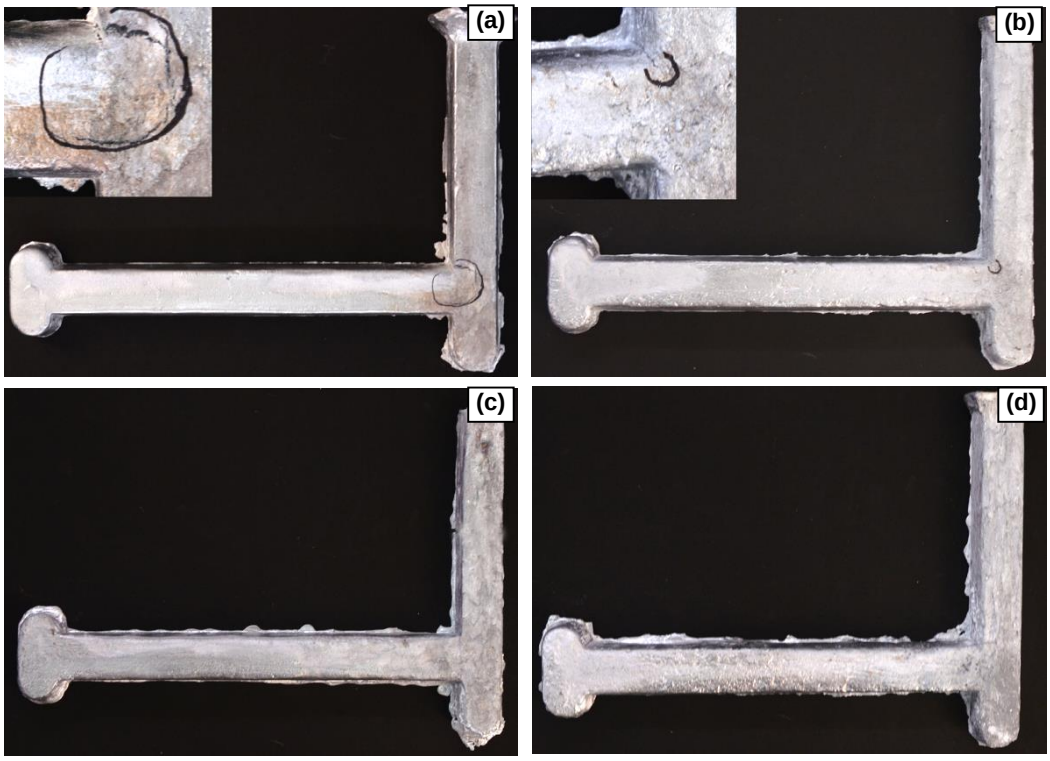

Fig 5.5 Hot tear image of Al-7Si-3Cu alloy of as cast and with addition of hot rolled 0.035 wt.% Ti (a) as cast; and at 250 ºC hot rolling temperature with (b) 25; (c) 50; (d) 75 % reduction level.

This was happened due to the larger number of nucleating sites were present in the hot rolled master alloys. Type D master alloy showed leading effect on minimizing hot tearing tendency of Al-7Si-3Cu alloy. Hot tear is completely eliminated at much lower addition level (0.035 wt.% Ti) in comparison to other type A, B and C master alloy.

5.1.6 Porosity analysis of L-shape casting

Porosity analysis has been carried out for as cast and with addition of Al-5Ti-1B grain refiner in Al-7Si-3Cu alloy. The samples were cut from 3 different positions of the L- shaped die casting of the alloy as shown in Fig. 5.6.

Fig 5.6 Chosen Positions for porosity, XRD and SEM analysis

1st position: The first part to solidify

2nd position: The middle part

3rd position: The last part to solidify (susceptible to cracks)

Fig 5.7 clearly displays the results of casting of as cast and with addition of type C grain refiner in A-7Si-3Cu alloy. It is clearly seen that the addition of grain refiner decreases the porosity level in the hot tear casting. At the 1st position, the porosity level is same in as cast and grain refined alloy. 2nd position has different porosity levels for as cast and grain refined Al-7Si-3Cu alloy. However, porosity level for as cast alloy is higher but not exceed to the level that this region became prone to hot tear. Though, 3rd position is more susceptible to hot tearing tendency. Fig. 5.7 shows that the porosity level is maximum for as cast alloy at 3rd position, resulting hot tearing took place in this region. At the same position the level

of porosity is reduced by introducing grain refiner up to 3.7 %. This reduced porosity level is not sufficient to cut the liquid melt in the last stage of solidification. So, addition of grain refiner reduces the chance of formation of cracks at the 3rd position by better feeding of liquid metal and faster solidification.

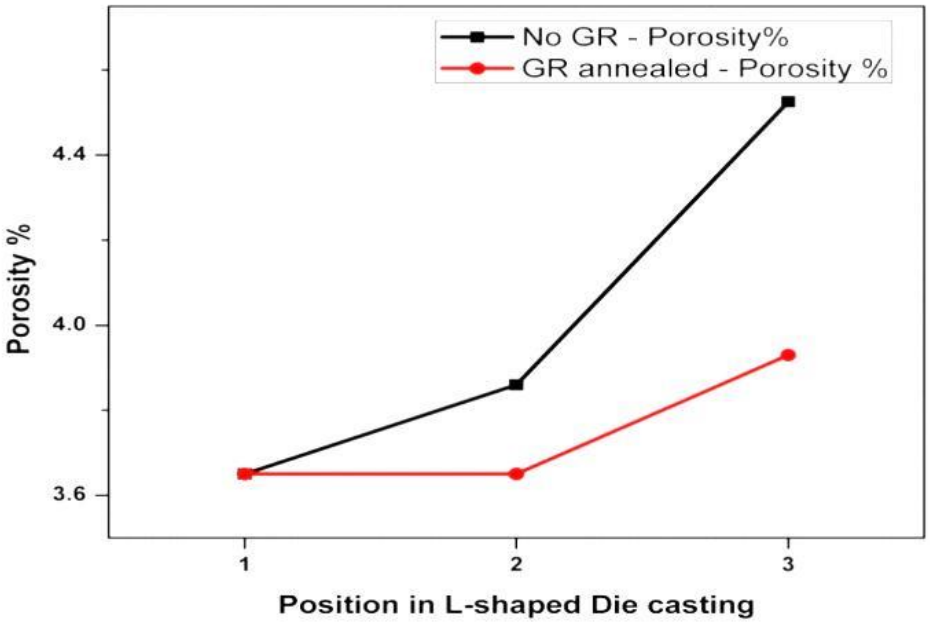

Fig 5.7 Porosity percentages at different positions of the L-shaped die casting

5.2 XRD analysis of L-shape casting

The XRD analysis of the three samples cut from different positions of the L-shaped die casting (Fig. 5.6) are shown in Figures 5.8 (a-c). The 1st position, which solidified first shows a high relative intensity of $TiAl_3$ (JCPDF No. 01-072-5006) phase in the XRD analysis (Fig. 5.8a). The relative intensity of $TiAl_3$ decreased at 2nd position and was the least at the 3rd position. From the above XRD analysis, it can be conclude that the casting part which contains least heterogeneous nucleating particles ($TiAl_3$) is more susceptible to hot tearing. Therefore, to minimize porosity and hot tearing tendency of the Al-7Si-3Cu alloy sufficient nucleating sites should be available in the alloy.

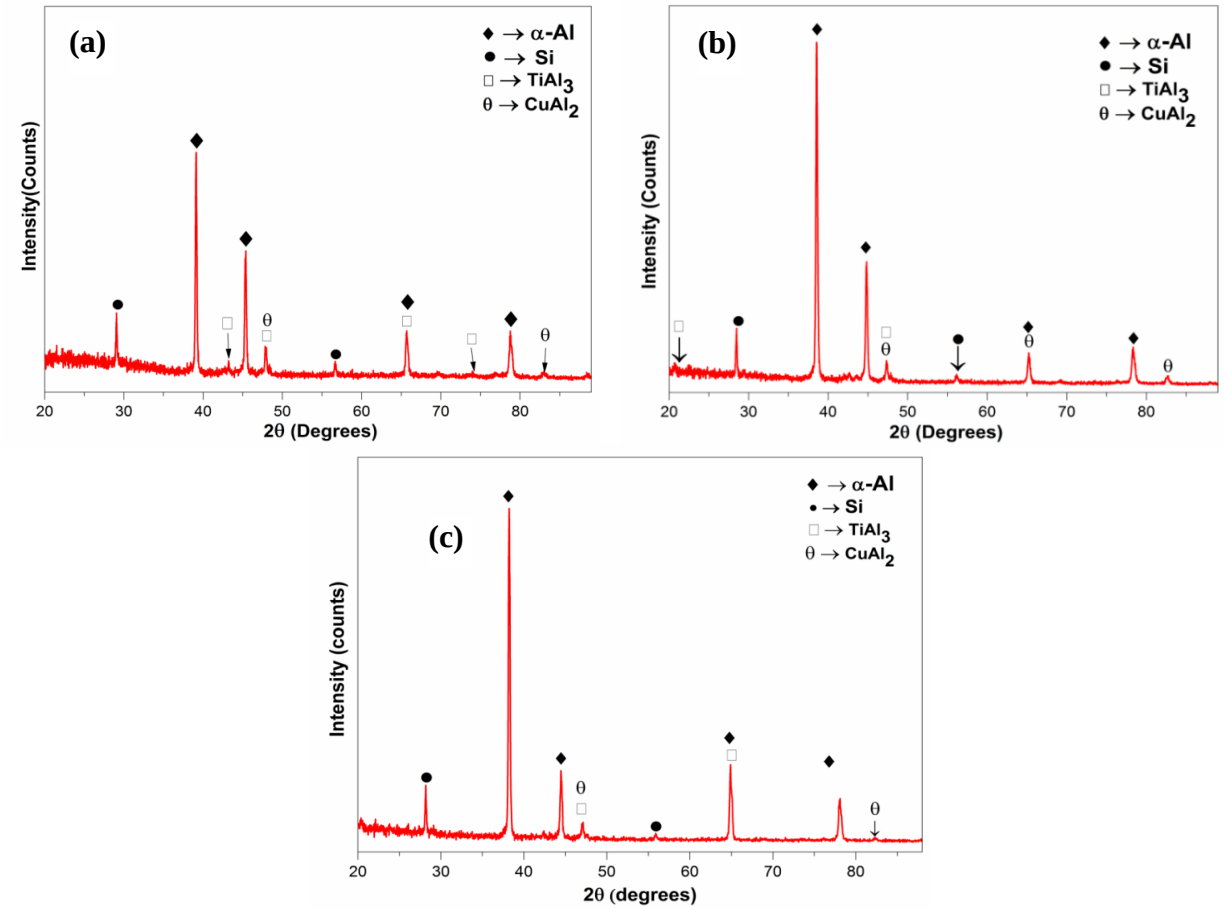

Fig 5.8 XRD analysis of (a) 1st position; (b) 2nd position; (c) 3rd position.

5.3 SEM analysis of Al-7Si-3Cu in L-shape casting

Figures 5.9 (a-d) show the SEM micrographs and their corresponding EDX mapping of Al-7Si-3Cu alloy at 1st position (Fig. 5.6). Form the micrograph analysis it is seen that this region consists more fine dendrites structure rather than equiaxed structure (Fig. 5.9a). However, the presence of titanium is observed and also confirmed with the help of mapping analysis (Fig. 5.9b). As shown in Fig. 5.9c and Fig. 5.9d that titanium is distributed thoroughly in the interdendritic region of α-Al phase. Which provide sufficient under cooling at the ahead of the liquid-solid interface and capable to eliminate hot tear from the casting.

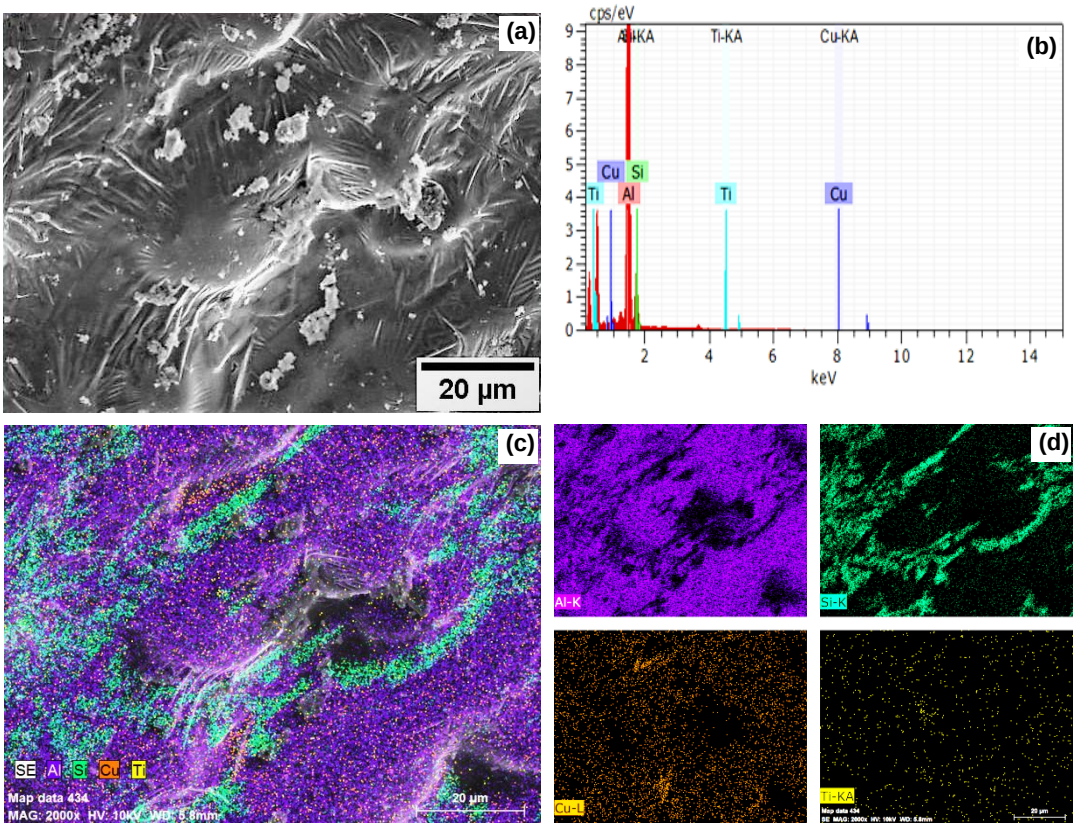

Fig 5.9 SEM analysis of 1st position, (a) SEM microstructure, (b) elemental analysis, (c) and (d) mapping analysis

Figures 5.10 (a-d) show the mapping of SEM micrograph of Al-7Si-3Cu of 2nd position (Fig. 5.6). In this region hot tear was not propagate. In this region (Fig. 5.10a), microstructure is dendritic in nature but are less in comparison to 1st position. The elemental analysis and mapping display the presence of titanium particles in the region, which may be in the form of both $TiAl_3$ and TiB_2 particles as shown in Fig. 5.10 (b-d). Boron was added in very low quantity so it is not detected with the limitations of machine. These particles contribute to break the dendritic structure and ultimately reduced the hot tear. There is presence of copper particle, but there effect is reduced by titanium particles. The SEM microstructure shows that this region consists less Cu content in comparison to 1st position. Copper is uniformly distributed throughout the α-Al matrix. However, silicon is present in great amount in this region, therefore, fluidity of liquid metal is quite high in this region. Higher fluidity of the melt reduces the hot tearing tendency of the Al-7Si-3Cu alloy.

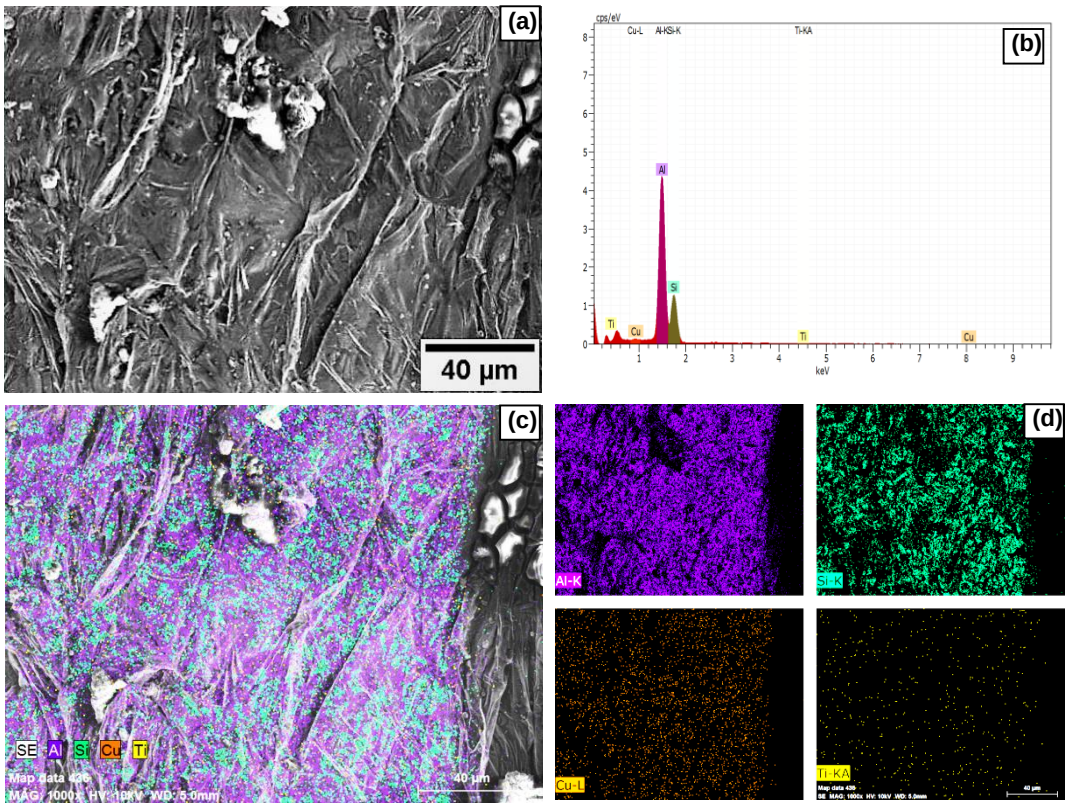

Fig 5.10 SEM analysis of 2nd position, (a) SEM microstructure, (b) elemental analysis, (c) and (d) mapping analysis.

Figures 5.11(a-f) show the SEM, elemental analysis and mapping of the 3rd position (Fig. 5.6). Fig. 5.11a shows a crack surface in the casting region. Major part of the crack surface shows the presence of aluminium and silicon content. From the elemental analysis (Fig. 5.11b and Fig. 5.11c) it is clearly seen that this region consists very less quantity of titanium. Where, $TiAl_3$ and TiB_2 particles help in reducing dendritic structure and ultimately reduce the hot tear tendency of the particle. Since there was less existence of titanium, so the hot tear was present in this casting region, which is last stage to solidify. Fig. 5.11d shows the formation of spikes on the hot tearing surface which is due to the lack of feeding at the last stage of the solidification. Mapping analysis of this region clearly shows the absence of titanium particles (Fig. 5.11e and Fig. 5.11f).

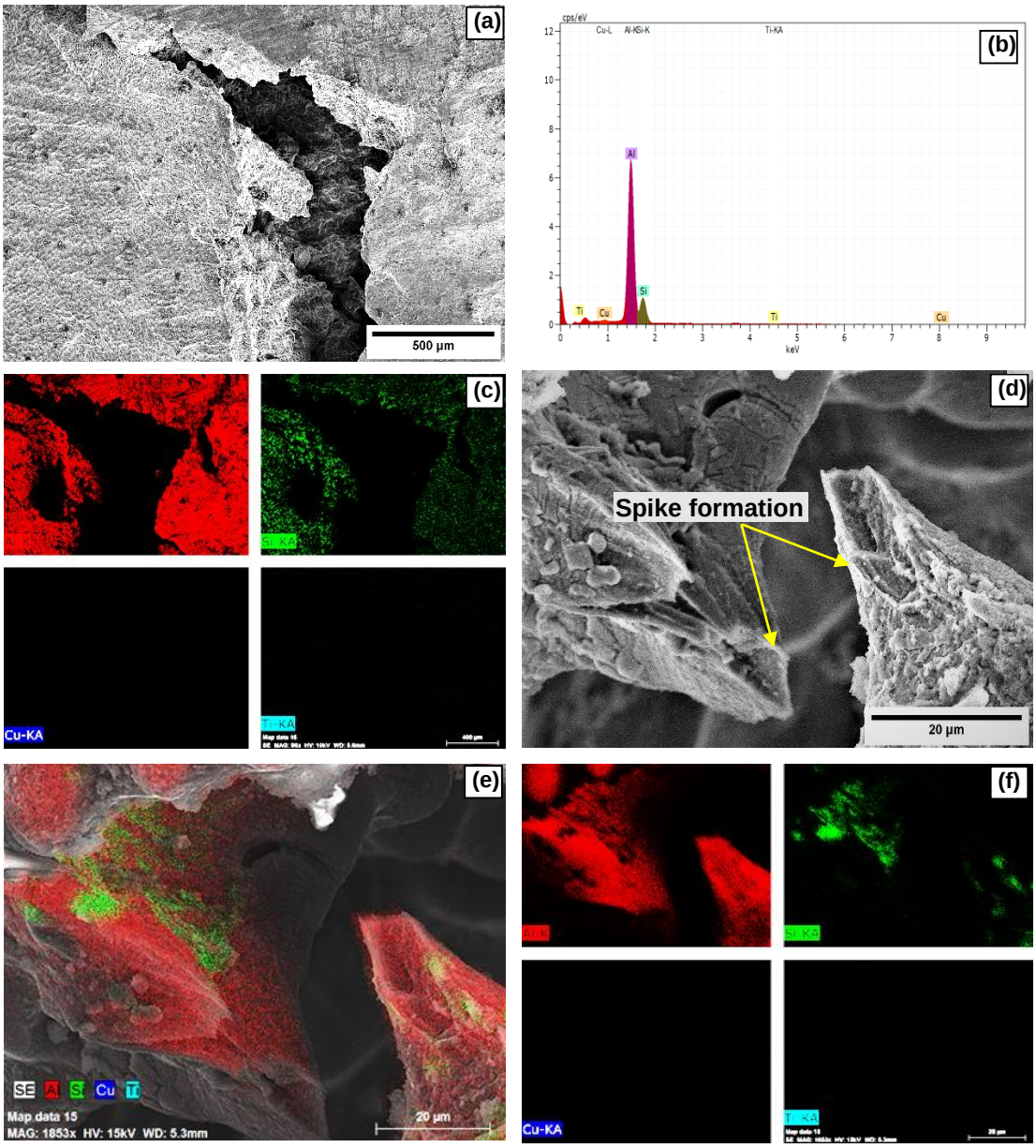

Fig 5.11 SEM analysis of 3rd position, (a) fracture surface; (b) elemental analysis; (c) mapping analysis; (d) spike formation; (e) and (f)mapping analysis.

For better understanding the mechanism of hot tearing in the Al-7Si-3Cu alloy the Scanning Electron Microscopy (SEM) images of the fracture surface acquired from a representative hot teared surface are shown in Figures 5.12 (a-g). Fig. 5.12a shows the fracture surface area cracked during the hot tear test. Fig. 5.12b and Fig. 5.12c show the fracture surface from the center areas, this is the latter stage of solidification of melt near the down-sprue and solidification mode was columnar as seen in earlier studies [62,96]. Fig. 5.12d and Fig. 5.12e show detached solid bridges and free dendrite structures, few of them are fragmented due to tensile loading in the mushy zone and outer dendrites are partially

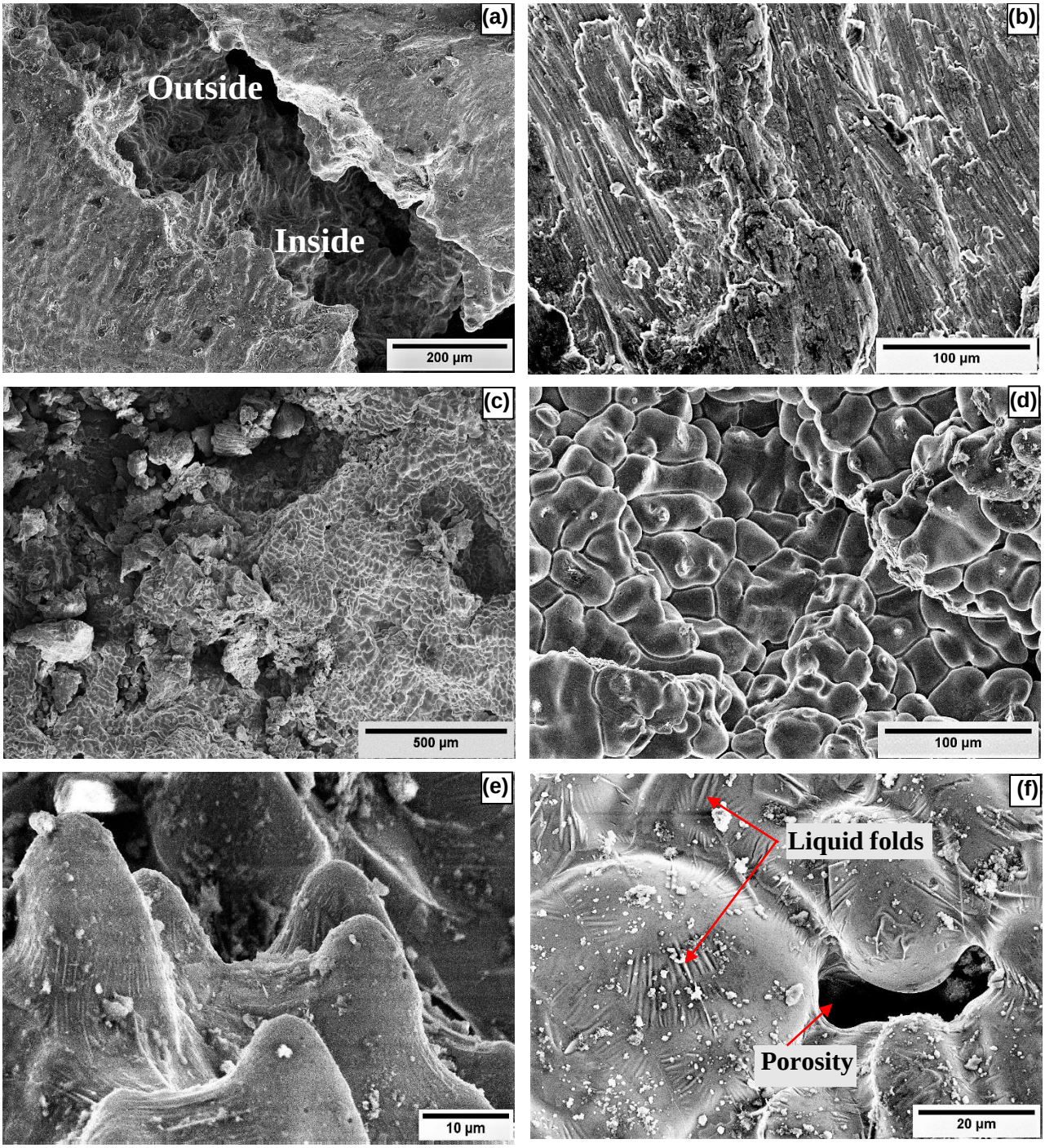

Fig 5.12 SEM fractographs of (a) hot tear surface of Al-7Si-3Cu alloy die casting showing the whole cross section area; (b); and (c) fracture surface from the internal areas showing connected dendrites which are rupture during the test; (d); and (e) Showing the bumpy nature of hot tear surface at during tensile loading in mushy zone at higher magnification respectively; (f); Feature of porosity and liquid folds on fracture surface.

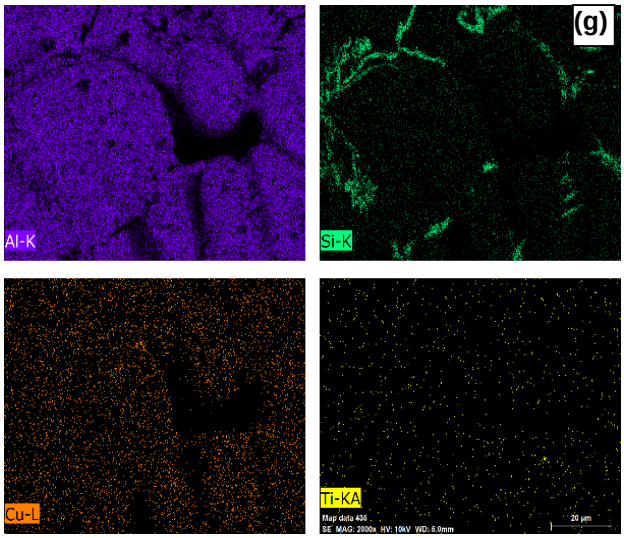

Fig. 5.12. SEM fractographs of (g) the corresponding EDX mapping of Fig. (f).

separated while inner dendrites are associated with each other. The conversion from a mushy state described hot tearing, where almost all the solidifying grains are detached by liquid films [85,157,171]. This can be attributed to shrinkage and porosity leading to either insufficient interdendritic feeding, or absence of eutectic liquid between interdendritic regions. Fig. 5.12f shows the presence of porosity in the hot tear region; this obstructs the continuous flow of liquid during the last stage of solidification. Investigators [56-58] confirmed that they all revealed the bumpy nature of fracture surfaces, made of additional dendrite arm tips. Hot tear persists by breaking the contacts between dendrites below the solidus temperature. However, during interdendritic separation, the liquid film is dense enough to facilitate the formation of dendritic tip, and can be observed in Fig. 5.12f as liquid folds on fractured surface. Fig. 5.12g shows the corresponding EDS analysis results. It can be observed that the hot tear region has lower titanium and higher copper content respectively. This observation supports the statement that the presence of copper in the alloy leads to higher probability of hot tearing. At higher concentrations, copper phase segregates in form of $CuAl_2$ and $MgCuAl_2$ during solidification [172], which leads to depletion of eutectic alloy, as lesser liquid is left for micro-feeding. Thus, the higher concentration of copper adversely affects the eutectic alloy and leads to formation of cracks. As titanium has a profound affinity for the solid phase, its concentration in the melt drops as the solidification continues and at low titanium concentrations of the peritectic horizontal, bulk titanium $TiAl_3$ particles are unstable in contact with the melt and dissolved quickly, resulting large columnar grains was observed at the center [173-175].

Crack susceptibility of Al-7Si-3Cu alloy due the presence of Fe and Cu elements

Figures 5.13 (a-e) show the SEM and EDX analysis of the grain refined and fracture surface of Al-7Si-3Cu alloy. Fig. 5.13a shows the presence of intermetallic, β-FeCu and α-MnFe which are in needle shape [176,177]. These intermetallics phases could bridge a gap between primarily solidified dendrites, in particular, where low Fe content was presented since the solid fraction was still small (around 0.60 wt.%). As it is observed that the θ-$CuAl_2$ phases remain in the interdendritic region at the fracture surface. Fig. 5.13b shows the hot teared surface of Al-7Si-3Cu alloy at lower magnification.

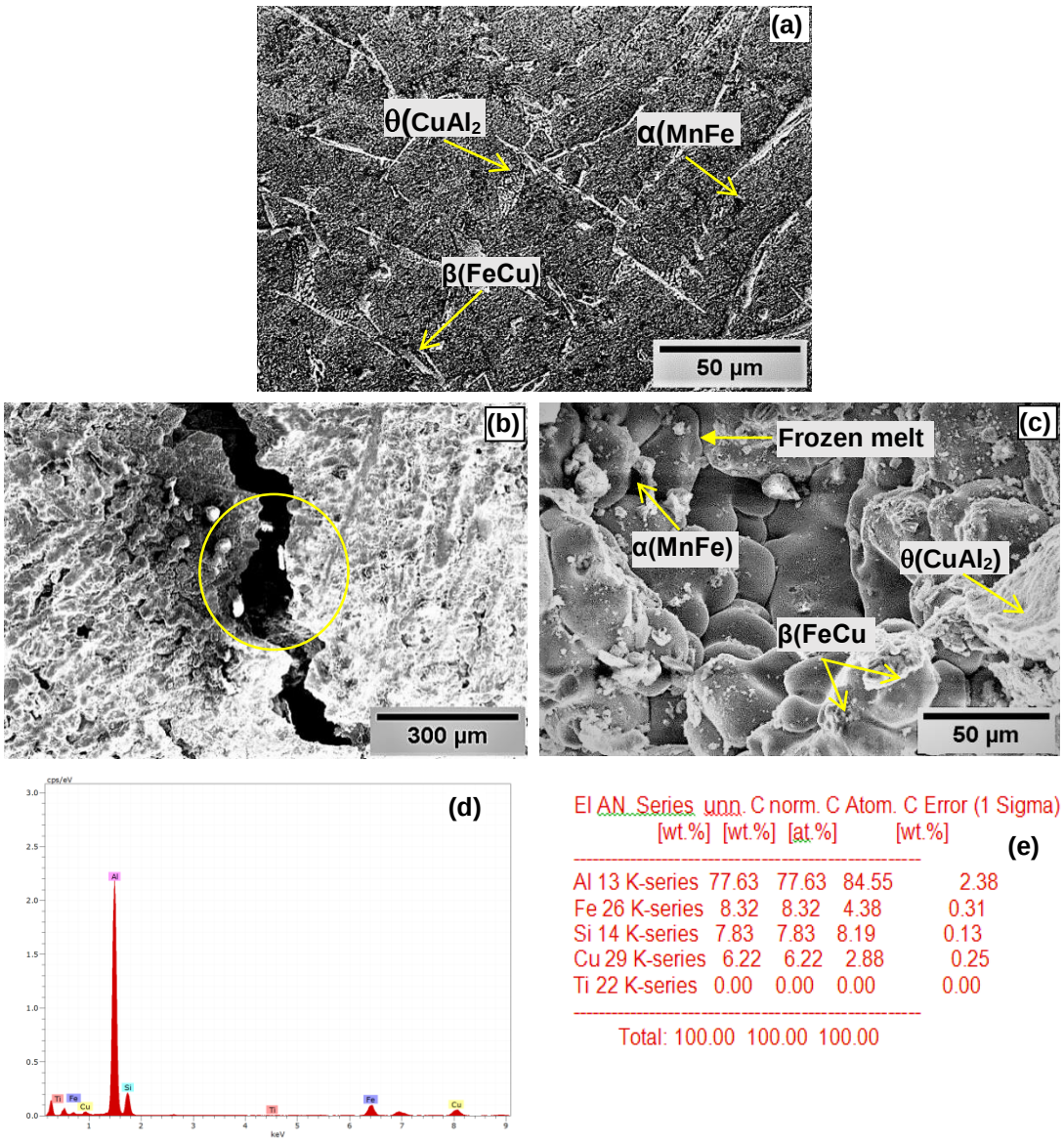

Fig 5.13 SEM analysis of Al-7Si-3Cu alloy; (a) Grain refined; (b &c) hot tear surface; (d &e) EDX analysis of the selected area of fracture surface.

The hot tear region created by breaking the remaining liquid folds have a very dissimilar behavior as this can be seen in Fig. 5.13c. The Al-7Si-3Cu alloy has much more β-FeCu than α-MnFe on the hot tear surface [176]. The EDX analysis has been carried out to detect the existence of elements on hot tear surface (Fig. 5.13 d& e). All other alloys contain a larger proportion of β-FeCu segments [177]. The presence of θ particles developed from the tear surface of the Al-7Si-3Cu alloy. Hot teared region with frozen liquid melt formed at surrounding temperature near the surface (last stage of solidification) [178]. Hot tears were still initiating at a lower temperature than the onset temperature of the eutectic reaction. The similarity in shape of the θ particles and their fine sizes result from eutectic precipitation and inadequate time to propagate since hot tearing arisen through solidification. At this point, solid skeleton formation begins to transfer tensile forces at the early stage, which suggests that a continuous dendritic network formed in the mushy zone starts to separate under the applied tensile force for hot tearing to occur.

5.4 TEM analysis of hot tearing surface

The TEM analysis of 1st and 3rd locations of test bar (Fig. 5.6) has been carried out to observe the effect of titanium and copper on hot tearing tendency of Al-7Si-3Cu alloy as shown in Figs. 5.14 (a-h). The results have been investigated with the help of crystals orientational relationship between Al and $TiAl_3$ particles. Fig. 5.14a shows the $TiAl_3$ particles which have a tetragonal structure with a = 0.3846 nm and c = 0.8594 nm. [151]. These $TiAl_3$ particles are found at the center of the α-Al grains, and boride particles are pushed along the grain boundary. According to the X-ray diffraction theory, the closed packed plane normally to the plane that has the highest structure factor e.g. the plane $\{001\}_{\mathrm{Al}}$ is the closed packed plane correspond to $\{002\}_{TiAl_3}$[76], which has the highest structure factor and low wetting angle. The other closed packed or nearly closed packed plane are identified in this TEM analysis as found in XRD analysis earlier which have perfect matching with Al matrix, these are $\{111\}_{Al}||\{112\}_{TiAl_3}$, $\{200\}_{Al}||\{200\}_{TiAl_3}$, and $\{200\}_{Al}||\{004\}_{TiAl_3}$.

Fig. 5.14b displays the TEM micrograph of the fracture surface (at, position 3rd). The corresponding SAED pattern is shown in figure Fig. 5.14c. The present planes $\{111\}_{Al}||\{101\}TiAl_3$ shows the poor matching between the Al and $TiAl_3$ (aluminide) phases, the minimum dis-registry is 31%, which is quite high. At the hot tear region, the two phase are not coherent resulting in the larger lattice strain [33]. This is a major cause

of opening of hot tears in this region. Although, at fractured region $TiAl_3$ particles were in much lower quantity as compared to 1st position. Subsequently, it was not capable of resisting the tensile load in the mushy zone between interdendritic regions. The EDS analysis confirmed that this surface (fracture) contained α-Al, Si, Cu and apart from the significant amount of titanium. The copper particle was equally distributed at the hot tear surface in a higher amount which favors the statement that copper increase the hot tear tendency of the alloy. Eskin et. al [232] performed inspections and support the same trend. The Cu-content has a dominating influence on hot tearing susceptibility in Al-7Si-3Cu-alloys (Fig. 5.14f). A high Cu-content result in a significant hot tearing susceptibility (high HCS, and high CSC), a high Ti content reduces hot tearing susceptibility (low HCS and low CSC) [229]. Furthermore, theoretically predicted phases were also taking into account. Many investigators [47,69,233] found that at higher Cu concentrations Cu-phases segregate in the form of $CuAl_2$, $Al_5Cu_2Si_6$, and $CuAl_2Mg$ during solidification; this has a negative influence and depletes the alloy of eutectic available for micro feeding. The aggregate of precipitated Mg-containing phases in the eutectic in the as-cast alloy is less [209]. Titanium was also present at the fracture surface, but in lesser quantity, it was not able to provide adequate heterogeneous nucleation sites for the grain refinement process, resulting in poor refinement on the α-Al surface, resulting hot tear occurred. To reduce the hot tearing tendency of Al-7Si-3Cu alloy, it is necessary to be presents aluminide particles of the minimum misfit. $TiAl_3$ particles should be present in each direction corresponds to an absolute a_H/a_B value, with basal facts larger than the critical α-Al nucleation size, for a given under cooling achieved during the casting. Edge-to-Edge matching is a governing approach that enables the prediction of those particles that can act as an effective nucleating substrate during solidification. From a crystallographic point of view [151], although AlB_2, $TiAl_3$, and TiB_2 are all active heterogeneous nucleants for Al-alloys industry, the predicted ability of the substrates varies.

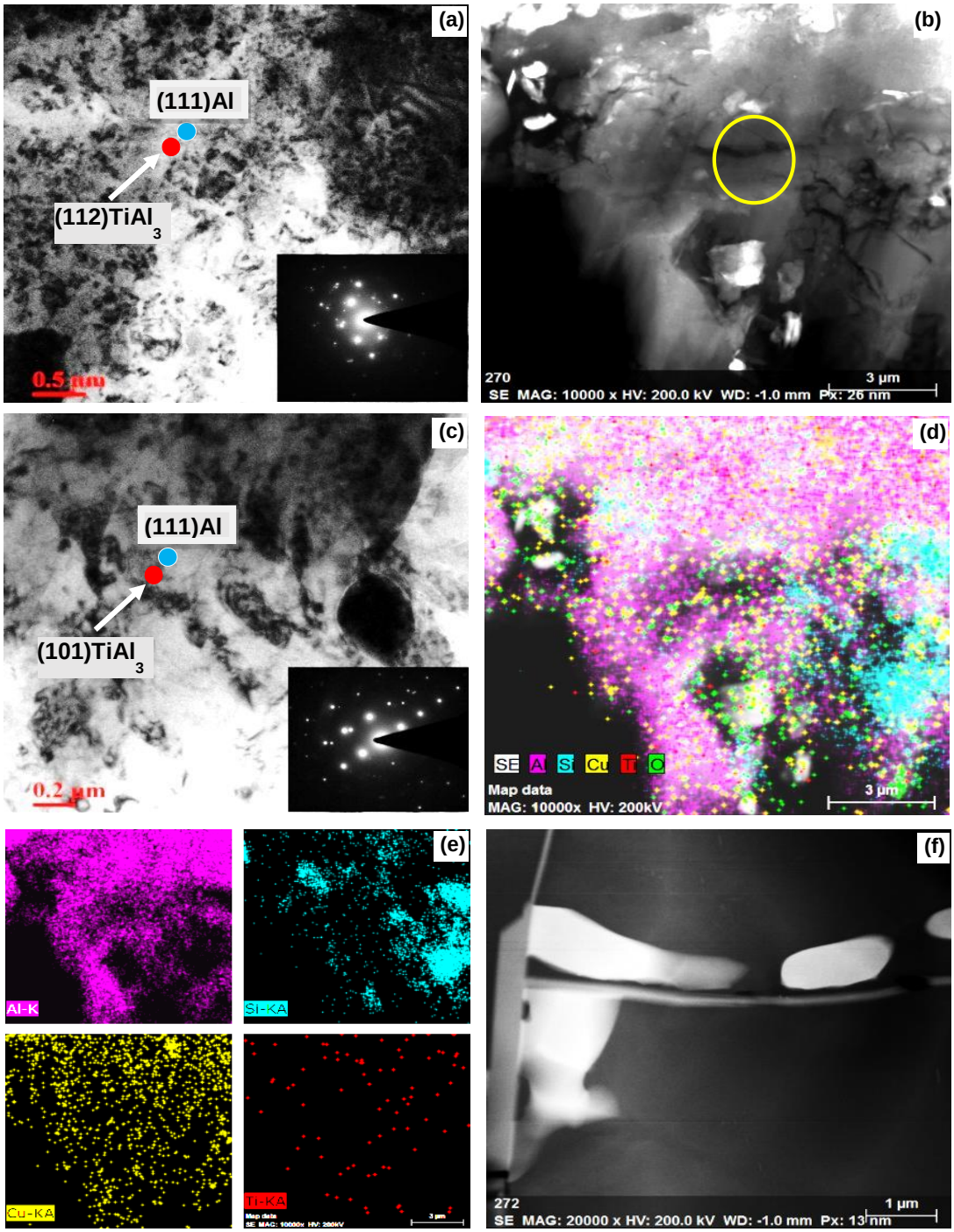

Fig 5.14 TEM analysis of Al-7Si-3Cu alloy; (a) Grain refined; (b &c) hot tear surface; (d &e) EDX analysis of fracture surface; (f) presence of copper on hot tear surface. TEM analysis of Al-7Si-3Cu alloy;

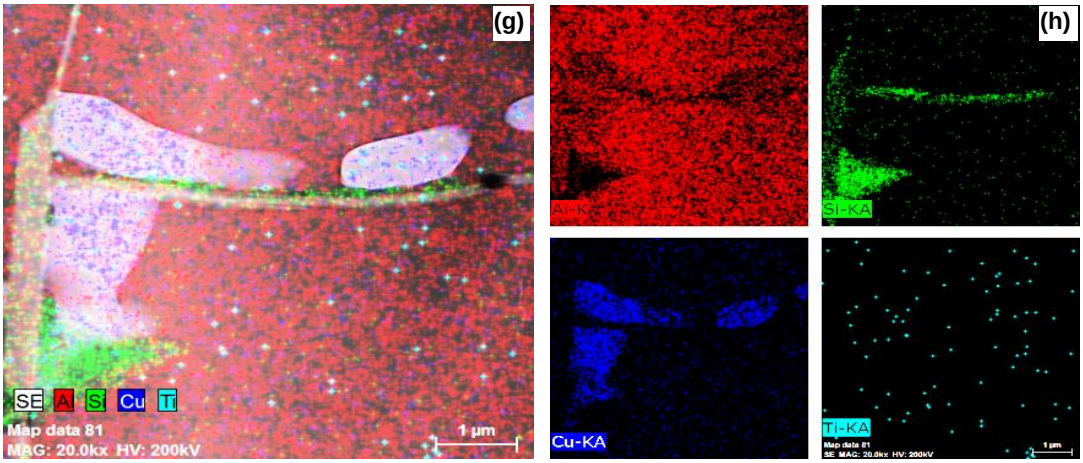

Fig 5.14 (g &h) EDX mapping of the selected area of fracture surface.

CONCLUSIONS AND FUTURE WORK

Based on present investigations the following conclusions are made.

- Addition of Al-5Ti-1B master alloy refined the α-Al phase in Al-7Si-3Cu alloy.
- The improved grain refining efficiency of Al-5Ti-1B master alloy after ball milling could be attributed to the decrease in $TiAl_3$ particles size but, excessive refining of $TiAl_3$ nucleating sites probably accelerates fading of particles hence decreasing of the grain refining efficiency.
- The improved grain refining efficiency of Al-5Ti-1B master alloy after annealing could be attributed to the increase in volume fraction of $TiAl_3$ particles.
- The better grain refining performance of the hot rolled Al-5Ti-1B master alloy as compared to the type A, type B and Type C master alloy could be attributed to the decrease in the particle size (15 μm) and the increase in the number of fine $TiAl_3$ particles due to the fracture of $TiAl_3$ during rolling.
- Addition of Al–5Ti–1B master alloy could result in significant improvement in the mechanical properties of Al–7Si–3Cu alloy to the extent of above 20.5%, 23.8%, 28.5% and 39%, respectively in UTS with addition of type A, type B, type C and type D master alloys separately.
- Hardness properties of Al-7Si-3Cu alloy were improved due to the addition of type A, type B, type C and type D master alloys in Al-7Si-3Cu alloy individually.
- At 300 ºC mould temperature, hot tear is completely disappeared from the test bar. At this temperature the initiation of hot cracks could be refilled by the remaining liquid and healed, which lead to the lower hot tearing tendency .
- The results showed a good correlation between hot tears and grain size, as a reduction in hot tearing tendency was attended by a decrease in grain size. The addition of type A master alloy at 0.050 wt.% Ti in Al-7Si-3Cu alloy hot tearing got eliminated at 230 ºC mould temperature.
- The addition of type B master alloy (0.045 wt.% Ti) with 30h and 50h ball milling completely eliminated hot tearing in Al-7Si-3Cu alloy. However, the optimum grain refinement of Al-7Si-3Cu alloy is attained with the addition for 30h, at 0.045 wt.% Ti with average particles size 20 μm. Al-7Si-3Cu alloy inoculated with type B master alloy at same addition level of Ti for 50h does not show the further refinement due to the additionally smaller size of $TiAl_3$ particles.

- The addition of 0.040 wt.% Ti annealed grain refiner for 8 hours at 700 ˚C eliminated hot tear in Al-7Si-3Cu alloy.
- The Al-7Si-3Cu alloy inoculated with type D master alloy at 0.035 wt.% Ti for 50% hot rolled reduction at 250 ˚C displayed that hot tearing got eliminated from the test bar at lower addition level in comparison to type A, type B, type C master alloys.
- SEM analysis of hot tearing surface shows that remaining intergranular liquid film and liquid bridge are dense enough to permit the formation of bumping tips and liquid folds.

Suggestion for Future Work

The suggestions for future work are;

- EBSD analysis can be performed on hot tearing surface to better understand the grain refinement mechanism.
- Tomography studies on Al-7Si-3Cu alloy can be explored to get the internal structure of the samples.
- Extensive study about the machinability and corrosion resistance of Al-7Si-3Cu alloy may also be performed.
- Investigate the mechanism of hot tear in welding and compare to the casting.
- Combined effect of grain refiner and modifier on hot tearing.

References

[1] Y. Zeng, B. Jiang, R. Li, H. Yin, S. Al-ezzi, Grain Refinement Mechanism of the As-Cast and Al. Alloys, (2017) 1–9. doi:10.3390/met7050172.

[2] G.L. Liu, N.C. Si, S.C. Sun, Q.F. Wu, Effects of grain refining and modification on mechanical properties and microstructures of Al-7.5Si-4Cu cast alloy, Trans. Nonferrous Met. Soc. China (English Ed. 24 (2014) 946–953. doi:10.1016/S1003-6326(14)63147-2.

[3] A.M. Samuel, H.W. Doty, S.V. Gallardo, F.H. Samuel, The effect of Bi-Sr and Ca-Sr interactions on the microstructure and tensile properties of Al-Si-based alloys, Materials (Basel). 9 (2016). doi:10.3390/ma9030126.

[4] M. Liu, Z. Wu, R. Yang, J. Wei, Y. Yu, P.C. Skaret, H.J. Roven, DSC analyses of static and dynamic precipitation of an Al–Mg–Si–Cu aluminum alloy, Prog. Nat. Sci. Mater. Int. (2015) 1–6. doi:10.1016/j.pnsc.2015.02.004.

[5] J. Campbell, Castings Practice: The Ten Rules of Castings, Butterworth-Heinemann, 2004. https://books.google.com/books?id=MS-JFA04n0QC&pgis=1 (accessed February 17, 2016).

[6] D.B. Karunakar, R.N. Rai, S. Patra, G.L. Datta, Effects of grain refinement and residual elements on hot tearing in aluminum castings, (2009) 851–858. doi:10.1007/s00170-009-2037-4.

[7] A. Srinivasan, Z. Wang, Y. Huang, F. Beckmann, K.U. Kainer, N. Hort, Hot tearing characteristics of binary Mg-Gd alloy castings, Metall. Mater. Trans. A Phys. Metall. Mater. Sci. 44 (2013) 2285–2298. doi:10.1007/s11661-012-1593-7.

[8] G.K. Sigworth, Grain Refining of Aluminum Casting Alloys, 67 (2001) 1–12. doi:10.1007/BF03355416.

[9] K. Nogita, A. Knuutinen, S.D. Mcdonald, A.K. Dahle, Mechanisms of eutectic solidification in Al – Si alloys modified with Ba , Ca , Y and Yb, 1 (2002) 219–228.

[10] S. Hegde, Æ.K.N. Prabhu, Modification of eutectic silicon in Al – Si alloys, (2008) 3009–3027. doi:10.1007/s10853-008-2505-5.

[11] G. Heiberg, L. Arnberg, Investigation of the microstructure of the Al ± Si eutectic in binary aluminium ± 7 wt % silicon alloys by electron backscatterd irraction (EBSD), 1 (2001) 43–49.

[12] A.K. Dahle, K. Nogita, S.D. McDonald, C. Dinnis, L. Lu, Eutectic modification and microstructure development in Al–Si Alloys, Mater. Sci. Eng. A. 413–414 (2005) 243–248. doi:10.1016/j.msea.2005.09.055.

[13] B. Level, R.A. Harding, Solidification Defects in Castings, (1994).

[14] D'Elia F, Ravindran C, Sediako D (2015) Interplay among solidification, microstructure, residual strain and hot tearing in B206 aluminum alloy. Mater Sci Eng A 624:169–180

[15] G. Cao, S. Kou, Hot tearing of ternary Mg-Al-Ca alloy castings, Metall. Mater. Trans. A Phys. Metall. Mater. Sci. 37 (2006) 3647–3663. doi:10.1007/s11661-006-1059-x.

[16] H. Huang, P. Fu, Y. Wang, L. Peng, H. Jiang, Effect of pouring and mold temperatures on hot tearing susceptibility of AZ91D and Mg − 3Nd − 0 . 2Zn − Zr Mg alloys, Trans. Nonferrous Met. Soc. China. 24 (2014) 922–929. doi:10.1016/S1003-6326(14)63144-7.

[17] A. Dissertation by Shimin Li, Hot Tearing in Cast Aluminum Alloys : by, (2010).

[18] K. Navyanth, Minimization of Defects in Aluminium Alloy Castings Using Sqc., 8 (2013).

[19] T.R. Society, P. Transactions, E. Sciences, Heterogeneous nucleation and adsorption, 361 (2013) 409–417.

[20] S. Shankar, M.M. Makhlouf, Eutectic Solidification of Aluminum-Silicon Alloys, (2004) 3038–3043.

[21] G.K. Sigworth, Fundamentals of Solidification in Aluminum Castings, 8 (2014) 7–20.

[22] M. Engineers, S.A. Scientific, The Effect of Mould Temperature and Cooling, (2009).

[23] N.E. Gmbh, Thermal Description Of Hypoeutectic Ai-Si-Cu Alloys Using Silicon Equivalency, (2016) 152–168.

[24] N Iqbal, N H Dijk, T Hansen, L Katgerman, GJ Kearley, The role of solute titanium and TiB_2 particles in the liquid-solid phase transformation of aluminum alloys [J]. Mater Sci Eng A, 386: (2004), 20-26.

[25] R. Haghayeghi, E.J. Zoqui, H. Bahai, An investigation on the effect of intensive shearing on the grain refinement of A5754 aluminium alloy, J. Alloys Compd. 481 (2009) 358–364. doi:10.1016/j.jallcom.2009.02.135.

[26] M. Easton, D. Stjohn, Grain Refinement of Aluminum Alloys : Part II . Confirmation of , and a Mechanism for , the Solute Paradigm, Metals 30 (1999) 1625–1633.

[27] M.A. Doheim, A.M. Omran, G.A. Sayed, Evaluation of Al-Ti-C Master Alloys as Grain Refiner for Aluminum and Its Alloys, (2011) 1–6. doi:10.1007/s11661-011-0689-9.

[28] T.K., P.hD. Thesis , The Effect of Grain Refinement on the Castability of Magnesium-Aluminium Alloys, (2007).

[29] T. Wang, Z. Chen, H. Fu, T. Li, Grain refining performance of Al-B master alloys with different microstructures on Al-7Si alloy, Met. Mater. Int. 19 (2013) 367–370. doi:10.1007/s12540-013-2012-3.

[30] Z. Chen, T. Wang, L. Gao, H. Fu, T. Li, Grain refinement and tensile properties improvement of aluminum foundry alloys by inoculation with Al-B master alloy, Mater. Sci. Eng. A. 553 (2012) 32–36. doi:10.1016/j.msea.2012.05.088.

[31] J. Wannasin, R. Canyook, S. Wisutmethangoon, M.C. Flemings, Grain refinement behavior of an aluminum alloy by inoculation and dynamic nucleation, Acta Mater. 61 (2013) 3897–3903. doi:10.1016/j.actamat.2013.03.029.

[32] R.Z. Valiev, T.G. Langdon, Achieving exceptional grain refinement through severe plastic deformation: New approaches for improving the processing technology, Metall. Mater. Trans. A Phys. Metall. Mater. Sci. 42 (2011) 2942–2951. doi:10.1007/s11661-010-0556-0.

[33] G.M. Sigworth G, 907, AFS Trans ,. 172 (2007) 907.

[34] P. Li, S. Liu, L. Zhang, X. Liu, Grain refinement of A356 alloy by Al-Ti-B-C master alloy and its effect on mechanical properties, Mater. Des. 47 (2013) 522–528. doi:10.1016/j.matdes.2012.12.033.

[35] Z. Wei Chen, Z. He, W. Qi Jie, Growth restriction effects during solidification of aluminium alloys, Trans. Nonferrous Met. Soc. China (English Ed. 19 (2009) 410–413. doi:10.1016/S1003-6326(08)60287-3.

[36] S. Yan, H. Wang, The Effect of Small Amount of Titanium Addition on the Grain Refinement and Mechanical Properties of ZA48 Alloy, 22 (2013) 1113–1119. doi:10.1007/s11665-012-0382-1.

[37] T. Wang, Z. Chen, H. Fu, L. Gao, T. Li, Grain refinement mechanism of pure aluminum by inoculation with Al-B master alloys, Mater. Sci. Eng. A. 549 (2012) 136–143. doi:10.1016/j.msea.2012.04.019.

[38] M. V Markushev, On the Principles of the Deformation Methods of Aluminum-Alloys Grain Refinement to Ultrafine Size : I . Fine-Grained Alloys, 108 (2009) 43–49. doi:10.1134/S0031918X09070060.

[39] L. Singh, G. Goga, R. Singh, Review of the Latest Developments in Grain Refinement, 2 (2012) 2724–2727.

[40] M. Nowak, L. Bolzoni, N. Hari Babu, Grain refinement of Al-Si alloys by Nb-B inoculation. Part I: Concept development and effect on binary alloys, Mater. Des. 66 (2015) 366–375. doi:10.1016/j.matdes.2014.08.066.

[41] F.D. Elia, A Study On Grain Refinement And Hot Tearing In Permanent Mold Cast Aluminum Alloys, (2009).

[42] M. Kenneth, Heterogeneous nucleation catalysis and grain refinement, (1990).

[43] T.E. Quested, A.L. Greer, Athermal heterogeneous nucleation of solidification, 53 (2005) 2683–2692. doi:10.1016/j.actamat.2005.02.028.

[44] M.A. Easton, D.H. Stjohn, A model of grain refinement incorporating alloy constitution and potency of heterogeneous nucleant particles, Acta Mater. 49 (2001) 1867–1878. doi:10.1016/S1359-6454(00)00368-2.

[45] J.G. Li, M. Huang, M. Ma, W. Ye, D.Y. Liu, D.M. Song, B.Z. Bai, H.S. Fang, Performance comparison of AlTiC and AlTiB master alloys in grain refinement of commercial and high purity aluminum, Trans. Nonferrous Met. Soc. China (English Ed. 16 (2006) 242–253. doi:10.1016/S1003-6326(06)60042-3.

[46] C.G. Shivaprasad, S. Narendranath, V. Desai, S. Swami, M.S.G. Prasad, Influence of Combined Grain Refinement and Modification on the Microstructure and Mechanical Properties of Al-12Si, Al-12Si-4.5Cu Alloys, Procedia Mater. Sci. 5 (2014) 1368–1375. doi:10.1016/j.mspro.2014.07.454.

[47] K.G. Basavakumar, P.G. Mukunda, M. Chakraborty, Influence of grain refinement and modification on microstructure and mechanical properties of Al-7Si and Al-7Si-2.5Cu cast alloys, Mater. Charact. 59 (2008) 283–289. doi:10.1016/j.matchar.2007.01.011.

[48] M. Farkašová, E. Tillová, M. Chalupová, Modification of Al-Si-Cu cast alloy, FME Trans. 41 (2013) 210–215.

[49] G. Timelli, G. Camicia, S. Ferraro, Effect of grain refinement and cooling rate on the microstructure and mechanical properties of secondary Al-Si-Cu alloys, J. Mater. Eng. Perform. 23 (2014) 611–621. doi:10.1007/s11665-013-0757-y.

[50] F.H.S. P. Ouellet, Effect of Mg on the Ageing Behavior of Al-Si-Cu 319 Type Aluminum Casting Alloys, J. Mater. Sci. 34 (1999) 4671–4697.

[51] F.D. Elia, C. Ravindran, Influence of grain refinement on hot tearing in B206 and A319 aluminum alloys, Trans. Indian Inst. Met. 62 (2009) 315–319. doi:10.1007/s12666-009-0072-3.

[52] H. Ghadimi, S. Hossein Nedjhad, B. Eghbali, Enhanced grain refinement of cast aluminum alloy by thermal and mechanical treatment of Al-5Ti-B master alloy, Trans.

Nonferrous Met. Soc. China (English Ed. 23 (2013) 1563–1569. doi:10.1016/S1003-6326(13)62631-X.

[53] K. Venkateswarlu, S.K. Das, M. Chakraborty, B.S. Murty, Influence of thermo-mechanical treatment of Al Á 5Ti master alloy on its grain refining performance on aluminium, Mater. Sci. Eng. A. 351 (2003) 237–243. doi:10.1016/S0921-5093(02)00842-0.

[54] K. Venkateswarlu, B.S. Murty, M. Chakraborty, Effect of hot rolling and heat treatment of Al – 5Ti – 1B master alloy on the grain refining efficiency of aluminium, 301 (2001) 180–186.

[55] U. Schulz, K. Fritscher, Grain refinement of 7075Al alloy microstructures by inoculation with Al-Ti-B master alloy, (n.d.). doi:10.1088/1757-899X/200/1/012029.

[56] M. Science, B. County, Effect of grain refinement on mechanical properties of ball-milled bulk aluminum of ball-milled bulk aluminum, (2015). doi:10.1016/j.msea.2008.01.045.

[57] N.H. leandro Bolzoni, Engineering the heterogeneous nuclie in Al-Si alloys for solidification, Appl. Mater. Today. 5 (2016) 255–259.

[58] H.K. M. Gorny, G. Sikora, Effect of Ti and B on the stability of grain refinement of Al-Cu alloy, Arch. Foundry Engg. 16 (2016) 35–38.

[59] F.L. P.R. Spena, M.D. Maddis, No Title, Met. Res. Technol. 114 (2017) 309.

[60] M.S.A. Shereen, No Titl, Met. Res. Technol. 114 (2017) 213.

[61] J. Zuo, L. Hou, J. Shi, H. Cui, L. Zhuang, J. Zhang, Materials Characterization E ff ect of deformation induced precipitation on grain re fi nement and improvement of mechanical properties AA 7055 aluminum alloy, Mater. Charact. 130 (2017) 123–134. doi:10.1016/j.matchar.2017.05.038.

[62] C. Nparc, K. Kamga, NRC Publications Archive (NPArC) additions Hot tearing of Aluminum-Copper B206 Alloys with Iron and Silicon Additions, (2010).

[63] D.G. Eskin, L. Katgerman, A quest for a new hot tearing criterion, Metall. Mater. Trans. A Phys. Metall. Mater. Sci. 38 A (2007) 1511–1519. doi:10.1007/s11661-007-9169-7.

[64] S. Li, D. Apelian, Hot tearing of aluminum alloys a critical literature review, Int. J. Met. 5 (2011) 23–40.

[65] M. Easton, H. Wang, J. Grandfield, D. Stjohn, E. Sweet, An Analysis of the Effect of Grain Refinement on the Hot Tearing of Aluminium Alloys, 28 (2004) 224–229.

[66] D. Ovono Ovono, I. Guillot b, D. Massinon, Determination of the activation energy in a cast aluminium alloy by TEM and DSC, Journal of Alloys and Compounds 432 (2007) 241–246

[67] S.G. Shabestari, M. Malekan, Assessment of the effect of grain refinement on the solidification characteristics of 319 aluminum alloy using thermal analysis, J. Alloys Compd. 492 (2010) 134–142. doi:10.1016/j.jallcom.2009.11.122.

[68] S. Bozorgi, K. Haberl, C. Kneissl, T. Pabel, P. Schumacher, Effect of Alloying Elements (Magnesium and Copper) on Hot Cracking Susceptibility of AlSi7MgCu-ALLOYS, 1–8.

[69] S. Robert, H. Building, Thermodynamic Prediction of Thixoformability in Alloys Based on the Al-Si-Cu and Al-Si-Cu-Mg Systems D. Liu 1 , H. V. Atkinson 1 and H. Jones 21, (2010) 308.

[70] A.T. Submitted by André Bernard Phillion, Hot Tearing and Constitutive Behaviour of Semi-Solid Aluminum Alloys , (2007).

[71] M. Bagheri, M. Alizadeh, H. Technology, The Effects of Hot Tear Segregations on the Rolled Product Quality of Continuously Cast Steel, 10 (2013) 11–17.

[72] Y. He, S. Li, K. Sadayappan, D. Apelian, Thermomechanical simulation and experimental characterisation of hot tearing during solidification of aluminium alloys, Int. J. Cast Met. Res. 26 (2013) 72–81. doi:10.1179/1743133611Y.0000000028.

[73] A. Hamadellah, A. Bouayad, Study of hot tear of AlCu5MgTi by restraining casting shrinkage in green- sand mold, 8 (2017) 3099–3105.

[74] N.H. T. Davis, L. Bichler, F.D. Elia, The effect of Grain Refinement on Hot Tearing in Az91D Mg alloy, Miner. Met. Mater. Ser. (n.d.) 653–660.

[75] W.R. Apblett and W.S. Pellini, Factors Which Influence Weld Hot Cracking, Weld. Res. vol.19 (1954) 83.

[76] M.G. Pokorny, C.A. Monroe, C. Beckermann, Z. Zhen, N. Hort, Simulation of Stresses during Casting of Binary Magnesium-Aluminum Alloys, (2010). doi:10.1007/s11661-010-0367-3.

[77] J. Song, Z. Wang, Y. Huang, A. Srinivasan, F. Beckmann, K.U. Kainer, N. Hort, Hot Tearing Susceptibility of Mg-Ca Binary Alloys, Metall. Mater. Trans. A Phys. Metall. Mater. Sci. 46 (2015) 6003–6017. doi:10.1007/s11661-015-3165-0.

[78] Transactions of the Indian Institute of Metals, 62 (2014) 6.

[79] H.J. Wang, J. Xu, Y.L. Kang, M.O. Tang, Z.F. Zhang, Effect of Al-5Ti-1B-1Re on the Microstructure and Hot Crack of As-Cast Al-Zn-Mg-Cu Alloy, J. Mater. Eng. Perform. 23 (2014) 1165–1172. doi:10.1007/s11665-013-0860-0.

[80] I. Farup, J. Drezet, M. Rappaz, In Situ Observation Of Hot Tearing Formation, Acta mater. 49 (2001) 1261–1269.

[81] K.C. Bala, R.H. Khan, Rate of solidification of aluminium casting in varying wall thickness of cylindrical metallic moulds, (2014) 19–30.

[82] M. Rappaz, I. Farup, J.-M. Drezet, Study an Modeling of Hot Tearing Formation, Mert. C. Flemings Symp. Solidif. Mater. Process. (2000) 213–22.

[83] Z. Lin, C.A. Monroe, R.K. Huff, C. Beckermann, Prediction of hot tear defects in steel castings using a damage based model, Proc. from 12th Int. Conf. Model. Cast. Welding, Adv. Solidif. Process. (2009) 329–336.

[84] J. Song, Z. Wang, Y. Huang, A. Srinivasan, F. Beckmann, K.U. Kainer, N. Hort, Hot tearing characteristics of Mg–2Ca–xZn alloys, J. Mater. Sci. 51 (2016) 2687–2704. doi:10.1007/s10853-015-9583-y.

[85] A.K. Birru, D.B. Karunakar, M.M. Mahapatra, A study on hot tearing susceptibility of Al-Cu, Al-Mg, and Al-Zn alloys, Trans. Indian Inst. Met. 65 (2012) 97–105. doi:10.1007/s12666-011-0112-7.

[86] A. Thesis, Hot tearing of Mg-Y and Mg-Y-Zn alloys Zhi Wang, Clausthal University of Technology Chairperson of the Board of Examiners, (2014).

[87] Z. Wang, J. Song, Y. Huang, A. Srinivasan, Z. Liu, K.U. Kainer, N. Hort, An Investigation on Hot Tearing of Mg-4.5Zn-(0.5Zr) Alloys with Y Additions, Metall. Mater. Trans. A Phys. Metall. Mater. Sci. 46 (2015) 2108–2118. doi:10.1007/s11661-015-2755-1.

[88] G. Cao, I. Haygood, S. Kou, Onset of hot tearing in ternary Mg-Al-Sr alloy castings, Metall. Mater. Trans. A Phys. Metall. Mater. Sci. 41 (2010) 2139–2150. doi:10.1007/s11661-010-0248-9.

[89] X.L. Ma, X. Wang, X.L. Li, L. Yang, Effect of Al5Ti1B master alloy on microstructures and properties of AZ61 alloys, Trans. Nonferrous Met. Soc. China (English Ed. 20 (2010) 1–5. doi:10.1016/S1003-6326(10)60505-5.

[90] A. Elsayed, C. Ravindran, Effect of Aluminum-Titanium-Boron Based Grain Refiners on AZ91E Magnesium Alloy Grain Size And Microstructure, I.J.M.C. 5 (2011) 29–41.

[91] T.R. Society, P. Transactions, E. Sciences, inoculation of melts, 361 (2013) 479–495.

[92] A.B. Pattnaik, S. Das, B.B. Jha, N. Prasanth, Effect of Al-5Ti-1B grain refiner on the microstructure, mechanical properties and acoustic emission characteristics of Al5052 aluminium alloy, J. Mater. Res. Technol. 4 (2014) 171–179. doi:10.1016/j.jmrt.2014.10.017.

[93] A. Amerioon, M. Emamy, G. Ashuri, Investigation the Effect of Al-5Ti-1B Grain Refiner and T6 Heat Treatment on Tensile Properties of Al-8 % Mg, 11 (2015) 32–37. doi:10.1016/j.mspro.2015.11.039.

[94] R. Barua, Kinetics of Phase Transformations : Nucleation & Growth, (n.d.).

[95] M.M. Makhlouf, H. V Guthy, The aluminum – silicon eutectic reaction : mechanisms and crystallography, 1 (2002) 199–218.

[96] F. Division, Effects and mechanisms of grain refinement in aluminium alloys, 24 (2001) 345–353.

[97] M. Modelling, M. Modelling, H.K.D.H. Bhadeshia, Lecture 8 : Growth Morphologies, 66 (1993) 243-266.

[98] M. Dash, M. Makhlouf, Effect of key alloying elements on the feeding characteristics of aluminum – silicon casting alloys, 1 (2002) 251–265.

[99] L. Zhigilei, Nucleation and growth kinetics Nucleation and growth - the main mechanism of phase transformations in materials, (1993).

[100] D. T. J. Hurle, E. Jakeman Lecture 3 : Solidification, (2014).

[101] J. Willard Gibbs Thermodynamics : Enthalpy , Entropy & Gibbs Free, 15 (2014) 1839–1903.

[102] P.S. Mohanty, Grain Refinement Al-Si Alloys of Hypoeutectic, 44 (1996) 3749–3760.

[103] P. Ashtari, H. Tezuka, T. Sato, Influence of Sr and Mn Additions on Intermetallic Compound Morphologies in Al-Si-Cu-Fe Cast Alloys, Mater. Trans. 44 (2003) 2611–2616. doi:10.2320/matertrans.44.2611.

[104] P.S. Mohanty, J.E. Gruzleskit, Mechanism of Grain refinement in Aluminium, 43 (2012).

[105] B. K. Dhindaw, Solidification under microgravity 26, (2001), 59–69.

[106] L. A. Jacobson and J. Mackittrick, "Rapid Solidification Processing" 11 (8), 1994, 355-408.

[107] O. Lashkari and R. Ghomashchi, The implication of rheology in semi-solid metal processes: an overview, J. Mater. Process. Technol. 182 (2007) 229–240.

[108] O.G. and H.C. M. Wessen, , Influence of holding time on particle size of an A356 alloy using new rapid slurry formation process, Int. Conf. High Tech Die Cast. Vicenza, Italy. (2006) 1–11.

[109] R.M. and M.C.F. D. B. Spencer, Rheological behavior of Sn-15% Pb in the crystallization range, Metall. Trans. 3(7) (1972) 1925–1932.

[110] http://www.rheomet.com.

[111] Z. D. Zhao and W.M. Mao, Preparation of semi-solid AlSi7Mg alloy slurry, Acta Met. Sin. 21(2) (2008) 139–145.

[112] L.D. and N.K. Y. Sirong, Microstructure evolution of SIMA processed Al2024, Mater. Sci. Eng. A. 420 (2006) 165–170.

[113] R.M. and M.C.F. D. B. Spencer, Rheological behavior of Sn-15% Pb in the crystallization range, Metall. Trans. 3(7) (1972) 1925–1932.

[114] M. Di Sabatino, L. Arnberg, Transactions of The Indian Institute of Metals Castability of aluminium alloys, 62 (2009) 321–325.

[115] S.K. Shaha, F. Czerwinski, W. Kasprzak, J. Friedman, D.L. Chen, Microstructure and mechanical properties of Al-Si cast alloy with additions of Zr-V-Ti, Mater. Des. 83 (2015) 801–812. doi:10.1016/j.matdes.2015.05.057.

[116] C. Liao, J. Chen, Y. Li, H. Chen, C. Pan, Modification performance on 4032 Al alloy by using Al-10Sr master alloys manufactured from different processes, Prog. Nat. Sci. Mater. Int. 24 (2014) 87–96. doi:10.1016/j.pnsc.2014.03.002.

[117] N.O.T. Restricted, Npl report, (2005).

[118] H. Huang, P. Fu, Y. Wang, L. Peng, H. Jiang, Effect of pouring and mold temperatures on hot tearing susceptibility of AZ91D and Mg − 3Nd − 0 . 2Zn − Zr Mg alloys, 24 (2014) 922–929. doi:10.1016/S1003-6326(14)63144-7.

[119] J. Song, F. Pan, B. Jiang, A. Atrens, M. Zhang, Y. Lu, A review on hot tearing of magnesium alloys, J. Magnes. Alloy. 4 (2016) 151–172. doi:10.1016/j.jma.2016.08.003.

[120] U. Patakham, J. Kajornchaiyakul, C. Limmaneevichitr, Grain refinement mechanism in an Al–Si–Mg alloy with scandium, J. Alloys Compd. 542 (2012) 177–186. doi:10.1016/j.jallcom.2012.07.018.

[121] Thermodynamic Modelling of Growth-Restriction and Poisoning Effects in Aluminium Alloys, Chapter 6 :(2007).

[122] L.Y. Pio, Enhancement of TiB Grain Refining Effect on A356 Gravity Die Casting with the Addition of Yttrium, Mater. Sci. Appl. 3 (2012) 713–718. doi:10.4236/msa.2012.310104.

[123] C. Jeong, High Temperature Mechanical Properties of Al-Si-Mg-Cu Alloys for Automotive Cylinder Heads, 54 (2013) 588–594.

[124] E. Aguirre-De La Torre, U. Afeltra, C.D. Gómez-Esparza, J. Camarillo-Cisneros, R. Pérez-Bustamante, R. Martínez-Sánchez, Grain refiner effect on the microstructure and mechanical properties of the A356 automotive wheels, J. Mater. Eng. Perform. 23 (2014) 581–587. doi:10.1007/s11665-013-0596-x.

[125] M. Zeren, E. Karakulak, Study on hardness and microstructural characteristics of sand cast Al – Si – Cu alloys, 32 (2009) 617–620.

[126] D.H. Xiao, J.N. Wang, D.Y. Ding, Effect of titanium additions on mechanical properties of Al-Cu-Mg-Ag alloy, Mater. Sci. Technol. 20 (2004) 1199–1204. doi:10.1179/026708304225022106.

[127] M. Vasheghani Farahani, E. Emadoddin, M. Emamy, A. Honarbakhsh Raouf, Effect of grain refinement on mechanical properties and sliding wear resistance of extruded Sc-free 7042 aluminum alloy, Mater. Des. 54 (2014) 361–367. doi:10.1016/j.matdes.2013.08.044.

[128] T. Al-cu, Copper Aluminum Alloys Cu-Al Phase Diagram, (n.d.).

[129] M. Vedani, G. Angella, P. Bassani, D. Ripamonti, A. Tuissi, DSC analysis of strengthening precipitates in ultrafine Al-Mg-Si alloys, J. Therm. Anal. Calorim. 87 (2007) 277–284. doi:10.1007/s10973-006-7837-2.

[130] A.M. Mitrašinović, F.C. Robles Hernández, Determination of the growth restriction factor and grain size for aluminum alloys by a quasi-binary equivalent method, Mater. Sci. Eng. A. 540 (2012) 63–69. doi:10.1016/j.msea.2012.01.072.

[131] K.R. Cardoso, D.N. Travessa, A.G. Escorial, M. Lieblich, Effect of mechanical alloying and Ti addition on solution and ageing treatment of an AA7050 aluminium alloy, Mater. Res. 10 (2007) 199–203. doi:10.1590/S1516-14392007000200017.

[132] E.C. De Paris, A Granular Model of Solidification as Applied to Hot tearing, Techniques. 3795 (2007). doi:10.5075/epfl-thesis-3795.

[133] J. Langlais, Fundamental study of hot tearing mechanisms of aluminum-silicon alloys, 2006.

[134] T.U.B. Itak, An improved practice to manufacture Al–Ti–B master alloys by reacting halide salts with molten aluminium, 420 (2006) 71–76. doi:10.1016/j.jallcom.2005.10.017.

[135] Z. Wei Chen, Z. He, W. Qi Jie, Growth restriction effects during solidification of aluminium alloys, Trans. Nonferrous Met. Soc. China (English Ed. 19 (2009) 410–413. doi:10.1016/S1003-6326(08)60287-3.

[136] T.E. Quested, Literature review Understanding mechanisms of grain refinement of aluminium alloys by inoculation, 20 (2004) 1357–1369. doi:10.1179/026708304225022359.

[137] V. Hassanbeygi, A. Shafyei, Investigation on Microstructure and Grain Refining Performance of a New Type of Al-3Ti-1C Master Alloy, (2014) 49–55.

[138] W.W. Ding, J.T. Zhu, W.J. Zhao, T.D. Xia, An Investigation on Grain Refinement Mechanism of Master Alloys Al-Ti, Al-TiC and Al-Ti-C Toward Pure Aluminum, Adv. Mater. Res. 652–654 (2013) 1072–1075. doi:10.4028/www.scientific.net/AMR.652-654.1072.

[139] W. Ding, T. Xia, W. Zhao, Y. Xu, Effect of Al-5Ti-C master alloy on the microstructure and mechanical properties of hypereutectic Al-20%Si alloy, Materials (Basel). 7 (2014) 1188–1200. doi:10.3390/ma7021188.

[140] M. Timpel, N. Wanderka, R. Schlesiger, T. Yamamoto, N. Lazarev, D. Isheim, G. Schmitz, S. Matsumura, J. Banhart, The role of strontium in modifying aluminium-silicon alloys, Acta Mater. 60 (2012) 3920–3928. doi:10.1016/j.actamat.2012.03.031.

[141] S.M. Jigajinni, S.A. Kori, K. Venkateswarlu, Development of New Combination of Grain Refiner-cum-Modifier for LM-21 Alloy, (2013) 1–7.

[142] M.O. Pekguleryuz, X. Li, C.A. Aliravci, In-Situ Investigation of Hot Tearing in Aluminum Alloy AA1050 via Acoustic Emission and Cooling Curve Analysis, (2009). doi:10.1007/s11661-009-9806-4.

[143] M. Easton, D. Stjohn, Grain Refinement of Aluminum Alloys : Part I . The Nucleant and Solute Paradigms — A Review of the Literature, 30 (1999) 1613–1623.

[144] L. Zhang, D. Eskin, A. Miroux, L. Katgerman, Role of Solute and Transition Metals in Grain Refinement of Aluminum Alloys Under Ultrasonic Melt Treatment, TMS (The Minerals, Metals & Materials Society), (2012) 1389–1394.

[145] M.I. Guo-fa, W. Kuang-fei, W.E.N. Tao, Z. Ming, W. Hong-wei, On grain refinement and titanium segregation in Al-Si alloy, (2007) 12–14.

[146] Y. Birol, An Improve Practice to Manufacture Al-Ti-B Master Alloys by Reacting Halide Salts with Molten Aluminum, J. Alloy. Compd., 2006, 420 (1–2), 71–76. doi:10.1179/1743133612Y.0000000017.

[147] A.M. Bunn, P. Schumacher, M.A. Kearns, C.B. Boothroyd, A.L. Greer, Mater. Sci., Technol. 15 (1999) 1115–1123.

[148] A.L. Greer, Grain refinement of alloys by inoculation of melts inoculation of melts, The Royal Society B Biological Sciences 361(2003):479-495. doi:10.1098/rsta.2002.1147.

[149] B.G. Thomas, I. Uiuc, Modeling of Hot Tearing and Other Defects in Casting Processes, 22 (2009) 362–374.

[150] M.X. Zhang, P.M. Kelly, Edge-to-edge matching and its applications: Part I. Application to the simple HCP/BCC system, Acta Mater. 53 (2005) 1073–1084. doi:10.1016/j.actamat.2004.11.007.

[151] M.X. Zhang, P.M. Kelly, M.A. Easton, J.A. Taylor, Crystallographic study of grain refinement in aluminum alloys using the edge-to-edge matching model, Acta Mater. 53 (2005) 1427–1438. doi:10.1016/j.actamat.2004.11.037.

[152] M. Zhang, P.M. Kelly, Edge-to-edge matching model for predicting orientation relationships and habit planes the improvements, Metals 52 (2005) 963–968. doi:10.1016/j.scriptamat.2005.01.040.

[153] C.L. Chen, W. Lu, Orientation relationships between TiB (B27), B2 , and $TiAl_3$ phases, (2009). doi:10.1557/JMR.2009.0220.

[154] J. Yang, J.L. Wang, Y.M. Wu, L.M. Wang, H.J. Zhang, Extended application of edge-to-edge matching model to HCP/HCP (α-Mg/$MgZn_2$) system in magnesium alloys, Mater. Sci. Eng. A. 460–461 (2007) 296–300. doi:10.1016/j.msea.2007.01.097.

[155] M. Johnsson, Grain refinement of aluminium studied by use of a thermal analytical technique ", Thermochimica Acta 256 (1995) 107-121.

[156] T. Ariwibowo, S. Subroto, Connection between hot tearing and cold cracking in DC-casting of AA7050 : Experiments and computer simulations (25-11-2014).

[157] U. Feurer, Quality Control of Engineering Alloys and the Role of Metals Science, Delft Univ. Technol. Delft. (1977) 131–145.

[158] G.J. Clyne, T.W. and Davies, The Influence of Composition on Solidification Cracking Susceptibility in Binary Alloy Systems, Br. Foundrym. 74 (1981) 65–73.

[159] H.F. Bishop, C.G. Ackerlind, and W.S. Pellini, Investigation of Metallurgical and Mechanical Effects in Development of Hot Tearing, Trans. AFS. 65 (1957) 244-47.

[160] J. Pumphrey, W.I., Jennings, P.H., , 75, (1948), p. 235-256, Inst. Met. 75 (1948) 235–256.

[161] M. D. Sabatino, L. Arnberg, Castability of aluminium alloys. Transactions of The Indian Institute of Metals 62 (2009) 321-325.

[162] S. Lin, “A study of hot tearing in wrought aluminum alloys” (Ph.D. thesis, University of Quebec, 1999), 7-68, 69-90.

[163] V. Metan, K. Eigenfeld, Controlling mechanical and physical properties of Al-Si alloys by controlling grain size through grain refinement and electromagnetic stirring, 150 (2013) 139–150. doi:10.1140/epjst/e2013-01803-6.

[164] Y. Estrin, A. Vinogradov, Extreme grain refinement by severe plastic deformation: A wealth of challenging science, Acta Mater. 61 (2013) 782–817. doi:10.1016/j.actamat.2012.10.038.

[165] A. R. Singer, S.A. Cottrell, Properties of the Aluminium-Silicon Alloys at Temperatures in the Region of the Solidus, J. Inst. Met. 73 (1947) 33-54.

[166] A. Bochvar, Optimum Content of the Eutectic in Cast Alloys, Izvest. Akad. Nauk. S.S.S.R, Tekhn. 6 (1944) 358–361.

[167] J. Vero, The Hot-Shortness of Aluminium Alloys, Met. Ind. 48 (1936) 431–34.

[168] P.H. Singer, ARR, Jennings, Hot-Shortness of the Aluminium-Silicon Alloys of Commercial Purity, J. Inst. Met. 73 (1947) 197–212.

[169] N. Hatami, R. Babaei, M. Dadashzadeh, P. Davami, Modeling of hot tearing formation during solidification, 5 (2007) 506–513. doi:10.1016/j.jmatprotec.2007.11.260.

[170] S. Bozorgi, K. Haberl, C. Kneissl, T. Pabel, P. Schumacher, Effect of Alloying Elements (magnesium and Copper), (2011) 113–120.

[171] D.C.G. Lees, The Hot Tearing Tendencies of Aluminium Casting Alloys, J. Inst. Met. 72 (1946) 343–364.

[172] D.C.G. Lees, Note on the Effect of Dissolved Gas on the Hot-Tearing of Aluminum Casting Alloys, J. Inst. Met. 73 (1947) 537.

[173] W.I. Pumphrey, P.H. Jennings, A Consideration of the Nature of Brittleness at Temperatures above the Solidus in Castings and Welds in Aluminum Alloys, J. Inst. Met. 75 (1948) 235.

[174] M. O. Pekguleryuz, S. Lin, E. Ozbakir, D. Temur, C. Aliravci, Hot tear susceptibility of aluminium–silicon binary alloys, Inter. J. of Cast Met. Research, 23 (2010) 310-320.

[175] H.F.T. U.K. Bhattacharya, CM. Adams, Stress Required to Hot Tear Plain Carbon Cast Steel, Trans. AFS. 62 (1954) 557.

[176] F. Kôrber, G. Schitzkowski, Determination of the Contraction of Cast Steel, Stahlund Eisen. 15 (1928) 128.

[177] U.K. Bhattacharya, C.M. Adams, H. F. Taylor, Hot-tear formations in steel casting, Trans. AFS. 60, (1952), 675.

[178] J.M. Middleton, Hot-tearing of Steel, J. Iron Steel Inst. 42 (1949) 407.

[179] C.W. Briggs, Hot Tear Formation, Metall. Steel Cast. (1946) 317.

[180] W.S. Pellini, Strain Theory of Hot-tearing Foundry, 80 (1952) 124.

[181] W.S.Pellini. H.F. Bishop, C.G. Ackerlind, Investigation of Metallurgical and Mechanical Effects in Development of Hot Tearing", Trans. AFS. 65 (1957) 247.

[182] E.J. Gamber, Hot Cracking Test for Light Metal Casting Alloys, Trans. AFS. 67 (1959) 237.

[183] T.W. Clyne and G.J. Davies, A Quantitive Solidification Test for Casting and An Evaluation of Cracking in Aluminium-Magnesium Alloys, Br. Foundrym. 68, (1975) 238.

[184] Novikov and O.E. Grushko, Hot Cracking Susceptibility of Al-Cu-Li and Al-Cu-Li-Mn Alloys, Mater. Sci. Tech.. no. 9, vol (1995) 926. 27.

[185] J.C. Borland, Generalized Theory of Super-Solidus Cracking in Welds and Casting, Br. Weld. J. Vol. 7 (1960) 508–512.

[186] S. Oya, T. Fujii, M. Ohtaki, S. Baba, J. Jpn. Inst. Light Met. 34 (1984) 511–516.

[187] R.A. Flinn, Fundamentals of Metal Casting., Addison-Wesley. (1963) 103–111.

[188] H.F.T. R.A. Rosenberg, and M.C. Flemings, Nonferrous Binary Alloys Hot-Tearing, Trans. AFS. 68 (1960) pp.518-528.

[189] S. Ohm, L. Engler, Festigkeiteigenschaften erstarrender Randschalen aus Aluminium-Iegierungen - Teil 1, GieBereiforschung. 42 (1990) 3.

[190] W.S. Bishop, H.F., Ackerlind, C.G., Pellini, Trans. Am. Foundrymen's Soc., Trans. Am. Foundrymen's Soc. 65 (1957) 247–258 12.

[191] J.O. Couture, A, Edwards, The Hot-Tearing of Copper-Base Casting Alloys, AFS Trans. 74 (1966) 709–721.

[192] J.M. Van Vlack, L.H., Riegger, O.K., Warrick, RJ., Dahl, Trans. Met. Soc. AIME. Vol. 221 (n.d.) 220–23.

[193] V.N. Saveiko, Theory of Hot Tearing", Russian Casting Production, 11 (1961) 453.

[194] U. Upadhya, G. Cheng, S. and Chandra, A mathematical model for prediction of hot tears in castings, Light Met. (1977) 133–142.

[195] G.J. Cylne, T.W. Pavies, the influence of composition on solidification cracking susceptibility in binary alloys system, Journ. Brit. Foundrymam. 74 (1981) 65–73.

[196] S. Chamberlain, B., Watanabe, A Natural Aging Aluminum Alloy, Designed for Permanent Mold Use, AFS Trans. 85 (1977) 133–142.

[197] R.T. Alcan, E. Road, - How to Optimise and Minimise, 630 (2010) 213–221. doi:10.4028/www.scientific.net/MSF.630.213.

[198] N.K.G.-S. H. Nishimura, No Title, 1 (1937) 8–39.

[199] Y. Matsuda, F., Nakata, K., Shimokusu, Effect of Additional Element on Weld Solidification Crack Susceptibility of Al-Zn-mg (Report I), Trans. Japanese Weld. Res. Inst. 12 (1983) 81–87.

[200] L. Bichler, A. Elsayed, K. Lee, C. Ravindran, Influence of Mold And Pouring Temperatures on Hot Tearing Susceptibility 0f Az91 D Magnesium Alloy, (2008) 43–54.

[201] S.S. J.A. Spittle, , Mater. Sci. Technol. 11 (1995) 533–537.

[202] Z. Zhen, N. Hort, Y.D. Huang, N. Petri, O. Utke, K.U. Kainer, Quantitative Determination on Hot Tearing in Mg-Al Binary Alloys, Mater. Sci. Forum. 618–619 (2009) 533–540. doi:10.4028/www.scientific.net/MSF.618-619.533.

[203] T.W. Clyne, M. Wolf, and W. Kurz, The Effect of Melt Composition on Solidification Cracking of Steel, with Particular Reference to Continuous Casting, Met. Trans. 13B (1982) 259.

[204] J.M. Middleton and H.T. Protheroe, The Hot Tearing of Steer, J. Iron Steel Inst. 168 (1951) 384.

[205] L. Katgerman, W.M. Van Haaften, W.H. Kool, Constitutive behaviour and hot tearing during aluminium DC casting, Mater. Forum. 28 (2004) 312–318.

[206] J. Van Eghem and A. de Sy, Mod. Cast. 48 (1965) 100.

[207] B.H. P. Pousset, M. Rappaz, Modeling of Inverse Segregation and Porosity Formation in Directionally Solidified Aluminum Alloys, Met. Mater. Trans. 26A (1995) 2349–2358.

[208] J.W. E. Scheuer, S.J. Williams, Foundry Properties of Aluminum Alloys, Met. Ind. 85 (1954) 63.

[209] J. Song, Z. Wang, Y. Huang, A. Srinivasan, Z. Wang, F. Beckmann, N. Hort, Hot tearing characteristics of Mg – 2Ca – x Zn alloys, J. Mater. Sci. 51 (2016) 2687–2704. doi:10.1007/s10853-015-9583-y.

[210] D. Stefanescu, Science and Engineering of Casting Solidification, Springer, 2015. https://books.google.com/books?id=ZFR1CgAAQBAJ&pgis=1 (accessed February 17, 2016).

[211] S. Gowri and M. Bouchard, Hot Cracking in Aluminium Alloys—Part 1. Literature Survey, Res. Report, Univ. Du Québec À Chicoutimi. (n.d.).

[212] Z. Lin, C.A. Monroe, R.K. Huff, C. Beckermann, I. City, Prediction of Hot Tear Defects in Steel Castings Using A Damage Based Model, (2009) 329–336.

[213] Q. Wu, Study of Hot Tearing in Cast and Wrought Aluminum Alloys, (n.d.).

[214] C.A. Aliravci, Investigation of Quantitative Methods to Measure the Hot Tearing Tendency in Wrought Aluminum Alloys, Univ. Du Québec À Chicoutimi. Alcan Chair Res. Rep. I. (1995).

[215] D. Warrington and D.G. McCartney, Development of a New Hot-Cracking Test for Aluminum Alloys, Cast Met. 2 (1989) 134.

[216] A. Couture and J.O. Edwards, The Hot-Tearing of Copper-Base Casting Alloy, Trans. AFS. 74 (1966) 709–721.

[217] D. Warrington and D.G. McCartney, Hot-Cracking in Aluminum Alloys 7050 and 7010, A Comp. Study", Cast Met. 3, no (1991) 202.

[218] A. Elsayed, C. Ravindran, Effect of Aluminum-Titanium-Boron Based Grain Refiners on Az91E Magnesium Alloy Grain Size and Microstructure, (2011) 29–41.

[219] D. Ovono Ovono, I. Guillot, D. Massinon, Determination of the activation energy in a cast aluminium alloy by TEM and DSC, J. Alloys Compd. 432 (2007) 241–246. doi:10.1016/j.jallcom.2006.05.132.

[220] M. T. S. balasubramanian, M. Balakrishnan, V. Balasubramanian, Influence of welding processes on microstructure, tensile and impaalloy iointsct properties of Ti-6Al-4V, Trans. Nonferrous Met. Soc. China. 21 (2011) 1253–1262. doi:10.1016/S1003.

[221] M.M.. Jaradeh, The Effect of Processing Parameters and Alloy Composition on the Microstructure Formation and Quality of DC Cast Aluminium Alloys, PhD Thesis, (2006) P46.

[222] B. Zlaticanin, B. Radonjic, M. Filipovic, Characterization of Structure and Properties of As-cast AlCuMg Alloys, Mater. Trans. 45 (2004) 440–446. doi:10.2320/matertrans.45.440.

[223] L. Kuchar, M. Br, A. Sládek, Influence of Chemical Composition on Porosity in Aluminium Alloys, 14 (2014) 5–8.

[224] H. Moller, G. Govender, W. E. Stump and R. D. Knutsen, Influence of temper condition on microstructure and mechanical properties of semi-solid metal processed Al–Si–Mg alloy A356, Int. J. Cast Met. Res. 22(6) (2009) 417–421.

[225] T.R. Society, P. Transactions, E. Sciences, Inoculation of Melts, 361 (2013) 479–495.

[226] Z. Zhang, X. Bian, Y. Wang, X. Liu, Microstructure and grain refining performance of melt-spun Al-5Ti-1B master alloy, Mater. Sci. Eng. A. Struct. Mater. 352 (n.d.) 8–15. http://cat.inist.fr/?aModele=afficheN&cpsidt=14762381 (accessed October 17, 2016).

[227] T. Chandrashekar, M.K. Muralidhara, K.T. Kashyap, P.R. Rao, Effect of growth restricting factor on grain refinement of aluminum alloys, Int. J. Adv. Manuf. Technol. 40 (2009) 234–241. doi:10.1007/s00170-007-1336-x.

[228] Z. Tang, T. Seefeld, F. Vollertsen, Grain Refinement by Laser Welding of AA 5083 with Addition of Ti/B, Phys. Procedia. 12 (2011) 123–133. doi:10.1016/j.phpro.2011.03.016.

[229] H.K. Kamga, D. Larouche, M. Bournane, A. Rahem, Hot tearing of aluminum – copper B206 alloys with iron and silicon additions, Mater. Sci. Eng. A. 527 (2010) 7413–7423. doi:10.1016/j.msea.2010.08.025.

[230] H. Nagaumi, S. Suzuki, T. Okane, T. Umeda, Effect of Iron Content on Hot Tearing of High-Strength Al-Mg-Si Alloy, 47 (2006). doi:10.2320/matertrans.47.2821.

[231] R. S.Kumar, J. Malisano, V.Ito, K.A.Q., Influence of Trace Element additions on Fe bearing Intermettalic solidification of a 6063 Al alloy, Miner. Met. Mater. Ser. (2017) 305–311.

[232] D.G. Eskin, V.I. Savran, L. Katgerman, Effects of Alloy Composition and Casting Speed on Structure Formation and Hot Tearing during Direct-Chill Casting of Al-Cu Alloys, 35 (2004) 3551–3561.

[233] W. Jiefang, X. Jingpei, Y. Shuqing, L. Zhongxia, W. Yonggang, Influence of titanium content on wear resistance of electrolytic low-titanium eutectic Al-Si piston alloys, 5 (2008) 3–7.

Appendix 1

Charge calculation for preparation of Al-7Si-3Cu alloy

For the production of 1 Kg of Al-7Si-3Cu alloy the raw material are following:

- Master alloy (Al-13%Si), let assume the value 'x' gm,
- Al-33Cu = y gm
- Pure Al = 1-x-y gm

Al	+	Al-13Si	+	Al-33Cu	→	Al-7Si-3Cu
(1-x-y)		x		y		1Kg

Balancing the Si from the both side, we have-

(x X 13)/100 = 70 gm

x = 538.46 gm

Balancing the Si from the both side, we have-

(y X 33)/100 = 30 gm

y = 90.90 gm

So equation becomes-

Al	+	Al-13Si	+	Al-33Cu	→	Al-7Si-3Cu
370.64gm		538.46gm		90.90gm		1Kg

Appendix 2

Table 4.3 Mean particle size of nucleating particles of as cast and after ball milling

Master alloy	Ball milling time (hour)	Mean (µm)	S.D.	min	max	Particle less than 25 µm
1	-	54.2	11.3	23	80	29
2	10	42.1	6.2	14	54	48
3	30	20.0	5.1	11	32	64
4	50	9.0	5.1	6	22	98

Appendix 3

Table 4.4 Mean particle size of nucleating particles of as cast and after annealing

Master alloy	Annealing temperature(˚C)	mean	S.D.	min	max	Particle less than 25 µm
1	-	54.2	11.3	23	80	29
2	400	50.1	9.2	22	80	48
3	500	47.2	8.1	19	79	54
4	600	46.0	7.1	18	78	58
5	700	36.8	5.9	14	78	72
6	800	53.9	10.7	23	80	32
7	800 upper part	60.3	9.3	32	80	13
8	800 lower part	36.3	6.3	13	54	76

Appendix 4

Table 4.5 Mean particle size of nucleating particles of as cast and after hot rolling

Master alloy	Rolling temperature(˚C)	Reduction level	mean	S.D.	min	max	Particle less than 25 µm
1	-	-	54.2	11.3	23	80	29
2	250	25	32.1	9.2	17	52	54
3	250	50	22.2	8.1	14	46	64
4	250	75	15.0	5.1	11	39	78
5	350	25	36.8	9.5	19	53	52
6	350	50	23.9	8.7	16	44	61
7	350	75	17.3	9.3	14	41	72

Appendix 5

Table 4.6 Phase transformations for exothermic reaction

Sample	*Wt.% Ti*	*Eutectic temperature (T_s)*	*Liquidus temperature (T_l)*
1	-	*549*	*583*
2	*0.10*	*550*	*589*
3	*0. 15*	*551*	*594*

Appendix 6

Table 4.7 Influence of grain refinement on the mechanical properties of Al-7Si-3Cu alloy

Type of grain refiner	*Wt.% Ti*	*UTS*	*QI (MPa)*	*Hardness (HB)*
A_0	*0.001*	*210*	*367*	*65*
A	*0.050*	*253*	*404*	*78*
B	*0.045*	*260*	*419*	*92*
C	*0.040*	*270*	*438*	*98*
D	*0.035*	*292*	*449*	*102*

Appendix 7

List of Publication from this Research work

1. **Sachin Kumar Rathi, Ashok Sharma, Marisa Di Sabatino**, "Effect of mould temperature, grain refinement and modification on hot tearing test in Al-7Si-3Cu alloy" Engineering Failure Analysis 79 (2017): 592-605.
2. **Sachin Kumar Rathi, Ashok Sharma, Marisa Di Sabatino**, "Performance of Al-5Ti-1B master alloy after ball milling on minimizing hot tearing in Al-7Si-3Cu Alloy" Trans Indian Inst. Met (2017) 75(3):827–831.
3. **Sachin Kumar Rathi, Ashok Sharma, Marisa Di Sabatino**, "Influence of Annealing of Al-5Ti-1B Master Alloy on Hot Tearing of Cast Al-7Si-3Cu alloy" Key Engineering Materials (2017) 717: 27-31.
4. **Sachin Kumar Rathi, Ashok Sharma, Marisa Di Sabatino** "Effect of Grain Refinement on Hot Tearing in Aluminium Alloys", Indian Foundry Journal, vol. No.12. December 2015.

Bio-Data

……

Name: Sachin Kumar Rathi

Address: Department of Metallurgical and Materials Engineering,
Malaviya National Institute of
Jaipur-302017 (India)

E- mail: sachin.baryons@gmail.com

Mobile: +919602161802, 7248805552

Career Objective:

To attain excellence in Science and Technology through innovations, capabilities and my zeal to explore. To pursue a career in knowledge sharing through research and development.

Academic Qualification:

Ph. D:	Thesis Title: Effect of Al-5Ti-1B Master Alloy Grain Refiner on Mechanical Properties and Hot Tearing Susceptibility of Cast Al-7Si-3Cu Alloy
Master of Technology:	In Metallurgical and Materials Engineering and have secured 7.3 CGPA in course work (MNIT Jaipur)
Master of Science:	Physics from CCS University Meerut Percentage: 63%.

Research Interest: Study of graphite and its effect in Al alloy, Influence of grain refinement on porosity and hot tearing in aluminium alloys

Professional Membership: Member of International Association of Engineers (IAENG), Student Member of IIF, Student Member of IIM

Research Publications:

1. **Sachin Kumar Rathi, Ashok Sharma, Marisa Di Sabatino**, "Effect of mould temperature, grain refinement and modification on hot tearing test in Al-7Si-3Cu alloy" "Engineering Failure Analysis" Elsevier 79 (2017) 592-605.
2. **Sachin Kumar Rathi, Ashok Sharma, Marisa Di Sabatino**, "Performance of Al-5Ti-1B master alloy after ball milling on minimizing hot tearing in Al-7Si-3Cu Alloy" Trans Indian Inst Met (2017) 75(3):827–831 doi: 10.1007/s12666-017-1065-2.